WIND FARMS IMPACT ON RADAR AVIATION INTERESTS - FINAL REPORT

FES W/14/00614/00/REP
DTI PUB URN 03/1294

Contractor QinetiQ

Prepared by Gavin J Poupart

September 2003

The work described in this report was carried out under contract as part of the DTI Sustainable Energy Programmes. The views and judgements expressed in this report are those of the contractor and do not necessarily reflect those of the DTI.

First published 2003

This page is intentionally blank

EXECUTIVE SUMMARY

Background

The Department of Trade and Industry (DTI) of the UK Government is committed to reducing carbon emissions and revising the UK energy infrastructure. As such, increased renewable energy generation is seen as a potential significant contributor to realising this vision. The UK's wind resource is significant and with the technology currently available, the UK has the potential to harness a significant proportion of the UK's energy requirements from this renewable resource.

The process of obtaining planning permission to build a wind farm involves many considerations, including consultation with various aviation stakeholders, both civil and military. These parties may raise objections for a variety of reasons. A known source of objection is that the wind farm may appear on the display of air traffic control radar. Decisions made regarding the likely impact that a wind farm may have upon radar operations are currently based upon assumptions. The electromagnetic interactions between a wind turbine and a radar signal are complex and there is currently limited understanding in this area and no accepted method for quantifying this potential impact.

A conflict of interest currently exists between the desire to encourage wind farm development as a renewable energy source and the desire to maintain the operational safety of air traffic. The practical manifestation of this conflict is that the UK has seen objections against a significant proportion of proposed wind farms on the grounds of aviation safety. This situation is obviously unsatisfactory to the wind energy industry. Often developers commit to the costs of site assessments that are subsequently refused permission, are subjected to planning delays or are significantly constrained regarding potential areas for development if they are to avoid this potential conflict.

Conversely, the current limited knowledge base and technical complexity of this subject area does not aid the aviation stakeholders when making assessments of the potential impact of wind farms upon aviation operational safety. The aviation stakeholders are often unable to provide clear and grounded comment as to whether a particular proposed wind farm presents a safety issue or what would be needed to mitigate and achieve the safety confidence required. The DTI has tackled this issue, in part, by commissioning this project to provide a detailed understanding of the interaction between wind farms and radar systems. It is anticipated that this study will provide input into the revision of the "Wind Energy and Aviation Interests interim guidelines" ref. ETSU W/14/00626/REP for the siting of wind farms.

Objectives

The main objectives of the study were as follows:

- Determine the effects of siting wind turbines adjacent to primary air traffic control radar;
- Provide the information required for the generation of guidelines by civil, military and wind farm developer stakeholders;
- Determine the extent to which detailed design of wind turbines influences their effects on radar systems;

- Determine the extent to which the design of the radar processing influences the effects of wind turbines on radar systems.

Methodology

As a mechanism to predict the Radar Cross Section (RCS) of wind turbines and understand the interaction of radar energy and turbines, a computer model has been developed by exploiting QinetiQ's stealth technology expertise. This model operates in a 'super-computer' environment and is designed to predict and simulate the impact of wind farms upon the primary radar display. The model considers the affects of the radar propagation over the terrain between the radar and the wind farm, the dynamic radar scattering from the wind farm and the processing in the radar. It can then display its results on a simulated radar display

The model has been validated through a full-scale trial and modelling process. Data have been collected from a number of sources: a single operational Enercon E-66 turbine located at Swaffham in Norfolk using a mobile experimental radar station, high fidelity RCS measurements of a scale model blade in a compact range chamber and from the radar display at RAF Marham (a radar having visibility of the Swaffham turbine).

The propagation code used as an input to the model was successfully validated by comparing its output with a validated public domain propagation model. A number of references are provided against other QinetiQ work that have in the past validated the QinetiQ propagation model as part of Ministry of Defence programmes.

In addition to the trial at Swaffham, some radar display video data were collected from Prestwick of a nearby multiple turbine wind farm appearing on the radar display. A model simulation was run of this wind farm with the turbines in a 'typical' configuration. Results provided additional confidence in the model's predictive ability.

In summary, a predictive computer model has been developed, validated against a single turbine scenario and has shown an accurate prediction capability. The reality is that most sites of concern will have multiple turbines, further model validation could be gained through a multiple turbine trial.

Stakeholder benefits

The experience gained and learning achieved during the development and validation of the predictive computer model have been used to perform a sensitivity analysis (identification of the sensitivity of sub-elements of the radar and wind farm interaction) and to compile a list of the key factors influencing the radar signature of wind turbines. Together, these have enabled us to provide a much more detailed quantification of the complex interactions between wind turbines and radar systems than was previously available.

The following points summarise some of the results of the project:

- The design of the tower and nacelle should have the smallest RCS signature possible. The RCS of the tower and nacelle can be effectively reduced though careful shaping;
- Large turbines do not necessarily lead to large RCS (i.e. tower height does not greatly affect RCS);

- Blade RCS returns can only be effectively controlled though the use of absorbing materials;
- For low probability of detection, but a large clutter return, set wind turbines such that they are mainly yawed close to ±90° from the radar direction;
- For high probability of detection, but a smaller area of clutter, set wind turbines such that they are mainly yawed close to 0° and 180° from radar direction;

It was noted that some of the RCS predictions used in the model are 4 to 6 dB lower than the measurements, near RCS peaks. This is a result of two main factors:

Firstly blade reflectivity. The blades are not metallic and therefore, have to be assigned a reflectivity in the modelling process. This has been estimated, and it appears from the measurements that the blades are more reflective than expected.

Secondly, the predictions carried out do not model any returns resulting from multiple interactions within the turbine structure. Given geometry that gives rise to paths back to the radar via multiple bounce these returns can be very large. Without this mechanism the predictions will be different from the measurement where strong multiple bounce returns are present.

To reduce this difference we must deal with both of these factors. The turbine blades need to be modelled with a more realistic reflectivity and the multiple bounce calculations must be included in the turbine calculations.

The model has the potential to be a valuable tool for the wind energy community and can provide a validated route to:

- Generate the detailed data required for more sophisticated initial screening than is currently available;
- Support the development of mitigation and solutions, including: siting optimisation, control of wind turbine RCS and enhanced radar filters (able to remove the returns from wind turbines);

This page is intentionally blank

LIST OF CONTENTS

This page is intentionally blank

1 INTRODUCTION

1.1 Project background

1.1.1 The Department of Trade and Industry of the UK Government has a policy of encouraging the development of renewable energy sources. One such renewable energy source is the power available from the wind. With the position of the UK on the edge of the continent of Europe, wind energy is particularly plentiful, so that wind is a promising renewable energy source for the UK.

1.1.2 The process of obtaining planning permission to erect a wind turbine or a wind farm (a group of wind turbines built on the same site) involves many considerations, including consultation with various aviation interests, both civil and military. These parties may raise objections to a proposed wind turbine for a variety of reasons. One common source of objection from the Royal Air Force is that the wind turbine, being a tall object (70 to 100 metres or more), is a threat to the safety of low-flying military aircraft on training flights. Another source of objections is that the wind turbine will appear as an echo on the display of radar used in air traffic control (ATC). This echo distracts the air traffic controller from the aircraft echoes which are his main interest, and can reduce the effectiveness of the radar by masking genuine aircraft returns. This is considered as a threat to the safety of air traffic, both civil and military.

1.1.3 There is, thus, a conflict of interest between the desire to encourage wind farm development as a renewable energy source, and the desire to maintain the safety of air traffic. In practice, a large fraction of proposed wind farms have objections lodged against them on grounds of aviation safety. This situation is unsatisfactory to the wind energy industry, as it involves them in the expense of preparing cases for wind farm development at sites that are subsequently refused permission, and considerably restricts the areas available for wind farm development.

1.1.4 The Department of Trade and Industry, contracting via Future Energy Solutions (FES) at Harwell has set up a working party under the title "Wind energy, defence and civil aviation interests". This provides a forum for representatives of the wind energy industry to meet with civil and military aviation authorities, and discuss these issues. Examples of wind farms in the vicinity of ATC radar exist in the UK. In some cases, problems have been reported and documented.

1.1.5 Cases are known where the presence of a wind farm adjacent to an airport is causing problems for the ATC of the airport. On the other hand, cases are also known where a wind turbine close to an airfield causes little or no problem to the airfield ATC. The reasons for this apparent inconsistency are not well understood.

1.1.6 This lack of understanding makes it hard for the aviation safety authorities to give clear and well-founded decisions on whether a particular proposed wind farm presents a safety issue or not.

1.1.7 The Department of Trade and Industry commissioned this study to clarify the interaction of wind turbines and radar systems, and to provide input into the production of guidelines for the siting of wind turbines near radar systems.

1.2 Radar cross-section

1.2.1 Throughout this report we will be using the term, radar cross-section (RCS). For readers unfamiliar with this term the following paragraphs are a description of its meaning.

1.2.2 An essential element in considering the detection of a wind turbine by a radar is the strength of the radar reflection from the turbine. This is measured by its RCS, which is an area, usually measured in square metres. It can have a wide range of values, and is often quoted in decibel square-metres (dBsm), which is a logarithmic measure. An RCS of 0dBsm means 1 square metre, every 3dB increase doubles the value in square metres, and each 10dB added means that the RCS is multiplied by 10.

1.2.3 In the special case of a large metal sphere, the RCS is equal to the area of the geometrical cross-section. For other targets it can be much greater than the geometrical area (e.g. a flat plate viewed at right angles, or the corner reflector used on buoys and small boats). In yet other targets it can be much smaller than the geometrical area (e.g. a stealth aircraft).

1.3 Objectives of work

1.3.1 The main objectives of the work are as follows:

- Provide information for the generation of guidelines for the siting of wind turbines near radar systems;
- Determine the effects of siting wind turbines adjacent to radar systems;
- Determine the extent to which the detailed design of the turbines influences their effect on radar systems;
- Determine the extent to which the radar processing influences the effects of wind turbines on radar systems.

1.3.2 To achieve these aims QinetiQ set out to complete the following tasks:

- Develop a computer model to simulate the effects of wind turbines on radar systems;
- Carry out radar cross-section (RCS) predictions of four wind turbine designs and analyse their radar signatures;
- Plan field trials to validate the predictions and computer model;
- Validate the predictions and model against the data collected in the field trials

1.3.3 After planning the field trials QinetiQ was also instructed to carry out these trials and this is also reported on here.

1.4 Report structure

1.4.1 The main report is split into sections, each containing details of one of the tasks carried out. Section 2 pulls together findings gained from the completion of this work into key factors influencing the radar signature of wind turbines, which should help the development of siting guidelines.

1.4.2 Section 3 reports on the development of a computer model to simulate the effects of wind turbines on radar systems. This model is developed using QinetiQ experience in radar scattering and radar propagation to allow the effects of a turbine on a primary radar display to be simulated.

1.4.3 Section 4 reports on RCS predictions carried out on wind turbines. The RCS of an object is a measure of how much energy is returned to the radar, and hence is critical in understanding, and simulating the effects of a wind turbine on radar. The predictions are done using QinetiQ prediction codes developed from 20 years of research in the UK stealth programme.

1.4.4 Section 5 contains the details and results of the radar measurements that have been made to validate the predictions and the computer model described in section 2. These measurements have been carried out on a scale model turbine blade in a QinetiQ measurement facility and of a real turbine using a QinetiQ mobile experimentation radar.

1.4.5 Section 6 explains the validation process and the results from this exercise. The validation uses all the data collected and explained in sections 3 and 4 to validate the computer model described in section 2. The model has been run to reproduce measured scenarios and the resulting output compared to the measured result.

1.4.6 Section 7 identifies the key parameters that influence the effects a turbine will have on a radar system. Examples would be the parameters which affect the RCS, and hence the returning power to the radar and radar settings and filters.

1.4.7 Section 8 contains the conclusions from the report, summarising all of the findings from the previous sections.

1.4.8 Section 9 describes the recommendations resulting from this study.

1.4.9 The following sections in the main body of the report concentrate on the results and findings of the study. All the technical detail and mathematics are presented in appendices at the back of the report and are referenced from the main text.

1.4.10 Appendix A includes details of how the modelling of the wind turbines was carried out, and reasoning for the simplifications made. It also includes results from the predictions carried out.

1.4.11 Appendix B includes a detailed description of the computer model, fully describing the functionality of each of the model parts. It also includes a section on the mathematics of radar shadowing caused by turbines.

1.4.12 Appendix C is the outline trials plan that was generated early in the project to define the trials to be carry out.

1.4.13 Appendix D includes details of the radar trials carried out, including calibration and instrumentation issues. It also includes more processed measurement results.

1.4.14 Appendix E includes a discussion of the issues surrounding circular polarisation and shows that the RCS prediction techniques used in this work can be applied to circular polarisation problems.

1.4.15 Appendix F details the work carried out by the subcontractor EMRAD in creating a database of radar sites within line of site (LoS) of wind farms in the UK.

1.4.16 Appendix G contains a review of the QinetiQ computer model by the subcontractor EMRAD, explaining their views on the work carried out and the validity of the model.

2 KEY FACTORS INFLUENCING THE RADAR SIGNATURE OF WIND TURBINES

2.1 Learning as potential inputs to the DTI guidelines

2.1.1 In order to detail the relevant input sections for the DTI guidelines, they are identified below under the following headings for clarity; Wind turbine, Wind farm, Terrain, and Radar.

2.1.2 Wind turbine

2.1.2.1 Design (Shape). A typical wind turbine is made up of three main components, the tower, the nacelle, and the rotor. We have carried out a study of the effects of shape on the RCS of these components (see section 7). We consider each of the turbine components and present the key factors influencing the radar signature.

2.1.2.2 The wind turbine tower is a constant return that should be minimised to aid the radar filtering of the turbine. Radar processing can suppress stationary objects, but if the RCS is too high then the object will still appear as clutter on the PPI display. It should be noted that although the tower is essentially stationary it does vibrate and sway under normal operation and this may have an effect on the radar filtering.

2.1.2.3 For a tapered cylindrical tower increasing the taper angle will greatly reduce the tower RCS (e.g. Enercon tower RCS is $\approx 100m^2$. Increasing taper angle by 2° reduces RCS to $\approx 10m^2$). Over the range of likely tower sizes the diameter and height of the tower only have a small effect on the tower scattering. As the tower does not move, squashing the tower into an oval cross-section and pointing the narrow cross section at the radar can further reduce its RCS. This is only effective if there is one illuminating radar system as the RCS will be lower only when looking at the narrow tower cross-section (for details see section 7.3). The tower of a wind turbine will bend under normal operation due to wind load and thermal heating. These effects are likely to be big enough to significantly effect the tower RCS, and need to be taken into consideration when designing a tower for RCS control.

2.1.2.4 Unlike the tower the turbine nacelle RCS is a function of the turbine yaw angle. It rotates only slowly with respect to the radar, hence will be suppressed by radar filters. As with the tower it is still important to keep this return to a minimum to give the radar the best chance of filtering the turbine return.

2.1.2.5 Curved surface nacelles send energy in all directions, giving a less variable but high RCS with changing yaw angle. Flat panel nacelles create a variable RCS return with very high spikes and regions of low returns as the yaw is varied (e.g. the Enercon curved nacelle varies between $2m^2$ and $160m^2$, where as the Vestas flat panel nacelle varies between $0.003m^2$ and $12{,}600m^2$). To create an all round low nacelle return flat panels angled away from the radar (tilted up or down) should be used (e.g. the Vestas nacelle maximum can be reduced from $12{,}600m^2$ to $50m^2$ with a 10° tilt angle. See section 7.4 for more details).

2.1.2.6 With current nacelle designs (rounded or flat panel) the yaw angles which give the lowest RCS are around ±45° and ±135° with the highest RCS occurring at 0°, ±90°, and 180°.

2.1.2.7 The turbine rotor is very important in considering the effect of wind turbines on radar. As it is spinning a proportion of the blades (depending on yaw angle and RPM) will be travelling fast enough to be unsuppressed by most radar stationary clutter filters. Hence, unless these returns are below the radar threshold then the turbine will appear as a target on the radar PPI display.

2.1.2.8 The RCS of a turbine rotor changes rapidly as the blades rotate, and also vary as the turbine yaws and the blades pitch. From the data collected in this work on a number of blade designs (see section 7.5 for details) it is clear that, during a single revolution of the rotor, for any yaw angle a large RCS will be seen at some point. Shaping to control the RCS is only effective over a limited region of aspects. The same energy is being reflected but if we can concentrate it into a small number of directions this will leave regions where there is little backscatter of energy. As the blades will present most aspects to the radar at some point in time, shaping will have little effect on minimising the rotor RCS over any significant time period. The only real answer is to try and absorb some energy through the use of materials.

2.1.2.9 Material. A study proposal from QinetiQ is under consideration by the DTI to investigate the radar reflectivity of different wind turbine materials and if carried out will more fully address this issue in due course.

2.1.2.10 However, it is safe to say that the materials used in the manufacture of a wind turbine will affect the wind turbine's RCS value. In particular, metals and other electrically conducting materials, such as carbon fibre, are reflective to radar and, therefore, will contribute to increasing the RCS signature. Where the material used has semitransparent properties (such as wood or glassfibre) to radar, the internal structure of the wind turbine may need to be considered.

2.1.2.11 Operation (Yaw). The wind turbine RCS varies with the Yaw i.e. with the relative orientation of the wind turbine and the radar.

2.1.2.12 The components of the turbine that are a function of yaw are the nacelle and the rotor. As already discussed the nacelle RCS is minimised at ±45° and ±135° yaw angles, but as this is likely to be suppressed by radar filters, it is not the key source of scattering as seen by the radar. So are there any preferable yaw angles for minimising the effect from the turbine rotor blades? We must take account of the stationary clutter filter which will affect how the rotor appears to the radar as the yaw is varied. As the yaw moter moves the rotor axis closer to facing the radar the relative speed of the blades towards and away from the radar decreases and so the radar return from a greater proportion of the blades length is suppressed by the radar filters. The maximum speed of the blades in the direction of the radar, and hence the least suppression of the blade RCS, occurs when the rotor is facing 90° from the radar.

2.1.2.13 From our analysis we see that that from yaw angles around 0° and 180° (i.e. when the turbine is facing towards or away from the radar) the RCS of the blades are consistently high (around 100 to 1000m^2) throughout a complete rotation (see section 7.5 for details). This means that whenever the radar looks at the turbine there is a high probability of seeing a large signal and detecting the turbine. But this does not take account of the radar filters which will be more effective at this yaw angle. The filter is likely to suppress a large amount of the turbine return leaving just a small signal (i.e. a small region of PPI clutter) that is just detectable but with a high probability of detection. At the other

extreme when the rotor is facing 90° from the radar (yaw of ±90°) the RCS of the turbine blades are very variable. When a blade edge is vertical (blade pointing up or down) a very large RCS is seen which is as large if not larger than the blade face return. But this only occurs for a short time during the blade rotation and for the rest of the time the RCS is low (below $1m^2$). Also as the blades are moving in the direction of the radar beam the radar filter will not suppress much of the returning energy for a vertical blade. This gives rise to a situation where the turbine will go undetected unless a vertical blade is observed, and if one is seen the resulting clutter on the PPI screen is large. The time periods in a turbine's rotation when the RCS is high are short, and the probability of detection low, but when seen the resulting clutter will be large.

2.1.2.14 Blade Pitch. If a turbine has pitching blades then the effect of this pitching angle results in an adjustment to the yaw angle at which the situations described above occur. If the blades are pitched back by x degrees then the large RCS seen close to 0° and 180° yaw due to the blade faces will now occur at x° and 180+x°. Large pitch angles can create larger clutter problems by moving the large RCS seen, when looking at the front or the rear face of the blades, to a yaw angle where the radar filter is less effective (see section 7.5 for details).

2.1.2.15 Blade Numbers. Whilst the current wind turbine is tending towards three-bladed systems, other blade configurations are feasible, the effects of which may be to vary the RCS. This requires further investigation although it should be noted that the model described within this report can manage any blade configuration that the manufacturer's may wish to consider.

2.1.2.16 Rotation Speed. The rotational speed and the diameter of the turbine rotor determine the velocity at the tip of the rotor. For a radar filter to suppress the whole blade, the tip speed of the blade in the direction of the radar must be less than the speed at which the radar filter passes incoming radar returns unsuppressed. For a typical filter the suppression becomes less effective at around 50kph.

2.1.2.17 Lower rotational speeds for a given rotor diameter would allow more suppression to occur, but given that typical rotor RPM are between 15 and 25, giving rise to tip speeds in excess of 160kph, high suppression over a wide range of yaw angles would require much slower rotational speeds. For example, a maximum tip speed of 50kph for a 60m rotor would limit the RPM to 4.5. Small reductions in rotational speed will have little effect on the radar impact.

2.1.3 Wind farm

2.1.3.1 Range. Current procedures have put a lot of emphasis on the range of the wind farm from the radar. This has led to an impression that the further from the radar the farm is placed the smaller the interference. The situation is not that simple. A greater range is only better because it will increase the chances of intervening terrain and the earth's curvature obscuring the radar LoS to the turbines. Due to the magnitude of scattering from a wind turbine, if the wind farm is within the operating range of the radar and LoS exists then the radar will receive clutter signals from the turbines.

2.1.3.2 Layout Spacing. Spacing of wind turbines within a wind farm is typically of the order of a few hundreds of metres. The resolution of the radar in cross range is a function of the distance between the radar and the wind farm and the radar beam width. The downrange

resolution is dependant on the pulse width of the radar involved and is typically in the range of 50-300 metres.

2.1.3.3 If the spacing between the towers of the wind farm were smaller or equal to the cross range and down range resolutions, then tracking of aircraft over the wind farm would be very difficult. This is because radar will not resolve two targets that are within the resolution of the radar and will just appear as one large target. Conversely, if the wind turbines were several resolution cells apart, then there is resolvable space between the turbines and a potential to see the crossing aircraft amongst the turbine returns.

2.1.3.4 Layout Geometry. It has yet to be established which wind farm layout is more acceptable and more research is needed to determine the optimal arrangement as far as radar operators are concerned. However the following statements can be made regarding how various layout arrangements will appear to any radar system.

2.1.3.5 A grid layout will display as a regular pattern on the radar. This may prove easier for the radar operator to identify on the display.

2.1.3.6 A line of wind turbines running parallel to the radar's boresight will tend to produce a deeper but narrow radar shadow due to the cumulative blocking effect of the line of wind turbines. A line of wind turbines that is offset at an angle to the radar's boresight will tend to produce a wider but less deep radar shadow as the angle increases. A line of wind turbines perpendicular to the radar's boresight will produce minimal radar shadow. A random layout, which in reality is more likely, will produce a combination of the above effects. Which of these layouts is best will depend on what the radar coverage requirements are at low level behind the wind farm.

2.1.3.7 In a circumstance where a single wind turbine in clear LoS to the radar is undetected then, assuming sufficiently wide spacing of wind turbines in wind farm, it is highly likely that a wind farm of similar wind turbines would also be undetectable.

2.1.4 Terrain

2.1.4.1 Line of Sight between Radar and wind farm. As radar operate on a Line of Sight (LOS) basis, it is obvious that direct LOS between wind farm and radar should be avoided wherever possible i.e. by using the intervening terrain to mask the wind farm from the radar. If there is a LOS and the radar is working effectively then any wind turbine will cause radar clutter.

2.1.4.2 Over the horizon effects. Wind farms can create a detectable radar return even when not in direct LoS of the radar. This is due to diffraction over the intervening ground between the radar and wind farm. The level of detectability of the wind farm is dependant on frequency of radar and the distance from the wind farm to the point of diffraction and the distance below the LoS horizon where the wind farm is located.

2.1.4.3 Effect of wind turbine/wind farm on more distant objects. The diffraction effects mentioned above, and the design of wind turbines, mean that wind turbines individually create 'radar shadows'. Any shadow that does exist behind wind turbine decreases in intensity with distance (e.g.) for a 3GHz radar, the shadow extends hundreds of metres behind a typical wind turbine (see Annex B.5).

2.1.5 Radar

2.1.5.1 Frequency. Frequency of radar systems varies but is generally in one of three bands: 10GHz (3cm wavelength), 3GHz (10cm) and 1GHz (30cm). Higher frequency radar provides greater resolution i.e. the individual radar tracks are smaller and easier to differentiate. Hence for those radar with the highest frequencies, there is a smaller chance of both an aircraft and a wind turbine being in the same radar resolution cell causing track merge.

2.1.5.2 Track Filtering. All radar contain filtering systems that are designed to extract out information that is of use for the particular radar purpose and to reject all other information (perceived as clutter). As already discussed above, operating wind turbines exhibit many of the characteristics associated with aircraft i.e. relatively large RCS with a strong Doppler shift. As current generation radar systems are not designed for the removal, by filtering, of clutter from wind turbines, we have a situation where wind turbines can cause clutter and false tracks on radar displays.

This page is intentionally blank

3 COMPUTER MODEL DEVELOPMENT

3.1 Benefits of the model

3.1.1 The benefit of this model is to allow the effects of any particular wind farm on a particular radar to be accurately predicted. This can assist in the production of the regulatory guidelines by highlighting the important parameters and allowing these parameters to be quickly modified and the effect on the radar observed.

3.2 Model philosophy

3.2.1 The purpose of this model is to investigate in detail what the effects of radar echoes received by radar from a wind turbine are, and to study the effects of the radar signal processing on these highly variable echoes. This will give an understanding of the circumstances under which a turbine is visible to radar and when it is not visible. It also enables the examination of proposed means to distinguish wind turbine echoes from other echoes, and then if possible prevent them from obscuring wanted targets on the radar operator's display.

3.2.2 The basic idea of the computation is to study the progress of each radar pulse transmitted during a specified interval of time. During this interval the radar dish rotates, a (wanted) target aircraft moves across the scene, and blades rotate on one or more wind turbines. The magnitude of each received pulse is calculated, taking into account the antenna beam pattern, the propagation from the antenna to the target aircraft and the turbines, and the variable RCS of the aircraft and turbines. These returns are then passed through a simulation of representative radar signal processing, leading to a list of confirmed echo detections. These are then displayed on a plan-position indicator (PPI) display typical of radar displays. A PPI is just a monitor on to which all the radar information is displayed for the operator to interpret.

3.2.3 QinetiQ's software suite for studying and analysing the interactions of wind turbines with the performance of radar systems is known as WHIRL.

3.2.4 The software has been designed in a modular way corresponding to each of the following stages that require simulation. These stages are:

- Radar transmission of a pulse;
- Propagation of pulse over terrain from radar to wind farm;
- Scattering of pulse by wind farm;
- Propagation of pulse over terrain from wind farm to radar;
- Radar receives returning energy pulse;
- Radar signal processing;
- Radar display.

3.2.5 WHIRL itself consists of two parts, and it uses output from two other programs to simulate these processes:

- WHIRL-COM: simulates the radar signal processing;
- WHIRL-DIS: simulates a radar PPI display, using radar echo information output by WHIRL-COM;
- Ocellus: computes the RCS, a measure of the energy scattered by the wind turbines (feeds into WHIRL-COM);
- NEMESIS: computes the propagation factor between the radar and the wind turbines and back to the radar (feeds into WHIRL-COM).

3.2.6 This is described in more detail in the following sections.

3.3 Code structure

3.3.1 Figure 3-1 is a diagram of how all the code modules fit together.

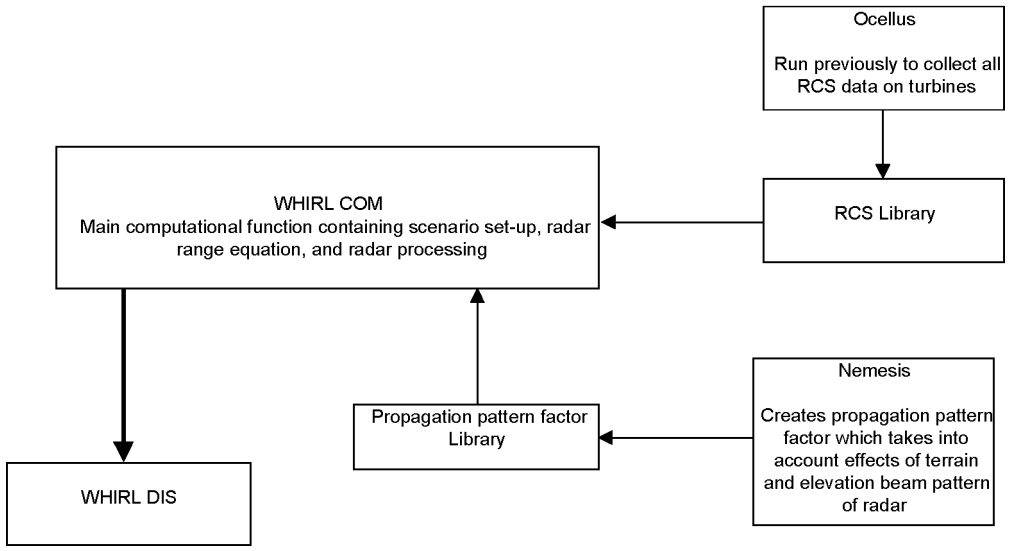

Figure 3-1; Diagram of how the QinetiQ software WHIRL fits together

3.4 Functionality

3.4.1 The functionality of each of the modules is briefly explained here. A more detailed explanation is contained in appendix B.

3.4.2 WHIRL-COM

3.4.2.1 WHIRL-COM performs the computational work of simulating the reflection of radar signals from a target aircraft and one or more turbines, and tracing the echoes through appropriate radar signal processing.

3.4.2.2 WHIRL-COM consists of four main sections:

- Graphical user interface, which allows the user to input data on the scenario to be modelled, and controls the running of the subsequent computation;
- Calculation of the geometry of motion of an aircraft target, and rotation of turbine blades;
- Radar equation calculation, which takes into account the rotation of the radar beam, the propagation factor from radar to aircraft target and turbines, and the RCS as the aircraft target moves and the turbine blades rotate;
- Simulates radar data processing, including pulse integration, moving target indication, and noise-related thresholding. Outputs the confirmed detections for input to WHIRL-DIS.

3.4.2.3 WHIRL-COM can model any number of turbines in any position in the UK (other sites would be possible given the relevant terrain data required). One aircraft target can be flown on a straight track across the display. Its start position, stop position and speed is set by the user. The code is currently set up to model a standard ATC primary radar, but all the radar parameters can be changed to suite different radar operations.

3.4.3 WHIRL-DIS

3.4.3.1 WHIRL-DIS is a program that simulates a radar operator's plan position indicator (PPI) display. It takes in the file from WHIRL-COM containing the accepted radar detections, and displays it in real time on the PPI display. This gives a visual indication of the effects of the various signal processing options.

3.4.3.2 The program was kept separate from WHIRL-COM so that it could be run on a portable computer for demonstration purposes. The separation ensures that WHIRL-DIS can run fast enough to display its output in real time, and is not held up by any time consuming calculations that are done in WHIRL-COM.

3.4.3.3 WHIRL-DIS does processing of its own: it accepts and displays the detections found in its input file. It contains additional thresholding with a user-adjustable range-dependent threshold. This allows the user to see the effect of adjusting the threshold without repeating the WHIRL-COM calculations.

3.4.3.4 When reading` an input file the user can select what threshold to set, and whether the moving target indicator (MTI) filter switch is on or off. Once a simulation is read in to WHIRL-DIS the user has a full range of viewing tools to enable the results to be evaluated. These are:

- Centre the simulation by mouse and keying in;
- Zoom in and out by increments, mouse and keying in;
- Variable display persistence of radar detections;
- Start and stop simulation at will;
- Move back and forth through simulation one second at a time;
- Reset simulation.

3.4.3.5 A comprehensive description of WHIRL DIS is contained in Appendix B.2.

3.4.4 Ocellus: RCS computation

3.4.4.1 QinetiQ's software for the computation of RCS is known as Ocellus. This is used more widely for QinetiQ's RCS prediction work.

3.4.4.2 This code calculates the RCS of the turbines for parameters such as:

- Frequency of radar energy;
- Position of the transmitting and receiving antenna (Do not have to be co-located);
- Distance to target;
- Polarisation of radar energy.

3.4.4.3 It does these calculations using several mathematical methods. Most of the contribution to the turbine's RCS comes from the method of physical optics. When the program detects the presence of a sharp edge, an additional factor is applied to the RCS according to the physical theory of diffraction.

3.4.4.4 In the context of the present study, this program is used to generate a table of RCS values for a particular turbine over a wide variety of parameters. Once complete the resulting table encapsulates all the data for a particular turbine and can be used in WHIRL to investigate many different scenarios.

3.4.5 NEMESIS: propagation calculation

3.4.5.1 NEMESIS is a QinetiQ program for calculating radar propagation factors taking into account the following factors:

- Radar frequency;
- Intervening terrain;
- Radar's elevation beam pattern.

3.4.5.2 This program uses the parabolic equation method, and is used more widely in QinetiQ where propagation calculations are required.

3.5 Model limitations

3.5.1 Currently the model does not include any of the following effects:

- Interactions between individual turbines within a farm;
- Interactions between aircraft targets and the turbines;
- Any shadowing effects caused by the turbines of the aircraft target;

3.5.2 These capabilities can be straightforwardly implemented, although they have not been specifically introduced within this study.

4 RCS PREDICTIONS OF WIND TURBINES

4.1 Reason for RCS predictions

4.1.1 As discussed in the introduction, the RCS is a measure of the energy returned from the turbine to the radar. This is one of the key factors in determining the effects of turbines on radar systems. All objects illuminated by the radar beam will return some energy to the radar receiver. The only way a radar can discriminate between a real target and some other object in the environment is if the RCS of the object is different in some way to that of the real target. So it is clear that without a thorough understanding of the turbines RCS its effect on radar cannot be calculated.

4.2 Input information

4.2.1 In order to predict the RCS of wind turbine we require detailed geometry information so that a computer aided design (CAD) model of the turbine can be created. This is used to generate an input file for the RCS prediction software. Also required are the electrical properties of the construction materials if not made from metal. The turbines we concentrated on were the Vestas V47 (used at the Hare Hill wind farm in south-west Scotland), and the Enercon E-66 (The turbine at Swaffham, Norfolk). The E-66 turbine was to be measured in the field trials and the data used to validate the predictions. We also acquired information on some other blade designs so the sensitivity of the turbine RCS to design change could be investigated.

4.2.2 Three companies were contacted to supply this information, Vestas (UK), Ecotricity (UK arm of Enercon), and NEG Micon Rotors. QinetiQ also took their own measurements of the turbines in order to build up accurate and comprehensive CAD models.

4.3 CAD Creation

4.3.1 All the models were created in a commercially available CAD package (SDRC I-DEAS). All the parts of the turbine are built separately and are then "joined" together to make different turbine configurations.

4.3.2 For details of all the approximations made in generating the CAD models see Appendix A.1. Figure 4-1 and Figure 4-2 show the models made as compared to the real turbines.

4.3.3 Four different CAD models were generated as follows:

- Enercon E66 turbine with a 66m diameter rotor;
- Vestas V47 turbine with a 47m diameter rotor;
- Enercon E66 tower and nacelle with a 80m rotor using NEG Micon blades;
- Vestas V47 tower and nacelle with a 52m rotor using NEG Micon blades.

4.3.4 All these CAD models are descriptions of the turbines' outer surfaces, and no attempt has been made to model the internal structure. The effect of internals on the signature is discussed in more detail in appendix A.4.

Figure 4-1; The CAD model of the Swaffham turbine compared to the real thing.

Figure 4-2; The CAD model of the Hare Hill turbine compared to the real thing. The turbine blade edges only appear serrated due to the resolution of the image.

4.4 Data collected

4.4.1 Far field RCS predictions on all four models described in section 4.3 have been carried out. Each of the turbines has the same predictions completed on it, carried out in the following way.

4.4.2 For each configuration there are three CAD model descriptions. One has a blade pitch of 0° (i.e. the blades are set to catch the maximum wind), one a pitch of 20° (feathered to spill some wind, and 90° (feathered right back to stall the turbine). For each of these pitches data were collected at 1.5GHz and 3GHz, and at 36 yaw angles of the rotor and nacelle (every 10°). At each of these yaw angles data from 2400 positions of the blades were collected to allow simulation of the blade movements in any of the yaw positions. This means over 2 million RCS calculations have been completed. Table 4-1 summarises the turbine set-ups predicted.

No of blade pitches	3	{0°, 20°, and 90°}
No. of frequencies	2	3GHz, 1.5GHz
No. of yaw angles	36	0° to 360° in 10° steps
No. of rotor positions for each yaw	2400	(every 0.05° of rotation)

Table 4-1; Summary of the turbine set-ups predicted on all four turbine configurations.

4.5 Results and analysis

4.5.1 All of the turbine predictions exhibited several basic characteristics. To explain these characteristics the examples of the Enercon turbine at Swaffham (with a blade pitch of 0 degrees, at yaw angles of 0 degrees and 90) degrees is used. The RPM for both of these were set to 12.4 RPM. A more complete set of the predictions from all the turbines can be found in Appendix A.5.

4.5.2 In all cases the yaw angle is specified relative to the direction of the radar. So when the yaw is 0° the radar is pointing along the axis of rotation of the turbine rotor, with the blades in front of the tower when viewed from the radar position. This means the turbine is face on to the radar. When the yaw is 90° the turbine rotation axis is perpendicular to the direction of the radar, i.e. the turbine appears side on to the radar.

4.5.3 We will, firstly, consider the results for the Swaffham turbine at 0 degrees yaw before examining the results for the Swaffham turbine at 90 degrees yaw.

4.5.4 The RCS at 0 degrees yaw is presented in Figure 4-3. It shows a number of features (labelled 1 to 8 on the figure) that can be attributed to the turbine blades. Since we are investigating the RCS with time, from a single yaw angle, any contribution to the RCS from the tower will be constant. There are two very broad peaks. At the top of which, either side of the maxima, are two further peaks. The symmetry between these is apparent and the likely cause of the observed peaks is the turbine blades. The positions in time of these features are summarised in Table 4-2.

Number	Time (secs)	Degrees rotated	Description
0	0.000	0.0	Initial blade positions (not marked)
1	~0.125	~9.3	Small peak
2	~0.850	~63.2	Large peak
3	~0.980	~72.9	Small peak
4	~1.125	~83.7	Large peak
5	~1.750	~130.2	Small peak
6	~2.450	~182.3	Large peak
7	~2.600	~193.4	Small peak
8	~2.740	~203.9	Large peak

Table 4-2; Summary of the main features of the RCS from the Swaffham turbine at 0° yaw

4.5.5 Figure 4-4 details the blade positions at the times indicated in the table above. Position 0 is the turbine configuration at time, $t = 0$. It can be seen that the blade position for the peaks 2 and 6, and, 4 and 8 are the same respectively. Likewise the small peaks observed at 1 and 5, and, 3 and 7 are also the same. The angular spread between all of these is ~120 degrees. This confirms that these small and large peaks are a result of some interaction with the blades.

4.5.6 We can explain the features observed by considering what is happening to the blades as they rotate. It may be noted from Figure 4-4 that the peaks (features 2,4,6 and 8 in Figure 4-3), occur when a blade is just either side of the tower.

4.5.7 As the blades move the returns from the blades combine with the constant returns from the tower and nacelle in different ways. As the returning signals are electromagnetic waves they have a magnitude and a phase (i.e. are phasor quantities). Hence, due to constructive (in-phase) and destructive (out-of-phase) interference between the different parts of the turbine, peaks and troughs arise in the RCS pattern.

4.5.8 Furthermore, the inclinations of the blades' surfaces are always changing due to the changing pitch and rotation of the blades with time. This has the effect of altering the projected area seen by the radar. The RCS of the blades is closely related to the surface area presented to the radar. This, coupled with the interference phenomenon described above, will give rise to maxima and minima in a cyclic fashion. The period of this behaviour should be equal to the angle between the individual blades, i.e. 120 degrees.

4.5.9 We can see from the results that at times the RCS drops to low levels (below -10dBsm). Here the destructive interference between the different parts of the turbine is so good that the RCS return from the turbine is nearly wiped out. This only occurs for very short times and could not be used to control the RCS of a turbine over a significant length of time due to the constant movement of the blades.

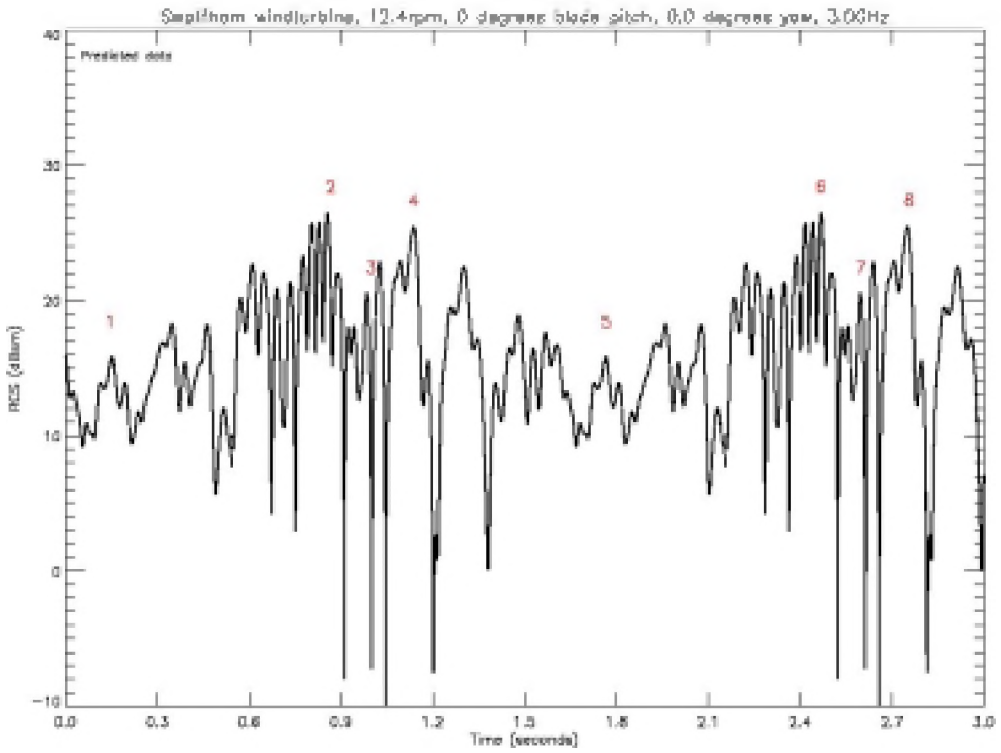

Figure 4-3; The Swaffham turbine RCS versus time at 0° pitch, 0° yaw.

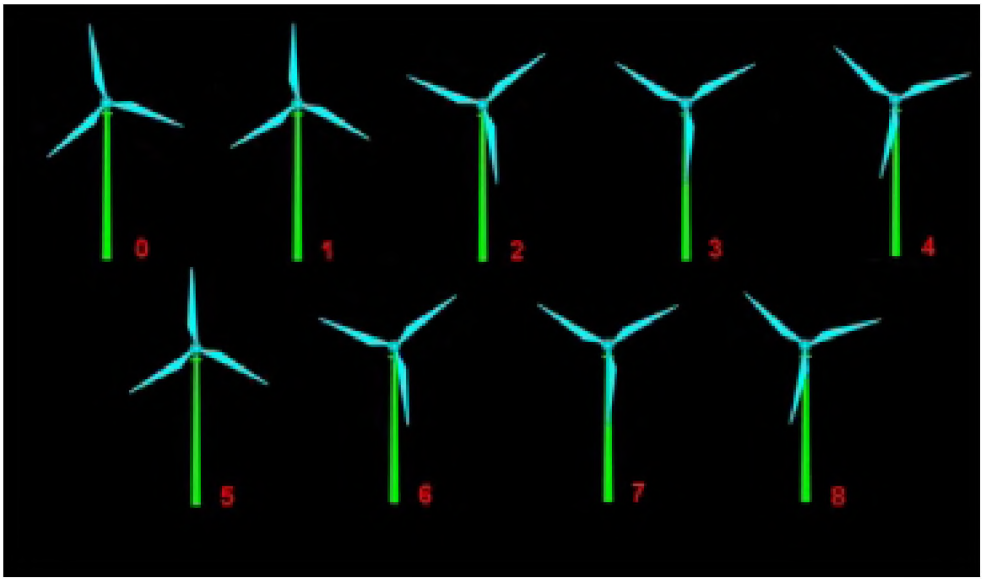

Figure 4-4; The Swaffham turbine rotor positions at 0° pitch , 0° yaw.

4.5.10 This is in fact what is observed in our results. To confirm that the effects seen are from the blades, the zero-Doppler (ZD) components were removed from the data. This process removes all the contributions from the data originating from non-moving parts, i.e. the tower and nacelle. Figure 4-5 presents the data without the ZD components. It can be seen that the same features observed in the complete RCS (Figure 4-3) are present. The difference being that the small peaks at points 1 and 5 are approximately 5 dB lower. When the blade positions at these points are considered (see Figure 4-4) we can see that the small peaks correspond to when the tower is at its most visible. Therefore the reason for the difference in levels is that at this point the RCS is dominated by the returns from the tower, which are removed by the ZD processing.

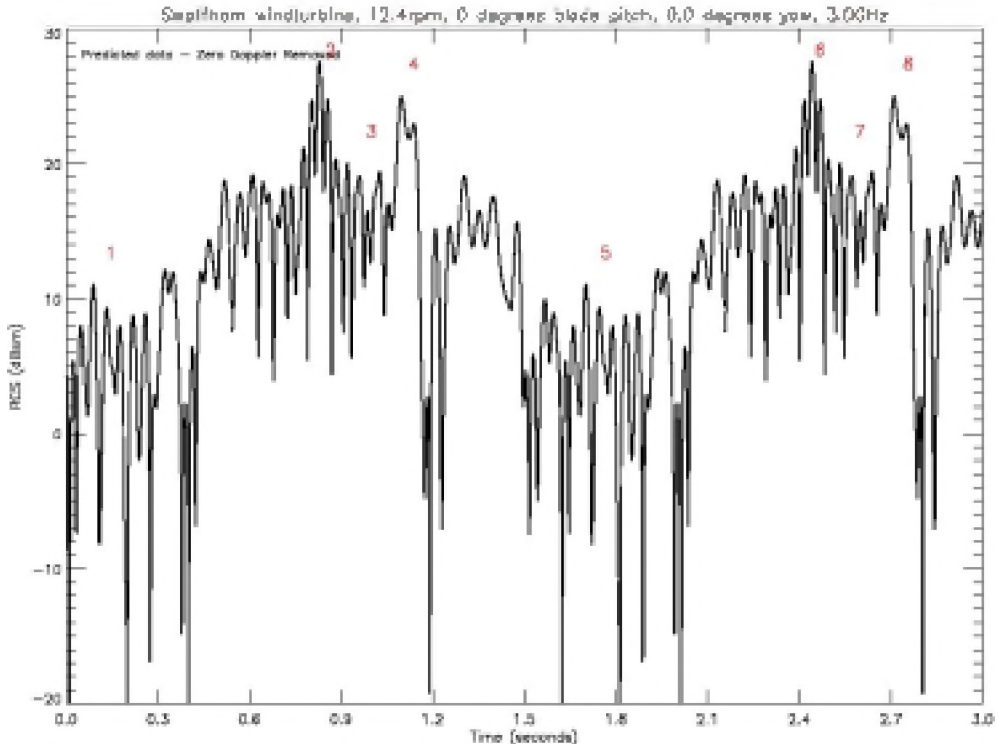

Figure 4-5; The Swaffham turbine RCS versus time at 0° pitch, 0° yaw, with the zero-Doppler component removed.

4.5.11 The RCS at 90 degrees yaw is presented in Figure 4-6. It shows four features (labelled 1 to 4 on the figure) that, as with the 0 degrees yaw case, can be attributed to the turbine blades. The figure shows two very sharp spikes in the RCS (labelled 1 and 3) and two less distinct features between these spikes (labelled 2 and 4). These are summarised in Table 4-3.

4.5.12 The two sharp peaks (1 and 3) can be seen to occur when a blade is pointing vertically downwards, as shown in Figure 4-7. The radar is looking from right to left in terms of the figure. When the blade is positioned as shown then the leading edge is both perpendicular and directed towards the radar. The spike is a result of this leading edge. At this point the return from the blade will be at its highest.

Number	Time (secs)	Degrees rotated	Description
0	0.000	0.0	Initial blade positions (not marked)
1	~0.375	~27.9	Peak
2	~1.150	~85.6	Slight Peak
3	~1.990	~148.1	Peak
4	~2.790	~203.9	Slight Peak

Table 4-3; Summary of the main features of the RCS from the Swaffham turbine at 90° yaw

4.5.13 Based on this we might expect to see some sort of event occurring in the RCS when a blade is pointing directly upwards. This is indeed the case with the very small peaks seen between the large spikes (i.e. 2 and 4). Again, the blade positions are shown in Figure 4-7. The general flatness of the RCS can be attributed to the fact that the profile of the blades when viewed from 90 degrees yaw is very flat and any subtle effects resulting from the blades will be swamped by the return from the tower and nacelle which will dominate.

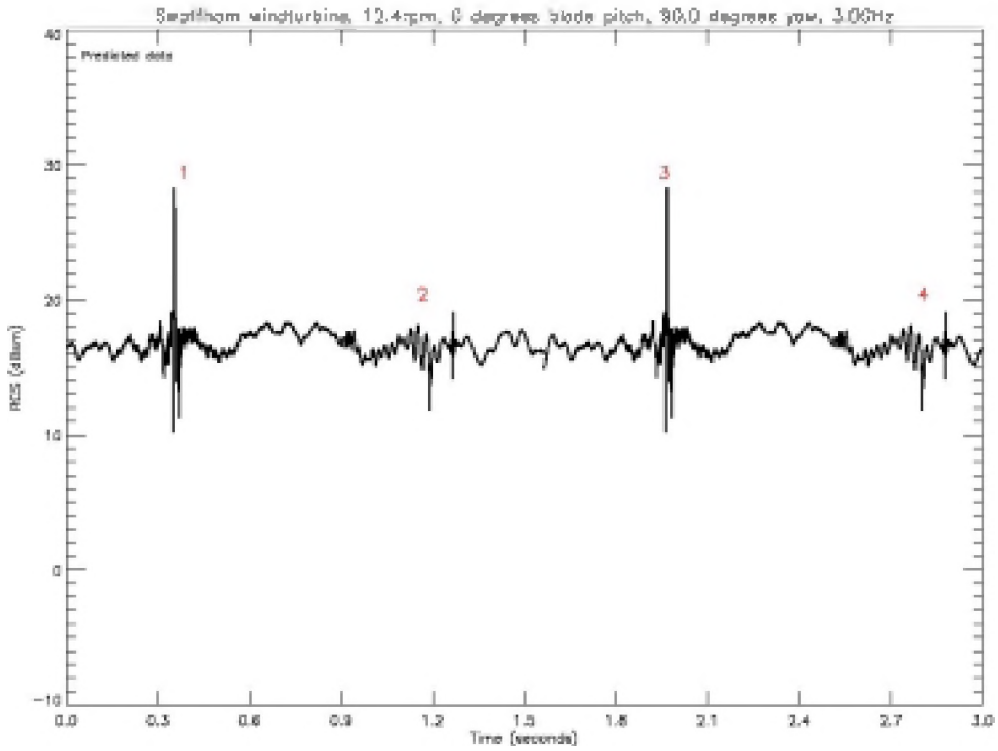

Figure 4-6; The Swaffham turbine RCS versus time at 0° pitch, 90° yaw

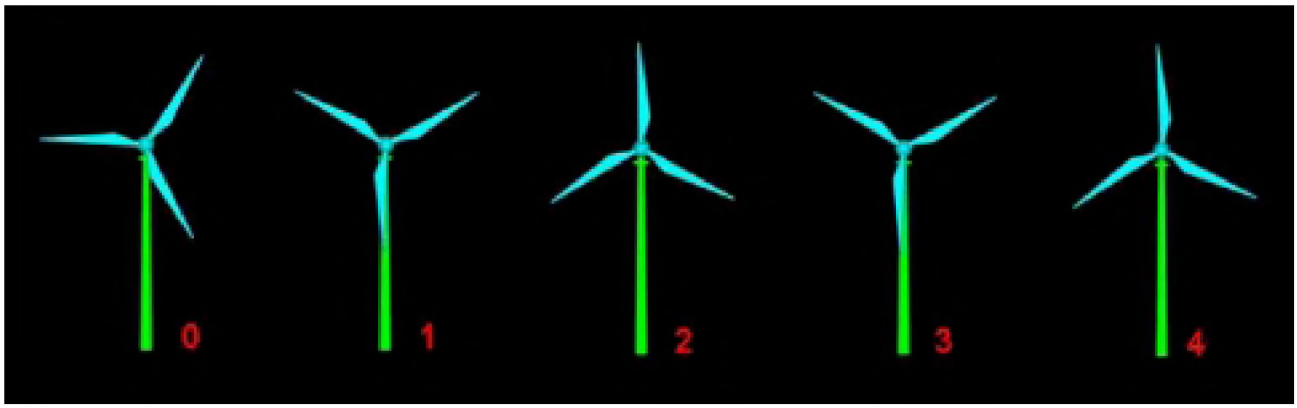

Figure 4-7; The Swaffham turbine rotor positions at 0° pitch, 90° yaw.

4.5.14 The angular "distance" between like features is, in both cases, approximately 120 degrees. This is good evidence that the peaks have originated from the blades. To confirm this we removed the ZD components. The data without the ZD are presented in Figure 4-8. The peaks (2 and 4) between the major spikes are significantly clearer when the ZD is removed. This is a consequence of removing the dominant return of the tower and nacelle.

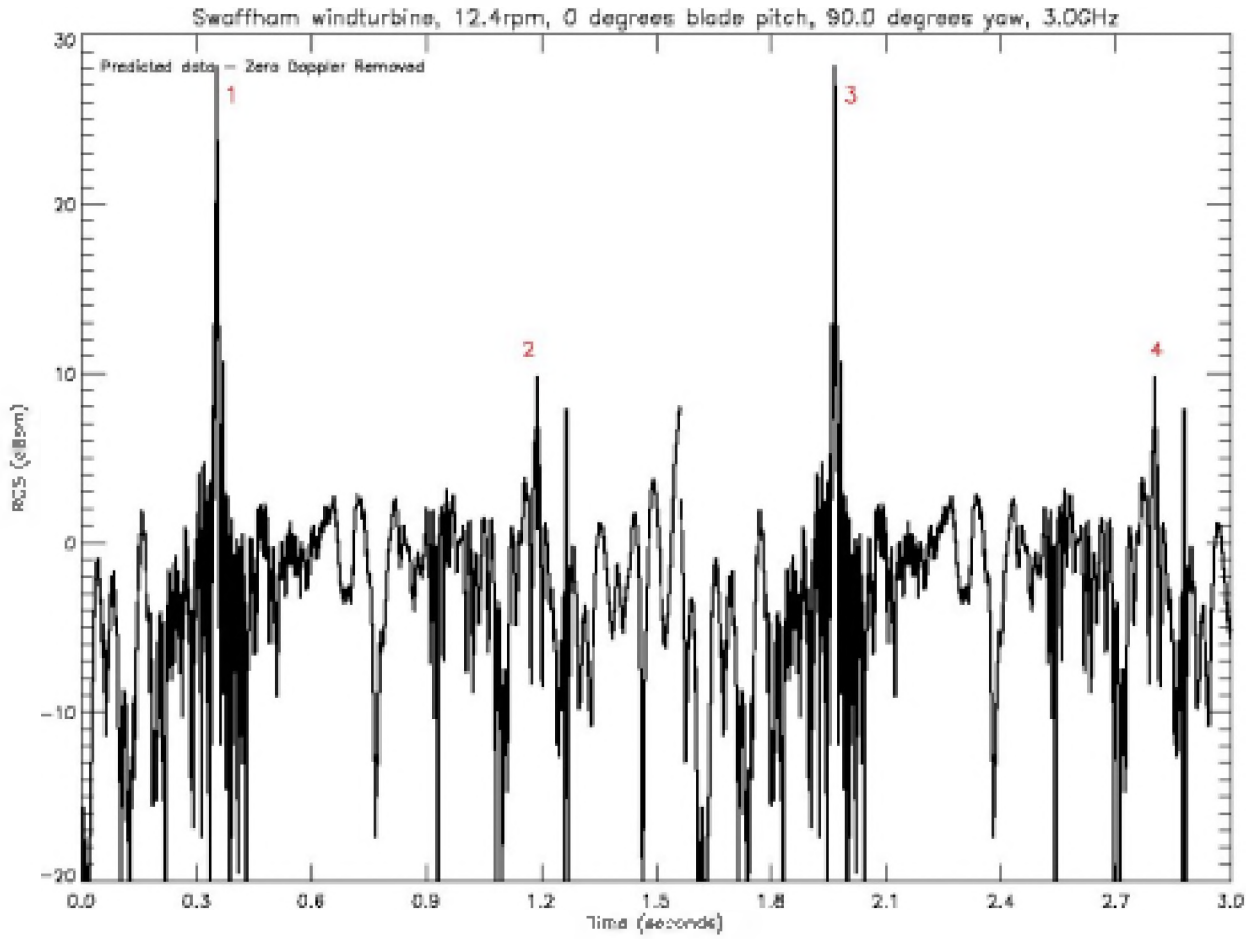

Figure 4-8; The Swaffham turbine RCS versus time at 0° pitch, 90° yaw, with the zero-Doppler component removed.

4.6 Summary

4.6.1 We have explained the various features (peaks and troughs) on the predicted RCS for the Swaffham wind turbine at two yaws (0 degrees and 90 degrees). The blades contribute less when viewed from side-on (90 degrees yaw) than at head-on (0 degrees yaw) in terms of average RCS. However, in both cases the dominant features, such as the peaks in the RCS, are a direct result of the turbine blades.

This page is intentionally blank

5 RADAR MEASUREMENTS

5.1 Scale model measurements

5.1.1 To add confidence and credibility to the RCS prediction process and the results for this project, one of the blade designs supplied by NEG Micon Rotors was made into a 1/15th scale model which was measured in the QinetiQ Compact Antenna Test Range, a RCS measurement facility at QinetiQ Malvern. By creating a 1/15th scale model, measuring it at 15 times the frequency of interest and adding a scaling factor, we get a realistic assessment of the RCS of the full-scale blade. The Compact Range comprises a pulsed radar system which operates in an anechoic environment which provides a low noise measurement background and, therefore, very accurate measurements. By using a parabolic reflector, far field measurements can be performed and thus we can find the absolute RCS of the blade. Figure 5-1 shows the compact range with a business jet under test supported in the test zone.

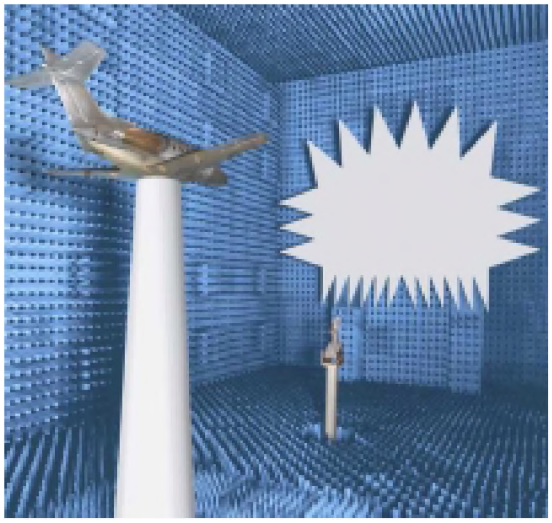

Figure 5-1; Compact Antenna Test Range

5.1.2 The blade was manufactured using a process known as stereolithography, where a resin is cured by a laser, which is controlled by a computer using the CAD representation of the blade. Once this is complete the blade must be coated with a metallic layer so it reflects radar energy. Figure 5-2 shows a photograph of the 1/15th scale blade before surface metallisation. The blade was mounted horizontally and full 360° rotational measurements were made. Measurements of different blade pitch angles were made in order to compare with the predictions for the same blade orientations.

5.1.3 Data were collected on four blade pitch angles: 0°, 10°, 20°, 30°, and 40°. At each of these pitches vertical and horizontal polarisations were collected, at five frequencies: 15GHz, 16GHz, 16.35GHz, 17GHz, and 18GHz. These correspond to full-scale equivalent frequencies of: 1GHz, 1.067GHz, 1.09GHz, 1.13GHz, and 1.2GHz. At 0° pitch the data were collected with an azimuth step of 0.1° giving 3600 data points, and at all other pitches at a step of 0.5° giving 720 points. An example of the data is shown in Figure 5-3. This data set was collected at 15GHz, and has been scaled to what the full-scale blade would give at 1GHz.

Figure 5-2 Non-metallised 15th scale NEG Micon Rotors blade.

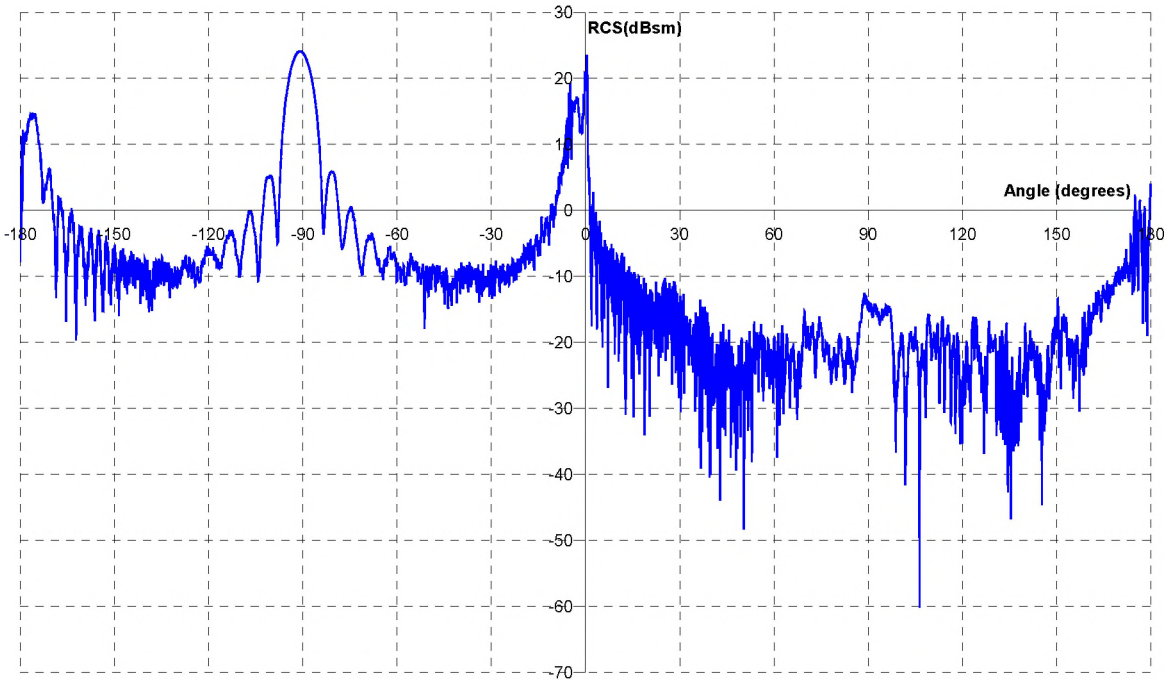

Figure 5-3; RCS of blade at full-scale frequency of 1GHz with blade at 0 degree pitch. Polarisation is vertical.

5.1.4 The leading edge of the blade is presented to the radar at 0°. Here the RCS rises to a maximum of 22dBsm. At 90° the tip of the blade is facing the radar, and the RCS is only -14dBsm. At 180° the trailing edge is facing the radar. This is angled slightly so producing a peak of 14dBsm at -175°. The return at -90° is when the blade root is facing the radar, which could not occur when attached to a turbine hub.

5.2 RCS prediction validation with a scale model blade

5.2.1 The blade was mounted horizontally and full 360° rotational measurements were made. Measurements of different blade pitch angles were made in order to offer comparison with the predictions of the same orientations. A blade was then modelled and a plot of one measurement compared to the prediction is shown in Figure 5-4.

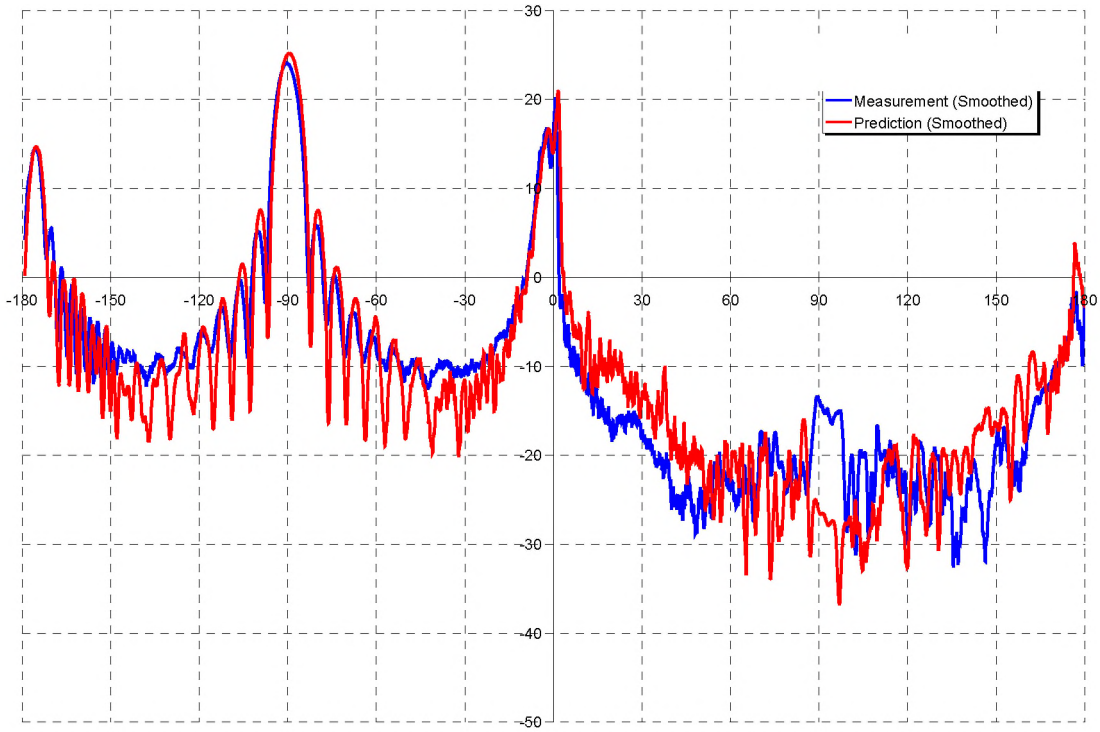

Figure 5-4; Prediction versus measurement. Blade pitch angle is 0°, Full scale frequency = 1GHz

5.2.2 The dark red and blue lines were obtained using a smoothing function in order to see the trends of the returns more easily. Given that the prediction software is only considering the physical optics and not geometrical second order effects, there is very good agreement between the two methods. From these results, we gained confidence that the predictions would give us a very good estimate of the RCS to be expected from a full-scale turbine.

5.3 Trial planning

5.3.1 This task was to specify field trials at two sites where wind farms are known to appear on displays of ATC radar. The specification was to include:

- the monitoring requirements of relevant radar parameters;
- the monitoring requirements of relevant wind installation parameters;
- the monitoring requirements of atmospheric, wind, and other meteorological conditions;
- the data capture and data handling requirements, including the necessary sample rate, and necessary arrangements for correlation of the data from different sources;
- the extent of the trials needed to achieve the purposes of the overall project.

This specification was to be sufficient for any third party to conduct the trials and would supply all the data needed to successfully validate the computer model. The outline trials plan generated from this task can be found in appendix C.

5.3.2 QinetiQ required full-scale radar measurements of wind turbines to provide radar data for validation of the computer model (WHIRL). The plan was to use an instrumentation radar to make radar measurements of a single wind turbine at Swaffham, Norfolk, and to record the information from the Watchman radar sited at Marham Royal Air Force (RAF) base. Also data would be recorded from the primary radar at Prestwick of the twenty-turbine wind farm at Hare Hill, Ayrshire, Scotland. Each site has particular characteristics: the Swaffham site is located about 5nmi from an ATC radar at the RAF airfield at Marham, and, being a single turbine, will form a good experimental 'control', and the Hare Hill site is well-known for the clutter it causes on the ATC PPI radar displays at Prestwick Airport. No instrumentation radar measurements were to take place at Prestwick.

5.3.3 In order to collect the data from the primary radar at Marham and Prestwick QinetiQ sought a contractor who would be able to offer this service. Contact with RAF Strike Command informed QinetiQ that Flight Refuelling Ltd (FRL) was the manufacturer of the RAF's current ATC displays for their Watchman primary airfield radar and also that the company had a display recording system that is used by FRL as a service tool. A visit was made by QinetiQ to FRL to discuss requirements, and to see a demonstration of PPI recording playback. FRL immediately understood the requirement and the demonstration showed that the PPI playback matched our need. The result was that FRL would be sub-contracted for these aspects of the trials.

5.3.4 Exploration of QinetiQ instrumentation radar resources showed that our Multiband Pulsed Radar (MPR), could match the needs of the trials programme. MPR, although classed as a mobile radar, is built into four shipping containers that are permanently attached to two 40 ft-long articulated trailers. MPR presently operates on the 3 GHz frequency of ATC primary radar systems.

5.3.5 Along with collecting the radar data the MPR also logs the current weather conditions, against time so that this information can be linked to the measurement. It also collects video footage of the wind turbine when it collects radar data, so that visual checks of the current state of the turbine can be made.

5.3.6 Another important part of the trial is the collection of data from the turbine. This must be logged against time so that the radar measurements and the turbine data can be linked together. We planned to collect the data direct from the turbines' control systems using a PC.

5.4 Swaffham trial

5.4.1 The Swaffham trial took place from 1 July 2002 to 5 July 2002, and was successfully completed.

5.4.2 The QinetiQ MPR was stationed at Swaffham Raceway, 3.45km from the Ecotricity wind turbine (see Figure 5-5). Radar observations of the turbine were made at regular intervals over a period of five days, during which a variety of weather conditions were experienced. Views of the turbine varied by more than 180° in yaw angle, with more than

half of the aspects being seen during both wet and dry conditions (see Figure 5-6). In total, nearly 250 RCS measurements of the turbine were recorded, lasting between one and two minutes each. These data are split roughly half-and-half between linear horizontal and linear vertical polarisations, and can be calibrated for absolute RCS using sphere measurements made at the site.

Figure 5-5; The MPR radar on site at Swaffham, with the wind turbine visible in the distance.

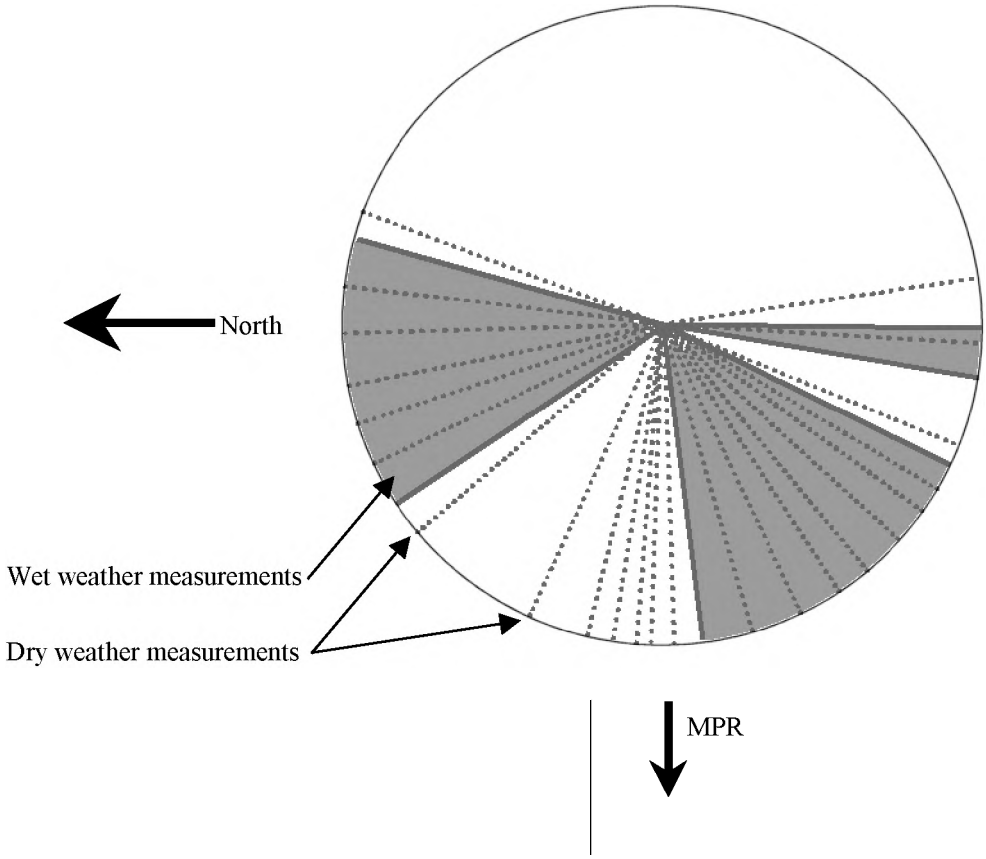

Figure 5-6: Rough sketch showing turbine heading during measurements. Dotted lines for dry measurements, shaded areas for wet-weather measurements

5.4.3 Output from the radar at RAF Marham was also successfully collected by FRL. This was later analysed at QinetiQ using kit supplied by FRL.

5.4.4 The data from the turbine control system were also collected without problems, largely thanks to the help and assistance of Ecotricity, the turbine operators. They supplied a PC that was hooked up to the turbine supervisory control and data acquisition (SCADA) system to record all the turbine settings every 3 seconds for the duration of the trial. Data collected from the turbine were rotor revolutions per minute (RPM), pitch of each blade, and yaw angle of the turbine. What this data set lacked was a means to identify where the blades were in their rotation cycle at any given time. To do this QinetiQ developed a sensor (see appendix D.4 for details) to record this from within the nacelle. This worked well in lab testing, but in the nacelle of the turbines it suffered problems from electromagnetic interference and vibration. Data lost due to these problems were interpolated and correlated to the turbine blade positions from the recorded RCS data, and from the MPR video footage.

5.5 Swaffham results

5.5.1 To give an example of the results collected from the MPR trial, a typical data set is examined. All the main scattering features of the turbine are identified. More results are contained in Appendix D.5.

5.5.2 To give a sense of scale to these results Figure 5-7 shows a range of RCS values and where different objects lie on this scale. This shows why wind turbines are easily detected by radar as their scattering magnitude puts then up with some of the largest aircraft targets. Any operating ATC radar must be sensitive enough to see the small aircraft, which tend to have RCS of about $1m^2$ to $10m^2$, where as the turbine return is up to $1000m^2$ in some instances.

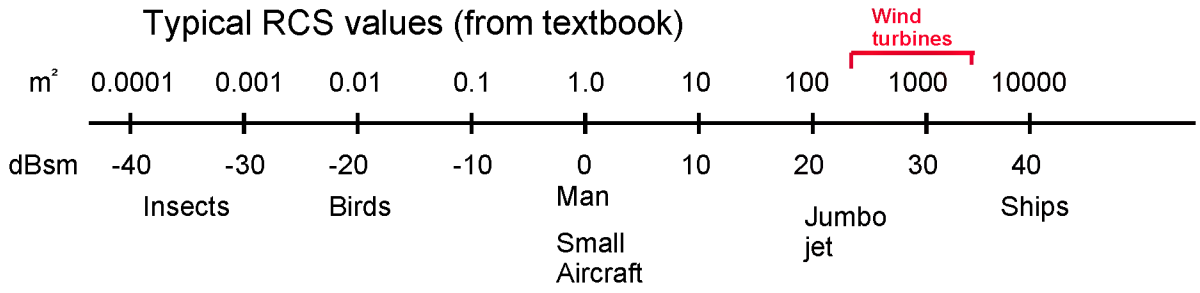

Figure 5-7; RCS scale showing the relative scattering magnitudes of different objects.

5.5.3 A set of data was identified during which the turbine was rotating at almost constant maximum speed (23 RPM). Using the video footage recorded by the radar, times were deduced for the start and end of three full rotations, so that RCS data could be extracted for just this period (16:25:00.02 to 16:25:08.00, 1/7/2002). The calibrated RCS and spectra for the first revolution are shown in Figure 5-8 and Figure 5-9. Doppler spectra for the whole period are shown in Figure 5-10.

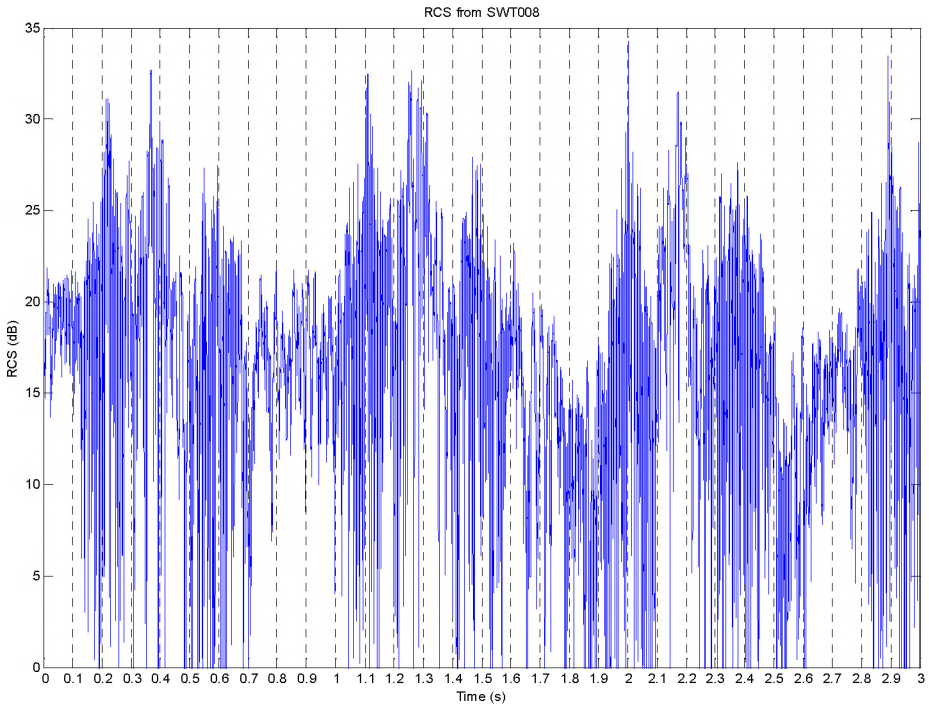

Figure 5-8; Calibrated RCS for (just over) one full revolution

5.5.4 Frame-by-frame analysis of the video allowed approximate timings to be deduced for the occasions when a blade was either vertical or horizontal with respect to the radar line of sight. These blade positions correspond to expected maxima and minima of the RCS for a single blade, and hence might be expected to give rise to peaks and troughs in the overall turbine RCS pattern. The times for these events are listed in Figure 5-11. Comparison with the peak positions in the RCS plot, Figure 5-8, shows a fair correlation between the video timings and the locations of peak RCS levels.

5.5.5 Considering Figure 5-8, it can be seen that there are three repetitions of approximately the same RCS variation during a single revolution, giving nine RCS peaks. Since there are three turbine blades, spaced at 120°, we expect to see 6 'flashes' as each blade passes through the vertical, above and below the hub. It is proposed that the three additional RCS peaks correspond to dihedral scattering, occurring half-way between the vertical flashes as incident radar energy is reflected from one blade onto the other before returning to the receiver. This scattering may be at a maximum when the blade furthest from the radar is horizontal, so that the radar is looking along the axis of the dihedral formed by the other two blades.

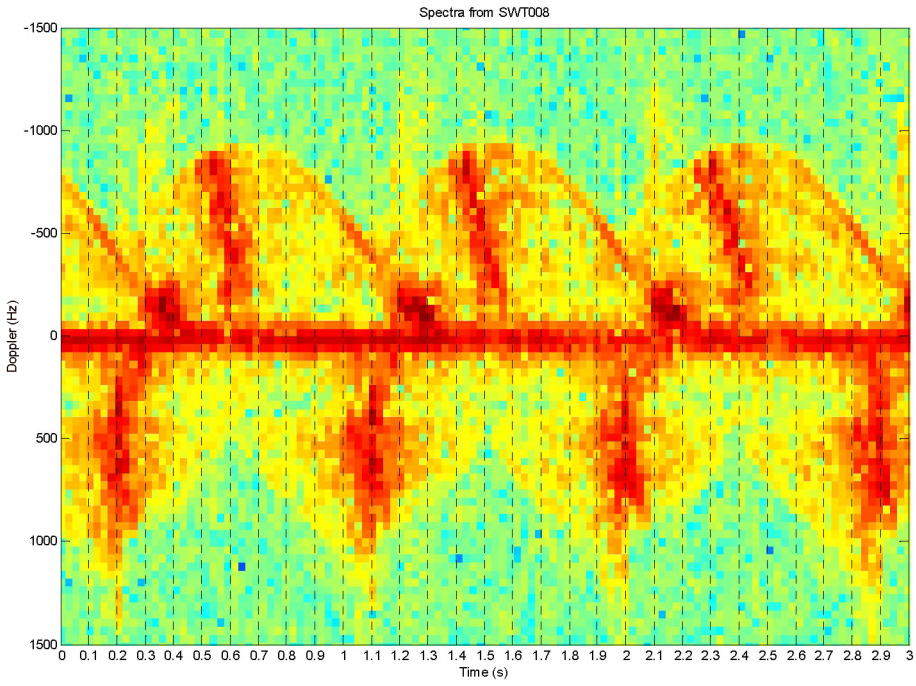

Figure 5-9; Doppler spectra versus time corresponding to the RCS plot

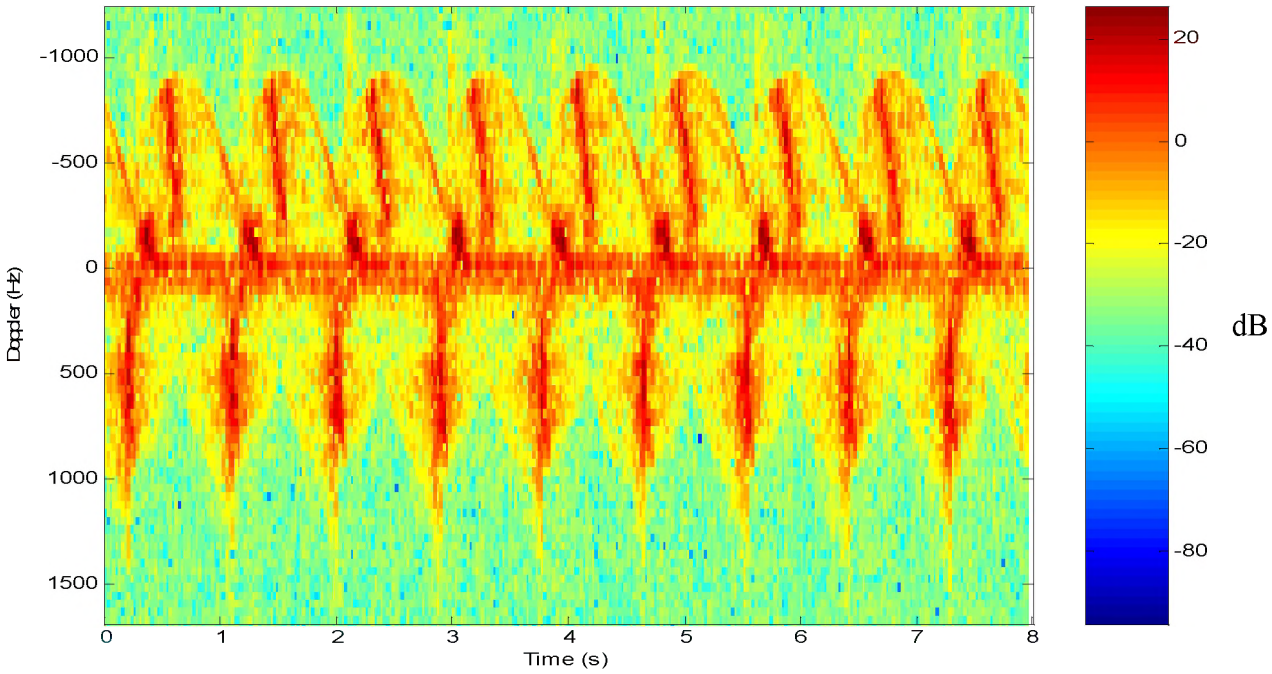

Figure 5-10; Spectrum against time for three full revolutions

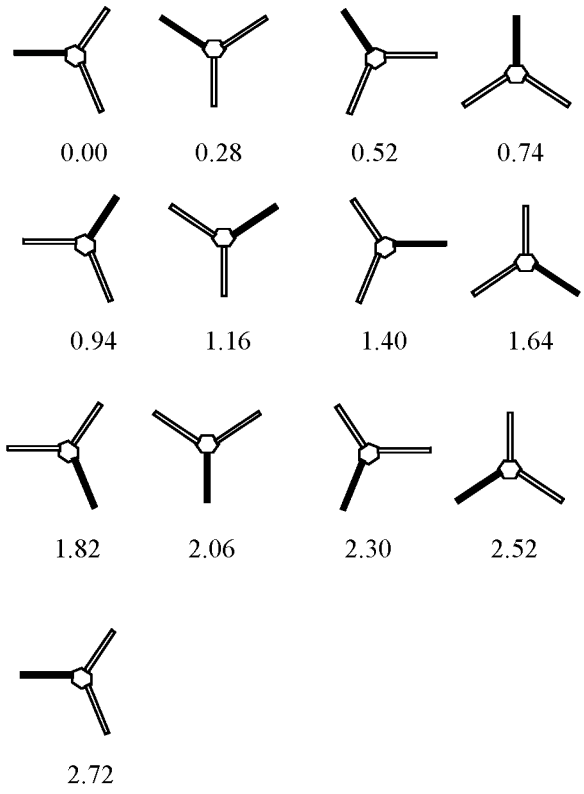

Figure 5-11; Approximate timings of blade positions (in seconds), taken from video

5.5.6 So at this point the blades are in the position shown in Figure 5-11, at 0.52 seconds, with the radar looking from the left of the page and the rotor turning clockwise. We will define blade 1 as the horizontal blade, blade 2 as the lower blade and blade 3 as the upper blade. As the blades continue to rotate blade 3 will approach vertical, where the blade tip's velocity vector is pointing directly away from the radar, hence negative Doppler frequencies are observed. The Doppler frequency generated by blade 2 is decreasing as the blade approaches horizontal, and is overtaken by the Doppler contribution from the approaching blade 1. When blade 1 reaches vertical (1.16 seconds in Figure 5-11), we get a maximum positive value in the Doppler frequency as now blade 3 has a velocity vector pointing directly towards the radar.

5.5.7 The spectrum from the vertical blade has a curved maximum region (dark red in the figures), which starts just before the blade reaches vertical and rapidly moves towards zero Doppler. This can be interpreted as a strong return moving from the blade tip down towards the root of the blade, and could be from the front or back edge, depending on the blade curvature.

5.6 Wind farm trial

5.6.1 A trial using the wind farm known as Hare Hill in Scotland was due to be completed to collect data from a wind farm with several wind turbines in site of a radar at Prestwick airport. Unfortunately the data available from the turbines was not suitable for the trial and budgetary constraints meant adding instrumentation to provide this data was not possible.

5.6.2 However some video of the PPI display at Prestwick was collected and this has been used for validation in section 6.5.5.

6 VALIDATION OF THE COMPUTER MODEL

6.1 Validation philosophy

6.1.1 To validate the WHIRL-COM model using the data collected at Marham, we have broken the process down in to three separate areas for which we wish to make comparisons against the real measurement data. This comes from the requirement to validate not only WHIRL but also the two data libraries it requires. This means we needed to validate not just against the output of WHIRL but also the input libraries that the code runs from. These two libraries contain the RCS data for the turbines used in the simulation and the propagation data for the particular radar in question. Both of these libraries were validated using the output from the MPR data collected at Marham. Once these libraries were shown to be correct we then validated the WHIRL software with the PPI data collected from the Watchman at RAF Marham.

6.1.2 The prediction data were collected sometime before the trial took place and hence a perfect match in the set up of the measured and the predicted scenarios was not possible. Nevertheless, the differences are small and should not greatly influence the results.

6.2 RCS validation

6.2.1 Overview

6.2.1.1 In order to validate the RCS predictions it was necessary to compare them with measurement data taken from equivalent turbine configurations.

6.2.1.2 We have measurement data from the Swaffham trial for a number of different scenarios (see section 5.4). The measurement configurations used in our comparison are summarised in Table 6-1.

Data set	Yaw (degs)	Pitch (degs)	Average RPM	Frequency (GHz)
1	0.4	0.96	12.4	3.05
2	100.33	0.99	12.5	3.05
3	39	0.99	20.6	3.05
4	0	0	10.7	3.05
5	50	5	22.5	3.05
6	100	0	13.6	3.05

Table 6-1; Summary of the measurement configurations used in the RCS validation

6.2.1.3 It should be noted that the turbine orientation of our prediction data does not exactly match those of the measurements. A comparison of the predicted orientations and the measured are summarised in Table 6-2. The differences are all very small and likely differences in the RCS will be small enough to allow effective comparisons. Also the measurement data refer to average or estimated values of yaw, blade pitch and RPM. We will be referring to the orientation of our modelled turbine throughout the following subsection.

Measured			Predicted		
Yaw (degs)	Blade Pitch (degs)	RPM	Yaw (degs)	Blade Pitch (degs)	RPM
0.4	0.96	12.4	0	0	12.4
100.33	0.99	12.5	100	0	12.5
39	0.99	20.6	40	0	20.6
0	0	10.7	0	0	10.7
50	5	22.5	50	5	22.5
100	0	13.6	100	0	13.6

Table 6-2, Summary of the measured and predicted turbine orientations

6.2.2 Swaffham turbine at 0 degrees yaw, 0 degrees pitch

6.2.2.1 The results of the comparison between the measurement and predicted RCS data for the turbine viewed from `head-on' (0 degrees yaw) are presented in Figure 6-1. It can be seen in this figure that the two sets of data match very closely in terms of a general trend and level. The main differences are a number of peaks that are not fully reproduced by the predictions. This is due to two effects; 1) the reflectivity of the blades and 2) a scattering phenomenon known as “multiple bounce” returns. The reflectivity of our blades was an estimate based on the reflectivity of fibreglass, but it appears the blades are more reflective than expected hence, the predictive values are lower than the measured values. The scattering due to multiple bounce returns was not computed as part of the predictions due to the computational overhead involved. Where paths exist back to the radar via two or three bounces from the turbine structure the predictions will be lower than the measurements. This is discussed more fully in the conclusions to this section.

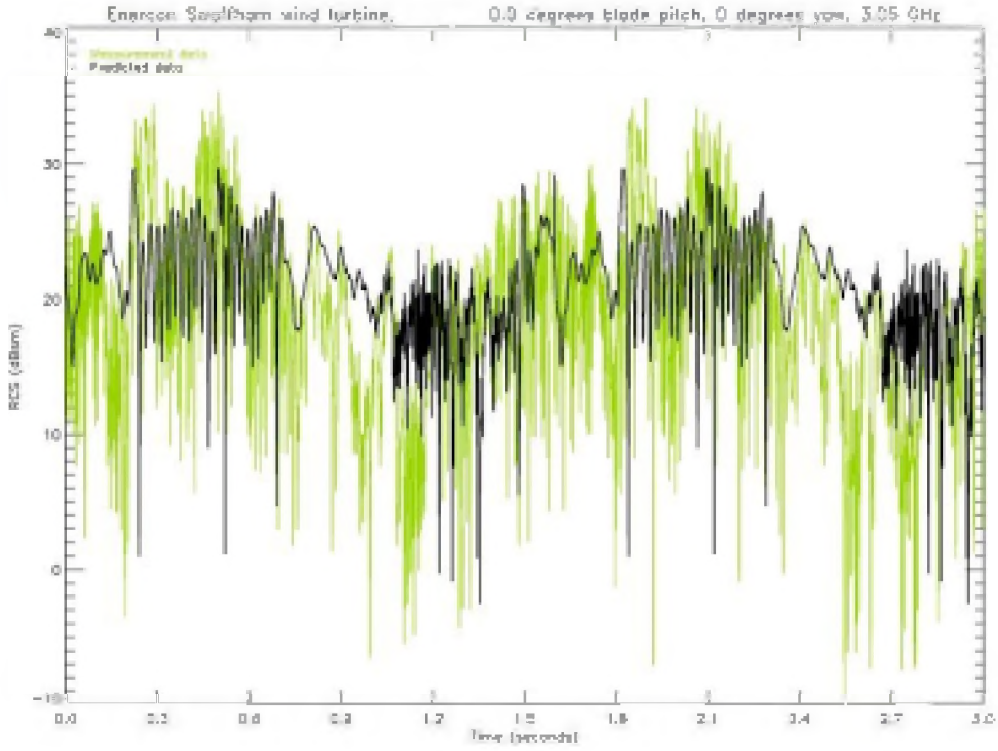

Figure 6-1; Comparison of the measured and predicted Swaffham turbine RCS versus time at 0° pitch, 0° yaw, 12.4RPM.

6.2.3 Swaffham turbine at 100 degrees yaw, 0 degrees pitch

6.2.3.1 At 100 degrees yaw we find that the measured and predicted RCS values are very close. The comparisons between the two data sets are presented in Figure 6-2. Here the mean RCS levels are within 2 to 3dB of each other and a very good match has been demonstrated. This indicates that the multiple bounce paths back to the radar are not significant at this yaw angle.

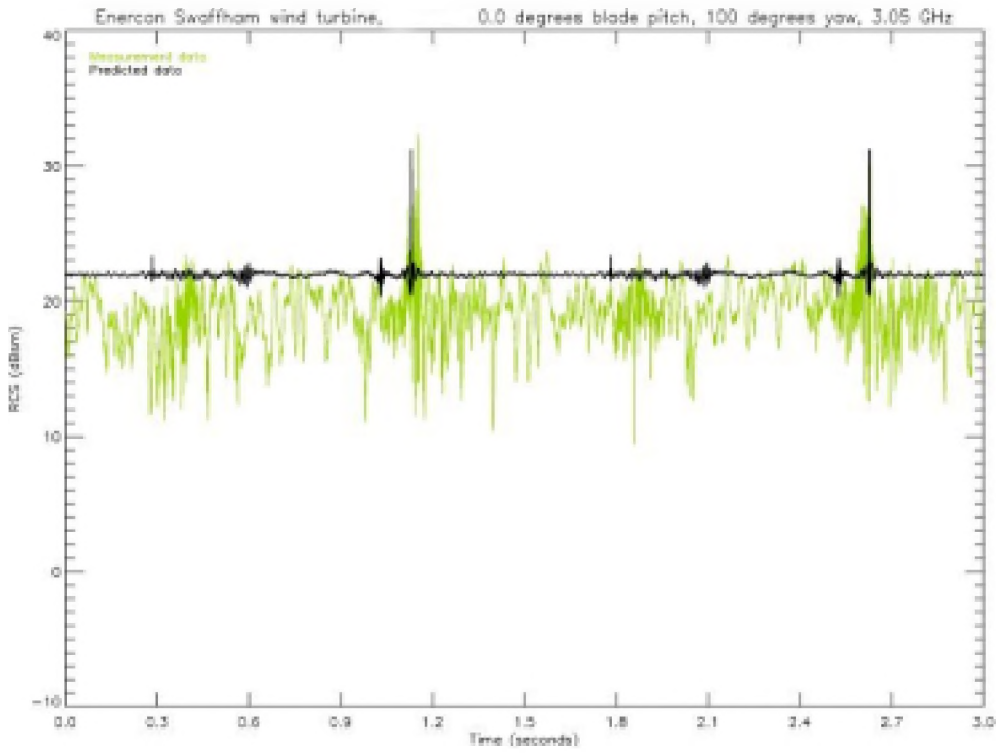

Figure 6-2; Comparison of the measured and predicted Swaffham turbine RCS versus time at 0° pitch, 100° yaw, 12.4RPM.

6.2.4 Swaffham turbine at 50 degrees yaw, 0 degrees pitch

6.2.4.1 In Figure 6-3 the comparison between the measured and predicted data is presented for the turbine at 50 degrees yaw. Overall the agreement is good with all the main features replicated by the predictions.

6.2.4.2 Away from the blade flashes the prediction data are higher than the measurements by around 5dB, and as with the 0° yaw data the peaks in the predictions are down on the measurement equivalent by around 4dB. These differences can be accounted for, as previously, by a lack of multiple bounce data in the predictions and differences in the blade reflectivity. The reason for the predictions being 5dB higher than the measurements away from the peaks is to do with the model of the nacelle used. In the predictions the nacelle is a perfectly smooth object and so produces a strong specula return at yaw angles near 40 to 50°. This effect in the measurements is smaller because the nacelle curvature is not as consistent and this causes the scattering to be incoherent. These differences are not critical in the modelling of the turbine response and the level of accuracy is sufficient.

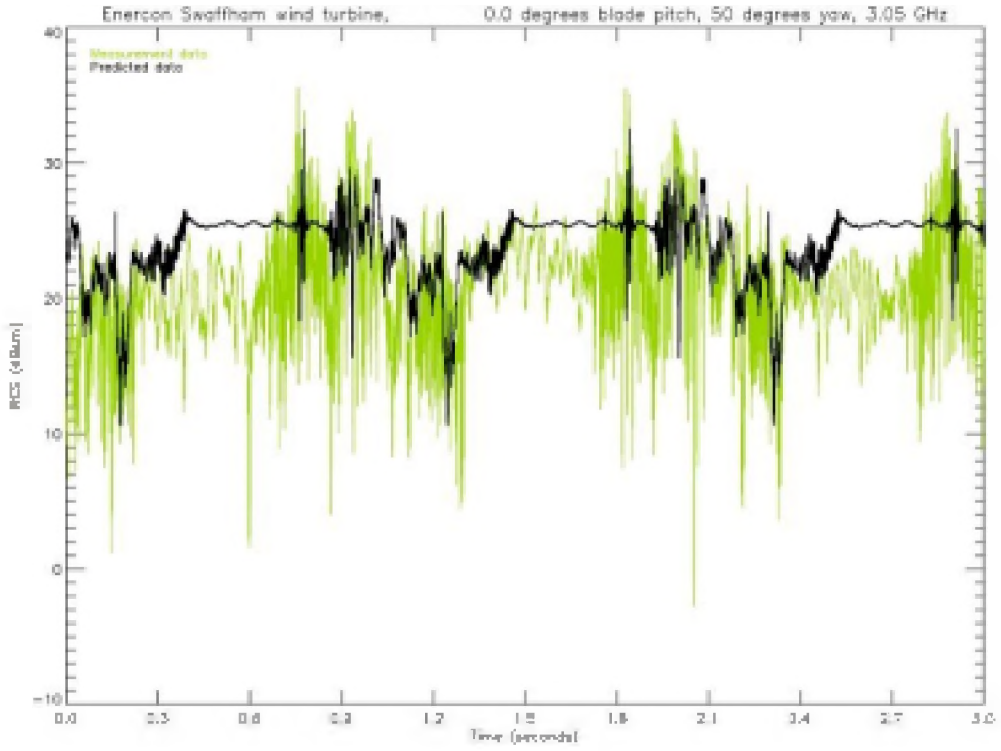

Figure 6-3; Comparison of the measured and predicted Swaffham turbine RCS versus time at 0° pitch, 50° yaw, 20.6RPM.

6.2.5 Swaffham turbine at 0 degrees yaw, 0 degrees pitch

6.2.5.1 In Figure 6-4 the radar is incident at 0 degrees yaw. The comparison between the measured and predicted trend is relatively good, apart from the peaks, which are lower by around 5dB. The reasons for these differences are, as stated previously, multiple bounce and blade reflectivity

6.2.5.2 Comparing this graph with Figure 6-1 shows the consistency of the measurement data collected. These graphs are of the same yaw angle position but were collected at different times during the trial period and show the very similar levels and features. This provides confidence in the results showing that random errors introduced by the measurement are not significant.

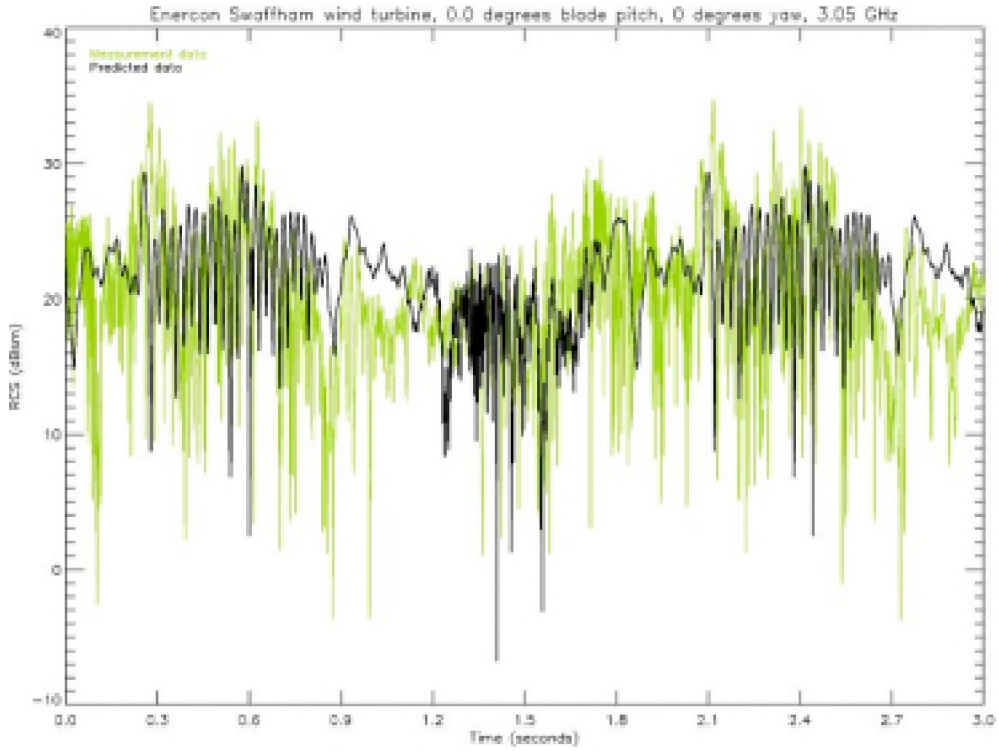

Figure 6-4; Enercon turbine at Swaffham, 0 degs pitch, 0 degs yaw, 10.7RPM.

6.2.6 Swaffham turbine at 50 degrees yaw, 5 degrees pitch

6.2.6.1 In Figure 6-5 we can see the prediction data compared with the measurement data for the turbine when the blade has been pitched at ~5 degrees. It can be observed that there is a reasonable level of agreement between the two data sets. The predictions are generally higher than the measurements, bar one repeating peak that is not found in the predicted data. The higher prediction levels are due to a strong return from the nacelle that is not present in the measurement due to imperfections in the nacelle which are not modelled in the predictions.

6.2.7 Swaffham turbine at 100 degrees yaw, 0 degrees pitch

6.2.7.1 There is exceptionally good agreement at 100 degrees yaw (see Figure 6-6) between the predicted and measured data in terms of trend and magnitude. The predicted data are lower than the trial data by around 2dB.

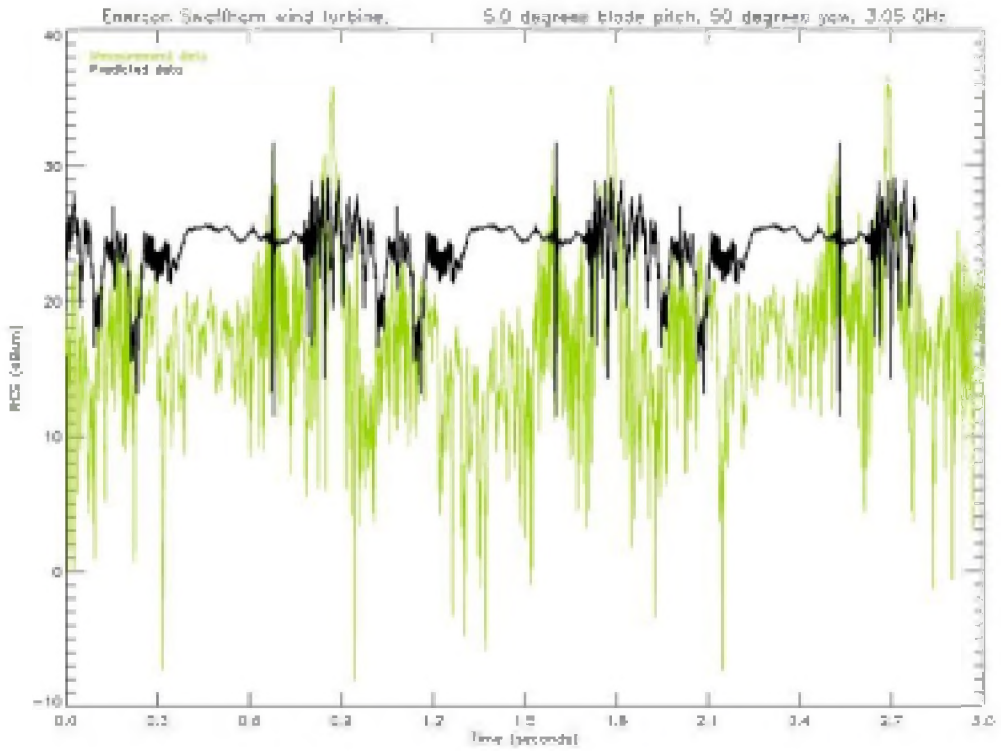

Figure 6-5; Enercon turbine at Swaffham, 5 degs pitch, 50 degs yaw, 22.5RPM

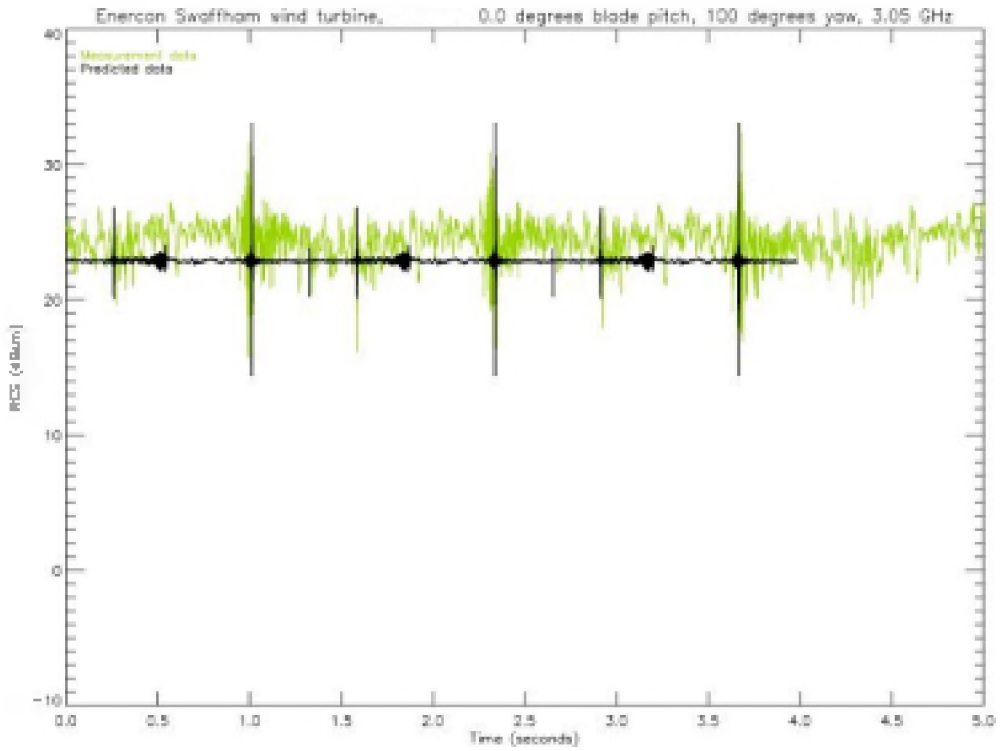

Figure 6-6; Enercon turbine at Swaffham, 0 degs pitch, 100 degs yaw, 13.6RPM

6.2.8 Conclusions

6.2.8.1 The RCS predictions of the Swaffham turbine discussed in the previous sub-section have been compared to measurement data successfully. The positions of the peaks and basic trend of the measurement data were shown to be accurately predicted. The level of agreement is sufficient for the current purpose and the differences are understood and explainable.

6.2.8.2 It was noted that some of the predictions are 4 to 6 dB lower than the measurements, near RCS peaks. EMRAD noted this in their review of the model – see appendix G. On further consideration it was concluded that this is the result of two main factors.

6.2.8.3 Firstly, the blades are modelled as solid fibreglass bodies. The properties of the fibreglass we used give rise to an 8dB reduction in the returns emanating from the blades. The blades appear to be more reflective increasing the level of the measurement data over the predictions.

6.2.8.4 Secondly, the predictions carried out do not model any returns resulting from multiple interactions within the turbine structure. An example of this would be energy reflected by a blade onto the tower and then returned to the radar. This effect is commonly referred to as "multiple-bounce" returns. The Ocellus prediction code is capable of predicting multiple bounce returns from a structure, but this has not been computed because of the computational overhead involved if calculated for a full rotation of the blades. Given geometry that gives rise to paths back to the radar via multiple bounce these returns can be very large. Without this mechanism the predictions will be different from the measurement where strong multiple bounce returns are present.

6.2.8.5 To overcome this difference we must deal with both of these factors. The turbine blades need to be modelled with a more realistic reflectivity. It should be noted that the genuine blades are fibreglass shells, containing lightning conductors and have metal tips. The shell structure and metallic elements will undoubtedly affect the level of the RCS. Reflectivity values would ideally come from small scale measurements of the materials involved, but if this was not possible then a more reflective blade could be modelled to make sure the predictions do not fall below the actual scattering levels.

6.2.8.6 The multiple bounce calculations must be included in the turbine calculations. To predict this mechanism for the complete detailed model is not impossible but is a time consuming process. A better solution might be to calculate the multiple bounce on a simplified turbine and then add these results into the final solution. Some investigation would need to be carried out to find the right trade-off between accuracy and computational efficiency, so that the predictions could be carried out in an optimum way.

6.2.8.7 At around 40 to 50° yaw the predictions showed a higher RCS than the measurements at times when the blades are not causing large returns. At these points the RCS is dominated by the scattering from the nacelle, which in the computer model of the turbine gives a stronger return than observed from the measurements. This is due to the model nacelle being a perfectly smooth object creating a large specula return at this yaw angle. This is not seen in the measurements due to imperfections in the nacelle surface.

6.3 Spectral content validation

6.3.1 To further validate the predictions we have looked at the spectral content of the returning signal as compared to the measured data. To make the comparison the measurement data and prediction data were processed using the same Fourier transform routine. The measurement data were re-sampled at the rate of the collected prediction data to allow a comparison to be made.

6.3.2 The spectra have been calculated using a complete revolution of the rotor, so shows the frequency content averaged over the whole cycle. We expect to see negative and positive frequency components for parts of the cycle when a blade is moving towards and away from the radar. The maximum significant frequency component should match up to the blade tip speed in the direction of the radar.

6.3.3 Yaw -100° and an RPM of 16.5 comparison

6.3.3.1 Figure 6-7 shows the results of this comparison. The main features to note are the large zero Doppler spike showing a large part of the turbine has no movement relative to the radar (tower and nacelle). This is present in both the prediction and the measurement and they are within 1dB of each other in magnitude.

6.3.3.2 The prediction data show a sharp cut-off at around ±1170Hz. This corresponds to a blade tip speed of $58.5ms^{-1}$. Calculating the tip speed from the rotation rate of 16.5 RPM gives a tip speed of $57ms^{-1}$, a good match. Beyond this frequency there are no data and we are left with the noise level. For the measurements this is around 50dB and in the predictions, a much cleaner data-set, this is down at –80dB. These differences are not important when studying these graphs.

6.3.3.3 The effect of the higher noise level on the measurement data is that the highest frequency component is not as distinct due to the higher noise level. Also the real turbine has more degrees of freedom. Vibration, sway and flex will all give rise to spectral components that are not modelled in the prediction.

6.3.3.4 Overall the measurements and the predictions show a good level of agreement with similar patterns and the same basic features.

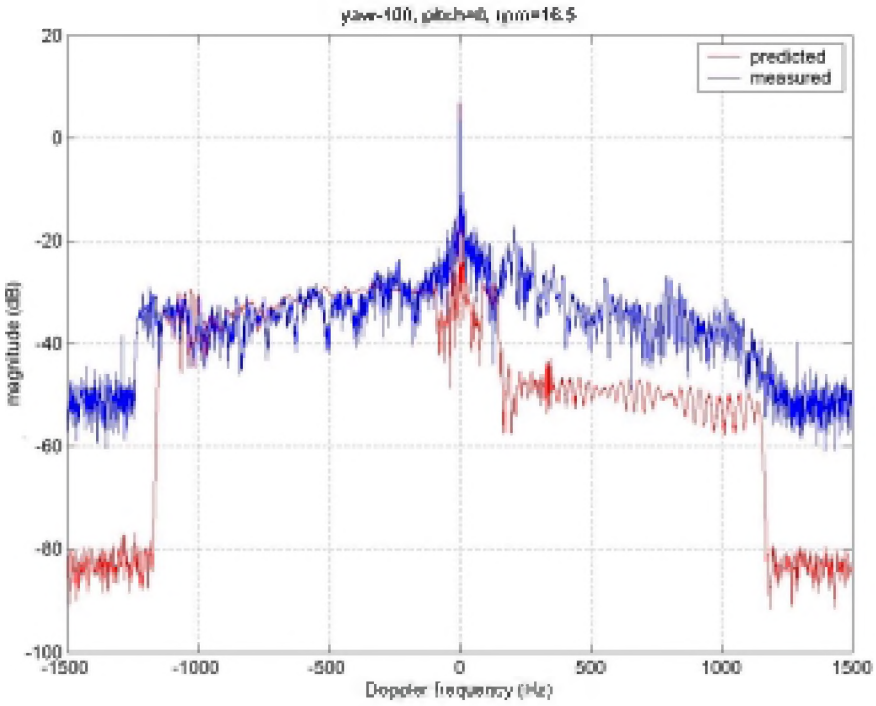

Figure 6-7; Frequency spectrum for one revolution of the Enercon E-66 turbine, measured and predicted comparison. Yaw -100°, Pitch 0°, RPM 16.5.

6.3.4 Yaw 10° and RPM of 12.4 comparison

6.3.4.1 Figure 6-8 shows the comparison when looking at 10° yaw. This is close to looking normal to the rotor when the spectral content will be smaller as the blades do not move much in the direction of the radar.

6.3.4.2 As before both the data-sets show a zero Doppler spike and then frequency components up to the blade tip speed in the direction of the radar. The slower drop-off in spectra components seen in the measurement data is probably due to the greater range of movement possible for the real turbine. The prediction roll-off frequency is ±160Hz which corresponds to a tip speed of $8ms^{-1}$ in the direction of the radar. Working from the RPM and the yaw angle we get a tip speed of $7.8ms^{-1}$ in the radar direction, a good match.

6.3.4.3 Results agree well out to the tip speed frequency of ±160Hz, then beyond this frequency there is some extra frequency components in the measurement data from movement not modelled in the predictions (i.e. flex and bending of the blades and tower). Data –50dB or lower are not significant as this is the noise floor of the measurements.

6.3.5 Yaw 90° and 12.5 RPM comparison

6.3.5.1 Figure 6-9 shows the comparison with a yaw of 90°. Again the main features to note are the large zero Doppler return shown in both data sets and the cut-off frequency that occurs at ±850Hz. This corresponds to a tip speed of $42ms^{-1}$. Using the RPM we find a tip speed of $43ms^{-1}$, a good match.

6.3.5.2 The comparison shows the main features are replicated, with the predictions being at a slightly lower level than the measurements.

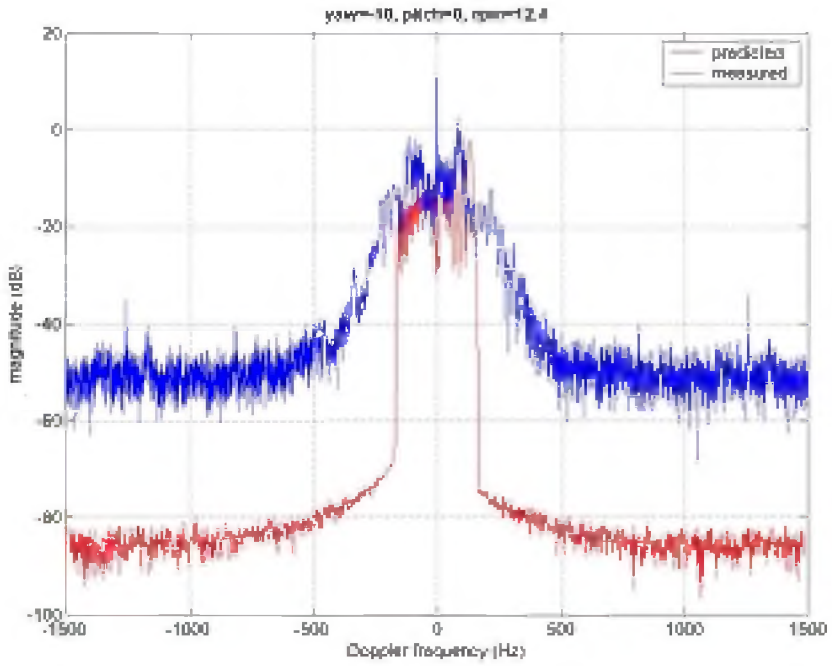

Figure 6-8; Frequency spectrum for one revolution of the Enercon E-66 turbine, measured and predicted comparison. Yaw -10°, Pitch 0°, RPM 12.4

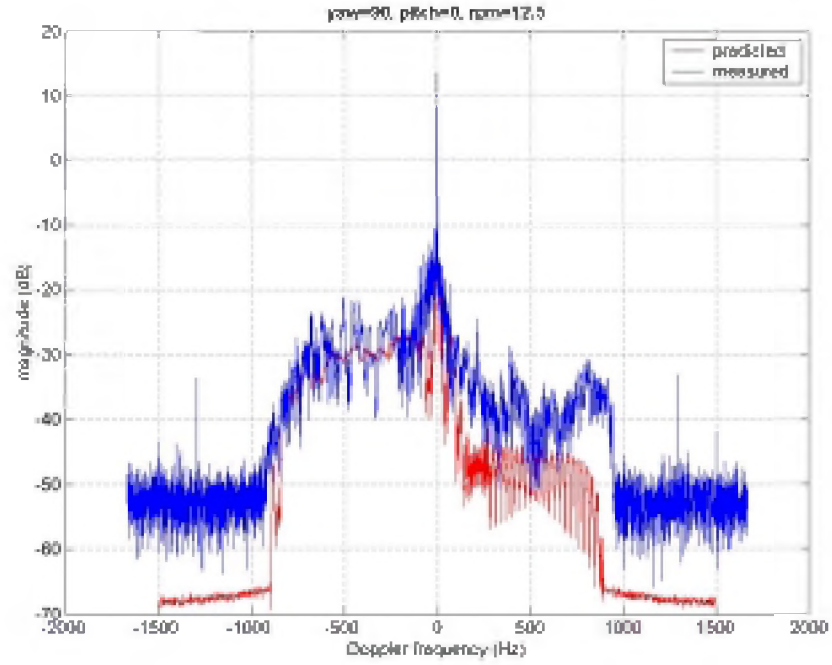

Figure 6-9; Frequency spectrum for one revolution of the Enercon E-66 turbine, measured and predicted comparison. Yaw 90°, Pitch 0°, RPM 12.5

6.4 Propagation validation

6.4.1 The validation of the propagation model has been limited to a simple comparison between NEMESIS (used for input to WHIRL) predictions and those from another widely used model, the Advanced Refractive Effects Prediction System (AREPS version 2.01.2014). This is produced by the Space and Naval Warfare Systems Center, San Diego, Atmospheric Propagation Branch.

6.4.2 The scenario chosen for comparison was a simulation of the MPR looking at the Swaffham wind turbine. The radar was placed at 52°39.2'N, 0°37.9'E, at a height of 2m above ground level. The direction of illumination was 085°, at 2° elevation, using a frequency of 3.05GHz. A vertical slice prediction was made with both models, showing the one-way path loss as a function of height and range. Results are shown in Figure 6-10 and Figure 6-11, which have been plotted using the same scales as far as possible. The graphs show the one-way path-loss for a bearing from the radar, taking into account the terrain. The terrain is a brown colour in both of the plots at the bottom of each graph, and the other colours show the path-loss at a range and height from the radar. The AREPS plot only shows data below an elevation angle from the radar of 45°, hence the area of no colour in the top left of the plot. We can see areas of high loss close to the ground where the terrain is screening the radar's view and a lobe structure as the elevation angle is increased. These lobes are caused by energy travelling via the ground and energy travelling directly from the radar constructively interfering with each other to create a lobing pattern. The NEMESIS output has more subtle variations in colour, making comparison difficult, but it shows broadly similar features to the AREPS output.

6.4.3 This is only a one-off comparison, but other projects within QinetiQ have used the NEMESIS propagation model successfully. One such project states that the model has been tested and accepted for maritime radar studies at 3GHz. This project confirmed that NEMESIS predictions of propagation factor, as a function of height and range, were consistent with measurements for the VHF band. Comparisons in the general literature indicate that NEMESIS agrees well with ray optics and diffraction solutions in their respective regions of validity, and that NEMESIS agrees with other parabolic wave equation solutions.

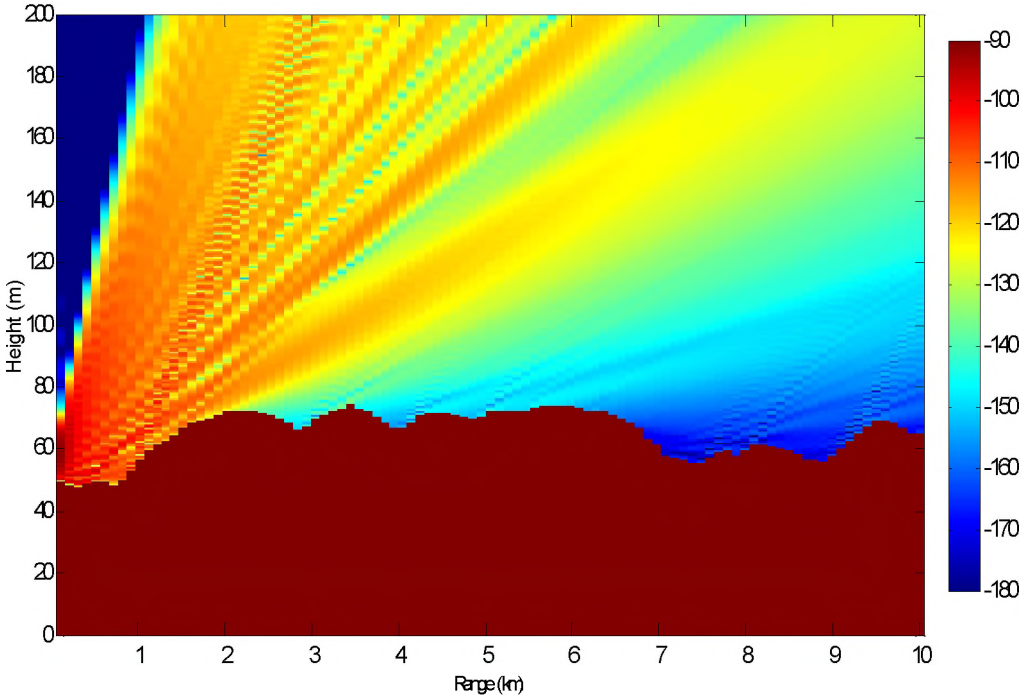

Figure 6-10; 1-way path loss from NEMESIS

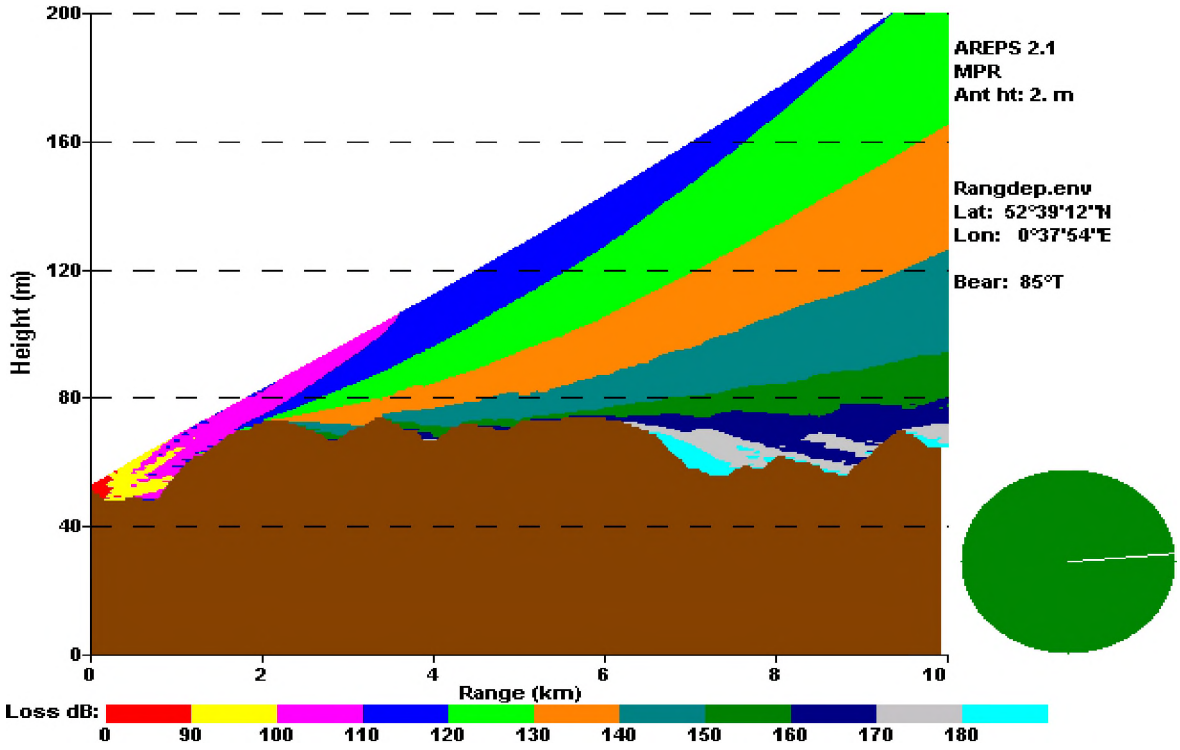

Figure 6-11; AREPS propagation loss prediction

6.5 WHIRL validation

6.5.1 Scenarios tested

6.5.1.1 To carry out the validation a few scenarios were picked so that the turbine returns could be studied and compared with the results from WHIRL. The comparison is done based on the physical size of the turbine return, and the number of times in 50 radar scans the turbine is "hit" or "missed" by the radar. We maintained a consistent approach when comparing the predictions with the real display. Table 6-3 lists the scenarios investigated.

6.5.1.2 As an example of the radar picture at Marham an image with a range of 13nmi is shown in Figure 6-12. Here the wind turbine can be seen as a small yellow return, along with other clutter that appears to be from trees, road traffic and other large man-made structures, plus several aircraft targets. To examine the clutter caused by the turbine we have zoomed right in on its position to get the best view. This is clearly not how the radar operators would use the PPI but is required to properly compare the simulation with the real data.

Date	Time	Turbine RPM	Turbine blade Pitch	Turbine Yaw angle (from radar direction)
02/07/2002	17:26	23	6	39
04/07/2002	16:06	12.4	1	0.4
05/07/2002	12:20	12.5	1	93
01/07/02	18:18	Turbine switched off	90	28

Table 6-3; Turbine configurations investigated for validating WHIRL

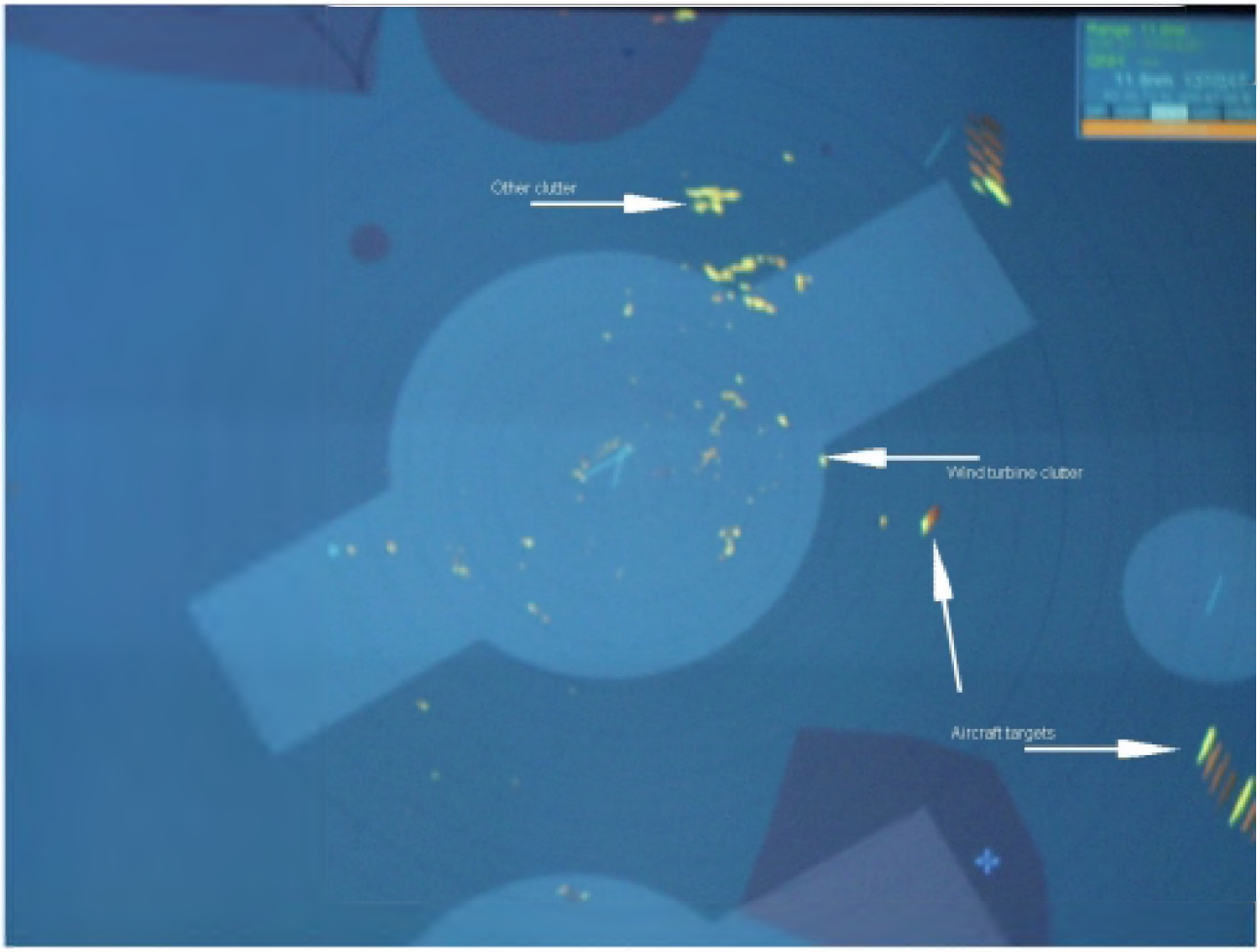

Figure 6-12; Screen shot from the recorded Marham data showing the turbine return and some air traffic.

6.5.2 Turbine at 40° yaw

6.5.2.1 The first scenario tested has the turbine at 40° yaw to the radar with a pitch of 6° and a rotation speed of 23 RPM. Referring to the RCS data from the turbine in Figure 5-8 and Figure 6-3, when not close to either 90° yaw or 0° yaw from the radar direction, the signature levels of the turbine have similar characteristics. The major differences in the scattered energy occur in the frequency spectrum.

6.5.2.2 To compare the data from WHIRL with the recorded picture, two parameters were considered; the size of the return on the screen and the amount of valid hits seen in a sample of 50 radar revolutions. Examples of a valid hit and a miss are shown for the simulation and the recorded data in Figure 6-13 and Figure 6-14. The radar display shows hits in the last scan as yellow and then this fades with each subsequent scan of the radar without a hit to orange though to black. The colours and persistence of the plots can be set by the user of the display. In WHIRL we have only modelled the clutter caused by the turbine, which is shown in Figure 6-13 and Figure 6-14 as the central orange or yellow plot. The other plots seen in the real radar display are from other clutter sources not associated with the wind turbine.

6.5.2.3 The size of the return from the wind farm when a good hit is returned in the real data is 410m in azimuth and 160m in down range. In the prediction large returns are 400m in

azimuth and 150m in down range. Out of 50 rotations of the radar 10 do not see the turbine in the recorded data. The WHIRL results miss 12 times in 50 radar scans.

6.5.2.4 These results show that the model accuracy reproduces the effects of the radar with the turbine in this configuration.

Figure 6-13; Results for turbine at 40 °yaw when the turbine is missed (orange is afterglow of display) for the real data (top) and WHIRL (bottom).

Figure 6-14; Results for turbine at 40 °yaw when the turbine is well seen (yellow marks recent hits) for the real data (top) and WHIRL (bottom).

6.5.3 Turbine at 0° yaw

6.5.3.1 In this example the turbine is facing the radar, meaning that there is a small radial velocity component return from the turbine in the direction of the radar. The blade pitch is 1° and the rotation speed is 12.4 RPM. If the MTI filter is working well then this is the yaw angle for which the turbine causes the least amount of clutter. When the real data were analysed the number of times the return signal from the turbine was rejected was little different to the results at 40° yaw. The radar missed detection of the turbine 11 times in 50 scans. What is apparent (see Figure 6-15) is that the size of the clutter on the display is smaller than at 40° yaw, so the turbine return has been better suppressed but not enough for the radar to reject the turbine altogether. The range cell size of a good hit on the radar display is 130m by 260m.

6.5.3.2 The simulation of this situation showed very little sign of turbine clutter. This is caused by the simulation using a perfectly repeating wind turbine signature and perfectly implemented radar processing. The real turbine has a more variable return due to minor fluctuations in its operational state and has more degrees of freedom to create Doppler shift than the predictions.

6.5.3.3 To further investigate the performance of the MTI filter the returns on the PPI display were viewed when the turbine was non-operational and only drifting in the wind. A small

return from the turbine was still intermittently appearing on the screen. Clearly the real MTI filter does not have the suppression capability to remove this target all of the time.

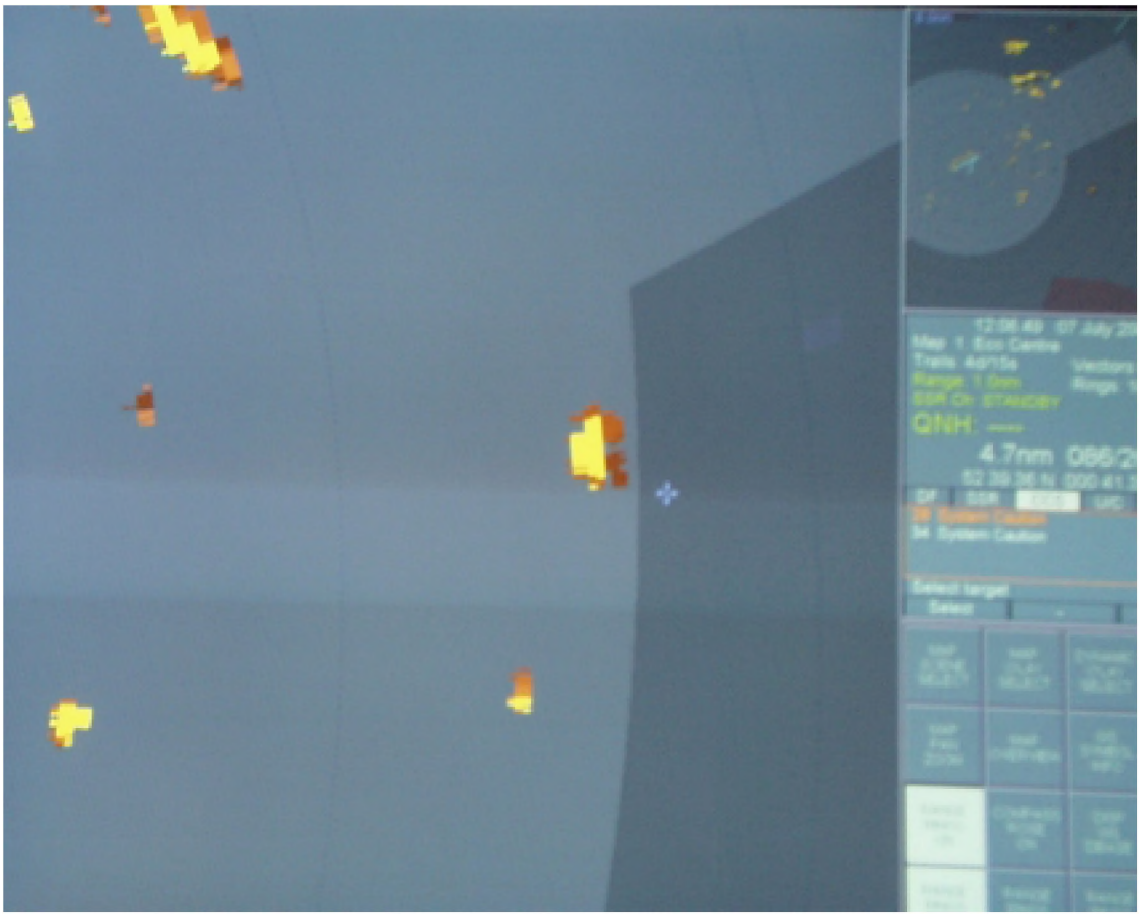

Figure 6-15; Typical maximum return from the turbine when at 0° yaw (i.e. facing the radar)

6.5.4 Turbine at 90° yaw

6.5.4.1 In this final example at Swaffham, the turbine is yawed 90° from the radar direction, has a blade pitch of 1°, and a rotational speed of 12.5 RPM.

6.5.4.2 The real data were investigated for 50 radar scans and only 13 good hits were seen. This makes sense as at this angle the bulk signature of the turbine is at its lowest and so the MTI will filter nearly everything but for the very large spikes from the blade flashes which have significant Doppler. A good hit on the radar display appears as 160m by 440m (see Figure 6-16).

6.5.4.3 The simulation of this scenario gave 11 good hits out of 50 radar scans, which agrees well with the real data. Also the size appears to be correct with large returns appearing at 150m by 400 - 500m. So the simulation gives good results in this situation.

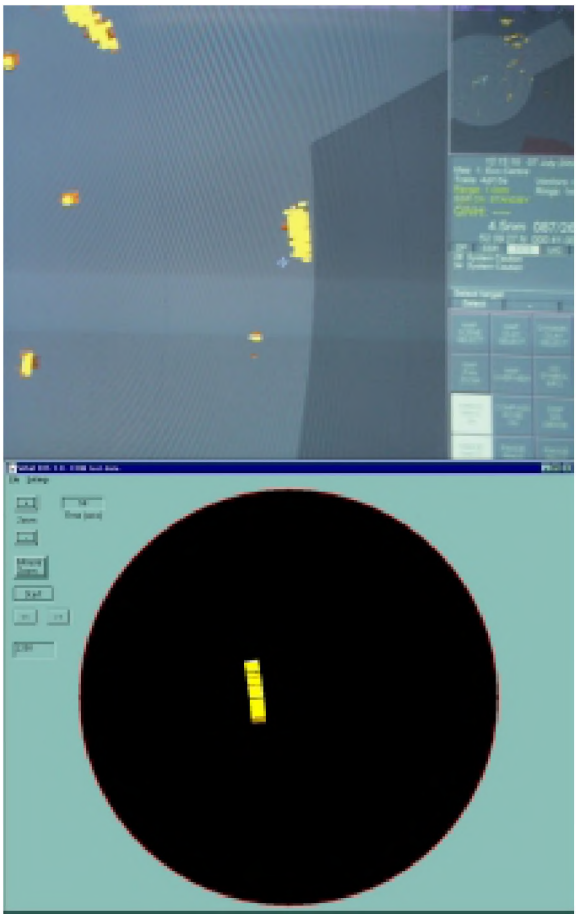

Figure 6-16; Results for turbine at 90 °yaw when the turbine is well seen (yellow marks recent hits) for the real data (top) and WHIRL (bottom).

6.5.5 Prestwick test

6.5.5.1 No official trial took place at Prestwick. While we were on site video data were collected from a PPI unit of the clutter caused by the Hare Hill wind farm. As a test of the model we ran a simulation of the Hare Hill site to compare with these data. Because no information is available of the wind turbines state while these data were recorded we have selected a yaw angle of 40° and a rotation speed of 23 RPM. All the turbines have exactly the same yaw and RPM and are all given random rotor start positions at the start of the simulation.

6.5.5.2 The data collected showed good correlation with the recorded data from Prestwick (see Figure 6-17). The display at Prestwick uses different colours from Marham with yellow used for a current plot and greens used for fading older plots. This is chosen by the user. The size of the clutter on the real screen extends approximately 2300m in down range and 3000m in cross range. In the simulation the extent of the clutter predicted is 2500m in down range and 4000m in cross range. This shows the predicted region of clutter appears wider than the recorded video. This may be due to the real turbines being at a yaw angle that is more easily filtered than the simulation. This would cause the cross-range extent to be smaller but without knowing the configuration of the turbines at this time no certain conclusions can be drawn.

6.5.5.3 This test has demonstrated that with a multiple turbine site the simulation gives useful information about radar impact.

Figure 6-17; Comparison of the simulation of clutter produced from the Hare Hill wind farm on the Prestwick primary radar (bottom) with a real video recording (top).

6.6 Summary

6.6.1 The RCS predictions of the Swaffham turbine discussed in the previous sub-section have been compared to measurement data successfully. The positions of the peaks and basic trend of the measurement data were shown to be accurately predicted. Some of the predictions are 4 to 6dB lower than the measurements, near RCS peaks but the differences are understood, explainable and could be corrected for.

6.6.2 The validation of the propagation model has been limited to a simple comparison between NEMESIS (used for input to WHIRL) predictions and those from another widely used model, the Advanced Refractive Effects Prediction System (AREPS version 2.01.2014). This is produced by the Space and Naval Warfare Systems Center, San Diego, Atmospheric Propagation Branch. The comparison showed good agreement between the two models. Also NEMESIS has been extensively used and validated in previous QinetiQ projects carried out for military customers.

6.6.3 The WHIRL model has been validated using the data recorded for a single turbine at Swaffham from the RAF Marham primary radar. The simulation agrees well with the recorded video picture for most turbine configurations. The turbine configuration that agrees least well is when it is pointing at the radar (0° yaw).

6.6.4 To quantify the accuracy of the model we can compare the number of scans a turbine is observed and detected by the radar with that predicted by WHIRL for each configuration. When the turbine is at 40° yaw the radar hit rate is 80%, whereas the WHIRL hit rate is 73%. This is a 7% error or expressed another way the model is correct 93% of the time. At a yaw angle of 90° the radar hit rate is 26%, and the WHIRL hit rate is 24%. This makes the model correct 98% of the time. At 0° yaw where the agreement is not so good the radar hit rate is 78%, and the WHIRL hit rate is 40%. This makes the model 62% accurate at this yaw.

6.6.5 The model has been shown to be sufficiently accurate to assess the effect of a turbine on radar. The results from Prestwick, although not a proper validation of a multiple turbine site, give encouragement and confidence that the model can give a realistic assessment of the clutter levels to be expected from a large wind farm.

This page is intentionally blank

7 PARAMETER SENSITIVITY

7.1 Current parameters

7.1.1 Currently only two parameters are initially considered when deciding whether a wind farm is satisfactorily located relative to a radar. These are whether LoS exists between the radar and the wind farm and the distance (range) between them. Generally if LoS does not exist, there is unlikely to be a siting issue. If LoS does exist further studies are required to deem whether the wind farm can be built without affecting radar operations.

7.1.2 These parameters, LoS and range to target, are important, but if they are used solely to control the siting of wind farms then large areas of the UK are unusable because of the high density of radar sites.

7.2 Further parameters

7.2.1 The other important parameters influencing the effect of a wind farm on a radar system are as follows:

- Radar sensitivity (Min detectable signal);
- Wind turbine rotor shape design;
- Wind turbine rotor material;
- Wind turbine tower design;
- Wind turbine nacelle design;
- Wind farm layout;
- Radar elevation beamwidth;
- Radar Frequency of operation;
- Radar range cell resolution;
- Radar MTI and other processing.

7.2.2 We will go though each of these parameters and discuss their impact and, if possible, how they can be modified to reduce this impact.

7.2.3 The radar sensitivity is clearly going to affect how the turbines appear to the radar. This is not a parameter that can be modified without reducing the performance of the radar. This is because the magnitude of the scattering from even a small turbine is large enough to reduce the radar sensitivity to such an extent that if the turbine is not seen it would also result in aircraft returns being lost.

7.2.4 The shape of the rotor defines how the turbine scattering changes in time. It is not a parameter that can be changed easily, as it must be designed to be aerodynamically efficient.

7.2.5 The material the rotor is manufactured from affects the amount of energy scattered and, hence, how easily the turbine is detected. Turbine blades are mostly made of fibreglass, and this could be modified with specially designed materials reducing the returns from the rotor.

7.2.6 The tower design has a large effect on the level of scattering produced from the turbine. Minimising this return makes the returns for the tower easier to remove by radar filters and reduces the possible detrimental effects to the radar. As the tower does not move it could be shaped to return very little energy back to the radar.

7.2.7 The nacelle design affects the turbine scattering in the same way as the tower. Minimising this return makes the returns from the nacelle easier to remove by radar filters and reduces the possible detrimental effects to the radar. The nacelle rotates only on one axis, so this leaves considerable scope for its signature to be reduced by altering its shape.

7.2.8 The layout and spacing of the turbines within a farm will affect how the clutter appears and the area it covers on the operators PPI display. To understand how the layout could affect the radar we must also consider the size of the radar resolution cell.

7.2.9 The radar resolution is defined as the distance between two targets at the point when they appear as one object on the radar display; i.e. objects with a separation smaller than the radar resolution cannot be distinguished from each other. A radar resolution is defined as three separate values. The radar downrange resolution is in the direction of the radar beam, hence is the radar resolution in range. The radar cross range resolution is in the direction 90° from the radar beam, hence is the radar resolution in bearing. The final value is the radar resolution in height. Many radar systems (including most ATC radar) have no height resolution, so an unconfirmed return (such as from a wind turbine) could be at any height.

7.2.10 Down range resolution is determined by the pulse length of the radar and any pulse compression algorithms used. Typical values are between 50 and 300m. The cross range resolution can be expressed as a bearing, and is typically between 1 and 3°. The cross range resolution in metres is a function of range and can be calculated using the formula $R\theta$, where R is the range and θ is the bearing resolution in radians. This shows that the cross range resolution increases with range from the radar. As an example the cross range of a radar system with a bearing resolution of 1.5° at 10km is 262m, at 20km is 524m, and at 30km is 785m. Hence if the wind farm is closer to the radar the cross range resolution will be smaller and the clutter caused on the radar display correspondingly smaller.

7.2.11 If the layout of the turbines is such that the turbines are not resolvable from each other then it will be very difficult to see any other targets passing over the site within the region of the farm as there are no gaps between the turbines. If the turbines are spread out so that they can be individually resolved then it may be possible to track aircraft between the turbines.

7.2.12 The radar elevation beamwidth affects how the turbines are illuminated, and hence the amount of energy returned by the turbines to the radar. In most situations reducing the beamwidth so the turbines are not illuminated will be most undesirable, as it will also limit the detection of real targets at low altitudes, and at long range.

7.2.13 The frequency of the radar will affect how the turbines appear to the radar. The RCS of wind turbines will vary with different radar frequencies. This is not a parameter that can be modified to reduce the effects of turbines, as these frequencies are well established and fixed. The amount of variation of the turbine scattering with frequency will depend

on the detailed design of the turbine. The turbines studied in this work were predicted at two frequencies and the difference between the results was not significant.

7.2.14 The radar processing is key to how the turbines appear to the radar. The more effective the MTI filter the bigger stationary turbines can be and be removed from the radar operators PPI display. There may also be yaw angles where an effective MTI filter would remove the turbine returns. Other filter designs are possible that could increase radar capabilities in the presence of wind turbines, but a discussion of this is outside the scope of this report.

7.3 Detailed tower sensitivity study

7.3.1 The turbine tower RCS return is a function of frequency, shape and material, and is not affected by pitch or yaw, as it is the stationary part of the turbine. We have looked at the variations with frequency and basic dimensions.

7.3.2 The tower contributes a constant return from the wind turbine and should be minimised to aid in the filtering of the tower return by standard MTI radar processing. This processing can suppress stationary objects, but if the RCS is very large the MTI will fail.

7.3.3 We have predicted the RCS from the tower for the Vestas V47 and the Enercon E66 in isolation to carry out this study.

7.3.4 Enercon E66 tower

7.3.4.1 A prediction of the tower has been carried out over a range of frequencies and the results are shown in Figure 7-1. It shows the tower RCS varies rapidly with frequency. This is due to its very large size when compared to the radar wavelength, and parts of the tower go in and out of phase with very small changes in frequency. This will only occur for a perfectly tapered cylinder as modelled in the prediction, but a real turbine tower will not vary as dramatically due to small imperfections in its manufacture. The average signature shown in Figure 7-1 is a more meaningful level for the tower RCS.

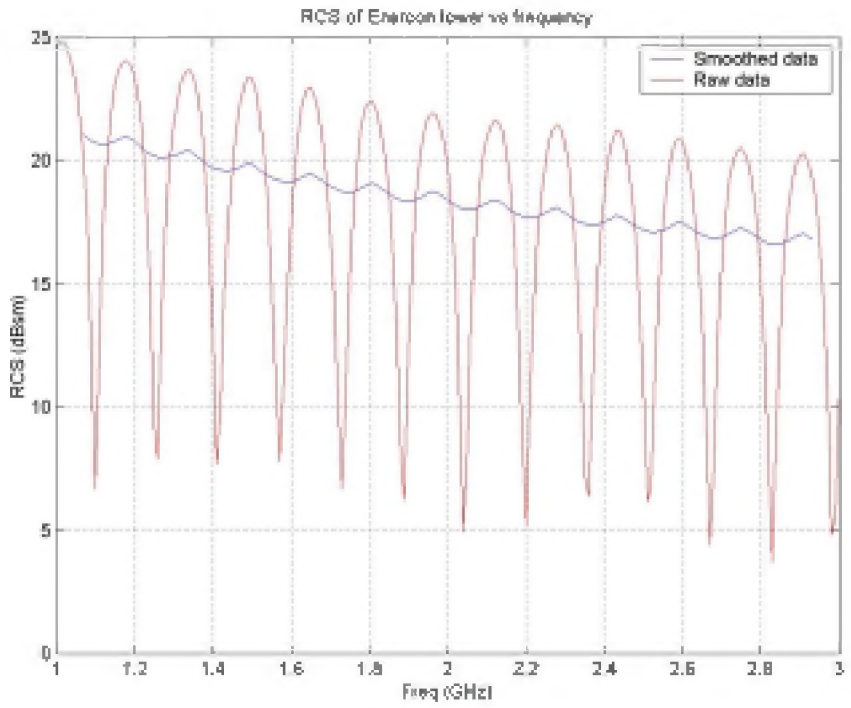

Figure 7-1; RCS of Enercon tower versus frequency. Red shows the raw prediction data and the blue curve is a more realistic smoothed curve.

7.3.4.2 From the results we see that as the frequency increases the RCS of the tower decreases. This will be true for any tapered cylinder tower. The angle of taper on the Enercon turbine is 0.88°. To assess the effect of this angle on the tower scattering predictions of different taper angles have been collected and the results are shown in Figure 7-2. The bigger we make this taper angle the smaller the tower RCS will become and small changes in this angle can have a large effect. At 0.88° the RCS is ~20dBsm ($100m^2$), at 2.88° it has fallen to 10dBsm ($10m^2$), and by 5.88° the RCS is ~3.5dBsm ($2.2m^2$). This is a key parameter.

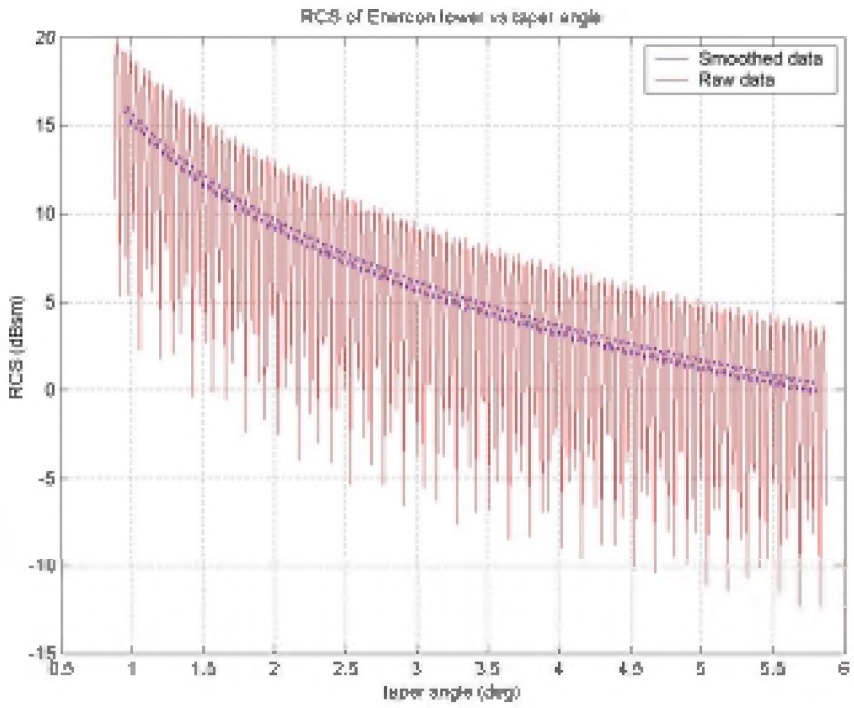

Figure 7-2; RCS of an Enercon sized tower as the taper angle is varied. The Blue curve is a smoothed version of the red showing the trend in the results.

7.3.5 Vestas V47 tower

7.3.5.1 Figure 7-3 shows a frequency sweep of the Vestas tower, and also a smoothed result that is likely to better represent a real tower due to small imperfections present in the real structure. The frequency variation is slower than with the Enercon tower due to its shorter length, but the RCS levels are similar. The variations with taper angle are also similar to the Enercon tower (see Figure 7-4). This shows that for a tapered cylinder tower the length and diameter are not the key parameters affecting the amount of energy reflected.

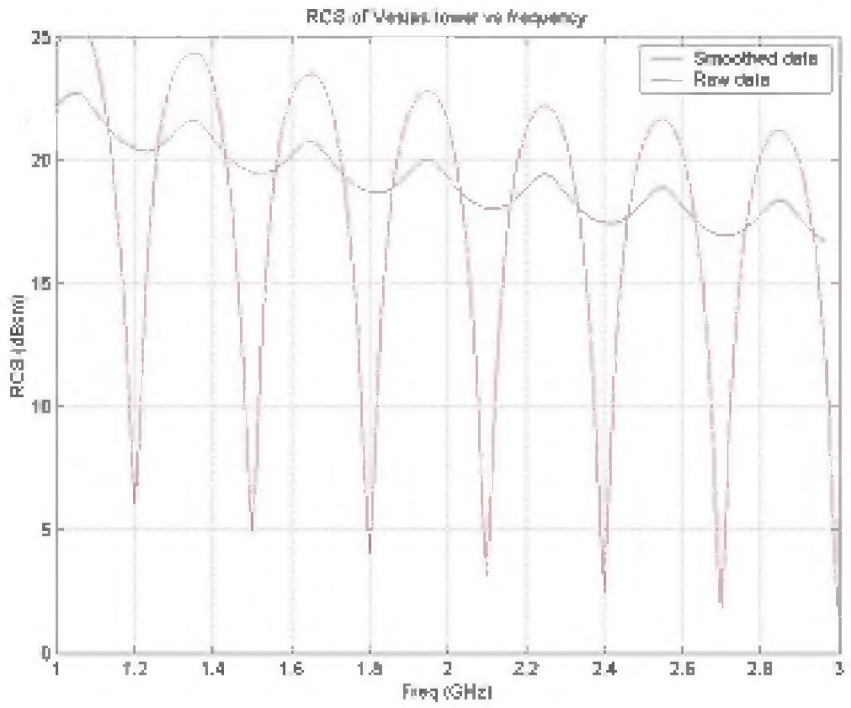

Figure 7-3; RCS of Vestas tower versus frequency. Red shows the raw prediction data and the blue curve is a more realistic smoothed curve.

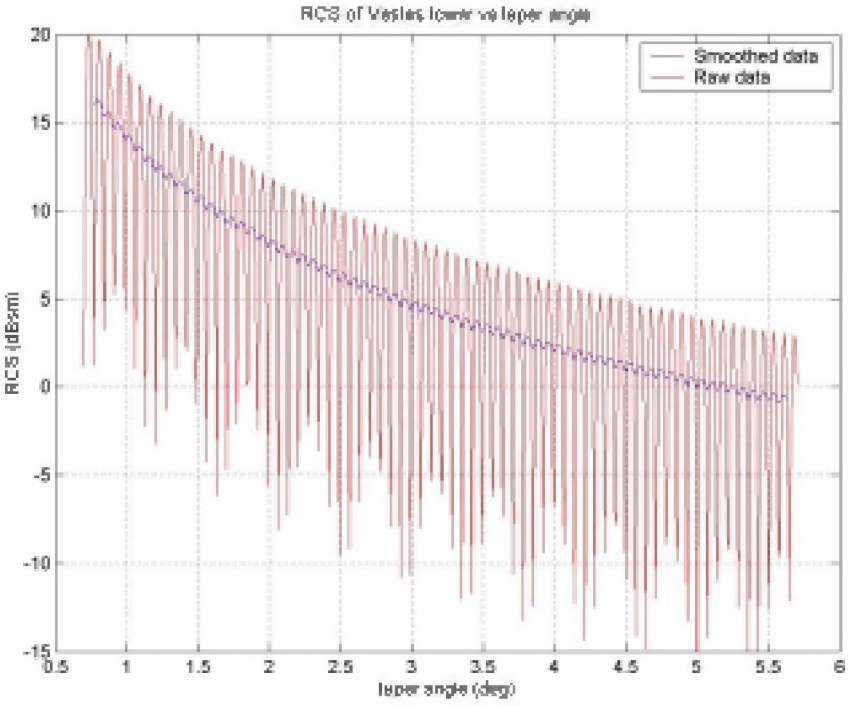

Figure 7-4; RCS of a Vestas sized tower as the taper angle is varied. The Blue curve is a smoothed version of the red showing the trend in the results.

7.3.6 Summary

7.3.6.1 Important points to note from this study are that for a tapered cylinder tower the key parameters are taper angle and frequency. Diameter and height are not as significant so long as the tower is many wavelengths high, which is always true above 1GHz. As the tower does not move, squashing the tower into an oval cross-section and pointing the narrow cross section at the radar can further reduce its RCS. This would require more work to assess the achievable RCS levels and its feasibility.

7.4 Detailed nacelle sensitivity study

7.4.1 The turbine nacelle RCS return is a function of frequency, shape and material, and yaw angle. It rotates with respect to the radar only very slowly so it will be suppressed by a radar MTI filter. It is still important to keep this return to a minimum so the MTI filter can easily filter this return, which is likely to be in good view of any nearby radar as it sits on the top of the turbine tower.

7.4.2 We have predicted the RCS from the nacelle from the Vestas V47 and the Enercon E66 in isolation at two frequencies as a function of yaw angle. All the results shown are from the prediction code and no measurement data are presented.

7.4.3 Enercon E66 nacelle

7.4.3.1 The Enercon nacelle is an egg shaped structure and hence is made up of curved surfaces with little flat surfaces. This will cause the reflected energy to be sent off in all directions quite evenly. The limit of this is a sphere whose backscatter RCS is the same from all aspects.

7.4.3.2 Figure 7-5 shows RCS of the nacelle for all yaw angles at two frequencies (1GHz and 3GHz). The RCS varies very rapidly with yaw angle, so the plots have been smoothed to show the trends with yaw. The RCS of the nacelle at 3GHz lies between 3.4dBsm and 21.8dBsm for all yaw positions. At 1GHz this range is –18.3dBsm to 22.9dBsm. The minimum RCS is very low at 1GHz and occurs when looking at 0° yaw. This is due to the rapid variation of the nacelle scattering with frequency from this yaw angle and is shown in Figure 7-6, which is the RCS at 0° yaw against frequency. It shows a large variation in scattering with small changes in frequency as parts of the nacelle go in and out of phase with one another.

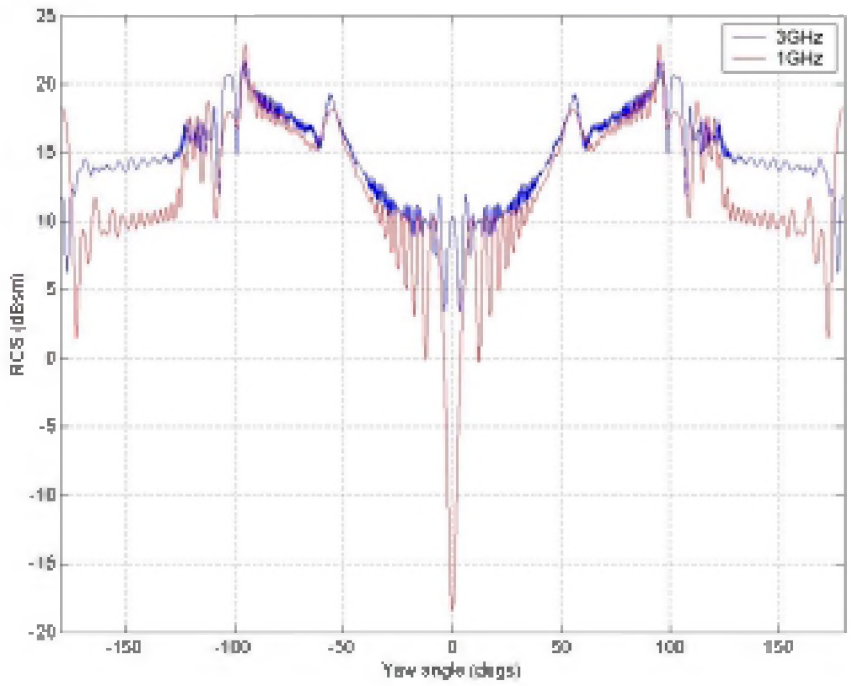

Figure 7-5; Variation in RCS of the Enercon nacelle with Yaw angle

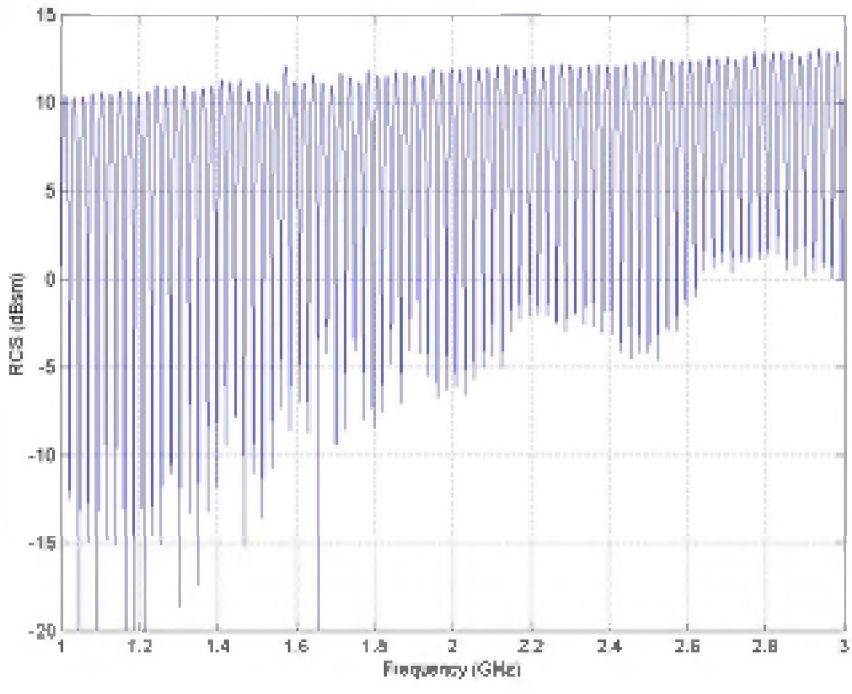

Figure 7-6; RCS looking at the Enercon nacelle at 0° yaw versus frequency.

7.4.3.3 The yaws which give the lowest returns are close to 0° with the maximum returns coming at yaws of ±90°.

7.4.4 Vestas V47 nacelle

7.4.4.1 The Vestas nacelle is a rectangular box shape, with no curved surfaces. This will cause the returns from the nacelle to be sharply spiked in yaw with quite low returns between these spikes.

7.4.4.2 Figure 7-7 shows the RCS of the nacelle for all yaw angles at two frequencies (1GHz and 3GHz). The RCS varies very rapidly with yaw angle, so the plots have been smoothed to show the trends with yaw. The large spikes in the RCS pattern occur at a yaw of ±90° when looking normal to the nacelle side panels. At 3GHz these spikes are 43.8dBsm and at 1GHz they are 41dBsm. This is large enough to defeat many radar MTI filters. At other yaws the returns can be much lower. In the 170° to 120° yaw positions the RCS falls as low as –25dBsm and is consistently below –10dBsm.

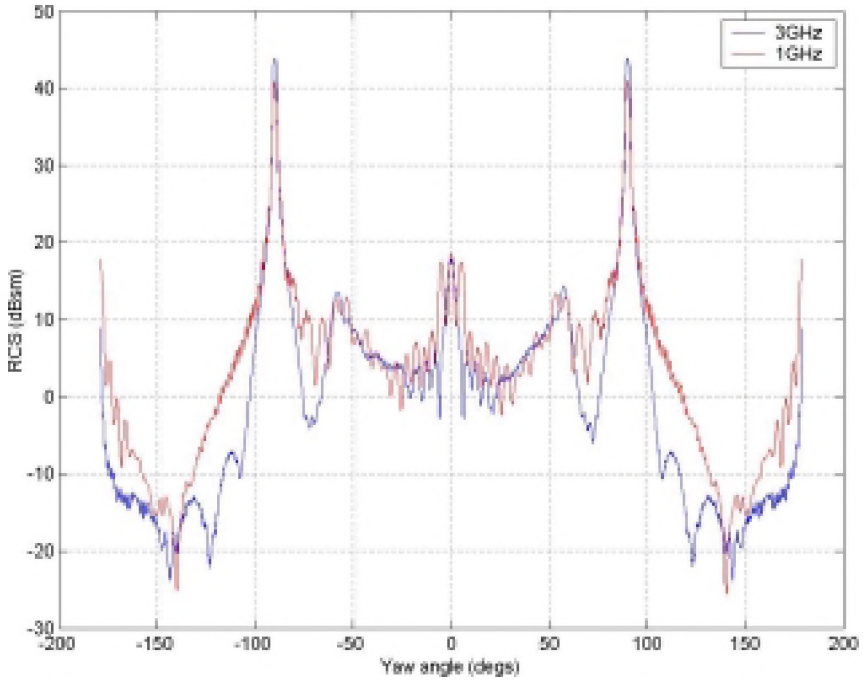

Figure 7-7; Variation in RCS of the Vestas nacelle with Yaw angle

7.4.4.3 To remove the large spikes seen at ±90° the side panels should be angled so that the surface normal cannot point at the radar. This can be done by tilting the face upwards. Figure 7-8 shows how the RCS of the side panel varies as this tilt angle is increased. Tilt angles of 10° can reduce these spikes from 40 to 50dBsm (10,000m^2 to 100,000m^2) to below 20dBsm (100m^2).

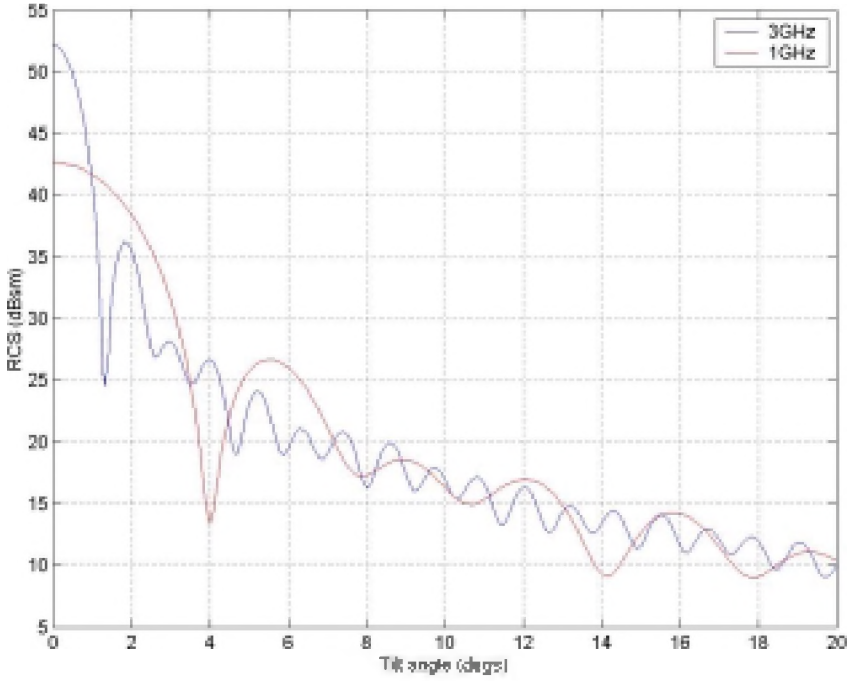

Figure 7-8; RCS return from the Vestas nacelle side panel for varying tilt angles

7.4.5 Summary

7.4.5.1 To avoid large spikes in the RCS, which can pass though MTI filters, curved surfaces can be used for the nacelle instead of flat surfaces. These curved surfaces spread the energy over wide aspects and can still give a large RCS. A better solution would be to build nacelles from flat panels, but angle them carefully so they do not point directly at the radar from any yaw angle. With careful design a nacelle could be designed to give low returns in all yaw directions.

7.5 Detailed blade sensitivity study

7.5.1 Introduction

7.5.1.1 The question as to whether or not there are any pitches and yaw angles that, together, are either advantageous or disadvantageous to the local radar was addressed.

7.5.1.2 The sensitivity of the turbine blades to the radar in terms of both pitch and yaw has been investigated on three different blades. A 40m NEG-Micon blade, the Enercon blade on the Swaffham turbine and the Vestas blade on the Harehill turbine.

7.5.1.3 The Vestas turbine blade was predicted with a pitch of 0 degrees. The Enercon blade and the 40m NEG-Micon blade were predicted at pitches of 0, 5, 10, and 20 degrees to investigate pitch effects.

7.5.1.4 The RCS of the different blades were predicted at a frequency of 3.0GHz. The blades were rotated from a vertical position (0 degrees rotation) in steps of 1 degree over an

azimuth sweep of –90 degrees to 270 degrees. The front of the turbine is considered to be at 0 degrees azimuth and the rear at 180 degrees azimuth.

7.5.1.5 The figures presented in the following subsections detail the RCS from a single blade with respect to azimuth. The RCS is presented when the blade has been rotated 0 degrees (vertically upwards), 60 degrees, 120 degrees and at 180 degrees (vertically downwards). The x-axis is the yaw angle of the turbine with respect to the radar that the blade would be attached to. Therefore these graphs show how the RCS of one blade varies in a fixed rotor position as the yaw is varied.

7.5.2 Vestas Harehill blade

7.5.2.1 It can be seen from in Figure 7-9 (when the blade is pointing vertically upwards) that there are a number of peaks in the azimuth (yaw) sweep that are 10dBsm or greater. These spikes occur when the yaw angle is such that the large front and rear surfaces of the blades are illuminated, or when looking directly at the leading and trailing edges. There are several peaks as the curved nature of the blade surfaces creates strong returns in a number of different directions.

7.5.2.2 As the blade rotates, from a vertical position, the peaks move across the azimuth range merging (when the blade is within 5 or so degrees from a vertical position) into two large prominent peaks that are centred around ~0 degrees and ~180 degrees azimuth. At these aspects the radar is incident on the front or the rear of the turbine respectively. The mean return at aspects away from these peaks is very low at around –20dBsm to –30dBsm. This very low return is a result of the radar being incident at non-specular angles on the blades. As the blade rotates further and approaches the downwards vertical position, the RCS from the blade returns to the state shown in Figure 7-9, but shifted by 180°. This is illustrated in Figure 7-9 to Figure 7-12.

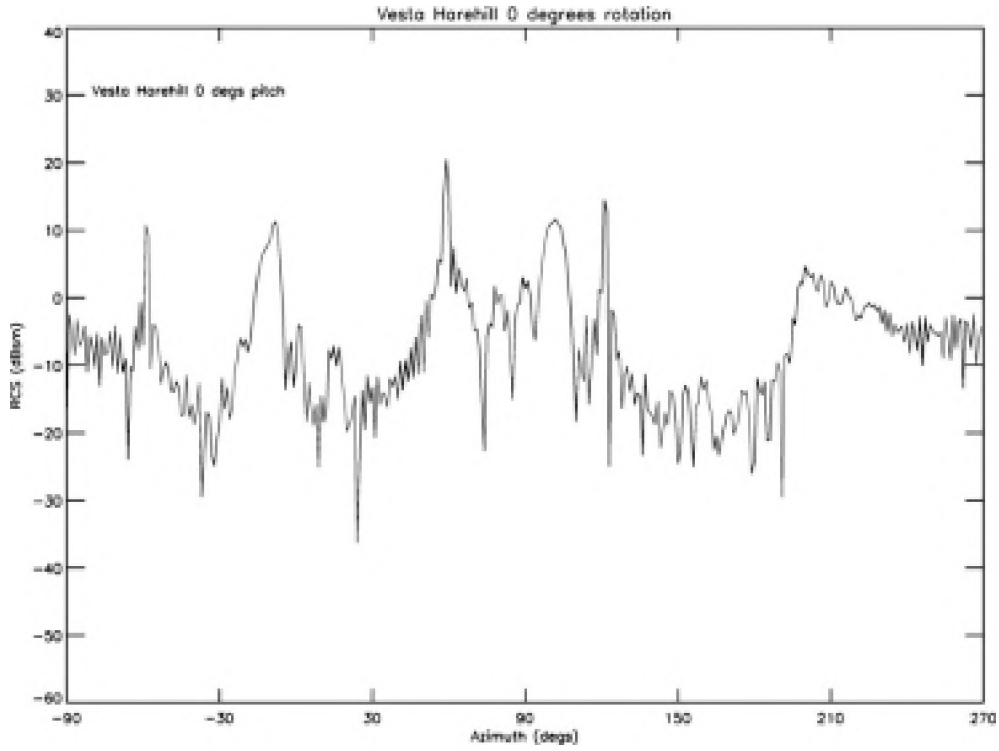

Figure 7-9; Vestas Harehill blade at 0 degrees rotation (Vertical)

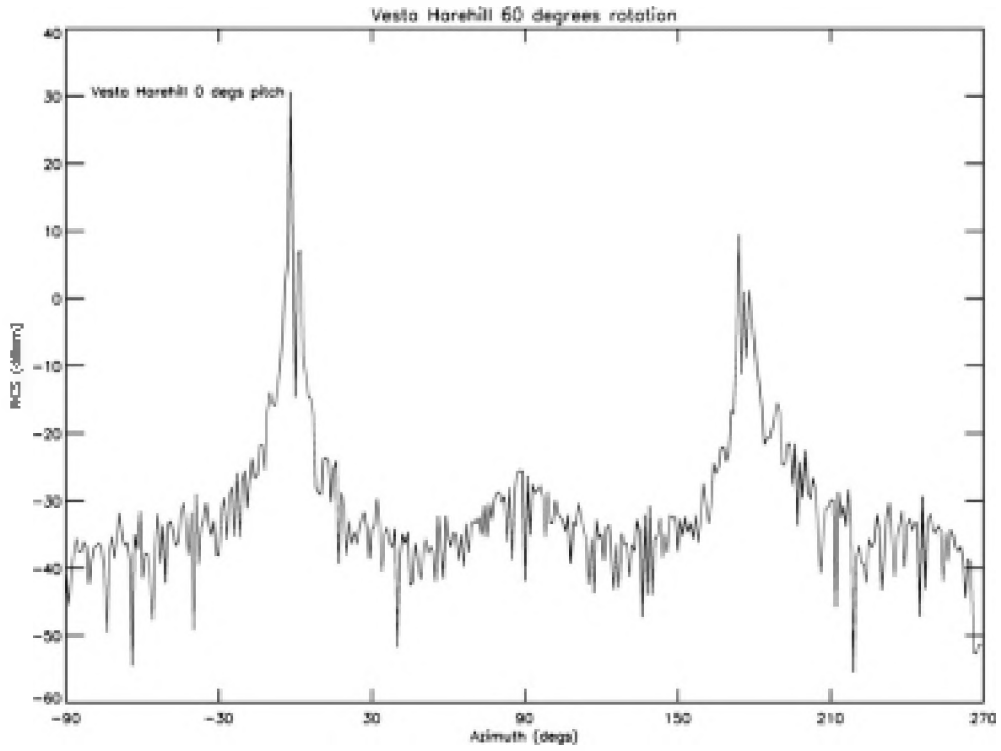

Figure 7-10; Vestas Harehill blade at 60 degrees rotation

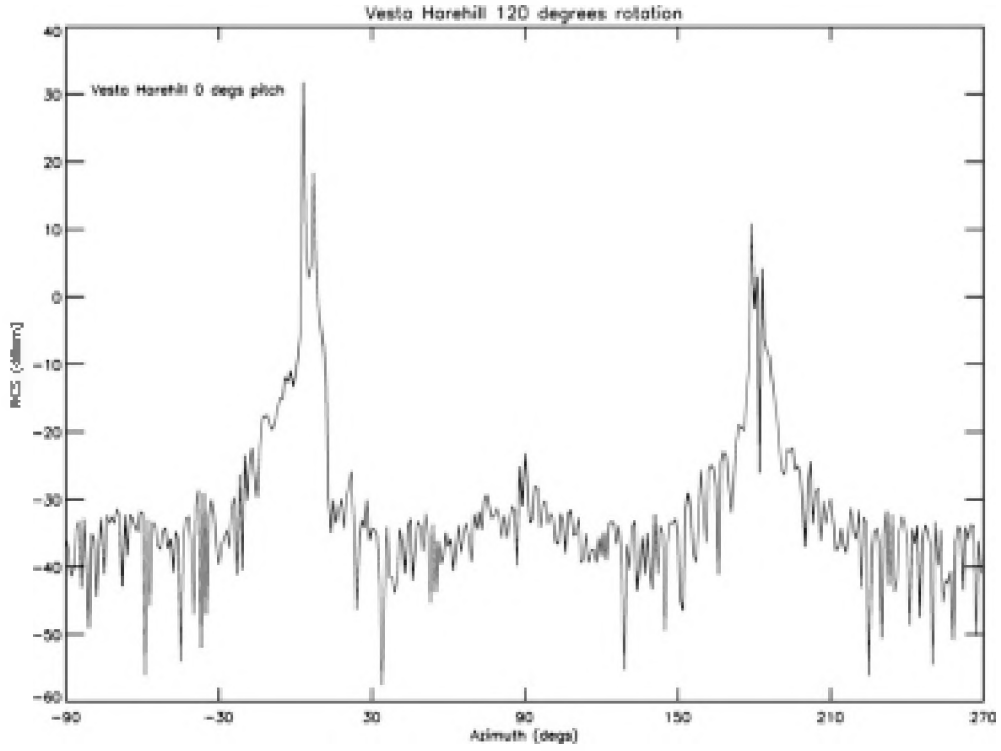

Figure 7-11; Vestas Harehill blade at 120 degrees rotation

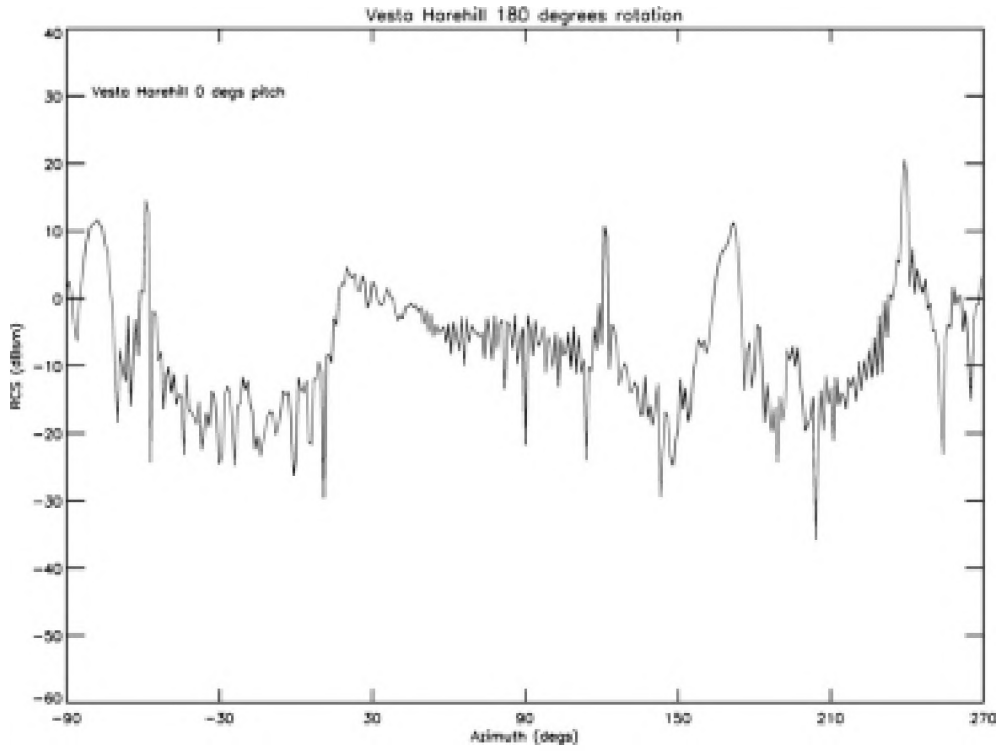

Figure 7-12; Vestas Harehill blade at 180 degrees rotation

7.5.3 Enercon Swaffham blade

7.5.3.1 We predicted this blade with a pitch of 0, 5 and 10 degrees. The RCS against azimuth when the blade is vertical can be seen in Figure 7-13. This figure shows how the pitch of the blade affects the position of the various peaks. For example when the blade pitch is zero degrees and the blade axis from root to tip is vertically upwards (figure 7-13) there is a peak at ~160 degrees azimuth. However, when the pitch is 10 degrees the equivalent peak occurs at ~170 degrees azimuth. Likewise, the same trend can be observed for the other features in the blade RCS. So a blade pitch of x° simply changes the yaw angle at which the large returns from the front and rear of the blades occur by x°.

7.5.3.2 As the blade rotates the peaks (as was seen for the Vestas Harehill blade) move position in azimuth and all the peaks, corresponding to the different pitches, merge into two large features. One at ~0 degrees and the other at ~180 degrees. As before this shows that away from the vertical (up or down) the blade only has a large RCS return when looking from the front or the rear of the blade. The width of the two peaks is around 20 degrees in azimuth meaning that for much of the azimuth sweep the RCS is very low. The trends are illustrated in Figure 7-13 to Figure 7-16.

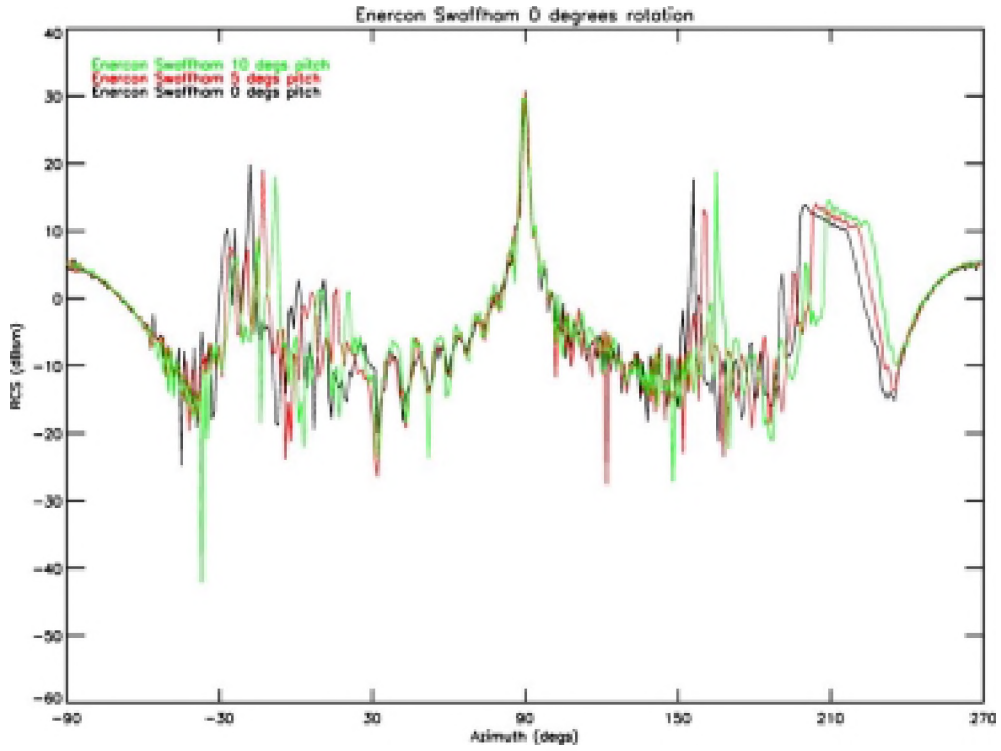

Figure 7-13; Enercon blade at Swaffham after 0 degrees rotation (vertical) for pitches 0, 5, 10 degrees

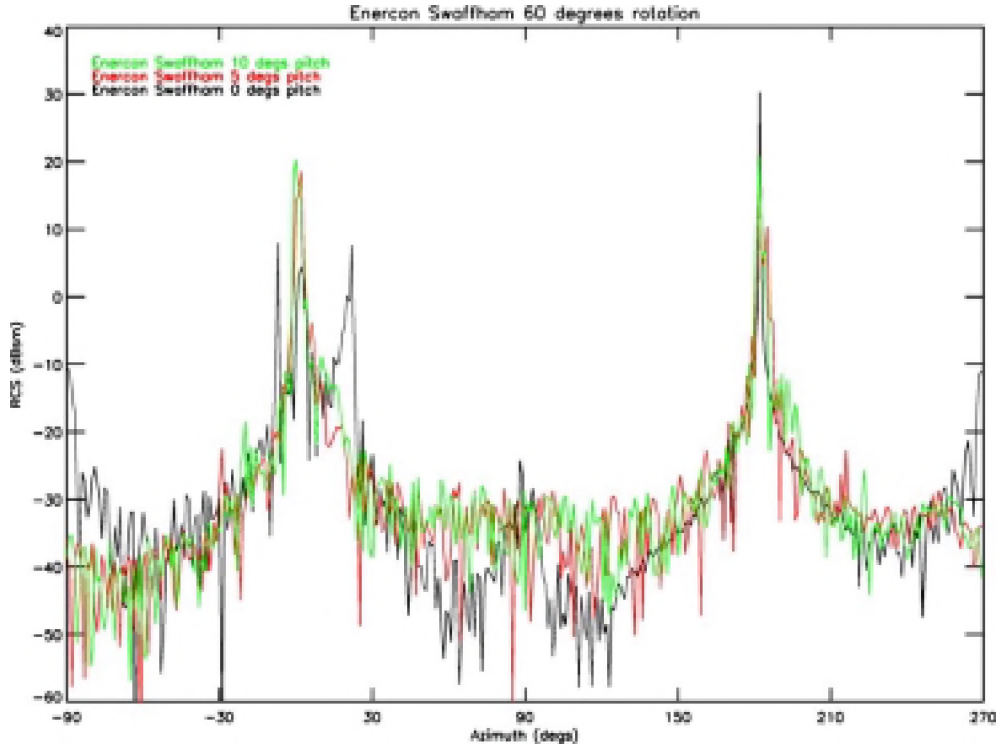

Figure 7-14; Enercon blade at Swaffham after 60 degrees rotation for pitches 0, 5, 10 degrees

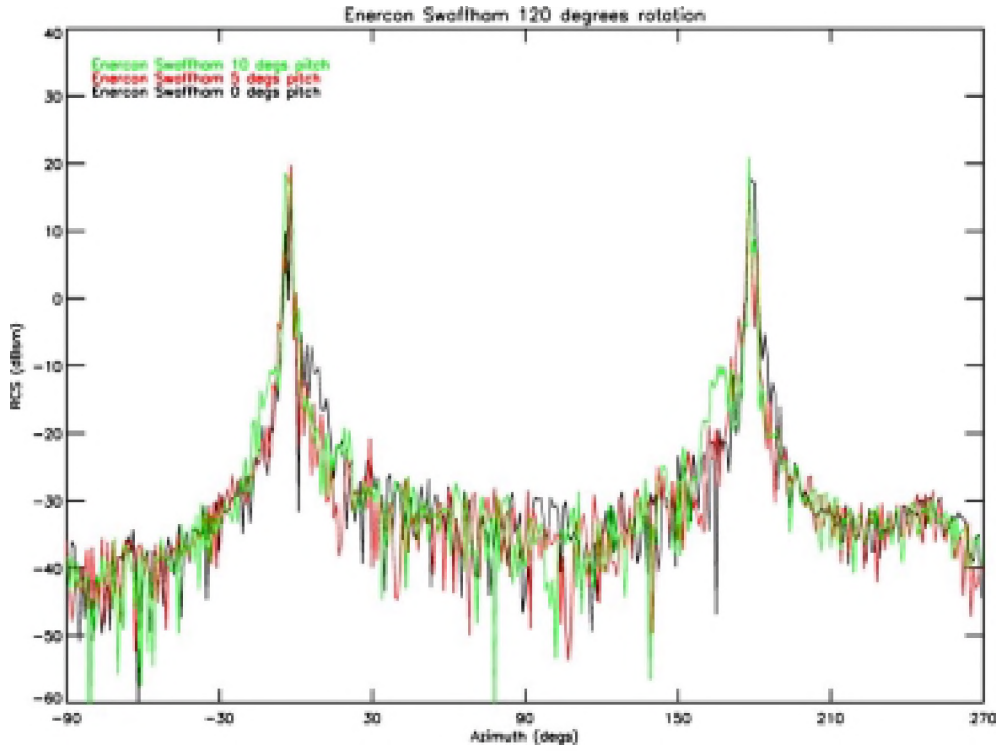

Figure 7-15; Enercon blade at Swaffham after 120 degrees rotation for pitches 0, 5, 10 degrees

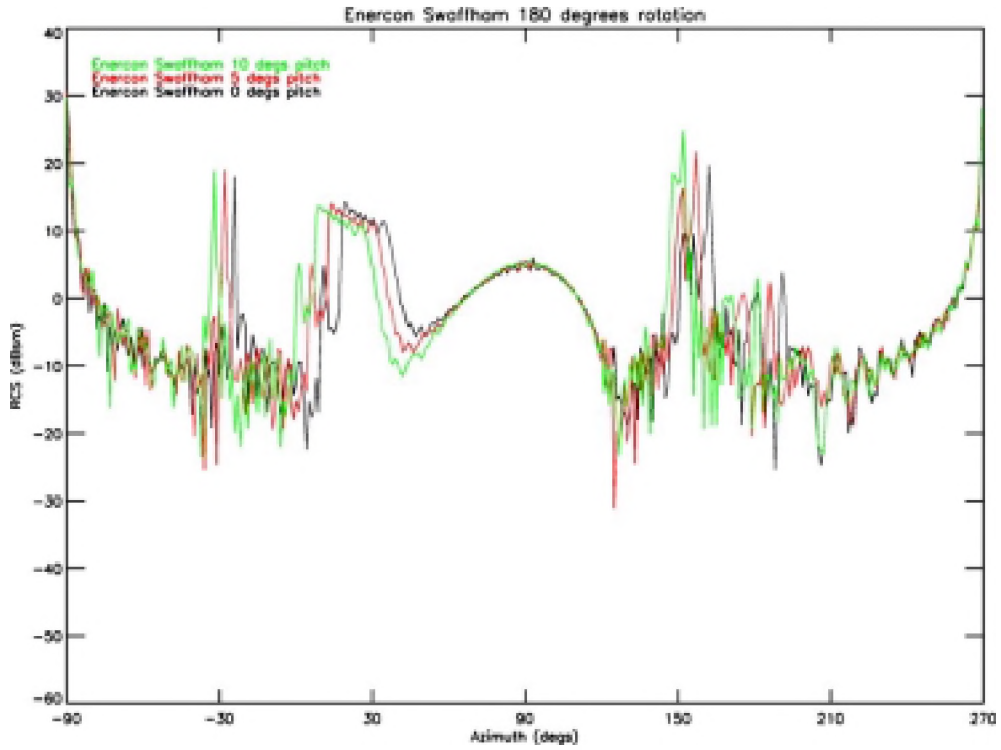

Figure 7-16; Enercon blade at Swaffham after 180 degrees rotation for pitches 0, 5, 10 degrees

7.5.4 40m NEG-Micon blade

7.5.4.1 The predicted RCS that was observed for this blade is similar to the blades already discussed. When the blade is pointing upwards a number of peaks can be seen through

the azimuth sweep. The pitches offset the position of these peaks (and the RCS as a whole) by the value of the pitch rotation. As was seen with the previous blades these peaks move in azimuth and merge into two peaks which correspond to the radar being incident at the front and back of the turbine. The RCS of the NEG-Micon blade at various rotations are shown in Figure 7-17 to Figure 7-20.

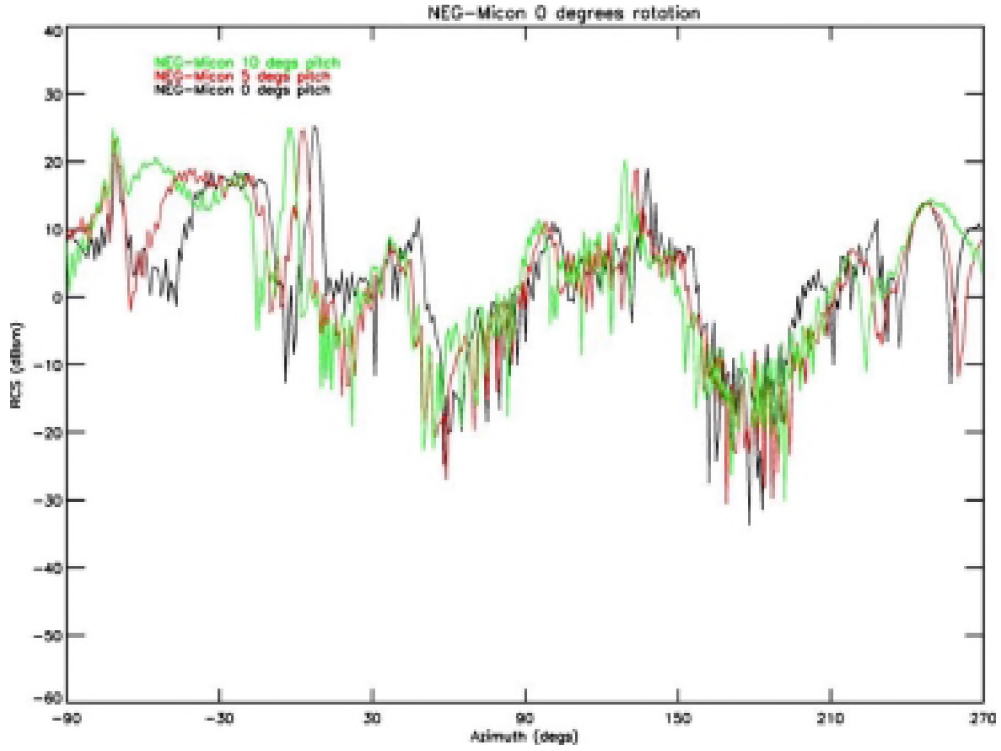

Figure 7-17; NEG-Micon blade after 0 degrees rotation (vertical)

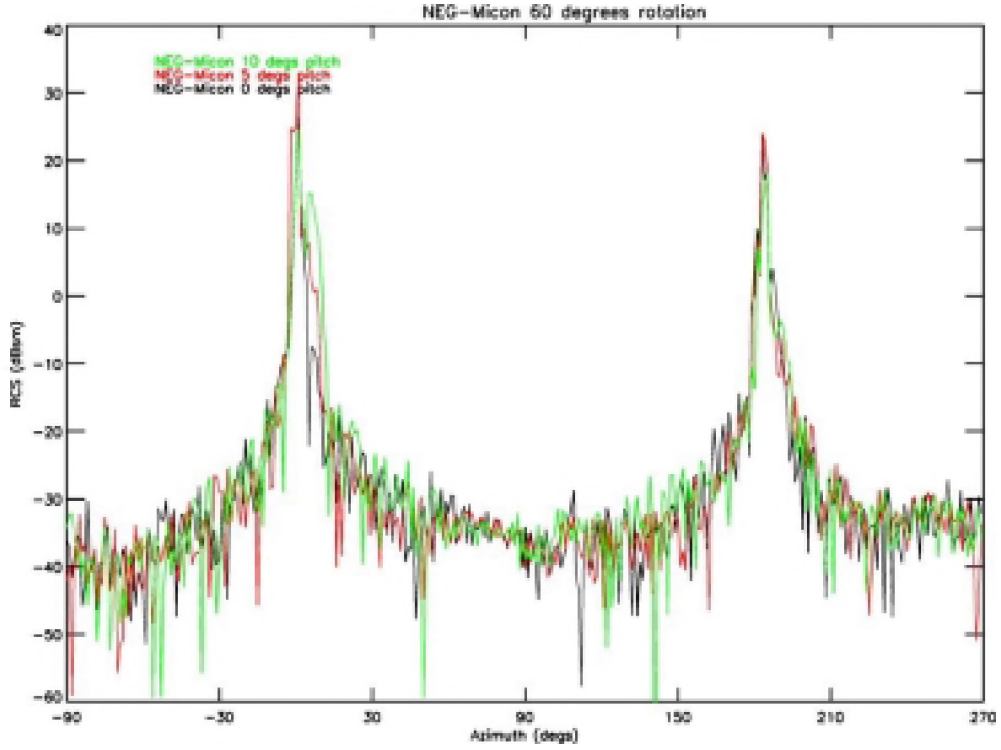

Figure 7-18; NEG-Micon blade after 60 degrees rotation

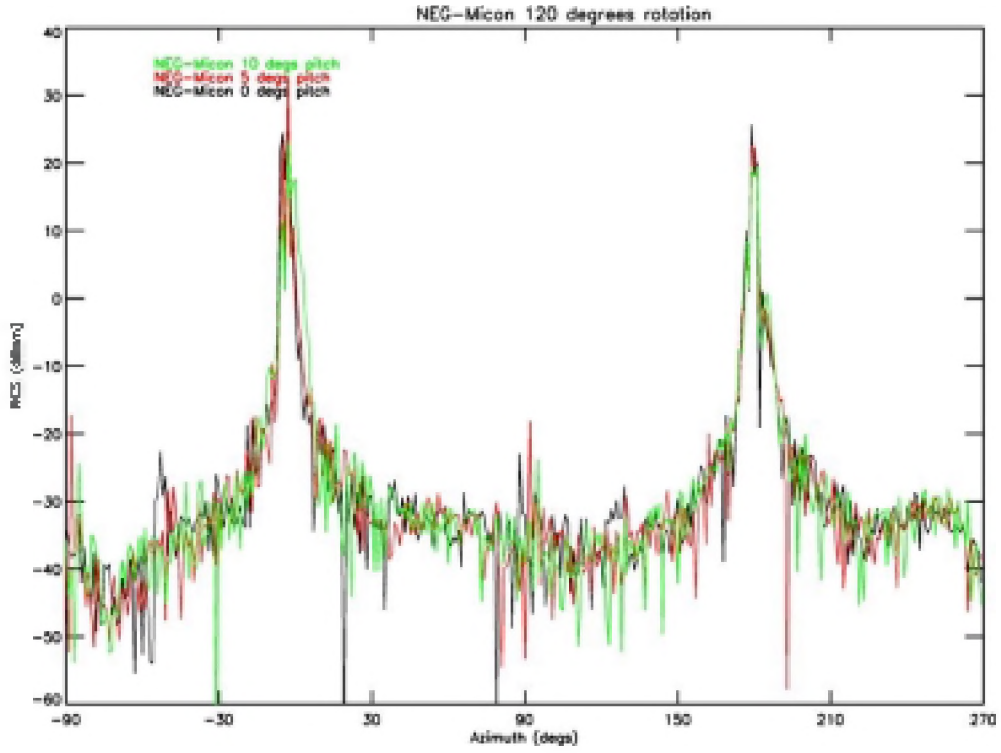

Figure 7-19; NEG-Micon blade after 120 degrees rotation

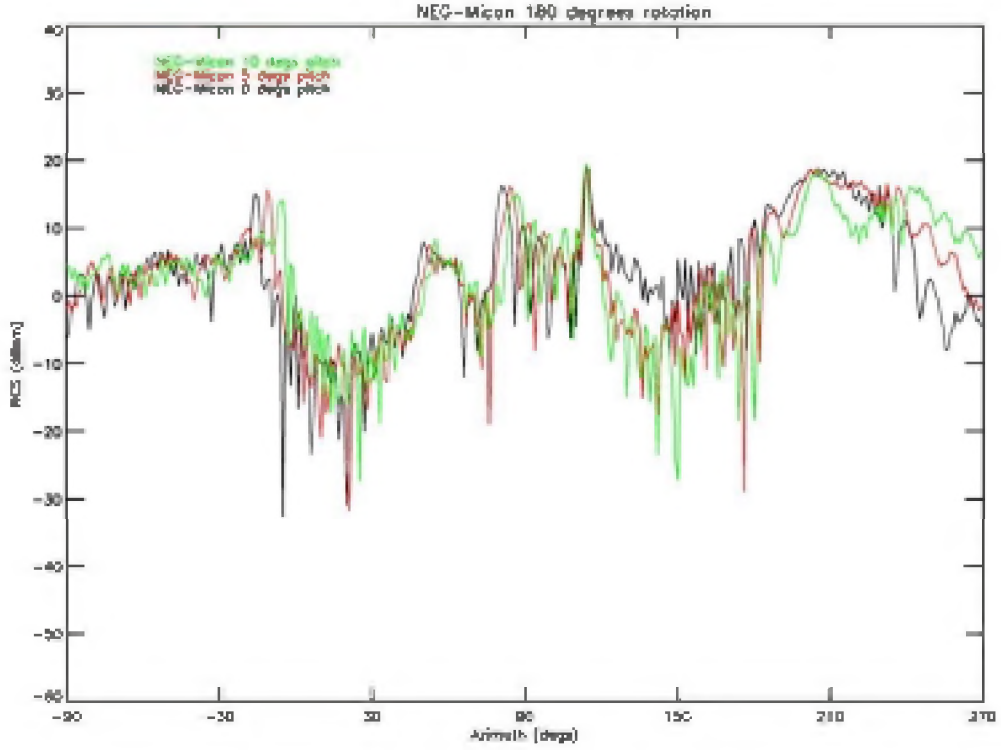

Figure 7-20; NEG-Micon blade after 180 degrees rotation

7.5.5 Discussion

7.5.5.1 From the results for the three blades investigated it can be seen that the trend of the RCS (with respect to yaw angle) during the blade rotation is broadly similar. In each case when the blade was in a vertical position the RCS has several peaks which, during rotation, move in azimuth, and merge into two prominent peaks. One (at 0 degrees azimuth) corresponding to the radar being incident at the front and the other (at 180 degrees azimuth) at the back for the turbine. As the peaks converge the average RCS outside the peak region can be seen to drop from ~0dBsm to below -30dBsm. Throughout the rotation (whilst the blade is away from vertical) the two large peaks remain at the same aspect.

7.5.5.2 The effect of the blade pitch on the RCS is to offset the position of the peaks in yaw angle (when the blade is vertical) by an amount equivalent to the pitch angle. It should be noted that once the blade has moved away from being vertical the effect of the pitch diminishes. The two peaks that emerge tend to be in a position in yaw that is dictated by the large return from the front and back of the blade and not by the pitch of the blade. With the blade away from a vertical position the pitch does not shift the peak returns in yaw but it will alter the magnitude of them as the orientation of the blade is shifted with respect to the radar.

7.5.5.3 From the results we have collected it is clear that finding yaw and pitch angles that result in smaller RCS is problematic. All though it is possible to find yaw and pitch angles which give small RCS from a blade in a fixed point of its rotation, for a complete cycle of the rotor the RCS level will always rise up for part of the cycle at any yaw and pitch angle.

7.5.5.4 To avoid large RCS returns from the blades over a large part of the rotation, avoid the yaw angles close to 0° and 180° (looking at the front and the rear of the turbine). As we move away from these angles towards ±90° the returns from the rotor become intermittent with large sort lived spikes that appear when the blade is close to vertical (up or down).

7.6 Summary

7.6.1 From these key parameters the most important are those that are realistically variable, and do not just reduce radar performance. These are:

- Wind turbine rotor material;
- Wind turbine tower design;
- Wind turbine nacelle design;
- Wind farm layout;
- Radar MTI and other processing.

8 CONCLUSIONS

8.1 Overview

8.1.1 The project objectives were to provide information for the generation of guidelines, by determining the effects wind turbines have on radar systems when sited nearby, and to determine the important parameters. To do this detailed RCS predictions of wind turbines have been carried out and measurements of a real turbine and a scale model blade have been made. A computer model has been built to simulate the effects of wind turbines on radar systems and validated using the measurement data collected.

8.2 RCS Predictions

8.2.1 Models of four turbines have been built in a CAD package to allow RCS predictions to take place. Over 2 million RCS calculations were generated for the turbines over a full range of blade and nacelle positions.

8.2.2 We have explained the features (peaks and troughs) of the RCS patterns for some typical turbine configurations. RCS returns of a whole turbine generally fall between 10 and 30dBsm ($10m^2$ to $1000m^2$). These are large returns typical of aircraft returns the radar is designed to receive.

8.2.3 The data collected have been processed to predict the Doppler spectrum of the wind turbine in different configurations, over a complete rotor revolution. These results show the large expected zero Doppler spike containing all the reflected energy from the stationary parts of the turbine, and significant returns out to the Doppler frequency equivalent to the tip speed of the blades.

8.2.4 For all the data the RCS peaks 6 times a revolution when a blade is either pointing up or down (i.e. a blade edge is pointing straight back at the radar). The main features that affect the RCS of the turbine and could be modified with little impact on turbine operation are:

- Nacelle outer shape and material;
- Tower taper angle.

Clearly the blades have a big effect on the RCS of the turbine and their shape is determined by the aerodynamic requirement of the turbine.

8.3 Computer model development

8.3.1 A computer model called WHIRL has been developed. It consists of two main parts and uses output from two other programs:

- WHIRL-COM: simulates the radar data processing, including radar echoes from wind turbines and an aircraft target;
- WHIRL-DIS: simulates a radar plan position indicator display, using radar echo information output by WHIRL-COM;
- Ocellus: used to compute the RCS of the wind turbines (feeds into WHIRL-COM);
- NEMESIS: used to compute the propagation factor between the radar and the wind turbines and the aircraft target over the local terrain (feeds into WHIRL-COM). The terrain has a resolution of 100m and does not include vegetation or man made structures.

8.4 Radar measurements

8.4.1 Radar measurements have been carried out to validate the RCS predictions, and the output of WHIRL.

8.4.2 High fidelity RCS measurements were carried out on a $1/15^{th}$ scale model of a wind turbine blade in the QinetiQ Compact Radar Range. These data were used to get the full scale equivalent RCS of a blade at 1GHz (using the highest frequency possible in the range). The RCS peaks at about 20dBsm when the leading edge is perpendicular to the radar however, most of the time the RCS is below -10dBsm. These measured data were used to validate the prediction techniques used. Comparison of predicted values with measured values showed excellent agreement and provides suitable evidence of the validity of the predictive modelling methods used.

8.4.3 The main measurement programme was to collect data on a real turbine. This was done on a turbine at Swaffham using the QinetiQ MPR. Data also collected were the turbine parameters (i.e. yaw, blade pitch, and RPM), so the RCS data could be correlated to the turbine configuration. The radar data displayed on the PPI screen of the nearby RAF base radar were recorded for the trials week for final validation of WHIRL. Data over a wide range of yaw angles and in wet and dry conditions were collected.

8.4.4 The results show the RCS of the turbine to be in the range of 20 to 30dBsm most of the time. The largest RCS is seen when a blade is horizontal or vertical (6 times a revolution). At yaw angles close to 90° to the radar (turbine side on) other peaks appear when one blade is horizontal and pointing away from the radar. These returns are likely to be due to multiple bounce returns from either the blades and the tower, or between the blades themselves.

8.5 Validation of WHIRL

8.5.1 The validation of WHIRL was carried out in two separate stages. Firstly, the inputs to WHIRL (propagation and RCS data) were checked against data collected on trial. Secondly, the PPI data collected from RAF Marham were compared with the output display of WHIRL.

8.5.2 The RCS predictions were shown to reproduce the peaks and basic trend of the measurement data for a number of representative turbine configurations. Differences in the absolute levels of the predictions and the measurements of between 4 and 6dBsm were observed. This is a result of two main factors:

- The blades are modelled as solid fibreglass bodies. The properties of the fibreglass we used give rise to an 8dB reduction in the returns emanating from the blades. The blades appear to be more reflective increasing the level of the measurement data over the predictions;
- The predictions carried out do not model any returns resulting from multiple bounce interactions within the turbine structure. The Ocellus prediction code is capable of predicting these returns from a structure, but was not computed because of the computational overhead involved. Without this mechanism the predictions will be lower than the measurement where strong multiple bounce returns are present.

8.5.3 To overcome this difference we must deal with both of these factors. The turbine blades need to be modelled with a more realistic reflectivity and the multiple bounce calculations must be included in the turbine calculations.

8.5.4 Having said that the difference in the current predictions is small and as the predictions follow the pattern of the RCS they are deemed appropriate and sufficient for use in WHIRL.

8.5.5 To further validate the predictions we have looked at the spectral content of the returning signal as compared to the measured data. The spectra were calculated using a complete revolution of the rotor and shows the frequency content averaged over the whole cycle.

8.5.6 The main features of the measurements and the predictions matched well. These were the large zero Doppler spike showing a large part of the turbine has no movement relative to the radar (tower and nacelle) and the sharp cut-off at a frequency that corresponds well with the tip speed of the turbine in each case. The measurement data are not as distinct in its highest frequency component as there are clutter returns in the measurements which cause the noise floor level to be higher. Also the real turbine has more degrees of freedom with vibration, sway and flex which will all give rise to spectral components which are not modelled in the prediction.

8.5.7 The propagation code used as an input to WHIRL was validated by comparing its output with a validated American propagation code. Both showed similar results. A number of references are also given to other QinetiQ work that have validated the QinetiQ code using measurement data in the past. The propagation code used only considers effects of the terrain and does not include any extra screening caused by vegetation or man-made obstacles.

8.5.8 The display output from WHIRL has been compared to the display recorded from RAF Marham's primary radar. The simulation agrees well with the recorded video for most turbine configurations. The model is shown to be between 93% and 98% accurate for these configurations. The turbine configuration that did not agree as well (62% accurate) was when the turbine was yawed straight at the radar. The MTI filter in the model is too idealised and filters the turbine more effectively than the real radar.

8.5.9 Although no actual trial took place at Prestwick some video data were collected of the nearby multiple turbine wind farm appearing on the radar PPI display. A simulation was run of this wind farm with the turbines in a "typical" configuration. Results are encouragingly similar, but without a proper trial no real conclusions can be drawn.

8.6 Key factors influencing the radar signature of wind turbines

8.6.1 In this section we have detailed the key factors influencing the radar signature of wind turbines identified to date and the respective lessons learned. These are at a high level and detailed below.

8.6.2 The key turbine factors influencing the effect of the turbine on radar are:

- the design of the tower and nacelle should have the smallest RCS signature possible;
- RCS of the tower and nacelle can be effectively reduced though careful shaping;
- Large turbines do not necessarily lead to large RCS (i.e. tower height does not greatly affect RCS);
- Blade RCS returns can only be effectively controlled though the use of absorbing materials;
- For low probability of detection, but a large clutter return, set wind turbines such that they are mainly yawed close to ±90° from the radar direction;
- For high probability of detection, but a smaller area of clutter, set wind turbines such that they are mainly yawed close to 0° and 180° from radar direction;
- If blades are pitched by x° avoid yaw angles near x° and 180+x° as a high probability of detection of clutter will occur here.

8.6.3 The key factors influencing the effect of wind farms on radar are:

- Spacing of wind turbines within a wind farm needs to be considered in the context of the radar cross range/down range resolutions. Spacing the turbines such that only one turbine can appear in any range cell has advantages in identifying the wind farm, filtering out the turbines and in tracking aircraft over the farm area;
- In a circumstance where a single wind turbine in clear LoS to the radar is undetected, it is highly likely that a wind farm of similar wind turbines would also be undetectable;
- No optimal layout or format has been prescribed as each wind farm will have its own specific requirements dependent on many factors;
- The resolution of the radar in cross range is a function of the distance between the radar and the wind farm and the radar beam width. The downrange resolution is dependent on the pulse width of the radar involved and is typically in the range of 50-300 metres.

8.6.4 Key terrain factors:

- In non LoS cases, the level of detectability of the wind farm is dependent on the frequency of radar and the distance from the wind farm to the point of diffraction and the distance below the LoS horizon, where the wind farm is located;

- Direct LoS between wind farm and radar should be avoided wherever possible. This does not mean that in some cases wind farms outside the LoS cannot be detected.

8.6.5 Key shadowing factors (for more details see appendix B.5):

- Single wind turbines do not create a significant 'radar shadow'; Any shadow region is only dark to a distance of a few hundred metres behind the turbine.
- Beyond this there is some reduction of the radar power, and a time-variation, but these will not prevent detection except possibly for very small targets.

8.7 Summary

8.7.1 So to summarise during this project the following things have been achieved:

- Detailed RCS predictions of wind turbines have been completed;
- Size of the scattering has been quantified and the key scattering sources have been identified;
- A model has been developed that will predict the effect of wind farms on primary radar systems;
- Detailed radar measurements of a real turbine have been collected and the radar returns related to the configuration of the turbine;
- The RCS predictions have been validated against the collected measurement data with a good level of agreement;
- The final output of the model has been validated against a single turbine and has shown encouraging results against a multiple turbine site.
- The key factors influencing the radar signature of wind turbines have been identified and interpreted.

This page is intentionally blank

9 RECOMMENDATIONS

9.1 All wind turbine/wind farm developer's and aviation stakeholders should read and digest the detailed factors influencing the radar signature of wind turbines, which have been generated by this project (Section 2).

9.2 Consider the influence of the turbine to include static and moving parts. Main areas for consideration are as follows:

- Design both the tower and nacelle such that they can never present a flat/concave surface to the radar boresight. (Consider the relative geometry of the radar boresight to the wind turbine).
- The nacelle material can be one of three options: *Reflective* – this implies a high RCS and thus no problems can be raised in regard to the internal mechanisms; *Radar Absorbent* – this implies a low RCS and thus no problems can be raised in regard to the internal mechanisms, however this also implies a potentially higher cost; *Transmissible* – this implies that the internal mechanisms will need to be considered.
- Accepting that fibreglass is currently the dominant material in blade manufacture, where possible the materials of the blades should follow the same process as for the nacelle detailed above. With specifically designed radar absorbing materials and structures reductions in the returns from the blades could be achieved.

9.3 Consider the influence of the layout of the wind farm. If one wind turbine with a clear LoS to the radar is unobservable then this implies that any number of the same wind turbine should also remain unobservable.

9.4 If the wind turbines are likely to be visible to the radar consider the following:

- The spacing needs to be considered in the context of both cross range and down range resolutions. Note: It is very difficult to discriminate genuine targets from wind turbines if the spacing is less than or equal to the resolution of the radar;
- Wind turbine layout needs to be chosen to incorporate the depth and extent of shadowing created.

9.5 Consider the influence of the radar functionality and set up. Specifically consider:

- The radar function (it may not be ATC);
- What are the cross-range and down-range resolution values;
- What is its respective scan rate i.e. what is acceptable in terms of target detection;
- What filters are they using (especially the MTI characteristics).

9.6 The results from the project (modelling and field trials data) have enabled us to provide a much more detailed quantification of the complex interactions between wind turbines and radar systems than was previously available.

9.7 The model has the potential to be a valuable tool to:

- Generate the detailed data required for a more sophisticated initial screening tool than is currently available;
- Support the development of future solutions – wind turbines (tower, nacelle and blades) with lower RCS signatures and enhanced radar filters which are able to remove the returns from wind turbines.

9.8 The model has shown accurate predictions for a single turbine; however, in reality most sites will have multiple turbines. As part of the project a simulation was run for an existing multiple turbine wind farm near to Prestwick airport and the results were compared to video data collected from the airport radar PPI display. The model predictions were encouragingly similar. However, to extend the validation of the model for the multiple turbine scenario, a further field trial should be carried out at a multiple turbine site.

10 ACKNOWLEDGEMENTS

10.1 QinetiQ would like to thank the following companies for their help with planning and running the trials:

- Enercon;
- Ecotricity (esp. Simon Vince for on site help);
- Flight Refuelling Limited;
- RAF Marham ATC personnel;
- Prestwick Airport ATC;
- Vestas;
- Scottish Power;
- Ingenco.

10.2 Information on turbine design and operation required for the predictions and setting up of the model were supplied by:

- NEG Micon Rotors;
- Vestas;
- Enercon/Ecotricity;
- Renewable Energy Systems Ltd;
- National Wind Power.

This page is intentionally blank

11 LIST OF ABBREVIATIONS

ATC	Air Traffic Control
BPSS	Blade Position Sensor System
CAD	Computer Aided Design
dBsm	Decibel square metres
FES	Future Energy Solutions
FRL	Flight Refuelling Limited
GPS	Global Positioning System
LoS	Line of Sight
MPR	Multiple-band Pulsed Radar
MTI	Moving Target Indicator
PPI	Plan Position Indicator
RAF	Royal Air Force
RCS	Radar Cross Section
RPM	Revolutions Per Minute
SCADA	Supervisory Control and Data Acquisition
TDC	Top Dead Centre
VHF	Very High Frequencies
WHIRL	Wind farms Having Interactions at Radar Locations
ZD	Zero Doppler

This page is intentionally blank

A RCS MODELLING OF WIND TURBINES

A.1 Approximations in CAD models

A.1.1 The drawings supplied on the wind turbine design allowed the basic turbine shape to be built as a CAD model, but not all the information required could be gained from this information. Therefore a number of estimates about the turbine shape had to be made. All the estimates are based on images of the turbines and QinetiQ measurements, and should be representative of the actual turbine.

A.1.2 Vestas V47 at Hare Hill

A.1.2.1 The following estimates were required to complete the model of the Vestas V47 turbine at Hare Hill:

- Curvature between blade root and aerofoil section;
- Curvature down the length of the blade aerofoil section;
- Attachment of the blades to the hub;
- No internals modelled;
- No minor features (external ladder, access doors, wind vane);
- Hub, nacelle, and nose cone all assumed to be metal (or as reflective as metal);
- Angle of blades when at minimum pitch

A.1.2.2 The following estimates were required to complete the model of the Enercon E-66 at Swaffham:

- Curvature between blade root and aerofoil section;
- Curvature down the length of the blade aerofoil section;
- Attachment of the blades to the hub;
- No internals modelled;
- No minor features (external ladder, access doors, wind vane);
- Hub, nacelle, and nose cone all assumed to be metal (or as reflective as metal);
- Nacelle size and where it is attached to the tower;
- Glass in viewing platform is transparent to radar;
- Position of platform on tower;
- Angle of blades when at minimum pitch.

A.2 Main Enercon turbine dimensions

A.2.1 The following table lists the key dimensions of the modelled Enercon turbine

Tower Height (m)	64.7
Tower base diameter (m)	4.17
Tower top diameter (m)	2.18
Blade length (m)	30.8
Rotor diameter (m)	66.4
Rotor Tilt angle (°)	3.5
Maximum Blade width (m)	3.97

Table A-1; Main dimensions of the modelled Enercon Turbine.

A.3 Details of data collection technique

A.3.1 Large quantities of data were required on each of the turbines built in the CAD package. To collect all these data in an efficient manner required developing a technique to do this with as little user intervention as possible. The following technique was devised.

A.3.2 In the CAD package the moving part of the turbine (the rotor) was modelled separately from the tower and nacelle. For each pitch angle required, a different rotor had to be created with the blades in the correct position.

A.3.3 The existing QinetiQ RCS prediction code is designed to read in a model and then carry out RCS predictions at different aspect angles and frequencies. We effectively had different models for each blade pitch angle and for every different position of the rotor. With 2400 blade positions, 4 turbines and 3 pitch angles this gives a total of 28,800 input models to predict. It was impractical to create this number of input models simultaneously. It was also very time consuming to output this many models from the CAD package. To overcome this problem we wrote code to take a base input model of the turbine and rotated the rotor by a set angle. This means we can create any rotor position from one output CAD model. This reduced the number of models needed from the CAD to 12 (4 turbines and 3 pitch angles).

A.3.4 The concept was to carry out a prediction on each blade position collecting all the required yaw angles and frequencies. Once one blade position is completed the rotor is rotated by an angular increment and the input file overwritten so avoiding disk storage problems.

A.3.5 This method creates an output file for each blade position, turbine and pitch angle. To make this data more manageable all the output files for a single turbine were compressed into one binary file. From this file, data can be read into post processing software and the data analysed.

A.4 Effects of internal structure

A.4.1 To assess the validity of ignoring internal structure from the predictions a few predictions were carried out. One of the blade designs supplied for the work was predicted on its own as a solid fibreglass model (see Figure A-1). Then in a separate prediction a lightning conductor running up the centre of the blade was predicted. This was modelled as a metal wire running the complete length of the blade. Its diameter is 50mm.

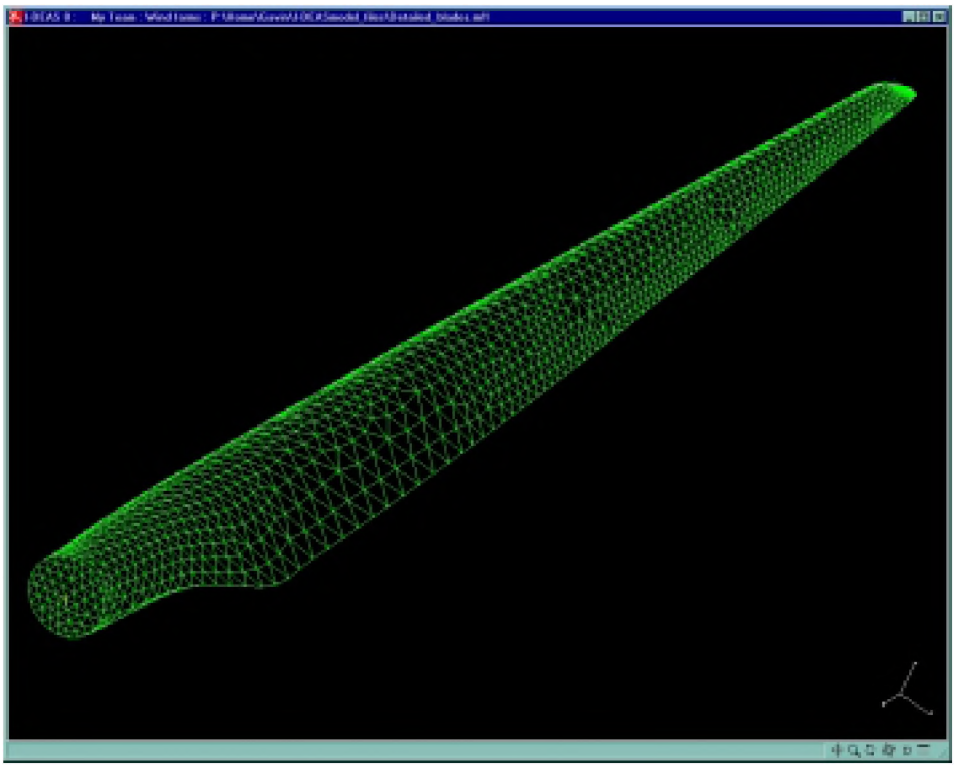

Figure A-1; Blade used for prediction

A.4.2 The results from the predictions are shown in the following three graphs. Figure A-2 shows the RCS of the blade and the conductor separately. It can be seen that for most angles the conductor RCS is significantly smaller than the blade RCS. Figure A-3 compares the blade RCS with the coherently combined RCS of the blade and the conductor. The differences are not great. To make this clearer Figure A-4 shows the same plot but with the data's rapid variation smoothed out. On the graphs the leading edge of the blade is normal to the transmitter at 180°, the trailing edge at 0°, the blade tip at 270° and the blade root at 90°. The return at 90° will not be seen when the blade is in use as this is the end where the blade joins the turbine.

A.4.3 This shows that with a wire conductor running down the blade its effect on the blade RCS is of second order, and so not of great significance.

A.4.4 The results show that when the returns from the wire conductor are added to the return from the blade the differences are small. The effects are likely to be even smaller than this in the real situation as the conductor is not directly illuminated by the radar, but only illuminated by the portion of the energy passing though the blade's fibreglass shell.

A.4.5 On the basis of these results and considering the complexities of modelling the internals of the blade it is sensible to concentrate on predicting the outer skin.

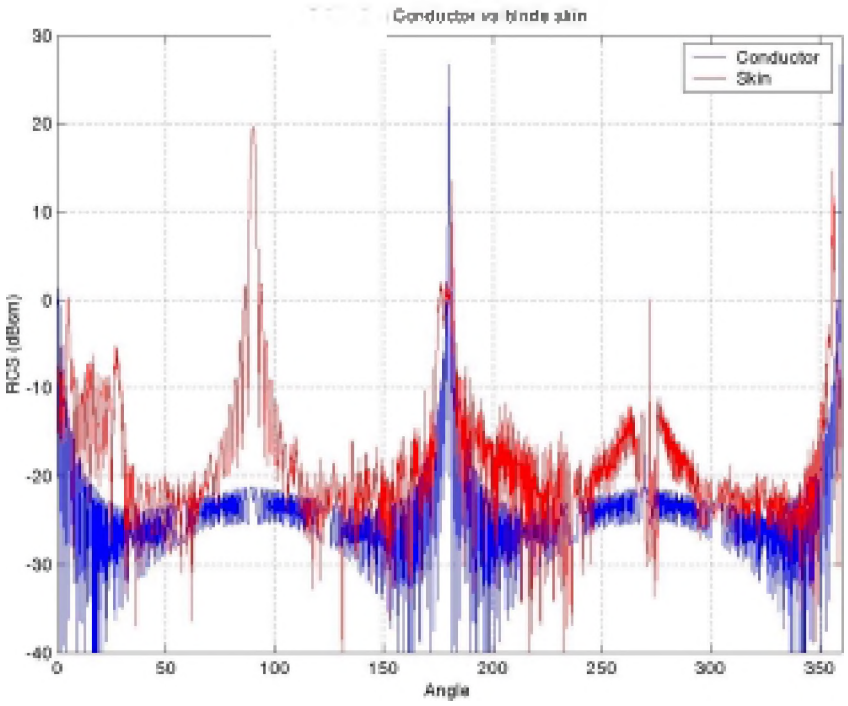

Figure A-2; RCS of lightning conductor and fibreglass blade

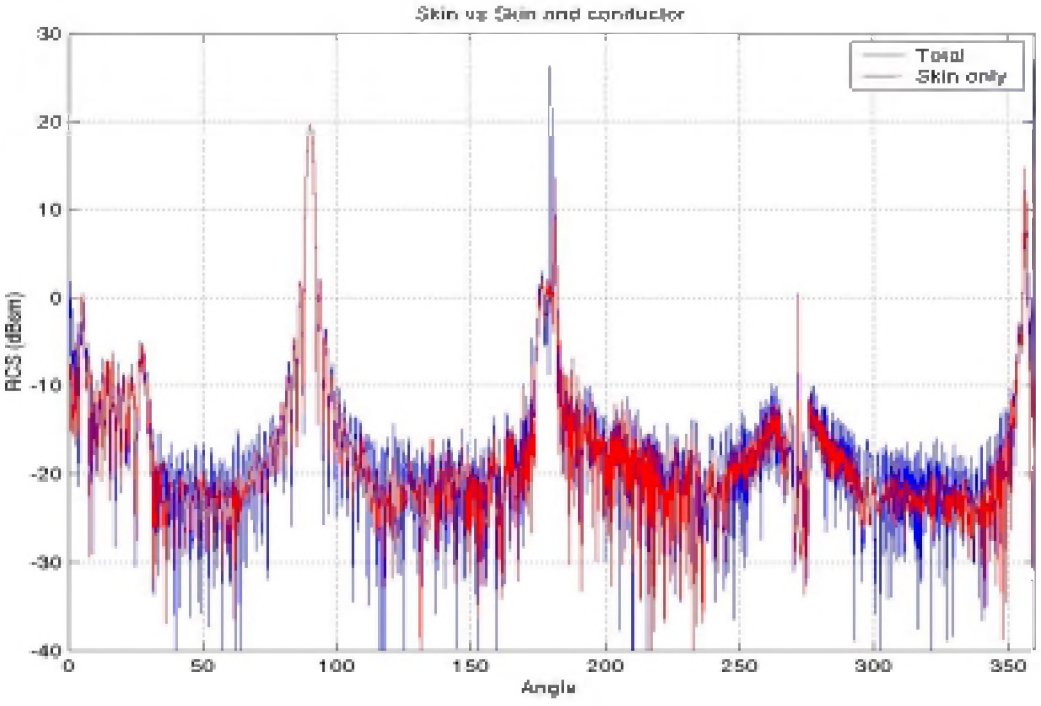

Figure A-3; RCS of blade with and without lightning conductor

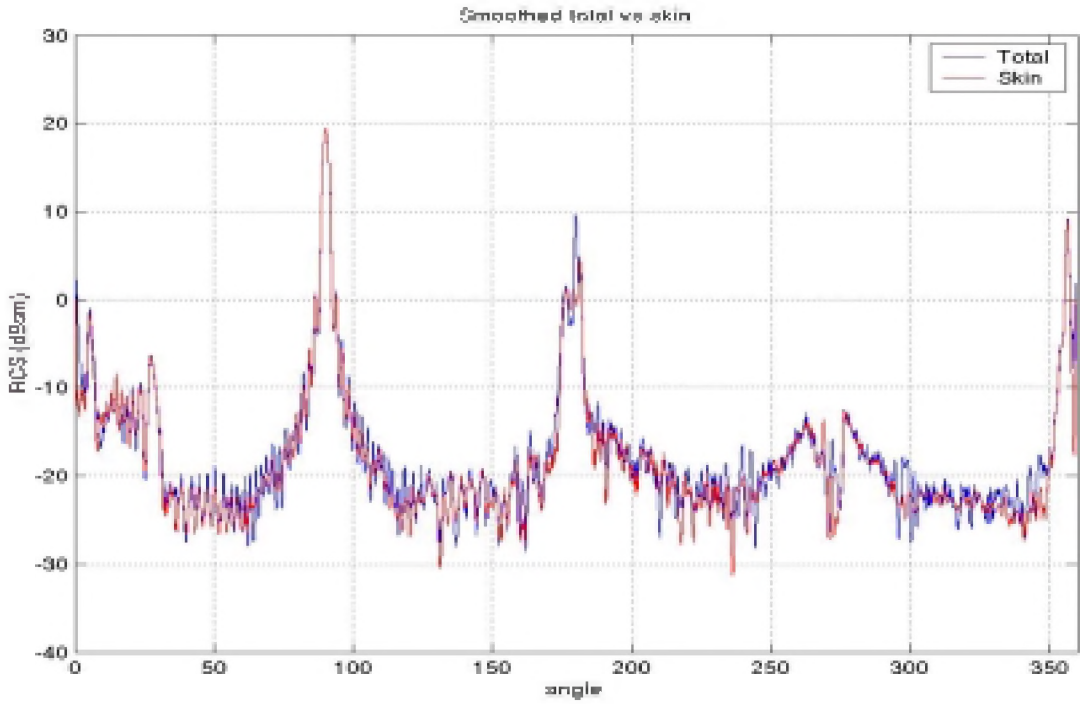

Figure A-4; Smoothed version of Figure A-3.

A.5 Further results

A.5.1 In this appendix a greater selection of RCS plots from the predictions of the turbines in different configurations is shown.

A.5.2 Figure A-1 to Figure A-3 show the changes in the RCS when varying the pitch angle of the blades on the Enercon E-66 turbine. Figure A-4 to Figure A-6 show the RCS of the Enercon tower and nacelle with different blades attached. Figure A-7 to Figure A-9 show the effects of different blades on the Vestas V47 turbine. It should be noted that Figure A-9 shows a very high RCS, as compared to all the other plots. This is due to the turbine nacelle, which at this yaw angle presents a large flat surface to the radar. This gives a very undesirable large return that could be eliminated by angling this surface so energy is not sent directly back to the radar.

A.5.3 Figure A-10 and Figure A-11 show the differences between 1.5GHz predictions and 3GHz predictions. The differences are quite small. The aspect angle axis in these graphs is the yaw angle of the nacelle and rotor, and the blades are not spinning. In all other plots the yaw angle is constant but it is the rotor's motion that gives the variation in RCS.

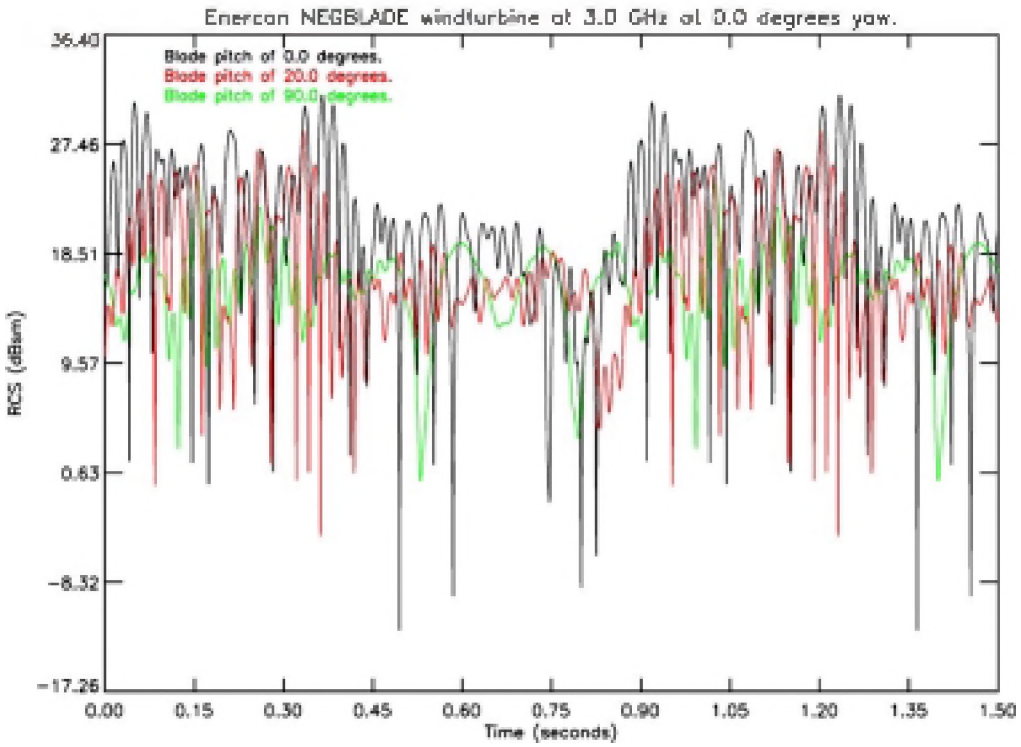

Figure A-1; Predicted RCS of Enercon E-66 showing variation with blade pitch at a yaw angle of 0°. Freq. = 3GHz, Linear polarisation.

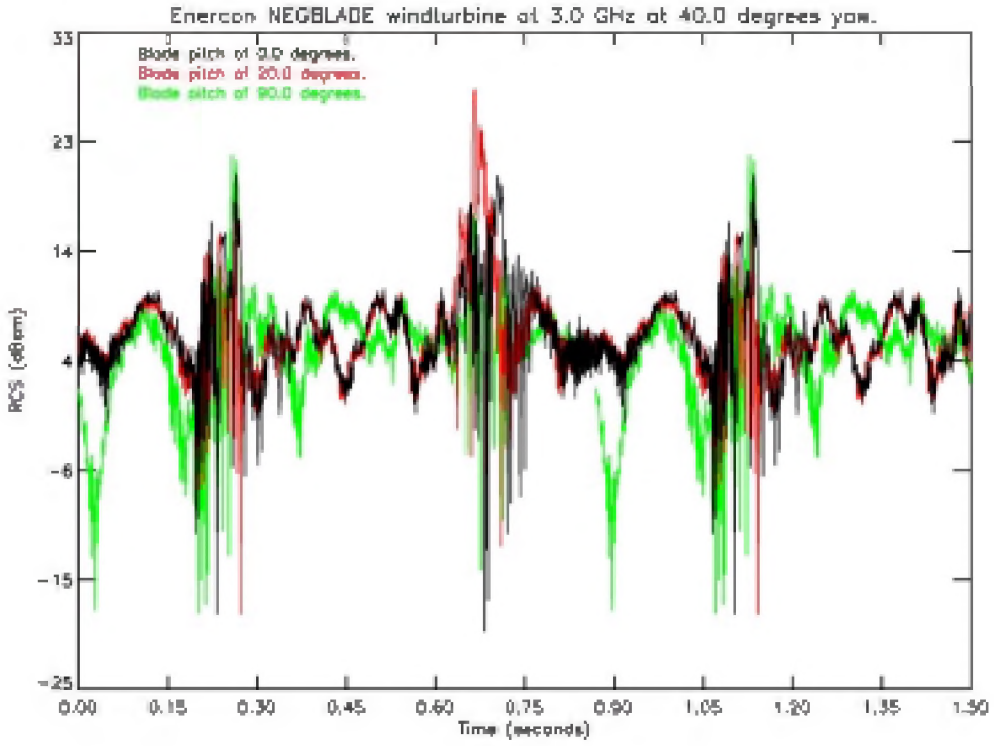

Figure A-2; Predicted RCS of Enercon E-66 showing variation with blade pitch at a yaw angle of 40°. Freq. = 3GHz, Linear polarisation.

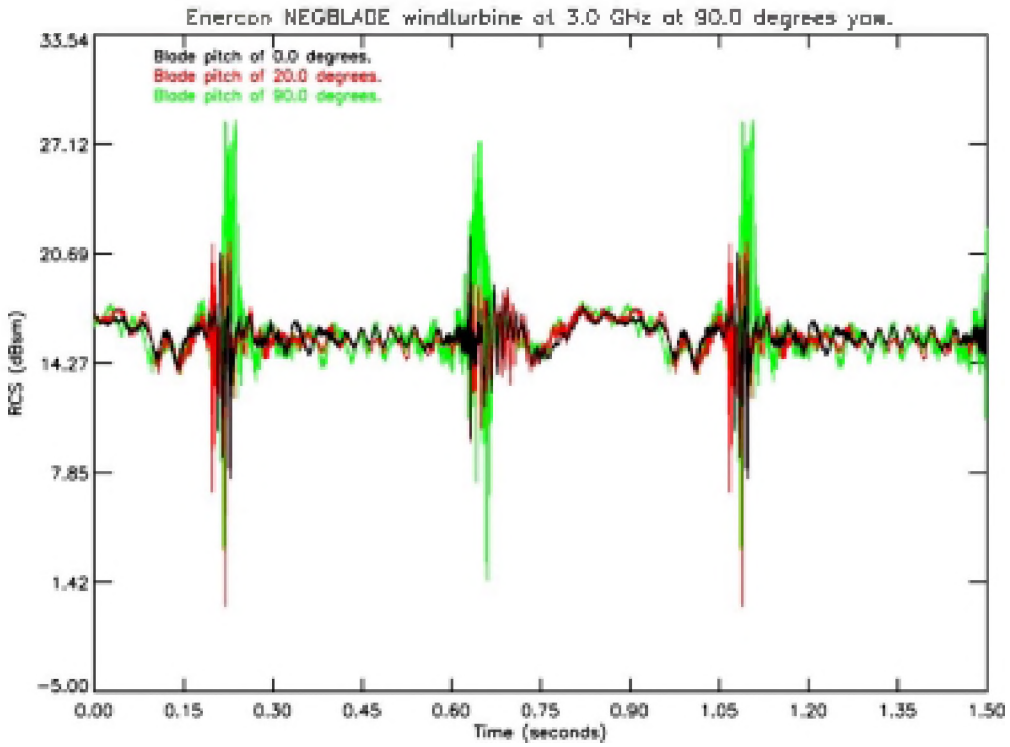

Figure A-3; Predicted RCS of Enercon E-66 showing variation with blade pitch at a yaw angle of 90°. Freq. = 3GHz, Linear polarisation.

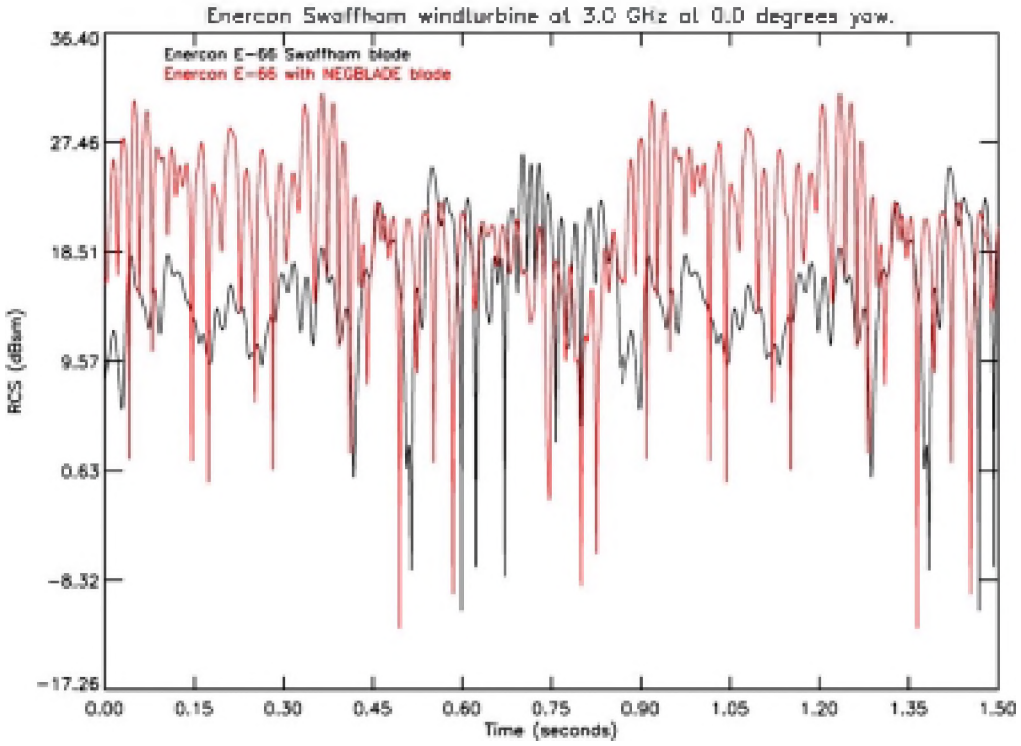

Figure A-4; Predicted RCS of Enercon E-66 showing variation with two different blade designs at a yaw angle of 0°. Freq. = 3GHz, Linear polarisation.

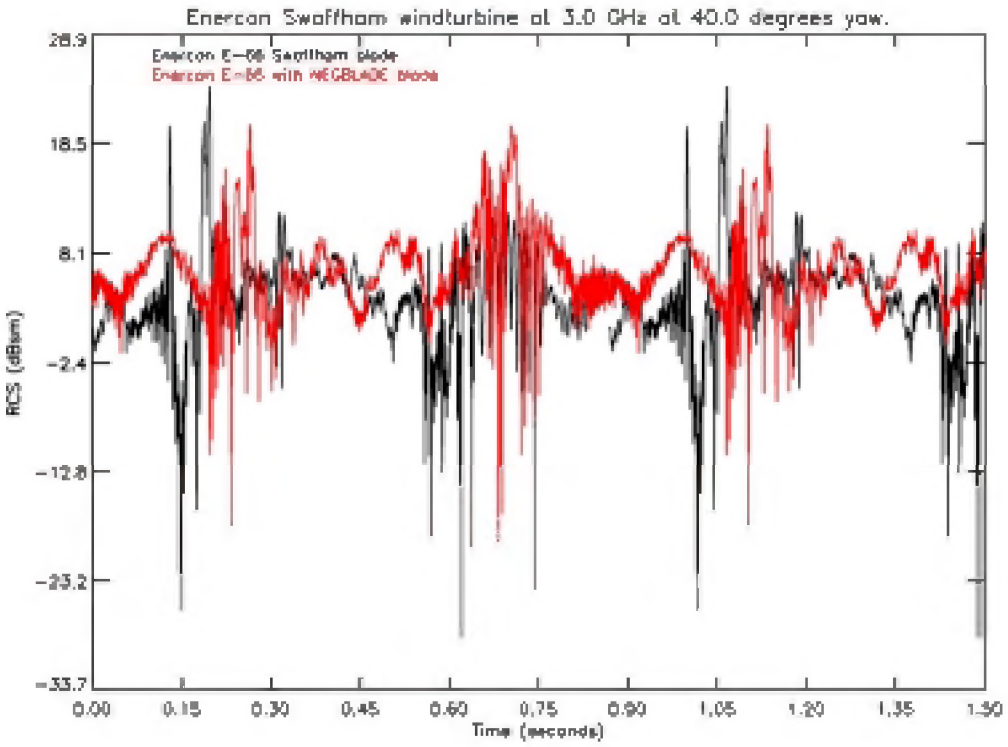

Figure A-5; Predicted RCS of Enercon E-66 showing variation with two different blade designs at a yaw angle of 40°. Freq. = 3GHz, Linear polarisation.

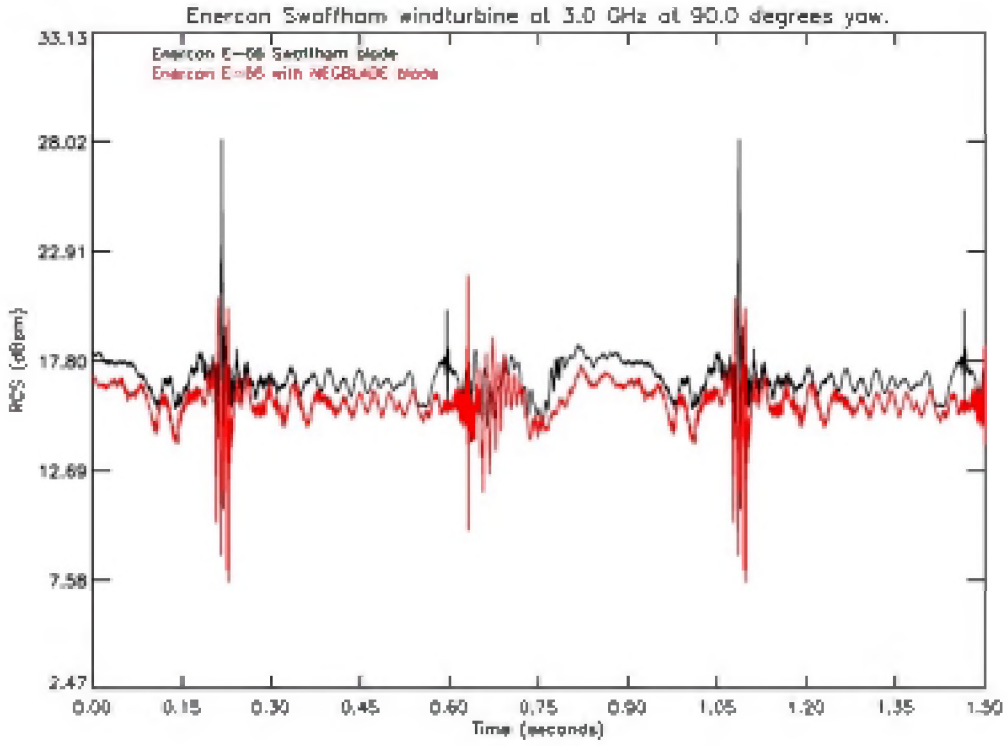

Figure A-6; Predicted RCS of Enercon E-66 showing variation with two different blade designs at a yaw angle of 90°. Freq. = 3GHz, Linear polarisation.

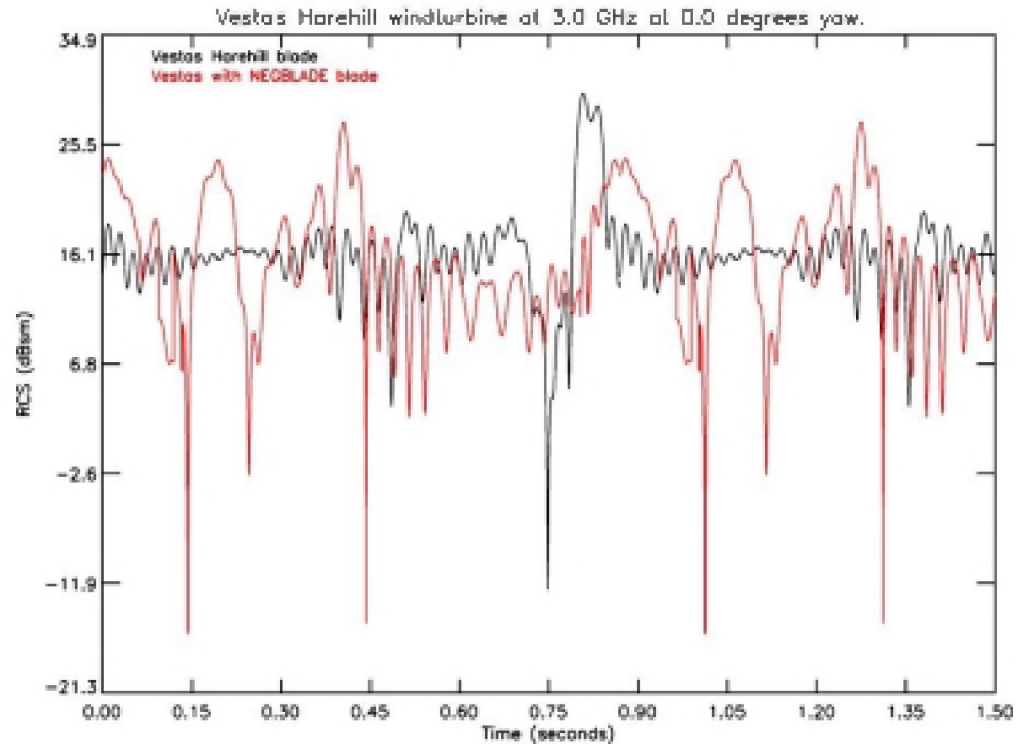

Figure A-7; Predicted RCS of Vestas V47 turbine showing variation with two different blade designs at a yaw angle of 0°. Freq. = 3GHz, Linear polarisation.

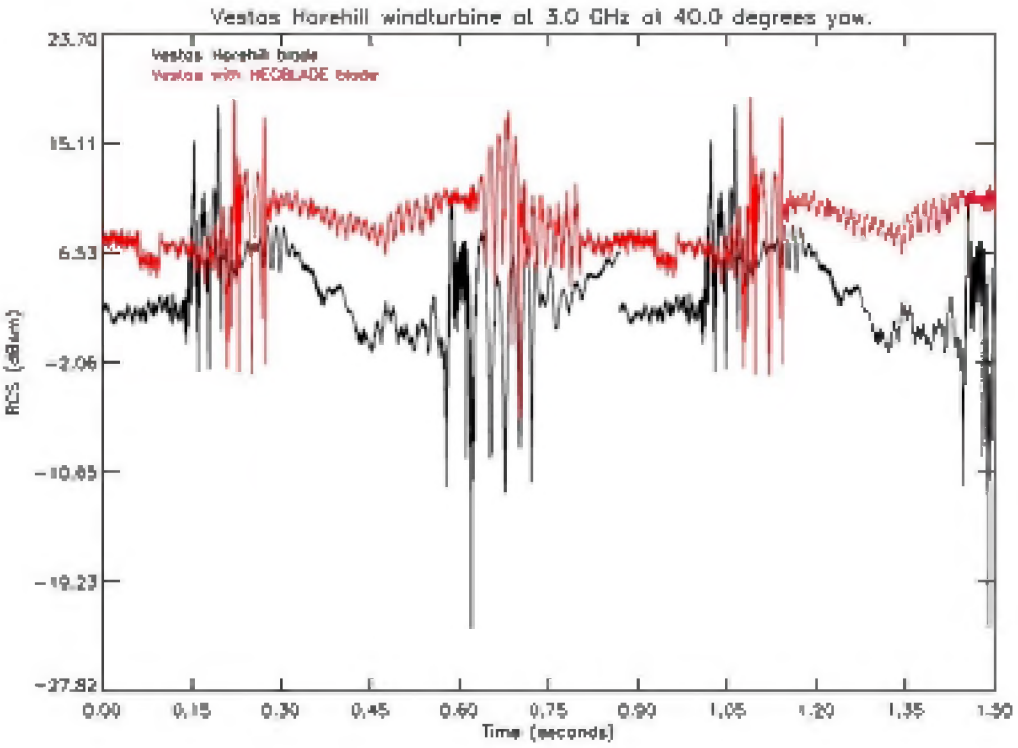

Figure A-8; Predicted RCS of Vestas V47 turbine showing variation with two different blade designs at a yaw angle of 40°. Freq. = 3GHz, Linear polarisation.

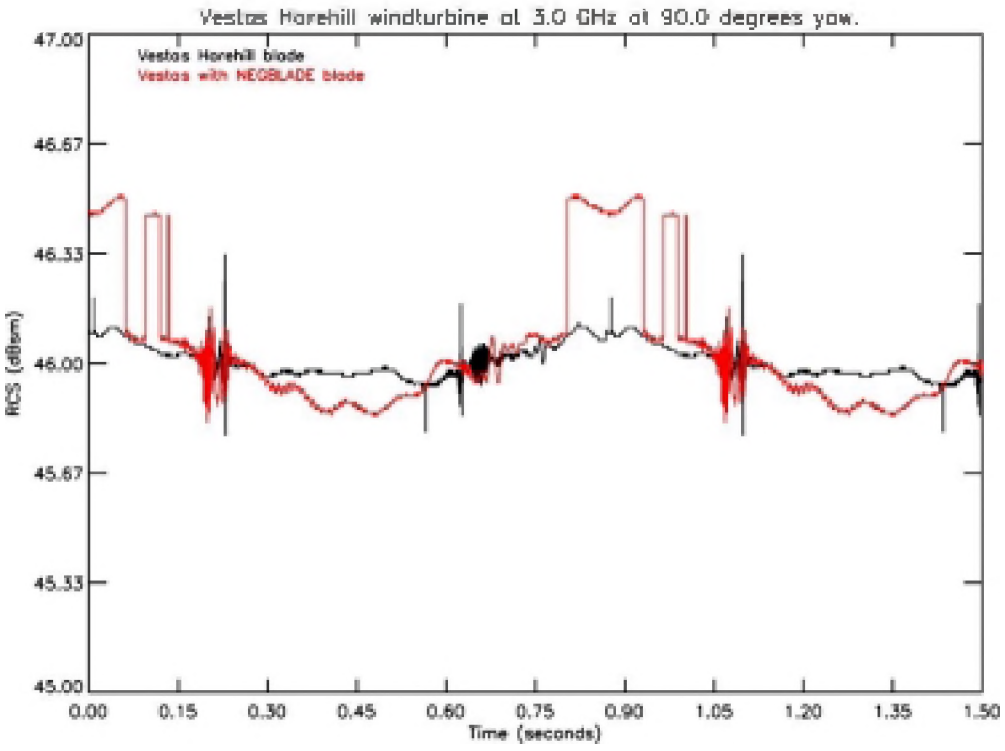

Figure A-9; Predicted RCS of Vestas V47 turbine showing variation with two different blade designs at a yaw angle of 90°. Freq. = 3GHz, Linear polarisation. (Very high RCS is due to the design of the nacelle when viewed from this yaw angle).

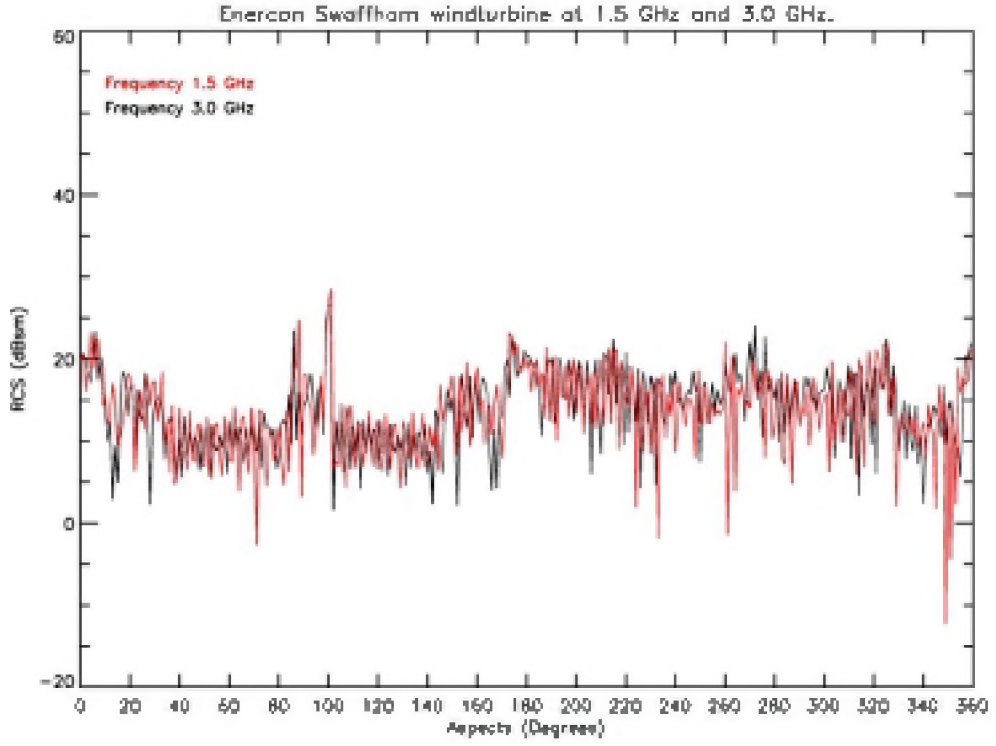

Figure A-10; Predicted RCS of Enercon E-66 turbine showing the difference between 3GHz and 1.5GHz. The turbine blades are stationary and the yaw angle is rotated though 360°. Linear Polarisation.

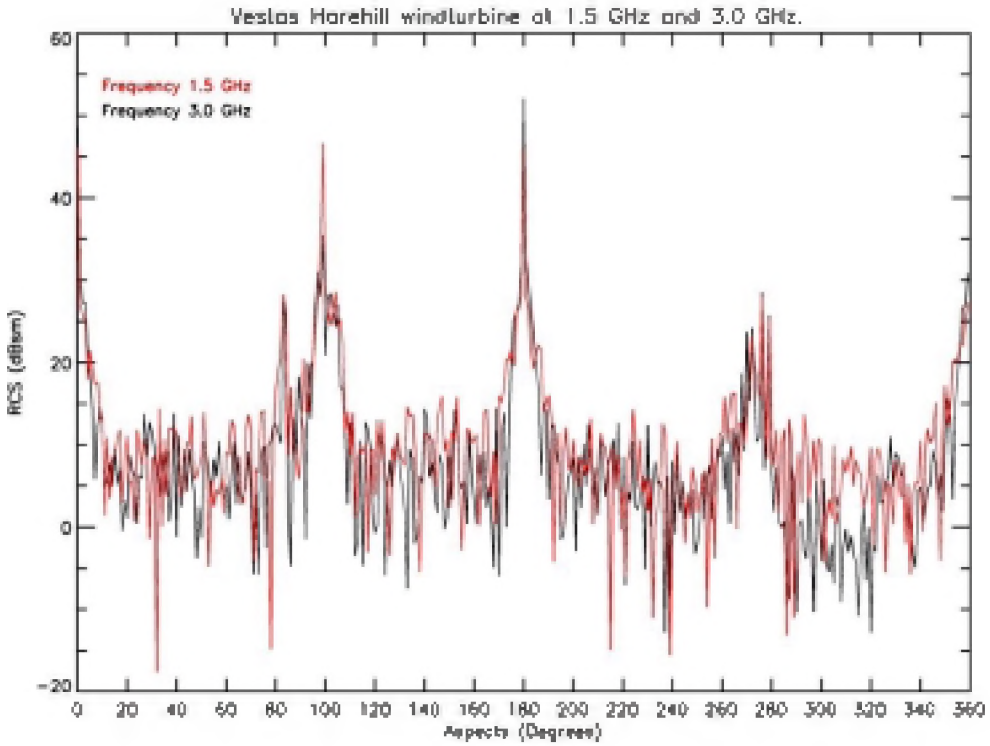

Figure A-11; Predicted RCS of Vestas V47 turbine showing the difference between 3GHz and 1.5GHz. The turbine blades are stationary and the yaw angle is rotated though 360°. Linear Polarisation.

This page is intentionally blank

B DETAILED MODEL DESCRIPTION

B.1 WHIRL COM

B.1.1 Introduction

B.1.1.1 WHIRL-COM performs the computational work of simulating the reflection of radar signals from a target aircraft and one or more turbines, and tracing the echoes through appropriate radar signal processing.

B.1.1.2 WHIRL-COM consists of four main sections:

- Graphical user interface, which allows the user to input data on the scenario to be modelled, and controls the running of the subsequent computation.
- Calculates geometry of motion of aircraft target, and rotation of turbine blades.
- Radar equation calculation, taking into account rotation of the antenna beam, the propagation factor from radar to aircraft target and turbines, and RCS as the aircraft target moves and the turbine blades rotate.
- Simulates radar data processing, including pulse integration, moving target indication, and noise-related thresholding. The outputs are confirmed detections for WHIRL-DIS to process.

B.1.2 Input data

B.1.2.1 The following variables defining the scenario to be modelled are input through the Graphical User Interface. The GUI also provides the means for saving the current scenario variables into a file, and to load the scenario variables from a pre-existing file. It also provides the means for obtaining a hard copy of the variables for record purposes.

B.1.2.2 Radar parameters:

- radar_x, radar_y, radar_z: position of radar (m).
- PRF: pulse repetition frequency (Hz).
- power: radar transmitted power (W).
- radar_frequency: radar frequency (Hz).
- radar_RPM: radar revolutions per minute.
- gain_start: initial azimuth angle of radar antenna (radians).
- pulses_integrated: number of pulses integrated.
- integration_efficiency: efficiency factor (0 to 1) of integration.
- dynamic_range: dynamic range of signal processing (dB).
- noise_bandwidth: noise bandwidth (Hz).
- tolerance: detection threshold relative to noise level (dB).
- Beamwidth: antenna beamwidth (degrees).
- pulse_length: Radar pulse length (secs).

B.1.2.3 Turbine parameters:

- turbine_number: Number of turbines present.

B.1.2.4 Arrays, with an entry for each turbine:

- turbine_x(), turbine_y(), turbine_z(): turbine position (m); z is the height of hub above mean sea level.
- turbine_z_above_ground(): hub height above ground level.
- turbine_tilt(): turbine pitch (degrees).
- turbine_bearing(): turbine bearing (yaw: angle about vertical axis).
- turbine_RPM(): turbine revolutions per minute.
- blade_pos_start(): Position angle of blades at start of simulation (degrees, from 0 to 120: -1 indicates a random starting position).

B.1.2.5 Target (i.e. aircraft) trajectory data:

- x_start, y_start, z_start: starting position (m).
- x_finish, y_finish, z_finish: finishing position (m).
- target_speed: target speed (m/s).
- target_rcs: RCS of target (square metres).

B.1.3 Computations: initialisation and geometry

B.1.3.1 The computations of WHIRL-COM are set in motion by the user pressing the {RUN} button of the Graphical User Interface. If the data have changed since the last save, the program asks the user whether the current scenario data should be saved; if "yes", the user is prompted for a file name, and the scenario data are saved in the file.

B.1.3.2 The program reads in a data file containing the RCS values for a turbine, as a function of the angular aspect of the blades (yaw: bearing of the rotation axis; pitch: angle of the blade rotated about its own length; and rotational position about the normal rotation axis), and frequency. This file is constructed from the output of the Ocellus RCS prediction program (see section 4).

B.1.3.3 The program also reads in another data file containing propagation factors from the radar, as a function of position (range, bearing, height). This file is output by the NEMESIS propagation software (see section 5).

B.1.3.4 The program computes the position of each turbine relative to the radar position, and expresses it in polar co-ordinates (range, elevation, bearing).

B.1.3.5 The program operates in a series of time-steps. One time-step occurs for each radar pulse, which means that the time step is typically 1 millisecond. The total time interval is defined by the starting and finishing positions of the target aircraft, and the speed of the aircraft. This should be at least several seconds to see the effects of the turbine blade as it rotates. Thus in order to model each pulse several thousand time steps are required.

B.1.3.6 At each time step, the program calculates the position of the aircraft target as it moves through the scene. The motion of the aircraft is assumed to be at a steady speed in a

straight line. It also calculates the aspect angles presented by each of the turbines to the radar, as the turbines rotate. Each turbine is assumed to rotate at a steady rate, but the rates need not be the same from one turbine to the next. Blade rotation is started either from a specified, or from a random angular position, and is controlled by the user input. Thus one can avoid the different turbines rotating in synchronism where this is unrealistic.

B.1.4 Radar equation calculations

B.1.4.1 The program also calculates at each time step the current beam pointing direction of the radar antenna. This is assumed to rotate at a steady speed. It is generally useful to avoid the antenna period being a simple multiple of the turbine rotation periods, to avoid unrealistic synchronism.

B.1.4.2 For each time step, the program calculates a return echo power from the aircraft target using the radar equation. This takes into account the range from the radar, the current antenna gain in the direction of the aircraft, the propagation factor, and the target RCS. This calculation includes a phase factor, as well as the received power. This is necessary for any coherent radar data processing, such as moving target indication.

B.1.4.3 The calculation of the antenna gain is done from the azimuth difference between antenna beam and aircraft; the functional form is built into a subroutine, which can be easily altered as required. This accounts for the azimuthal shape of the antenna beam: the elevation pattern is accounted for in the calculation of the propagation factor in NEMESIS. This assumes that the antenna pattern can be adequately approximated as a product of azimuthal and elevation functions.

B.1.4.4 The propagation factor from radar to target position is extracted from the NEMESIS data table, previously read in. It depends on the relative range, bearing, and height.

B.1.4.5 The aircraft target is assumed to have a steady RCS. This is a simple approximation, which results in the aircraft being constantly visible (provided the RCS is not too small). A fluctuating value (e.g. one of the Swerling models) could eventually be included if appropriate. If the target is manoeuvring the radar signature can be predicted. This is computationally more expensive and can be implemented when necessary.

B.1.4.6 A similar radar equation calculation is performed for each of the turbines. The antenna gain, the range and the propagation factor are obtained as for the aircraft target. The turbine RCS is extracted from the Ocellus RCS data file, previously read in. It depends on the current rotational position of the turbine blades, and so varies rapidly with time.

B.1.5 Radar data processing

B.1.5.1 A simple Moving Target Indicator processor is simulated. The current version is a three-pulse comparison processor, which calculates the second difference of three successive complex signals ($S_{n+1} - 2S_n + S_{n-1}$). This has the effect of suppressing targets with steady or linearly varying signal (including the phase). Because of the Doppler effect this suppresses stationary and slow-moving targets, while fast moving targets are passed because of the changing phase. From this point on, the program carries both the pre-MTI and post-MTI received powers. This enables one to visualise the effect of the MTI processing without repeating the whole calculation. Other MTI filter processing configurations can be implemented as appropriate.

B.1.5.2 The program performs post-detection integration, by adding up the power in a series of successive pulses. The result is multiplied by an integration efficiency factor (less than 1), to account for inefficiency in this process in practical implementations.

B.1.5.3 The signals are compared to a radar power threshold, with smaller signals being rejected as noise, and larger signals accepted as genuine target detections. The threshold is set to a specified ratio above the noise level, where the ratio is set by the user. The threshold controls the trade-off between too many false alarms (threshold too low) and missed genuine targets (threshold too high). There is also a simple simulation of an automatic gain control: if a very large signal is received, the threshold is temporarily raised to the large signal value divided by a user-specified dynamic range factor. This suppresses the reception of simultaneous small signals which fall below the raised threshold.

B.1.5.4 Other radar data processing can be included as required.

B.1.5.5 The program then writes out a file containing details of all the accepted radar detections, i.e. those that have passed the thresholding test. This file is read by the WHIRL-DIS program.

B.2 WHIRL-DIS: Simulated radar display

B.2.1 Introduction

B.2.1.1 WHIRL-DIS is a program that simulates a radar operator's PPI display. It takes in the file from WHIRL-COM containing the accepted radar detections, and processes and displays them in real time on the PPI display. This provides a visual demonstration of the effects and benefits of various signal processing options.

B.2.1.2 The program was kept separate from WHIRL-COM so that it could be run on a portable computer, for demonstration purposes. The separation ensures that WHIRL-DIS can run fast enough to display its output in real time, and is not held up by any time consuming calculations that are done in WHIRL-COM. The software has been coded in C++ and uses Microsoft Foundation Classes to perform the basic dialogue control functions.

B.2.1.3 WHIRL-DIS thus does some processing of its own: it accepts and displays the detections found in its input file. It contains additional thresholding, with a user-adjustable range-dependent threshold. This allows the user to see the effect of adjusting the threshold without repeating the WHIRL-COM calculations. Clearly, thresholding operates as an additional rejection mechanism, along with the noise-related rejection mechanism in WHIRL-COM. It was found desirable to include the thresholding in WHIRL-COM to avoid excessive size of the accepted detection file passed from WHIRL-COM to WHIRL-DIS.

B.2.2 Functionality of WHIRL-DIS

B.2.2.1 When starting up WHIRL-DIS the user is presented with the main window as shown in Figure B-1. The user must first load in a data file from WHIRL-COM and this is done by going to menu→file→ load. This allows the user to browse for an input file and load it into the program. Before the data are loaded into the program the user is presented with a dialogue box asking the user what threshold to use when reading the data and whether to read the data from the MTI channel or the raw channel. This is shown in Figure B-2.

B.2.2.2 Once the data are loaded the start button is activated. Clicking on **<start>** causes the clock to start and the display simulation to begin. Once the display simulation is running the start button becomes a **<stop>** button to allow the user to pause the run at any time.

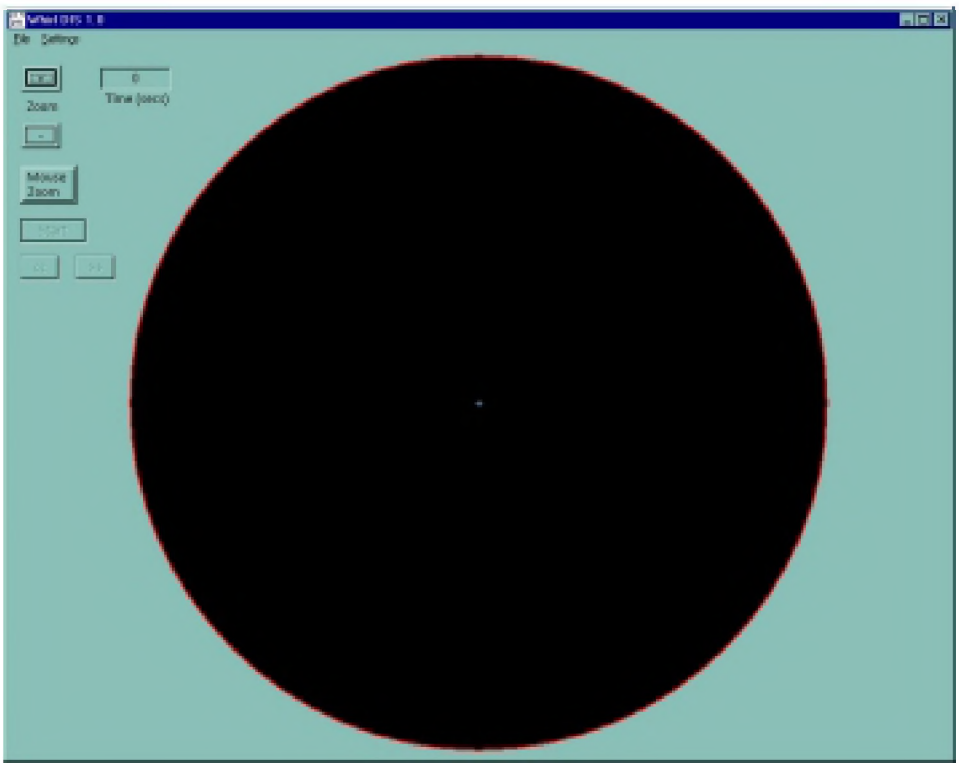

Figure B-1; Initial look of main WHIRL-DIS window when the program is started.

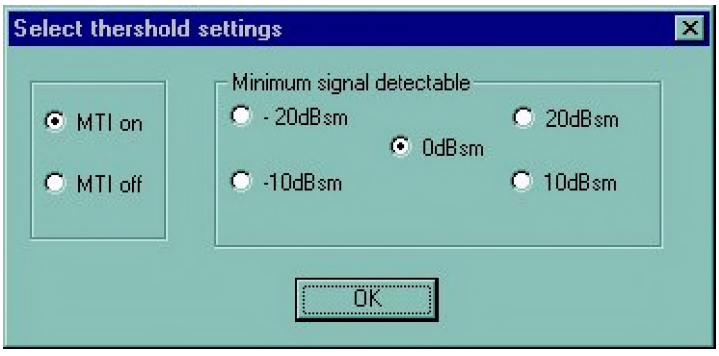

Figure B-2; Read in options presented to user when inputting data to WHIRL-DIS.

B.2.2.3 As the simulation runs the targets are displayed as the radar sees them according to the input file from WHIRL-COM. An example of this is shown in Figure B-3, using a test file containing two moving targets. The green cell marks where the target was on the last sweep and the yellow and orange cells mark the tracks of the targets over the past few sweeps.

B.2.2.4 To allow the user to study different parts of the PPI display in detail there are several zoom options available. On start up the centre of the PPI display corresponds to the radar position and the maximum range is set to 60km. During the simulation the user can zoom in or out about the current centre point using the zoom buttons in the top left hand corner of the window (see Figure B-3). The plus button decreases the range of the area

displayed by 10km (hence a zoom in) and the minus button increases the range by 10km (zoom out). For more precise zooms the user can switch the mouse zoom button and then pull out a rectangle on the display using the mouse marking the edges of an area to view. The screen then zooms in to just this zone, as illustrated in Figure B-4.

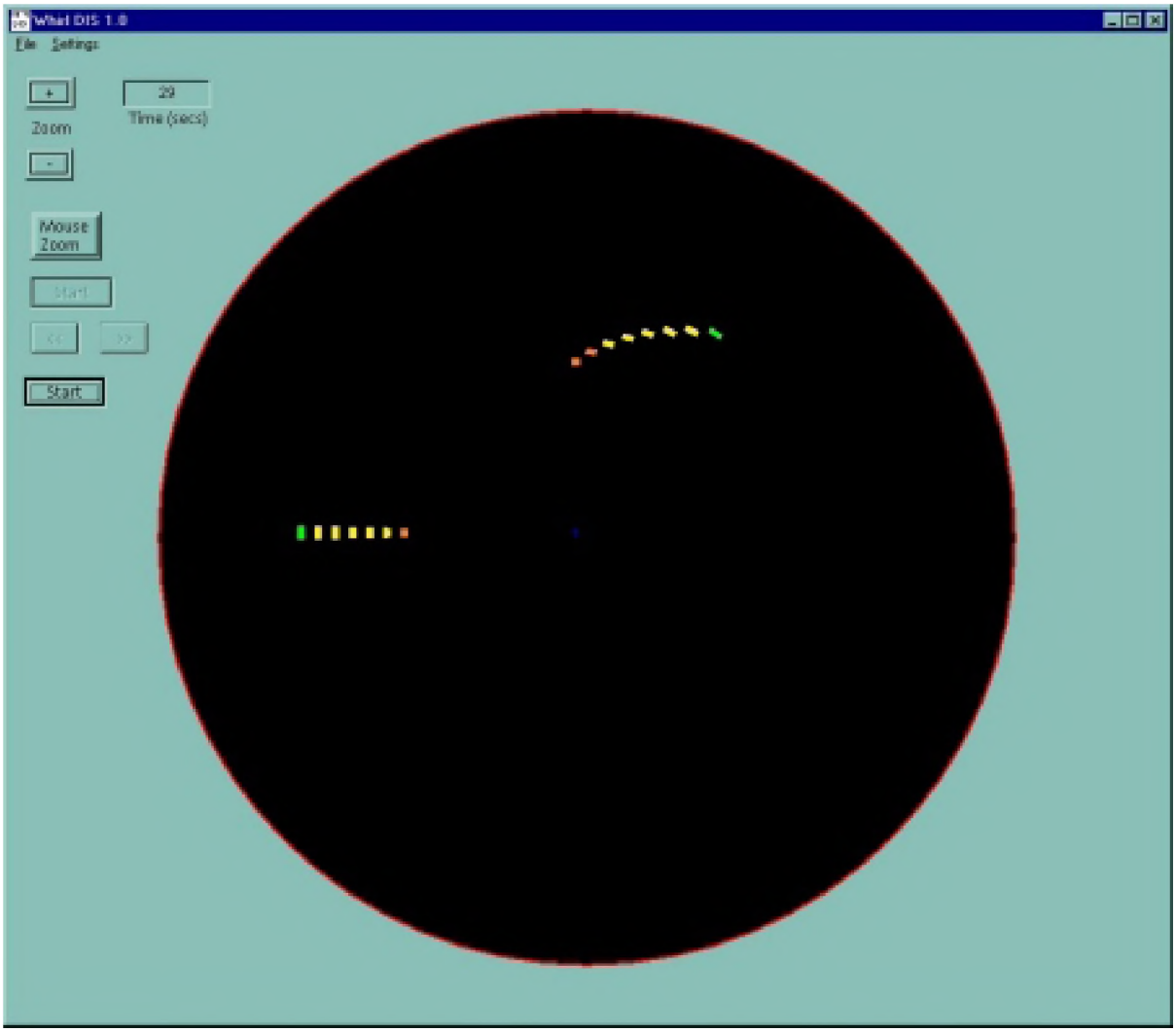

Figure B-3; Current screen shot of WHIRL DIS displaying test data.

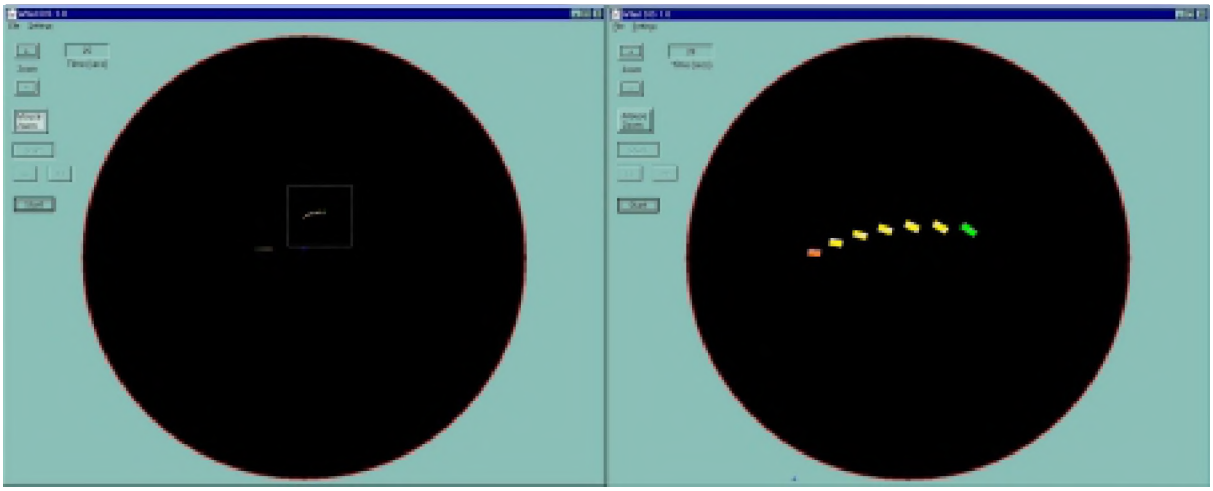

Figure B-4; Example of the mouse zoom function. Left shot shows a rectangle selected using the mouse and the right shot shows the resulting zoomed in display.

B.2.2.5 If the user wants to modify how the display looks or zoom into a very particular area then a series of options can be accessed via **menu→settings→options**. This menu is shown in Figure B-5. Opening this window does not stop the simulation and as items are changed the display is automatically updated. The variable parameters are:

- Centre of display (km. Note: radar is always at {0,0});
- Diameter of display (km);
- Tail length: the number of scans a target remains on the screen after detection;
- Beamwidth (Degrees)
- Pulse length (seconds)

B.2.2.6 It should be noted that changing the beamwidth and the pulse length from the values read from the COM output file should be done with caution. Changing these values should mean re-running WHIRL-COM, as they may have an effect on the detection capabilities of the radar. Changing these values in WHIRL-DIS shows how the wind farm may look if the resolution of the radar changes, for these parameters control the size of the cells produced from a large radar return.

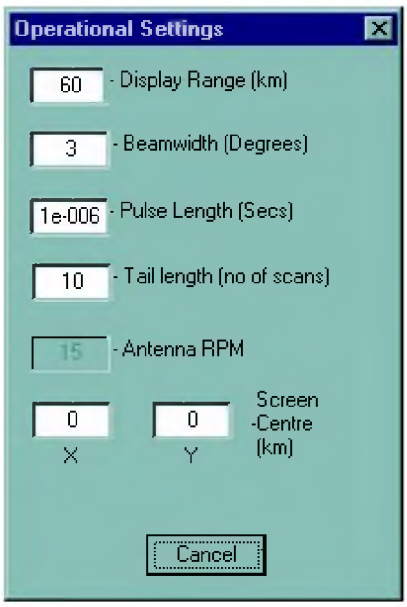

Figure B-5; Options box to control WHIRL-DIS while a simulation is running

B.2.2.7 There are also a number of functions to help the user move through the simulation. The arrow keys under the start/stop button (see Figure B-1) move the simulation one second forward or backwards when the simulation is paused, to examine what is happening in slow time. Also, the simulation can be reset back to the start by going to **menu→settings→reset**.

B.3 Ocellus: RCS computation

B.3.1 QinetiQ's software for the computation of RCS is known as Ocellus. This software was not written specifically for the present project, but is used more widely for QinetiQ's RCS prediction work.

B.3.2 The target whose RCS is required is represented in the form of a mesh covering the external surface of the target. The mesh may consist of triangular or plane quadrilateral elements, which form an approximation of the true target surface. The meshes can be supplied in a number of standard geometry formats. They are usually generated using the meshing capabilities of a commercial Computer-Aided Design package: the package I-DEAS has been used for the modelling of wind turbines in the present study.

B.3.3 By default, the surface of the target is assumed to be perfectly conducting, so that it totally reflects radar energy. The radar scattering from a smooth surface is computed by the method of physical optics. This is a good approximation for scatterers that are reasonably smooth and are much greater than the radar wavelength in size.

B.3.4 One can also specify that different portions of the surface are covered with different materials. The material is specified as a series of layers, each of which has a thickness, a complex dielectric constant, and complex permeability. The structure may, but need not, have a metal back. The program then computes the complex plane wave reflection coefficient for the structure as a function of frequency, angle of incidence and polarisation. Alternatively, a table of reflection coefficients can be supplied from an external source, either by calculation or measurement. This is then used to modify the physical optics scattering appropriately.

B.3.5 The user also specifies the frequency of the illuminating radar, and the position of the transmitting and receiving antenna. Each of these data items can be specified as an evenly-spaced series of values, to obtain repeated calculations, such as a frequency sweep or an azimuth cut of the RCS. By default the program assumes that the radar is monostatic, i.e. the receiver is always in the same place as the transmitter. However, this is not necessary: the user can specify a bistatic calculation in which the receiver is in a different position from the transmitter. In the context of wind farms, this is useful for studying indirect reflections from a wanted aircraft, via a turbine, to a radar.

B.3.6 The transmitter and receiver antennas are normally at a large distance from the target (technically "in the far-field"). But the user may specify the range of one or both antennas from the target, which need not be in the far-field. The phases of the reflections from different parts of the target are then added up taking into account the true distances to the antennas, giving a near-field RCS. The far-field is considered to be at any distance larger than $2L^2/\lambda$, where L is the target diameter, and λ is the radar wavelength. Particularly for large targets and short wavelengths, this distance can be very large, and in these cases the use of far-field RCS will be inappropriate.

B.3.7 The physical optics method does not give the complete RCS when a target has sharp edges. The presence of a sharp edge violates the assumption of smooth surfaces implicit in the physical optics method. The program automatically detects the presence of a sharp edge, when adjacent facets of the mesh are at a large angle to each other. It then applies a correction to the RCS, computed according to the Physical Theory of Diffraction (PTD). This method uses an "incremental length diffraction coefficient" for each element of the sharp edge. These are then summed along the edge, with appropriate angles of incidence and phases. This calculation is optional, although it is normally included as it is not very time-consuming.

B.3.8 The software is also capable of handling shadowing of one part of the target by another. If one part of the target lies directly behind another, as seen from the radar transmitter, then it is not illuminated, and should be omitted from the physical optics computation. The program is capable of automatically detecting occurrences of such shadowing, and omitting the shadowed portions from the computation. Shadowing does not happen for convex targets such as a single turbine blade, but it is possible for the blades of a turbine to shadow each other, or to shadow or be shadowed by the turbine tower. The detection of shadowing can increase the computation time considerably, so the detection can be performed with various degrees of refinement, or switched off altogether, thus giving the user a trade-off between computation time and the accuracy of the result.

B.3.9 Another scattering mechanism is multiple bouncing, in which energy is reflected more than once from different parts of the target before returning to the radar. An important case of this occurs if the target contains re-entrant faces at right-angles to each other, forming a "dihedral" (two surfaces) or "trihedral" (three surfaces). These structures give strong retro-reflection over a large range of angles of incidence where they are illuminated, so it is important to include this effect if they are present. Multiple bounces will not occur for a single wind turbine blade. But multiple bounces may possibly occur in a complete turbine, between different blades or between the turbines and the tower. The program can compute such multiple bounce reflections. This computation is time-consuming. The user can set the maximum number of bounces that will be considered, according to the effects likely to be important; or the multiple bounce detection can be

switched off altogether. Thus there is a trade-off between computer time and the accuracy of the result.

B.3.10 When studying radar scattering from buildings on the ground, a significant contribution can come from reflections that return to the radar via a double bounce from the surface of the building and the ground, especially where the ground surface is flat for some distance in front of the building. Where the surface of the building is vertical, it forms a right-angled "dihedral" with the ground, which produces strong retro-reflection. Even a triple bounce contribution (ground-building-ground) can sometimes be significant. The program can compute such ground reflections, and add them to the direct reflection with the correct phase. This computation is optional.

B.3.11 It is possible to request that the program outputs separately the different contributions to the RCS discussed above (physical optics, diffraction, multiple bounce, ground bounce). This is useful as a diagnostic tool for determining the mechanism responsible for strong reflections. In the context of the present study, this program has been used to generate a table of RCS values, for a particular turbine at a particular radar frequency, giving the monostatic RCS calculation for the necessary set of directions of incidence angle. The set of directions depends on the yaw angle(s) of the turbine blade(i.e. the angle about a vertical axis as the wind direction changes),the blade pitch (i.e. rotation about its own axis),and the normal rotation of the blade during electricity generation. The output from one or more Ocellus runs is converted by a small separate translator program to a binary format suitable for efficient reading by WHIRL.

B.3.12 The computation of the RCS table can be very time-consuming, but the computer can be left to get on with the computation without human intervention. Once the computation is done the resulting table encapsulates all the information about the turbine at the particular radar frequency. The table can then be re-used in many different radar scenarios, different wind-turbine layouts, etc. It thus allows efficient exploration of different scenarios without re-computation of the RCS values.

B.4 NEMESIS: propagation calculation

B.4.1 NEMESIS is a QinetiQ program for calculating radar propagation factors taking into account the intervening terrain. It is based on the Parabolic Equation Method (PEM), an approximation of the full wave equation, which models propagation for small angular deviations with high accuracy. Appropriate boundary conditions are applied at the ground to take into account ground reflections. The method also automatically accounts for diffraction over hilltops into shadowed areas. The program was written by James Branson *et al*, at QinetiQ Portsdown West, using Matlab. It was not written specially for the present project, but is used more widely in QinetiQ where propagation calculations are required. It has (in other work) been verified against experimental measurements, and against other software.

B.4.2 Input to the model consists of:

- radar system parameters:
  - frequency;
  - polarisation;
  - antenna beam shape and elevation beamwidth;

- Antenna position (latitude and longitude) and elevation angle (propagation predictions can be made at a single azimuth angle, or a range of angles);
- Optionally, transmitter power, pulse duration, antenna transmit and receive gains, system noise and losses, and some other parameters can be specified.

- Environmental features:
  - terrain elevation data;
  - refractivity profiles (if available — there are standard settings);
  - clutter characteristics (if available — there are standard settings);

- Calculation parameters:
  - maximum range;
  - number of range steps to use;
  - maximum height;
  - maximum angle (elevation);

B.4.3 The beam pattern of the radar can be modelled as omni-directional, sinc or cosecant squared, and there is a user-defined option for non-standard antenna patterns. This reads values from a file in a number of formats, including gain versus angle and measured signal voltage against height, which are then converted into the form required by the rest of the program. Gain is normalised to unity on boresight.

B.4.4 Terrain data are supplied as digital terrain elevation data (DTED) in either latitude longitude format, or using UK grid co-ordinates. Such DTED files are available to QinetiQ to cover most of the UK.

B.4.5 The model can output a number of parameters, but the one we are concerned with here is the pattern propagation factor. This is calculated as a function of range, height and azimuth (if required). The maximum height, maximum range, number of range steps and maximum angle for prediction are chosen by the operator. NEMESIS then determines the height interval for the calculation, which is performed using the Fourier split step method, as described in [1]. In essence, the model creates an output grid with height samples treated as elements of a fast Fourier transform (FFT), which is evaluated at each range step in turn, from the antenna out to the maximum desired range. Total run time therefore depends on the number of range steps, and the number of height samples (the FFT size).

B.4.6 There are limitations on the elevation angle for which the parabolic equation model is valid. NEMESIS allows the user to select a maximum angle for calculation, but values higher than 15 degrees are not recommended. The value chosen should take into account both the antenna beamwidth and the antenna elevation angle.

B.4.7 As described in [2], there are limitations on the terrain slope for which PEM solutions are valid — approximately 20 degrees for the formulation described in that paper. In order to cope with this situation, NEMESIS checks the terrain slope at each range step, and invokes a modified version of the algorithm if the gradient is too steep.

B.4.8 The development of PEM theory is described in [3].

B.4.9 The Matlab model consists of a number of Graphical User Interfaces (GUIs), which are used to set the input parameters and view the outputs. Once the scenario has been defined, the main "nemesis.m" module performs three tasks:

- The initial conditions are set-up, taking into account the antenna beam pattern, required range steps, maximum height etc. This occurs in the "beam_cast.m" module.
- The "m_cast.m" module performs interpolation of the refractivity and terrain data, to suit the output grid settings.
- The main parabolic equation solution is then performed by the "drapem.m" module. Other modules then display the calculation results graphically, and allow the user to view propagation factors, signal to noise, pathloss etc.

B.4.10 In the present work, the calculation is made over a sector of terrain centred on the radar, and containing the target aircraft and turbine positions. The output is a propagation factor from the radar to specified positions (defined by range, bearing, height), relative to an antenna with unit gain, propagating in free space. The results are written into a file, which is read by WHIRL-COM.

B.5 Shadowing

B.5.1 WHIRL-COM does not contain any shadowing effects from the turbines. This is mainly to do with the level of complexity this would introduce, but also because we do not believe it is a particularly significant effect. The following section explains the analysis we have carried out to investigate this.

B.5.2 The term "shadowing" appears to be used for more than one effect in the context of radar systems and obstacles such as wind turbines, as follows:

- The detection of a target, which is directly behind the wind farm, as seen from the radar, may be distorted by the passage of the radar energy through the wind farm.
- In the context of the computation of RCS, the term is used to refer to the hiding of one part of a single turbine behind another, which prevents the illumination of the rear part. This occurs at much closer range than the shadowing in the first meaning; for example the tower may be hidden behind a blade that is only a few metres away.
- The radar echo from an aircraft flying over a wind farm may be shadowed (or "masked") by the clutter echoes from the wind turbines at the same range and bearing. This is a quite different use of the term.

B.5.3 In this section we discuss shadowing in the first of these meanings.

B.5.4 One normally thinks of light rays travelling in straight lines, except when reflected or refracted from some material object. Then an opaque obstacle casts a dark shadow behind it, where the light does not penetrate. Pursuing this analogy might lead one to think there would be a dark radar shadow behind an obstacle, so that a target entirely within the shadow would not be seen by the radar. On this analogy, the radar shadow of a wind turbine would be only a few metres wide, comparable to the width of the turbine tower and blades. Thus a small moving target would not remain in the shadow for long, and a larger target would never be entirely within the shadow.

B.5.5 However, the concept of rays is not strictly correct, because of the wave nature of all electromagnetic radiation, including light and radar waves. It is a very good approximation for light waves in ordinary situations, because the wavelength of light (around 1/2000 millimetres) is very small. But for radar, the wavelengths used are in the range of centimetres, which are not very small compared to the size of practical objects. Then the straight-line ray approximation is less good, and wave effects have to be taken into account.

B.5.6 When a radar antenna sends out a pulse of energy, the energy spreads out according to the beam pattern of the antenna. The wave travels at the speed of light in all directions, so that a wavefront of the pulse is a sphere with the antenna at its centre. According to Huygens' principle, the propagation of the wave can be calculated by considering each part of the wavefront to radiate "secondary wavelets", and adding up their contributions at the desired observation point. The mathematical expression of Huygens' principle can be derived from the basic equations of electromagnetism, and so have a solider foundation than Huygens himself could have known. If the wavefront is completely unobscured, the adding-up process merely leads to the continuation of the original spherical wave, as indeed it must for the theory to make sense.

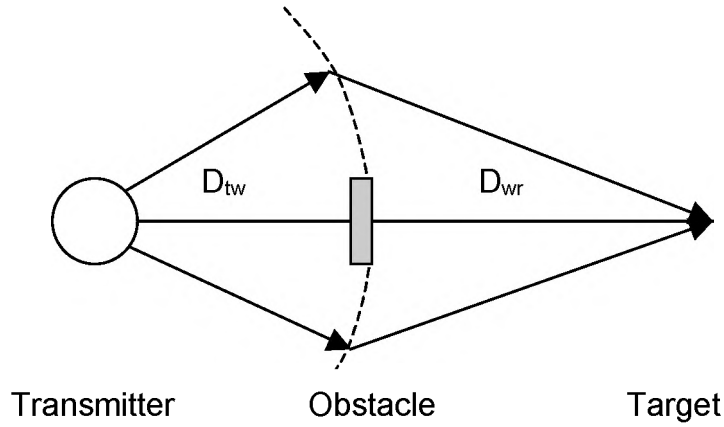

Figure B-6; Illustration of Fresnel zone around straight ray path

B.5.7 One finds according to this theory that energy travelling from one point to another does not travel only along the straight line between the points, but also travels along a tube of neighbouring paths. A neighbouring path is obviously somewhat longer than the straight line path. If the extra path length is less than 1/8 wavelength, the paths all add up in phase and contribute to the total energy transmitted. Energy travelling by longer paths arrive out of phase (significantly late), and the contributions from different paths cancel each other out, and so have no net effect.

B.5.8 Consider an intermediate plane, at distance D_{tw} from the transmitter and D_{wr} from the receiver (see Figure B-6). The contributing paths pass through a circle in this plane. This circle is technically known as the first Fresnel zone. Its diameter L_f is given by:

$$L_f = \sqrt{D\lambda} \quad where \quad \frac{1}{D} = \frac{1}{D_{tw}} + \frac{1}{D_{wr}}, \qquad (B\text{-}1)$$

and λ is the wavelength.

B.5.9 For typical distances of (say) 10km, and a radar wavelength of 10cm, the Fresnel zone diameter is $L_f = \sqrt{(5000 \times 0.1)} \approx 22$ metres. We see that this is much wider than the width of a turbine, but shorter than its length. This has the consequence that a turbine blade (or tower) does not obscure the whole of the width of the Fresnel zone, and so it does not cast a completely ``black'' shadow behind it.

B.5.10 That the Fresnel zone diameter is shorter than a blade length also has the consequence that only part of the blade length acts to scatter coherently in any particular direction. Then the normal "far-field" RCS of a blade may well be an overestimate. This shows that we must take the actual distances from turbine to radar and target into account in doing calculations, and cannot blindly assume that these distances are large.

B.5.11 Going back to Huygens' principle: if the wavefront is partially obscured, one adds up the contributions only from the open parts of the wavefront, since no energy passes through the obscured parts. If the obstacle is comparatively small, it is easier to take the continuation of the original wave (from the completely open wavefront), and subtract the contribution blocked out by the obstacle. This method can be used to compute the disturbance to a radar pulse at a point behind an obstacle.

B.5.12 If we idealise a turbine blade or tower as a long rectangular obstacle, then according to this method we find that the subtracted electromagnetic fields due to the obstacle (E_s) are related to the incident field in the absence of the obstacle (E_i) by

$$\frac{E_s}{E_i} = \frac{W}{L_f} = \frac{W}{\sqrt{D\lambda}}, \qquad (B\text{-}2)$$

where W is the obstacle width. (The obstacle length does not enter provided it is longer than the Fresnel zone diameter, as discussed above). Since the width of the obstacle is less than the Fresnel zone diameter, the subtracted field is small, so the shadow is not at all black. Because of the factor D in the denominator of this expression, the subtracted field becomes even smaller the further away the target is from the turbine.

B.5.13 The power density at a point behind the obstacle is reduced by a factor $(1\text{-}E_s/E_i)^2$, where the squaring occurs in going from electromagnetic fields to powers. In a radar, this factor applies to both outward signal and returned echo, so that the echo is reduced by the square of this factor, i.e. $(1\text{-}E_s/E_i)^4$. Figure B-7 shows a graph of this quantity as the distance between the target and the turbine changes, assuming that the obstacle width is 2 metres, the wavelength is 10 cm, and the distance to the radar is very large. The reduction factors are not very large, and would not prevent the detection of a target unless it is so small that it is already quite close to the lower limit of detection. An extended target would not all be in the most deeply shadowed position, and so its combined RCS would be reduced by a smaller factor.

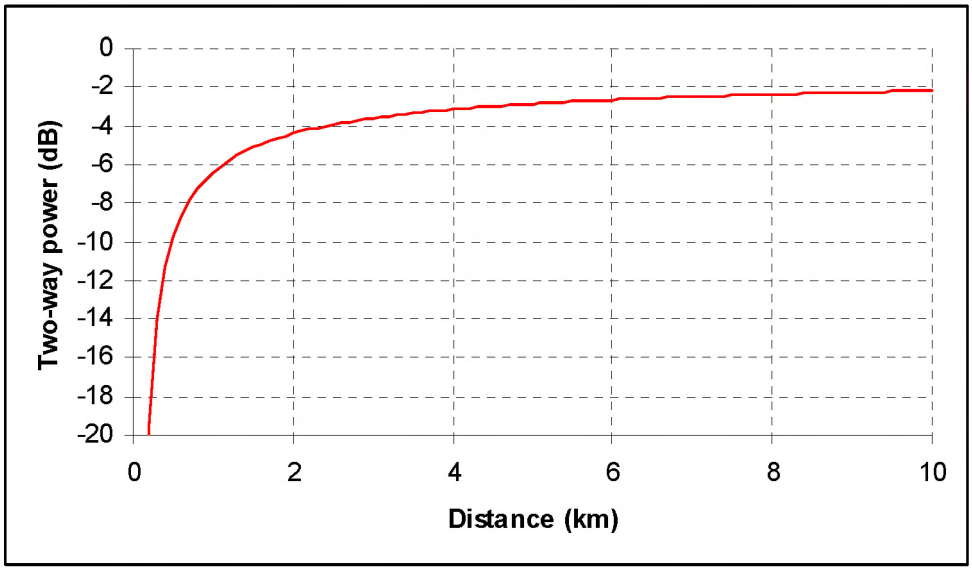

Figure B-7; Reduction in radar echo from point target behind 2 m wide obstacle (transmitter 18 km away, radar frequency 3 GHz)

B.5.14 Only if one comes close to the turbine is the radar echo greatly reduced. At a distance of $D = W^2/\lambda$, the interference field is comparable to the incident field, and then there is a dark shadow (and some approximations made in obtaining the above equation break down, so that a more refined theory must be used). For a 3 m wide obstacle and a 3 GHz radar, this distance is 90 metres. Within this distance there is significant shadowing (which applies to the second meaning of "shadowing" above).

B.5.15 When a target is behind a turbine, the shadow of the blade moves as the blades rotate. This produces a periodic variation in the power transmitted to a fixed point behind the turbine. This is illustrated in Figure B-8, which shows the power density at a point behind a rotating turbine as a function of time. The turbine is modelled with only one blade; though unrealistic, this helps to show its effects more clearly. The position of the target at height 0 is directly behind the hub of the turbine. We then get a roughly constant reduction of 1.3 dB (it is not precisely constant because the target has some width). With the target at height 25m, it is behind the centre of the blade when the blade is oriented vertically upwards (0 degrees). There is then a maximum attenuation of 4 dB, but only briefly when the blade is in the vertical position. At other orientations it has less effect on the transmitted power. At 50 m height the target is level with the end of the blade when the blade is vertically up: the maximum reduction is 2 dB. At 75 m height the target is clear of the shadow, and there is very little effect. With three blades the sharp excursions would occur three times per cycle, as each blade passed in front of the target.

B.5.16 The time variation of the transmitted power would have the effect that the apparent RCS of the target would vary from pulse to pulse and from sweep to sweep. However, one can expect the RCS to vary anyway, because any motion of the target will bring different scattering centres within the target into and out of phase. Thus the turbine-induced variability does not itself make detection of the target by the radar more difficult than it is already. The average reduction in RCS over a cycle is quite small, unless the target happens to be precisely behind the turbine hub.

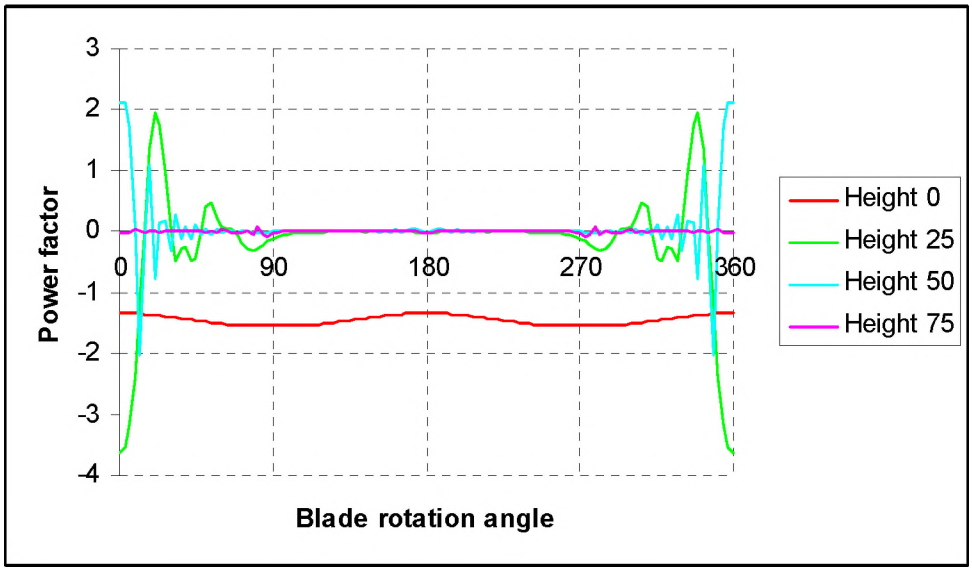

Figure B-8; Time variation of power behind rotating 50x3 m turbine blade (18km to transmitter, 1 km to target; radar frequency 3 GHz)

B.5.17 In summary, because of the wave nature of radar energy, the shadow behind a wind turbine is only dark to a distance of a few hundred of metres. This shadowing exists only for a width of a few metres, directly behind the turbine. This can only prevent the detection of a target if the target is no more than a few metres in size, positioned directly behind a turbine, and stationary so that it stays in the shadow. This is unlikely to be a problem in practice for realistic aircraft. Beyond this there is some reduction of the radar power, and a time-variation, but these will not prevent detection except possibly for very small targets.

C OUTLINE WIND TURBINE TRIALS PLAN

C.1 Introduction

C.1.1 The trials outlined here are required to validate output from computer models which will be developed as part of this work. These models will enable experimentation with wind turbine design and location, and radar parameters, to investigate how the effects on radar systems can be minimised.

C.1.2 These trials must validate all parts of the simulation from RCS modelling to the generation of PPI (Plan Position Indicator) displays of radars affected by turbine clutter.

C.1.3 Two sites have been proposed for trial measurements. The first is near Swaffham, Norfolk. This site has been selected for the trial because it consists of only a single turbine sited in flat terrain: results from it should make a good, simple test of the computer model. It is located within sight of the RAF airfield at Marham, Norfolk, where an ATC radar is located. The second site is at Hare Hill, 31 km / 17 nmi east of Prestwick Airport, near Ayr, Scotland. It comprises a wind farm of 20 turbines, and is well known as a source of returns on the ATC PPI displays at Prestwick Airport. Radar display data will be readily available, and the multiple turbines will offer a challenging problem for the computer model. Model validation using the data from this site will give a good idea of the model's capabilities.

C.2 Concept of necessary trials data

C.2.1 The following sections describe the three kinds of trials data that must be collected. These are described as:

- PPI video collection from ATC primary radars
- Calibrated RCS data from instrumentation radar
- Raw (uncalibrated) radar data from instrumentation radar

These data will test the computer model at different stages during its development: the calibrated RCS data will validate the RCS modelling of the wind farms, the raw data will then include RCS and propagation effects, and the PPI video will include the validation of the radar processing.

C.2.2 Consideration is presently being given to using sub-contractors for collection of the PPI video data and the wind turbine dynamic data. QinetiQ will collect the RCS data and raw radar data, using a QinetiQ-owned radar system.

C.2.3 Common reference standards will be necessary for all data types. For directional pointing data the reference will be True North. Discussions will be necessary between all the involved trial agencies to agree a time standard. It is suggested that the broadcast MSF (Rugby Radio Clock) might be convenient.

C.2.4 For any data recording equipment which is not automatically time synchronised (e.g. video cameras), a separate time synchronising event will be needed to link it to the other equipment.

C.2.5 It is thought likely that, to the turbine owners, each blade of a turbine will have a unique identity (e.g. Nos 1, 2 & 3). For the duration of the trial, it might be useful to have Blade 1 identified externally by attachment of a bright coloured marker

C.3 PPI Video Collection

C.3.1 Introduction

C.3.1.1 The data collected in these trials will be recorded video from a live PPI display. This is the type of display that air traffic controllers use to monitor the airspace covered by the radar in question. It presents a circular picture, with its centre representing the radar location. Its circumference represents a compass rose (with north at the top), and target range is measured radially.

C.3.1.2 The video data driving a PPI is the final output from an airport's primary radar, and is what the simulation code will aim to reproduce. This data will therefore be collected to compare with the final output of the simulation code when it is run for several different scenarios.

C.3.1.3 Both turbine sites are well within radar range of airfields (RAF Marham is close to Swaffham). Co-operation of the ATC authorities at both airfields is assured, so video data will be recorded at both locations. Because Swaffham has only one turbine, it will be regarded as the control site.

C.3.2 Measurement details

C.3.2.1 The following information describes briefly what is needed from the trials data, and is not intended to reflect the detail of how it will be achieved.

C.3.2.2 All the radar and turbine information must be collected and recorded at the time of the trial for each measurement type. All of the measurements are to be repeated at both Prestwick/Hare Hill and Marham/Swaffham.

C.3.2.3 As well as the trial data streams, detailed site information for use in the simulation will also be required. For the turbines it will comprise their latitude and longitude and their height above mean sea level (amsl): for the ATC radars the latitude and longitude and height amsl of their antennas will be required.

C.3.2.4 It is realised that the pointing direction of the turbines will be governed principally by the prevailing wind. It is hoped that, during the trial time frame, the wind direction will shift sufficiently to allow a significant amount of the following 'wish list' to be achieved. The listed pointing directions are, therefore, regarded as nominal.

C.3.3 Measurement 1

C.3.3.1 All the turbines will be facing the radar (blade axis of rotation pointing at the ATC radar location, or within a few degrees of it). The yaw angle of the turbines will be recorded relative to true north. So that there is no water in the air or on the turbines themselves, the weather should be dry. The pitch of the blades and the speed of rotation should be near constant as possible for the length of the measurement.

C.3.3.2 During the measurement the radar parameters must not change. Data to be recorded is frequency, pulse width, PRF, threshold, antenna gain as a function of aspect, rotation speed and direction (clockwise or anti-clockwise) and details of MTI/MTD settings.

C.3.3.3 The measurement will then record 10 minutes of PPI video (time stamped) while the conditions described above are steady.

C.3.3.4 To synchronise the blade rotation with the radar we will need to know the exact orientation of the blades at the start time of the video, for each of the turbines, and the bearing the radar antenna is pointing at the start time of the video. Some instrumentation may be required to ensure that there is time synchronisation between the PPI video signal, the turbine blade orientation, and the radar azimuth position. Table C-1 lists all the parameters that must be recorded in this measurement.

RADAR PARAMETERS	
Location	Deg, lat & lon and OSBB ref
Antenna height	m (amsl)
Frequency	Hertz
Pulse width	Seconds
Pulse repetition frequency	Hertz
Threshold	Voltage
Antenna gain (over 360°)	No units (0° at bore sight)
Antenna rotation speed	RPM
Bearing of antenna at start of video data	Degrees wrt True North
MTI/MTD settings	
WIND TURBINE PARAMETERS	
Location	Deg, lat & lon and OSBB ref
Hub height	m (amsl)
'Blade 1' position at data start	Degrees from vertical
Average yaw angle wrt bearing to radar	Degrees
Average blade pitch	Degrees (0° = stalled)
Average blade rotation speed	RPM

Table C-1; Parameters required from the video data collection measurements.

C.3.3.5 It is hoped that the wind farm variables of blade speed, pitch and turbine yaw will be virtually constant though out the length of the measurement. Recording time series data files of the parameters will enable evaluation of their average values. The recording period will be set by the time that a turbine maintains the yaw angle, but a period of between 10 and 30 seconds would be ideal.

C.3.3.6 The video data will be supplied as a mpeg file with the pictures containing a running clock to help sync the data.

C.3.3.7 Error bars associated with all the measurement data must be supplied, so that the success of the verification can be assessed, with respect to the errors in the measurement data.

C.3.4 Measurement 2

C.3.4.1 As measurement 1 but with the blade axis of rotation 45° (or as close as possible) to the radar line of site for all the turbines. All turbines should be generating.

C.3.5 Measurement 3

C.3.5.1 As measurement 1 but with the blade axis of rotation 90° (or as close as possible) to the radar line of site for all the turbines. All turbines should be generating.

C.3.6 Measurement 4

C.3.6.1 Measurement 1, 2, or 3 rerun in wet conditions. Turbines should be wet and rain falling for the duration of the measurement.

C.4 RCS and raw radar data collection

C.4.1 Introduction

C.4.1.1 This set of measurement trials will use a QinetiQ instrumentation radar to collect turbine RCS and raw radar data for validation of the RCS models used, and the raw data produced by the simulation before any radar processing. The trials radar is designed for radar target RCS data measurement and collection. It is not a scanning radar and will thus maximise data collection by pointing at the turbines throughout the measurement period.

C.4.1.2 This section describes a set of measurements to collect the data required to validate these aspects of the theoretical program.

C.4.1.3 Once at a trials site, the radar will lose some of its mobility, but there remains a reasonable probability of being able to move it sufficiently to meet the requirements for measurements at three, specified, turbine yaw angles.

C.4.1.4 For all the following measurements, it is essential to record the latitude and longitude of the radar. All of its other parameters will be known prior to the trial.

C.4.2 RCS measurements

C.4.2.1 The radar should be set up in a fixed position facing the windfarm and the same four measurements as described in section 2 carried out. This is a measurement of the turbines in the dry with the blade rotation axis 0°, 45°, and 90° from the radar line of sight. One of

these three measurement scenarios must be repeated in wet conditions. Again, the pitch and speed of the blades is not defined but must remain constant though out the duration of the measurement; with blade speed and pitch recorded throughout.

C.4.2.2 The objective will be to record 5 minutes of time stamped calibrated RCS data of the turbines at two frequencies, 3GHz and 1GHz: 3GHz will simulate an ATC primary radar, and 1GHz will simulate a Secondary Surveillance Radar (SSR) (it may prove difficult to obtain a radar to work at the second frequency). To synchronise the data with the turbine positions, the exact position of the blades of each turbine must be recorded at the start of the data recording period. Daily radar calibration will be carried out. Table C-2 shows the data that must be recorded for each measurement.

C.4.2.3 It is hoped that the wind farm variables of blade speed, pitch and turbine yaw will be virtually constant though out the length of the measurement. Recording time series data files of the parameters will enable evaluation of their average values. The recording period will be set by the time that a turbine to maintains the yaw angle, but a period of between 10 and 30 seconds would be ideal.

C.4.2.4 Although weather conditions will be a major factor, the optimum method may be the collection of a much longer period of data, with a preferred data set being extracted post-trial.

RADAR PARAMETERS	
Geographical location	Degrees, lat & lon & OSGB ref
Antenna height	m (amsl)
Frequency	GHz
WIND TURBINE PARAMETERS	
Geographical location	Degrees, lat & lon & OSGB ref
Hub height	m (amsl)
Blade 1 position at data start	Degrees from vertical
Average turbine yaw angle wrt radar boresight	Degrees
Average blade pitch	Degrees (0° = stalled)
Average blade rotation speed	RPM

Table C-2; Parameters required from the RCS data collection measurements

C.4.3 Raw data collection

C.4.3.1 This data item does not actually require any extra measurements to take place. The uncalibrated data from the RCS measurements will suffice. The data must be collected in a time stamped file as before.

C.4.3.2 The data to be recorded is listed in Table 3-2.

RADAR PARAMETERS	
Geographical location	Degrees, lat & lon & OSGB ref
Antenna height	m (amsl)
Frequency	GHz
Pulse width	μs
Pulse repetition frequency	pps
Averaging details	No of pulses
Antenna gain	dB
WIND TURBINE PARAMETERS	
Geographical location	Degrees, lat & lon & OSGB ref
Hub height	m (amsl)
'Blade 1' position at data start	Degrees from vertical
Average turbine yaw angle wrt radar boresight	Degrees
Average blade pitch	Degrees (0° = stalled)
Average blade rotation speed	RPM

Table C-3; Parameters required from the raw data collection measurements

C.5 Summary of trials

C.5.1 These trials will collect three types of data to test the computer model at three stages of its simulation. The RCS data will test the models of the scattering characteristics of a turbines, the raw radar data will test the turbine scattering models and the propagation model, and the PPI video data will test the turbine scattering models, propagation model, and radar processing models.

C.5.2 The results of the validation will highlight where differences arise in the computer code, and allow its output to be used sensibly.

C.5.3 Any errors in the trials will limit the sensitivity of the validation, so it will be important to keep these small and also to know what the error bars are to allow the results of the validation to be interpreted correctly.

This page is intentionally blank

D RADAR MEASUREMENT DETAILS

D.1 MPR site

D.1.1 Arrangements were made to allow MPR to be located at Swaffham Raceway, Downham Road, Swaffham. The site is private land, with a house also on site, and is partially secured by a fence, thus giving some small overnight security to the radar.

D.1.2 The position selected for MPR was in the south-east corner of the site. This gave the radar an unobstructed line of sight to the turbine, but the combination of the intervening topography and trees on the horizon obscured the turbine tower up to a point a few metres below the tip of a blade pointing vertically downwards.

OS grid ref	TF 782095
Range to turbine	3.45 km / 1.86 nmi
Site elevation	53 m AMSL
Heading to/from turbine	085° T / 265° T
Magnetic variation	approx. 2.5°W

D.2 MPR parameters

A.1.1 For the purposes of the trial, MPR mimicked a primary ATC radar system. At RAF Marham, the radar is a Watchman. Although MPR cannot match the Watchman parameters exactly, it was sufficiently close. The following parameters were used:

Frequency	3.05 GHz
PRF	2 kHz
Pulse width	1.0 μs
Polarisation	VV and HH (as consecutive measurements)
Watchman heading to/from turbine	081° T / 261° T

D.2.2 Note that MPR is a track-only radar without any scanning function. During the trial it operated in 'staring' mode, with its boresight aligned with the turbine.

D.3 Radar calibration and performance checks

D.3.1 MPR has a built-in 'loopback test', which is used routinely and very frequently, for performance testing. This test tests the whole radar system, apart from the radar antenna, and gives a performance 'value' that is compared with a known standard 'value'. If there is agreement between the two figures, then it is known that the system, apart from the antenna, is performing as expected.

D.3.2 MPR also has a standard performance test which uses a tethered kite or helium-filled balloon to carry aloft a 12in diameter light aluminium sphere (i.e. a target of known RCS, independent of its attitude): wind conditions dictate whether a kite or balloon is used. The sphere is flown at an altitude of about 1000ft AGL, at a range of about 1 km from MPR, and therefore it constitutes a discrete target in free space. By comparison of this test result with the expected result, there can be confidence that the whole radar system, including the antenna, is performing satisfactorily. This was carried out to the satisfaction of the operators on the first day of the trial.

D.3.3 The loopback test was performed at Funtington before MPR departed. Once MPR became operational (a multiple-hour task) at Swaffham on day one of the trial, a standard performance test was made. A further performance test was also made later during the trial period. Both showed the radar to be operating correctly

D.3.4 Additionally, as a continuous performance monitor, the loopback test is performed automatically at the start of every RCS measurement, and its result is recorded along with each set of measurement data. The received radar signals during each measurement were also monitored visually on an oscilloscope.

D.4 Blade position sensor

D.4.1 As the Swaffham trial most likely represented the first time that the RCS of a wind turbine was to be characterised, it was necessary to record as much data as possible. It was recognised that the position of a blade as it rotated (in a "clock sense"), would influence its individual RCS, and hence the turbine's bulk RCS. Blade position is not of interest to wind turbine operators, so it is not included in the instrumentation data set. In-house knowledge and facilities were utilised to design and manufacture a blade position sensor system (BPSS).

D.4.2 Enercon wind turbines are direct drive i.e. the generator rotor turns at the wind-driven rotor speed. Since the Enercon E-66 rotor has three blades (labelled, by Enercon, as "A", "B", and "C"), the rotor RCS would have a pattern that would repeat three times per rotor revolution. Therefore, assuming a constant, known, rotor speed, it was only necessary to sample blade position through a specified 120° of rotation. Enercon supplied custom trial software for sampling turbine operational parameters, including speed, and its sampling interval was agreed to be 3 seconds. We were told that the mass of the turbine rotor plus the attached generator rotor (i.e. its armature) was of the order of 20 tonnes, so rotational inertia was obviously very large. Therefore, it seemed reasonable to assume that any change of speed would be very slow. The MPR timestamps its recorded data with time of day (hh:mm:ss at one second resolution) and it was reasoned that we could achieve the objective by recording the time of day on each occasion that Blade A passed through top dead centre (TDC).

D.4.3 The E-66 armature drum is about 3 m diameter, and its exposed rear edge rotates in very close proximity to the massive generator supporting structure. This physical arrangement offered a few options for the use of different sensor types, and the choice was a photo-electric sensor. The sensor contained a transmitter that emitted a beam of red light, and an optical receiver with sensitivity adjustment: by attaching a bright reflector to the dull metal of the armature edge, the sensor sensitivity was adjusted so as to give a sensor output each time the reflector passed it. With the turbine braked with Blade A at TDC,

the reflector was attached to the armature in alignment with the sensor. Figure D-1 shows the sensor mounted in position.

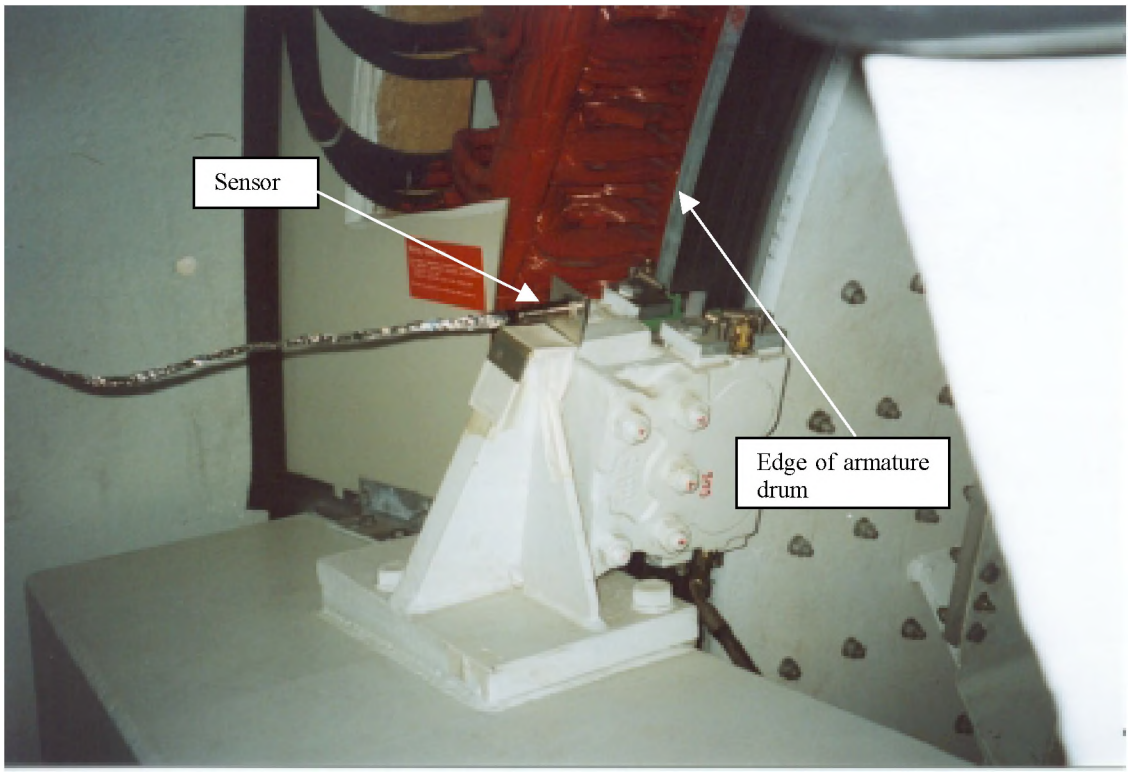

Figure D-1; The blade position sensor in position in the E-66 turbine at Swaffham.

D.4.4 It was judged that a positional resolution of about 5° would be sufficient, so with the E-66's maximum speed of 22 RPM, a time resolution of about 40 ms would thus be necessary. Global Position System (GPS) navigation receivers can provide a useful, very accurate time of day output, but its resolution is only 1s. The BPSS integrated a GPS receiver and the sensor with a laptop computer. Using QinetiQ-developed software, the program detected the GPS second time signals (hh:mm:ss), then measured the incremental time (:sss) between the last GPS signal and the next sensor signal. In post-trial data analysis, the sensor time became the time logged from the GPS plus the measured sensor offset time (i.e. hh:mm:ss + :sss).

D.4.5 The pre-trial testing for the BPSS was limited to basic functional testing in the laboratory; no equipment suitable for testing in a simulated environment was available. The system was taken to Swaffham and tested in place three days before the trial. It was very easily and quickly installed, with the sensor mounted on a simple, folded, sheet metal bracket adequately fastened to the turbine structure with double-sided adhesive tape. Although the sensor sensitivity adjustment was found to be very sensitive, the BPSS otherwise worked well on that occasion. The procedure for the trial was to start the BPSS each morning and return at the end of each day's trial to collect the day's data and then switch it off.

D.4.6 Operational problems were encountered during the trial week. The major problems were caused by gusting winds strong enough to drive the turbine at maximum output. These conditions produced moderate nacelle vibration and a harsh electromagnetic interference

(EMI) environment in the nacelle. The EMI arose from the basic design concept of the Enercon design which generates "frequency wild" alternating current which is rectified to direct current in the nacelle before transmission down the tower to ground level where it is inverted to stable 50 Hz current: the control electronics associated with the power rectification transmitted transient signals which were received by the BPSS. It was only in high output conditions that the rogue transients presented a problem. Vibration caused flexing of the sensor mounting bracket and sensor mis-triggering, and the EMI caused data corruption. A stiffer mounting bracket was put in place, and the problem was eliminated. The EMI effects were minimised by firstly wrapping the cable connecting the sensor to the laptop in a metal foil "screen", then routing/suspending the modified cable away from metal structure within the nacelle. During the week, some data were lost when the computer stopped data logging for unknown reasons: on each day, the nacelle was visited at least once during the day, so no complete days were lost.

D.4.7 The post-trial view of the BPSS was that some valuable knowledge had been gained, and it would enable us to build a better sensor on a future occasion. A major lesson learned was that, in high, gusting winds, the generator, despite its great mass, could change speed very quickly indeed (within a small fraction of a revolution). The reason for this behaviour was that, under high generator output conditions, the magnetic coupling force between the generator armature and stator was very strong, and fluctuated in unison with the wind speed. It was therefore not sufficient to sample blade position using a single sensor trigger (i.e. only a single detection per rotor revolution). Some good and useful blade position data were recorded, and it was usefully supplemented by the use of a high specification VHS video recorder to analyse MPR's video camera record of the turbine behaviour.

D.5 Full results

D.5.1 This section contains analysis of more of the measurement data for a number of different situations. Table D-1 lists these configurations:

Date	Time Start	Time End	RPM	PITCH	YAW	Run	Comment
02/07/02	17:26:24.00	17:26:32.00	23	6	39	SWT070	Raining
04/07/02	16:06:30.78	16:06:45.66	12.4	1	0.4	SWT194	
05/07/02	12:20:10.33	12:22:18.33	12.5	1	93	SWT247	
03/07/02	10:07:50.32	10:08:01.20	15	1	-92	SWT092	Poor Visibility

Table D-1; Details of the data analysed in this section

D.5.2 Results from each measurement run will now be presented, and some explanations offered for the observed features.

D.5.3 SWT070 (39° yaw)

D.5.3.1 This measurement was made under the same conditions as the data in the main report, but during wet weather. The features observed in the RCS and Doppler plots are essentially the same, with perhaps a slight increase in the RCS level of various parts of the target, such as the blade tips (visible at the edges of the spectrum plot). Results are shown in Figure D-2 and Figure D-3.

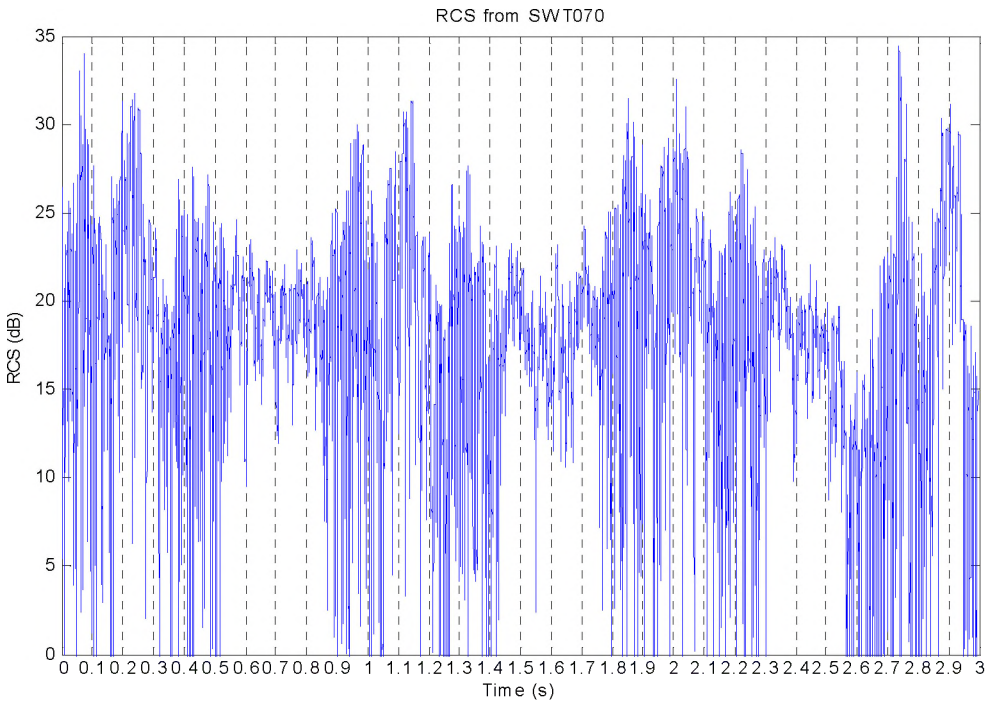

Figure D-2; RCS of the Swaffham turbine for slightly more than one rotor revolution. See Table D-1 for turbine conditions (run No SWT070).

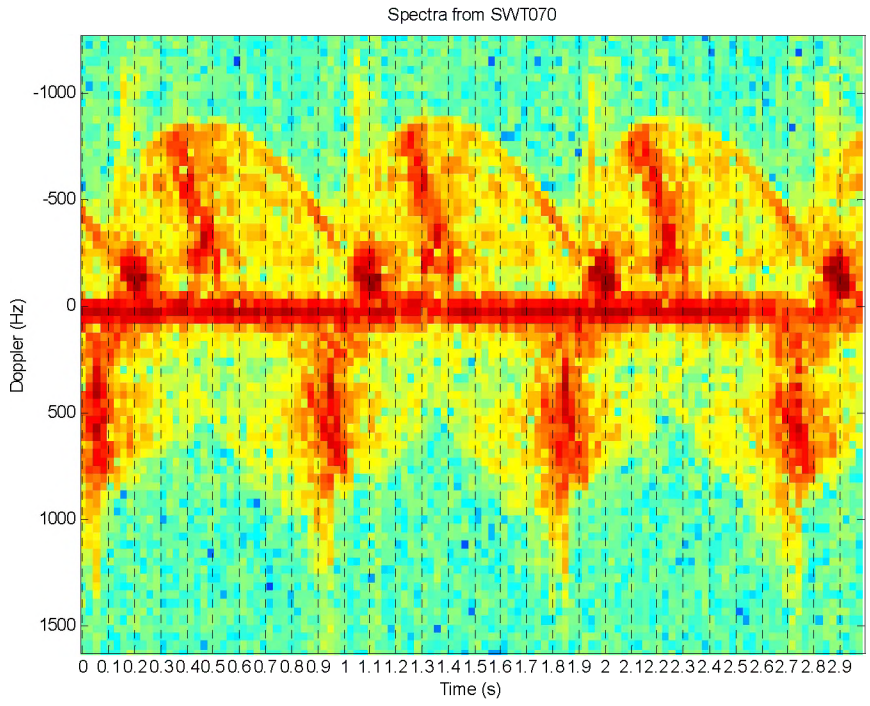

Figure D-3; Doppler spectra plot for the Swaffham turbine for 3 seconds of data. See Table D-1 for turbine conditions (run No SWT070).

D.5.4 SWT194 (0.4° yaw)

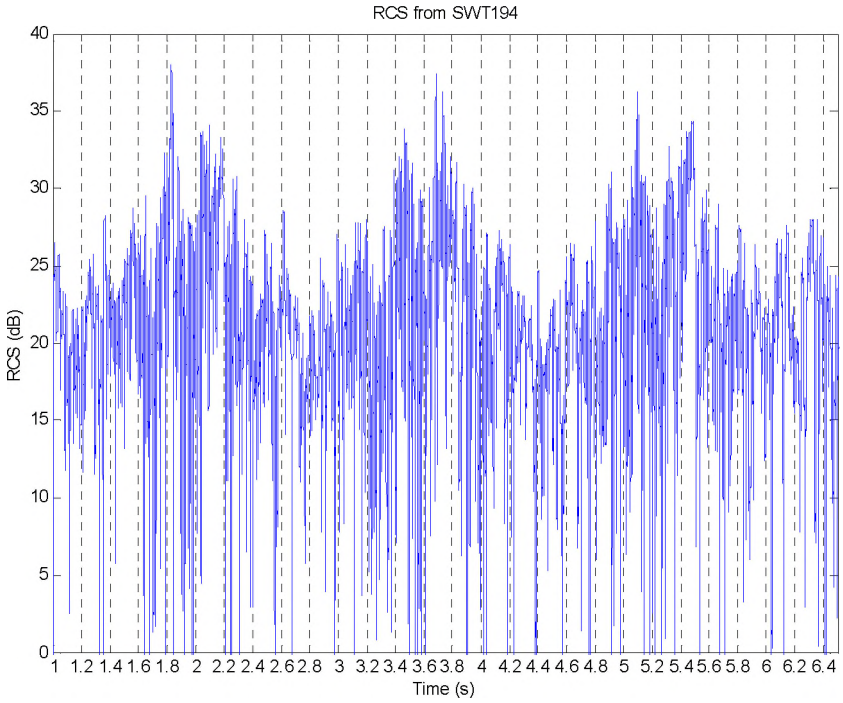

Figure D-4; RCS against time, for turbine facing radar

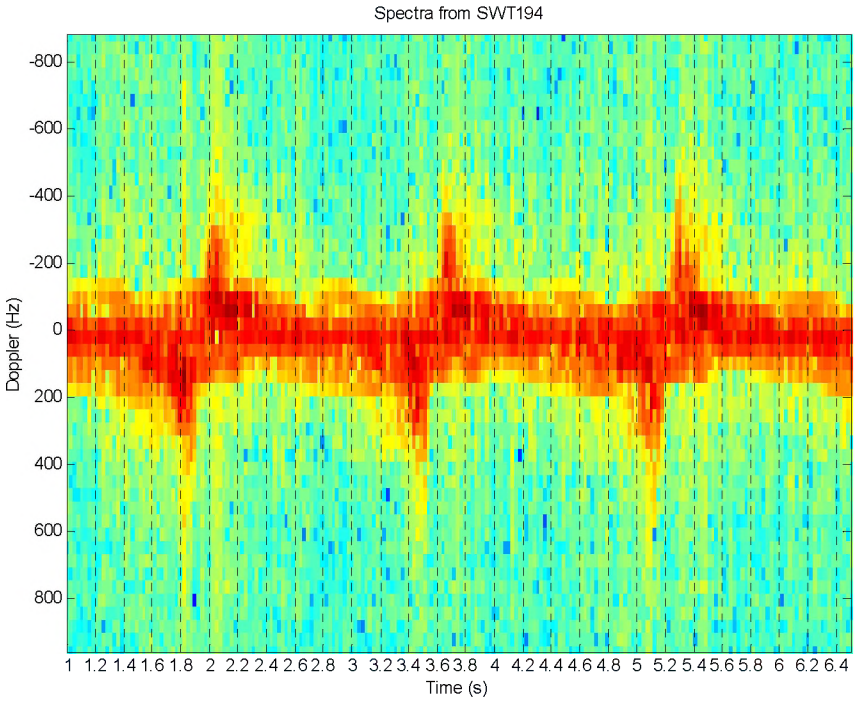

Figure D-5: Doppler spectra versus time, for turbine facing radar

D.5.4.1 Comparing the results shown in Figure D-4 and Figure D-5 with the turbine blade positions in Figure D-6, it is clear that the periods where there are a significant Doppler spread correspond to the times when the lower blade becomes vertical, and passes in

front of the tower. A possible explanation is that the action of the blade passing in front of the tower effectively shifts the reflection point from the tower, first towards the radar, and then away from the radar – giving a positive Doppler shift followed by a negative shift. A peak Doppler shift of approximately 320Hz implies a velocity of 16ms^{-1}, using the formula:

$$f_d = 2\frac{v_r}{\lambda} \qquad (D - 1)$$

where f_d is the Doppler frequency, v_r the relative velocity, and λ is the wavelength corresponding to the radar frequency, 3.05GHz. From Figure D-5, the time period during which the Doppler frequency changes is approximately 0.4s, giving the base of a simple triangle with height 16ms^{-1}, and area 3.2m. This is the same order of magnitude as the distance between the front surface of the tower and the front surface of the turbine blade, approximately 4.6m.

D.5.4.2 When the blade is alongside the tower, the overall echoing area from that region is maximised, producing a peak in the RCS, followed by a dip as the blade obscures the tower, and another increase in RCS as both blade and tower become visible again. The curvature of the blade surface ensures that the phase centre of the reflection is always moving, so the peak RCS levels are almost unaffected by zero-Doppler filtering, as seen in Figure D-7. The point at which the lower blade is vertical seems to occur closer in time to the negative Doppler shift, rather than the positive. This may be due to the detailed shape of the front surface of the blades, or may simply result from the difficulty in estimating exact timings from the video. Similarly, it is difficult to determine whether the 'blade up' position corresponds to a null or a narrow peak in the RCS pattern. Further analysis of the static measurements, and more slowly rotating dynamic measurements, are required to clarify these issues – but this is beyond the scope of the current contract, and may be of purely academic interest given the good agreement seen so far between predictions and measurement data.

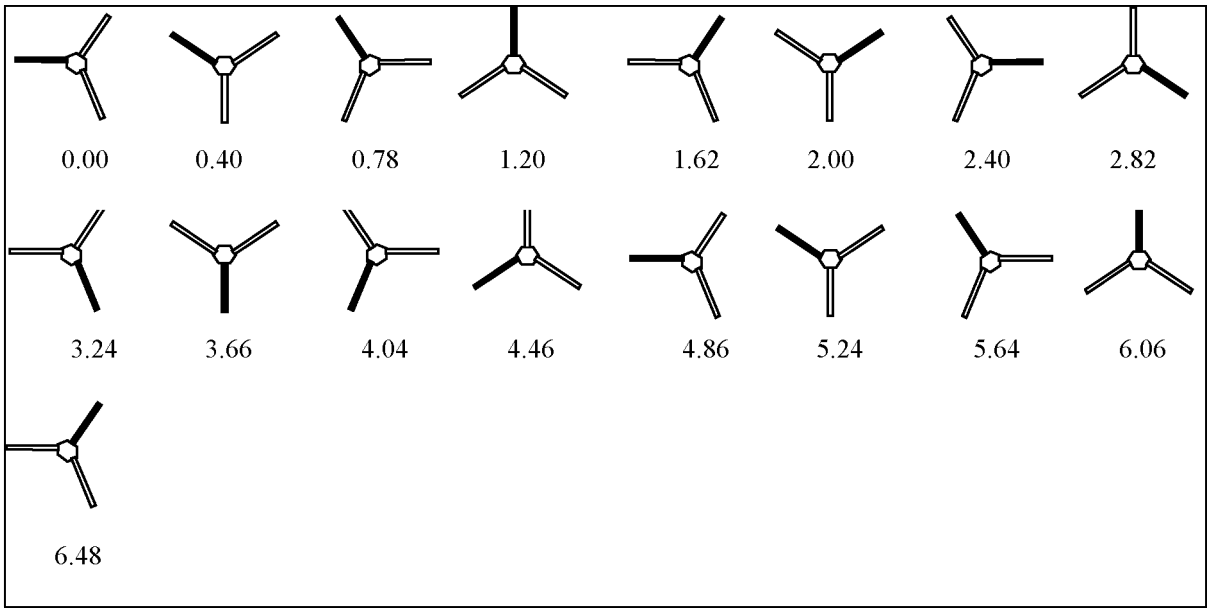

Figure D-6: Approximate times (seconds) for blade positions, turbine facing radar, SWT194

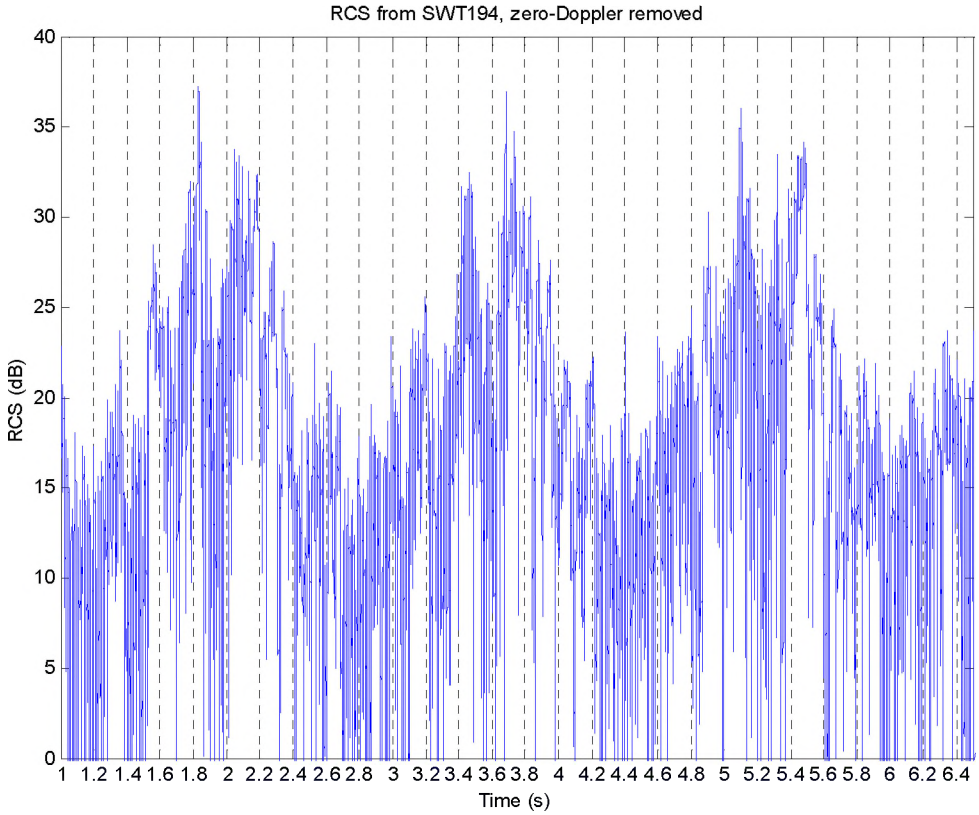

Figure D-7: RCS of moving parts for turbine facing radar

D.5.5 SWT247 (93° yaw)

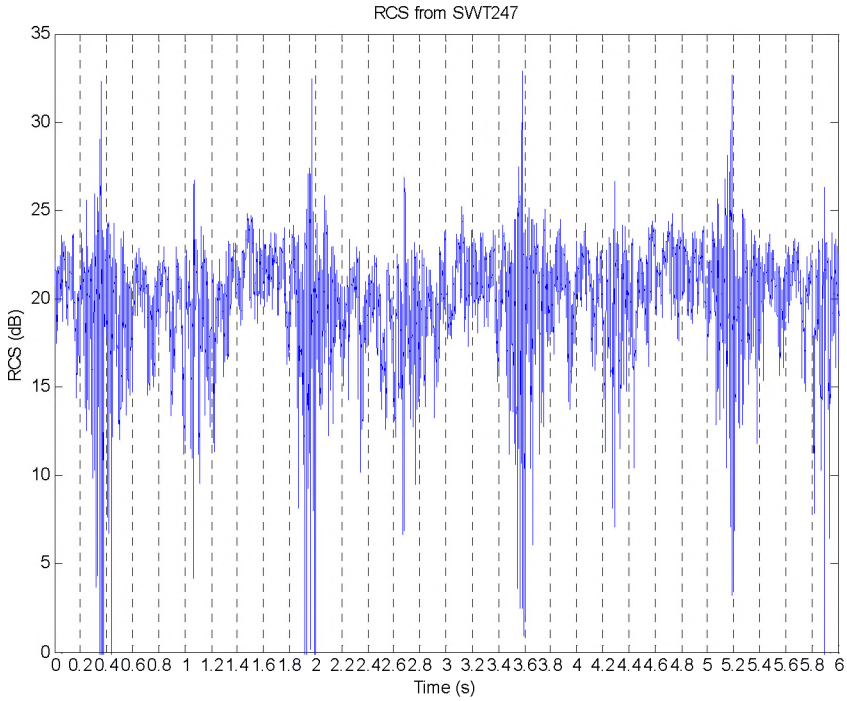

Figure D-8: RCS versus time for turbine facing to the south

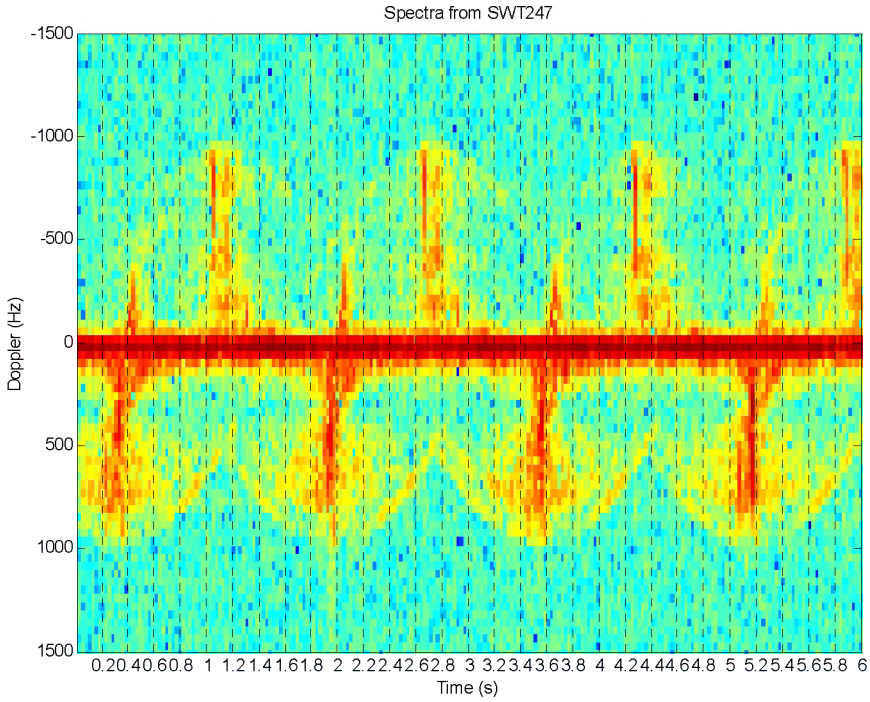

Figure D-9: Doppler spectra for turbine facing to the south

D.5.5.1 In this example, the turbine was side-on to the radar, facing approximately south. The blades rotate in a clockwise direction, so that when they are vertical, the top blade moves

away from the radar, and the bottom blade moves towards the radar. At these times, negative and positive regions of Doppler spread are produced, respectively – see Figure D-9. The weather was very misty during these measurements, giving poor visibility of the wind turbine on the video. However, it was possible to determine that at approximately 4.7s, the blade pointing towards the radar was horizontal, and moving upwards. Given that the rotation speed during this run was approximately the same as that during SWT194, we can therefore deduce the blade positions corresponding to major features on the plots. This confirms the previous statement on positive and negative Doppler flashes, showing that, once again, the RCS peaks corresponding to a blade pointing vertically downwards, are higher than those produced by a blade pointing vertically upwards. The smaller negative Doppler flash occurring moments after each positive flash, is probably caused by the same mechanism as the Doppler flashes observed during the head-on measurement, SWT194. That is, the phase centre of the combined reflection from the tower and the blade, moves rapidly away from the radar as the blade rotates upwards. The positive Doppler contribution, as the reflection point moves towards the radar, coincides with that from the moving blade itself.

D.5.5.2 This measurement does not show any evidence of a third RCS peak in-between the two caused by neighbouring blades passing through vertical, as was seen in the 38° yaw data. This suggests that the multiple bounce mechanism is not very strong at this aspect, possibly due to the curved shape of the turbine blades.

D.5.6 SWT092 (-92° yaw)

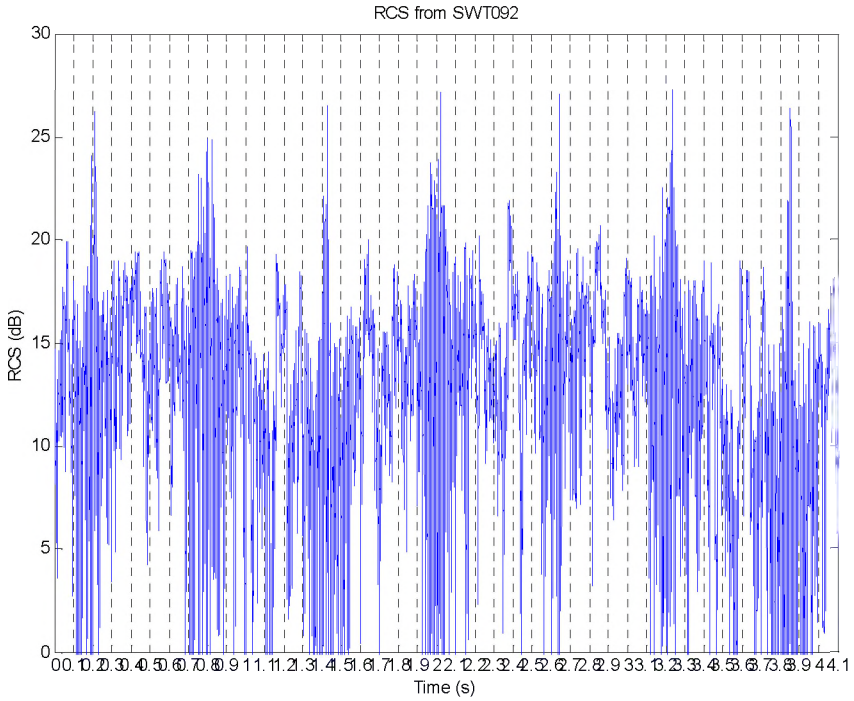

Figure D-10: RCS versus time for turbine facing to the North

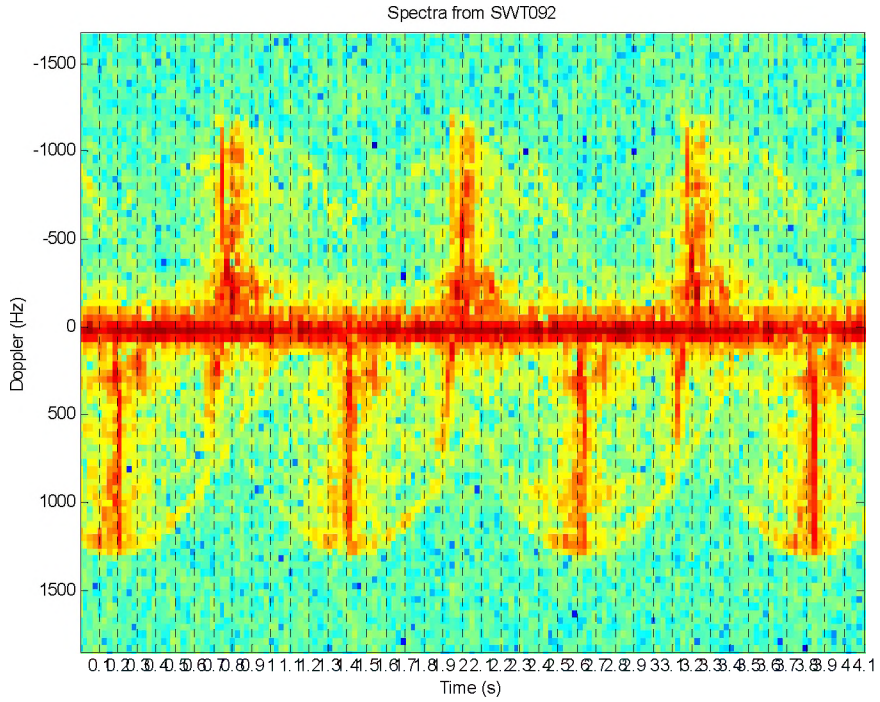

Figure D-11: Doppler spectra for turbine facing to the North

D.5.6.1 In this example, the turbine was side-on to the radar, facing roughly to the north. The blades rotate in a clockwise direction, so that when they are vertical, the top blade moves towards the radar, and the bottom blade moves away from the radar. At these times, positive and negative regions of Doppler spread are produced, respectively – see Figure

D-11. This view of the turbine makes it difficult to estimate blade positions, except when there is a horizontal blade pointing towards the radar. Two such instances occur at times of 0s and 1.18s, when the horizontal blade is moving downwards, just before a positive Doppler flash from the blade passing over the top of its trajectory. There is evidence of smaller positive Doppler flashes (i.e. corresponding to a lower speed range) occurring just after each blade passes upwards vertical, and just before the blades reach downwards vertical. These could be caused by multiple bounce interactions between the blades and the observation platform, with some contribution from the mechanism proposed in the previous sections (movement of the phase centre of the combined reflection).

E CIRCULAR POLARISATION

E.1.1 Questions have been raised about the ability of the WHIRL to model radar using circular polarisation. This is possible and can be configured by setting up configured input files and processing the output data to obtain circular polarised fields. This would then make a circular polarisation RCS library that could be used by the model.

E.1.2 Many surveillance radar use circularly polarised radiation, with the aim of improving the detection of wanted targets in the presence of weather clutter. A circularly polarised wave has its electric field vector rotating continuously as it travels, in contrast to a linearly polarised wave in which the electric field vector oscillates in a fixed plane. Circular polarisation can be left-handed or right-handed, depending on which way the electric field is rotating relative to the direction of travel. When a circularly polarised wave is reflected from a simple surface, the hand of circular polarisation is reversed, since the reflected electric field rotates in the same sense in the plane of the reflector surface, but the direction of travel is reversed. This is also true of raindrops, which are approximately spherical. Thus a radar which receives the same hand of circular polarisation as it transmits will tend to reject echoes from raindrops; and it is intended that this will improve visibility of other objects in rain.

E.1.3 Other objects are often complex in shape. The radar energy may bounce back directly to the target, or it may bounce back after two or more bounces, if the target contains concave parts in its structure. In these cases the polarisation of the reflected energy is often more equally split between the two hands of circular polarisation. In particular, a significant fraction of the energy comes back in the same hand as the transmitted energy, and so is detected by the radar. The use of circular polarisation does reduce the RCS of most targets relative to linear polarisation, because that part of the reflection which comes from smooth surfaces is not detected. But if the RCS of rain drops is reduced by a larger factor than the RCS of wanted targets (as is generally the case), then the visibility of wanted targets is improved by the use of circular polarisation.

E.1.4 Circular polarisation can be represented by a combination of vertical and horizontal linear polarisations with a 90 degree phase shift between them. Using this, the RCS of circular polarisation can be computed, if we know the RCS to both vertical and horizontal linear polarisations, including their phases. The average of the vertical and horizontally scattered electric fields is the part reflected from smooth surfaces, which is rejected by the circular polarisation radar. In the computations, this is the physical optics contribution, which is the same in both linear polarisations, and is generally the largest part. The remainder is the difference between the two scattered fields, which is detected by the circular polarisation radar. In the computations, this can arise from multiple-bounce reflections, or from edge scattering which is different in the two linear polarisations. For a convex object such as a turbine blade, there are no multiple-bounce effects (though there may be for a complete turbine set with tower). Thus the computed circular polarisation RCS arises from edge diffraction from the fairly sharp edge of the blade. Strictly speaking, there is another contribution to the circular polarisation RCS, from any cross-polar (vertical to horizontal or vice versa) scattering by the target. In the case of the turbine blades the computations show this to be small, so we will omit it.

E.1.5 Figure E-1 shows the circular polarisation RCS for the 26 metre turbine blade of which a scale model has been made earlier in this work. The red curve is obtained from the vertical and horizontal linear polarisation RCS values measured on the scale model, and scaled up to full size. The blade is tilted with its comparatively flat surfaces at 40 degrees to the viewing direction. On the angle scale, 0 and 180 degrees are looking at the inner and outer ends of the blade, and 90 and 270 degrees are looking perpendicular to its length. The green curve shows the circular polarisation RCS obtained from our computed linear polarisation RCS values. We see that there is good general agreement on the overall shape of the curves, and also on the position and height of the two main peaks. These peaks occur when we are looking perpendicular to the length of the blade, as one would expect. This agreement demonstrates that our RCS software is able to compute the circular polarisation RCS satisfactorily. The peak RCS is around +10 dBsm. This is considerably lower than the linear polarisation RCS, which is +25 to +30 dBsm for this blade in this orientation, but still large enough to be detectable.

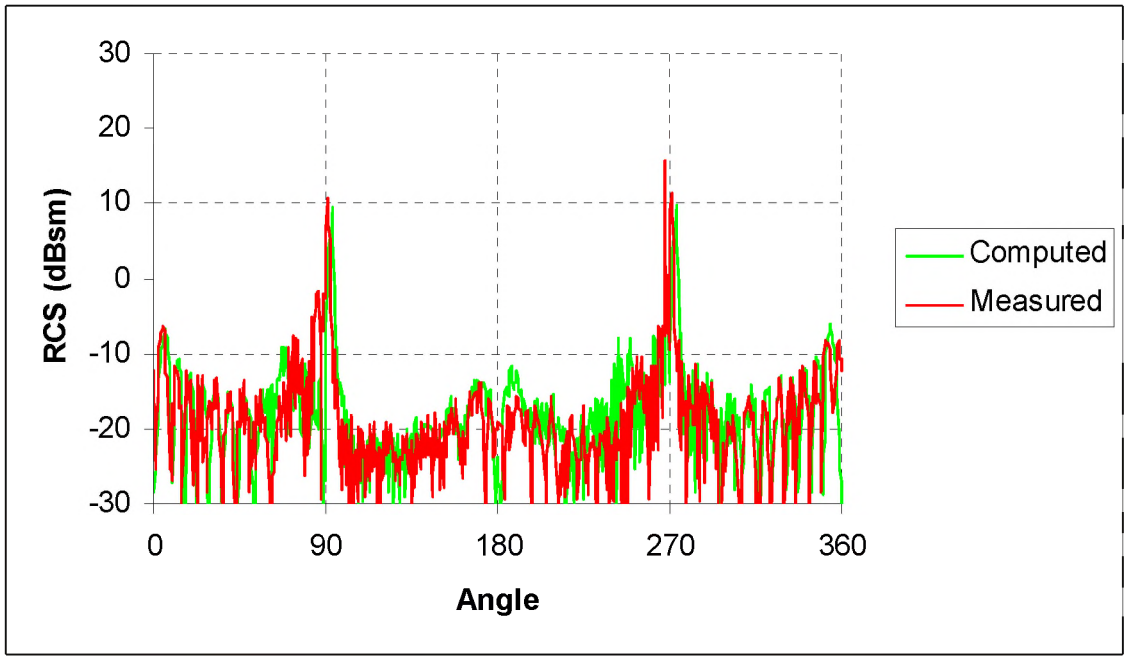

Figure E-1; Circular polarisation RCS of 26 m turbine blade

F IDENTIFICATION OF UK WIND FARMS WITHIN LINE-OF-SIGHT OF PRIMARY RADAR

F.1 QinetiQ introduction

F.1.1 One of the deliverables of this contract was to identify and catalogue all of the wind farms in the UK within site of primary radar installations. This is to provide a useful database of information that can be accessed by aviation and wind farm stakeholders when dealing with siting issues.

F.1.2 This task was sub-contracted by QinetiQ to Emrad Ltd the research and consultancy department of Pipehawk PLC. Emrad have had experience dealing with the electromagnetic interference of wind turbines with respect to TV signals and data links.

F.1.3 This work has generated a searchable database of all the current UK wind farms within LoS of primary radar. As this contains the positions of many of the UK military radar installations it is deemed unsuitable by the MoD for release into the public domain in its entirety. Therefore a suitable custodian (to be identified) will control the database and will release information within the database as required.

F.1.4 The rest of this appendix is a description of the database as supplied by Emrad Ltd.

F.2 Emrad Introduction

F.2.1 The main objectives of this task is to identify all current UK wind farms operating within the line-of-sight of primary radar installations and then collate geographical and technical information with regard to these wind farms and radar installations.

F.2.2 The general location of wind farms was obtained from BWEA, FES and by contacting wind farm operators directly. A 1:50,000 Scale Colour Raster Ordnance Survey map was used to obtain the corners of relevant wind farms to an accuracy of 10m; this is within one-second accuracy.

F.2.3 The UK's civil aviation radar consists of NATS and civil aerodromes. Information pertaining to UK's aerodromes and NATS' radar sites were obtained with the aid of CAA and NATS personnel. Furthermore, the CAA provided contact information for relevant civil aerodromes. This information was used to contact senior ATC personnel from specific aerodromes to establish the existence of respective line-of-sight wind farms. NATS provided a detailed verification list of their radar sites, which complemented the information received from CAA.

F.2.4 The MoD provided detailed technical data and contact information for their ASACS and ATC radar sites. Squadron Leader K. Smart provided information pertaining to ATC radar in the line-of-sight of wind farms. Squadron Leader G. Phillip provided contact information for the ASACS radar sites. This information was then used to contact ASACS radar sites in order to verify line-of-sight exists.

F.2.5 The location of each radar mast and wind turbine was verified against a 1:50,000 Scale Colour Raster Ordnance Survey map. This map was also used to determine the terrain between radar sites and line-of-sight wind farms.

F.2.6 A Microsoft Access database has been designed to aid the analysis of the collated information. The database consists of four relations (tables): Wind Farms, Radar Sites, Terrain and Wind Turbine Co-ordinates. The analysis of the information is achieved by the use of queries and reports. A general description of the terrain between a line-of-sight radar installation and a specified wind farm is given in the "Radar and Wind Farm" database.

F.3 Wind Farms

F.3.1 The majority of the data collated pertaining to wind farms was obtained from the BWEA and FES. This data included the wind farm name, operator, quantity, manufacturer and geographical location. A 1:50,000 Scale Colour Raster Ordnance Survey map was used to verify the location of the wind farms and to find the corners of relevant wind farms to an accuracy of 10m; this is within one-second accuracy. Where necessary, the co-ordinates of wind farms and wind turbines were obtained by contacting the wind farm operators.

F.3.2 Currently, a total of 98 wind farms operate in the UK (Feb 2003), 18 of these wind farms are in line-of-sight of a radar installation and 4 are in line-of-sight of more than one radar installation.

F.4 UK Radar Installations

F.4.1.1 There are two types of radar used for air traffic control and air defence control; these are primary radar and secondary surveillance radar (SSR). Primary radar is used to determine the range and bearing of a detected object; it can neither differentiate between objects nor determine their height. Secondary surveillance radar employs a transponder, which is located in the detected aircraft, to determine the aircraft's range and height. Therefore secondary surveillance radar is able to differentiate between airborne aircraft and wind turbines; consequently, only primary radar installations have been investigated.

F.4.2 Air Traffic Control

F.4.2.1 Air traffic control consists of aerodrome surveillance and en-route (or area) radar. Aerodrome surveillance radar allows air traffic controllers to provide air traffic service to aircraft in the vicinity of an airport. Area radar, which in the UK is operated by the NATS, provides a service for both civil and military aircraft in transit. Area radars have a longer range (typically 333km) than aerodrome radars (typically 139km), particularly at high altitudes.

F.4.2.2 A total of 51 UK ATC radar sites have been identified, 9 of these radar sites operate with one or more wind farm in line-of-sight of their radar.

F.4.3 Air Defence

F.4.3.1 Air defence radar provides air traffic service to military traffic; this is a similar role to that of the ATC for civilian aircraft. Furthermore, the MoD's ASACS monitor air traffic activity within the UK and its approaches with the aim of preserving the integrity of UK airspace.

F.4.3.2 A total of 42 ATC radar sites have been identified, 8 of these radar sites operate with one or more wind farm in line-of-sight of their radar.

F.4.3.3 A total of 30 ASACS radar sites have been identified, 3 of these radar sites operate with one or more wind farm in line-of-sight of their radar.

F.5 Description of the Database

F.5.1.1 Emrad Ltd has developed a database containing the relevant details of wind farms, UK radar sites and a description of the terrain between wind farms and line-of-sight radar installation. The database consists of four relations (tables):

- Radar Site.
  - Information pertaining to UK civil and military radar sites.
- Wind Farm
  - Information pertaining to UK wind farms.
- Terrain
  - A description of the terrain between radar sites and respective line-of-sight wind farms.
- LoS Turbine Location
  - Geographical Co-ordinates of wind turbines which are in line-of-sight of radar installations

F.5.1.2 The relationship between the tables is shown in Figure F-1. Each table consists of a primary key (one field whose value uniquely identify each record in the table) which provide matching data in key fields in other tables. A relationship works by matching data in key fields; usually a field with the same name in both tables. The primary keys in these tables specify that the value in the field 'Name' can never be duplicated within the table 'Radar Site'. The two primary keys in the table 'Terrain' specify that the combined value in the fields 'Radar Site' and 'Wind Farm' can never be duplicated within the table 'Terrain'. The one-to-many relationship between tables 'Radar Site' and 'Terrain' specifies that the value in the field 'Name' (in table 'Radar Site') can only occur once and that the same value in the field 'Radar Site' (in table 'Terrain') may occur many times.

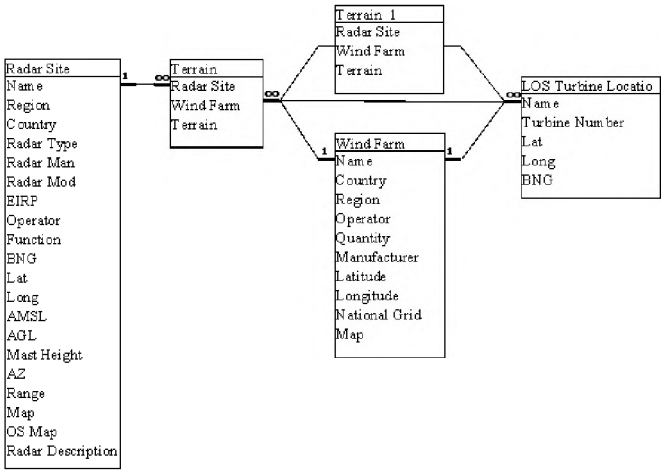

Figure F-1 Relationships for the Wind Farm Database

F.5.2 Radar Site

Field	Description
Name	The radar site's name
Region	County
Country	England, Scotland, Wales, Northern Ireland
Radar Type	Primary or secondary radar
Radar Man	Radar manufacturer
Radar Mod	Radar model number
EIRP	This is the highest peak instantaneous power within the antenna pattern. The peak gain of the beam pattern will be set to occur at an elevation of 2-3 degrees. (dBW)
Operator	Radar operator (NATS, RAF, RNAS, Aerodrome etc.)
Function	Radar function (en route, approach, SMR etc.)
BNG	The radar antenna's British National Grid location to 10m accuracy
Lat	The radar antenna's latitude (World Geodetic System 84) to 1 degree accuracy
Long	The radar antenna's longitude (World Geodetic Systems 84) to 1 degree accuracy
AMSL	The above mean sea level height to the centre of the antenna in meters
AGL	The above ground level height to the centre of the antenna in meters
Mast Height	Mast height to the centre of the antenna/scanner in meters
AZ	Azimuth propagation in degrees (generally 360 degrees)
Range	The maximum range, in km, at which the radar is used. Radar may be capable of detecting objects further than this distance but they would be ignored.
Map	This is a hyperlink to either www.streetmap.co.uk or www.multimap.com , which displays a detailed map of the radar
OS Map	This is a hyperlink to the relevant OS tile, which must be located on a local hard drive
Radar Description	This is a Microsoft Word document contain any further information about the radar site
Confirmed	The name of the person that gave confirmation about the line-of-sight wind farms or who provided information about the radar site
Contact	The telephone number of the person who provided information about the radar site

F.5.3 Wind Farm

Field	Description
Name	The wind farm's name
Region	County
Country	England, Scotland, Wales, Northern Ireland
Operator	The company that owns the wind farm
Quantity	The number of operating wind turbines on the wind farm

Manufacturer	The Wind turbine manufacturer
Latitude	The wind farm's latitude (World Geodetic System 84) to 1 degree accuracy.
Longitude	The wind farm's longitude (World Geodetic Systems 84) to 1 degree accuracy.
National Grid	The wind farm's centre British National Grid to 10m accuracy
Map	This is a hyperlink to either www.streetmap.co.uk or www.multimap.com , which displays a detailed map of the wind farm (in some cases this is an aerial view)
OS Map	This is a hyperlink to the relevant OS tile, which must be located on a local hard drive

F.5.4 Terrain.

Field	**Description**
Radar Site	The radar site's name
Wind Farm	The wind farm's name
Terrain	A description of the terrain between the radar site and the line-of-sight wind farm

F.5.5 RAF St. Mawgan

RAF St. Mawgan is chosen as an example, to illustrate how the database can be used to extract information about radar installations and wind farms operating in line-of-sight of their radar.
Information pertaining to RAF St Mawgan can be found in the table 'Radar Site', and can be displayed in a report form by running an Access report called 'Radar Installation'. Double clicking the 'Radar Installation' icon will execute a query, which will prompt the user to enter the name of a radar installation; in this case RAF St Mawgan is entered into the prompt box. Figure F-2 shows the output from the query, which can then be printed.

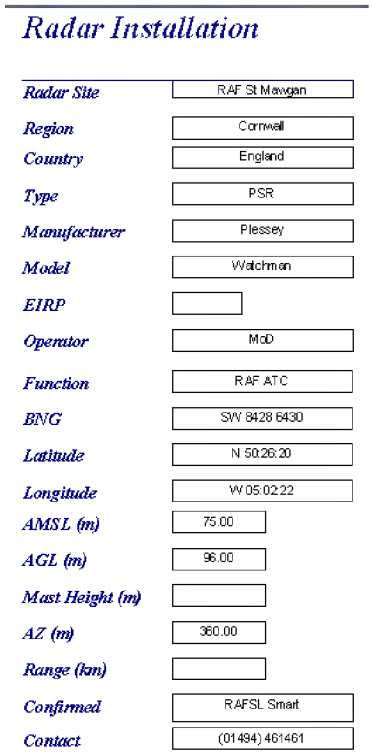

Radar Installation

Radar Site	RAF St Mawgan
Region	Cornwall
Country	England
Type	PSR
Manufacturer	Plessey
Model	Watchman
EIRP	
Operator	MoD
Function	RAF ATC
BNG	SW 8428 6430
Latitude	N 50:26:20
Longitude	W 05:02:22
AMSL (m)	75.00
AGL (m)	96.00
Mast Height (m)	
AZ (m)	360.00
Range (km)	
Confirmed	RAFSL Smart
Contact	(01494) 461461

Figure F-2 Information about RAF St. Mawgan from table 'Radar Site.

Another Access report, named 'LOS Wind Farms', is used to display information about the wind farms operating in line-of-sight of RAF St. Mawgan. Figure F-3 shows the output from the query, which can then be printed.

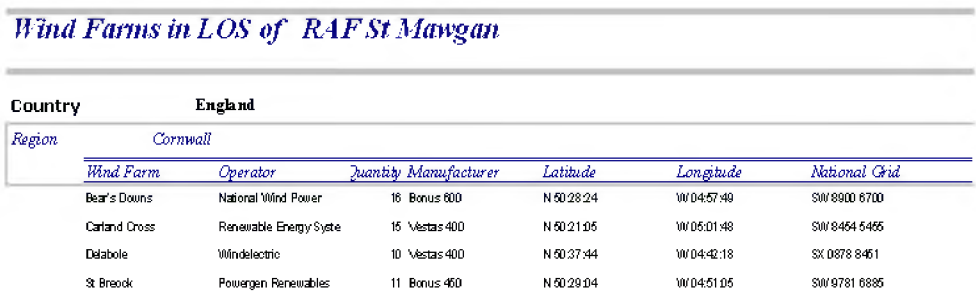

Wind Farms in LOS of RAF St Mawgan

Country **England**

Region *Cornwall*

Wind Farm	Operator	Quantity	Manufacturer	Latitude	Longitude	National Grid
Bear's Downs	National Wind Power	16	Bonus 600	N 50:28:24	W 04:57:49	SW 8900 6700
Carland Cross	Renewable Energy Syste	15	Vestas 400	N 50:21:05	W 05:01:48	SW 8454 5455
Delabole	Windelectric	10	Vestas 400	N 50:37:44	W 04:42:18	SX 0878 8451
St Breock	Powergen Renewables	11	Bonus 450	N 50:29:04	W 04:51:05	SW 9781 6885

Figure F-3 Wind Farms operating in line-of-sight of RAF St. Mawgan.

F.5.5.1 A description of the terrain between RAF St. Mawgan and each of the wind farms is held in a Microsoft Word document. This document is embedded within the database and can be accessed via the 'terrain' column in the 'terrain' table. A description of the terrain is as follows:

- Bear's Down consists of 16 wind turbines, 150m to 160m AMSL, located 7km E of RAF St. Mawgan. The wind farm has a spread of 1.5km. Denzell Downs is 185m AMSL and is 6.5km from RAF St. Mawgan. This may block 4 of the turbines.
- Carland Cross consists of 15 wind turbines, 120m to 150m AMSL, located 9km South of RAF St. Mawgan. The wind farm has a spread of 1km.
- Delabole consists of 10 wind turbines, 240m to 260m AMSL, located 33km NE of RAF St. Mawgan. The wind farm has a spread of 1km. Higher Tynes is 205m AMSL and is 28km from RAF St. Mawgan.
- St. Breock Downs consists of 11 wind turbines, 170m to 200m AMSL, located 14km NEE of RAF St. Mawgan. Nine Maidens is 170m AMSL and is 10km from RAF St. Mawgan.

This page is intentionally blank

G INDEPENDENT REVIEW OF WHIRL

G.1 QinetiQ introduction

G.1.1 As part of this study a contractor was appointed to conduct an independent review of the modelling work carried out during this study. The Contractor was EMRAD the research arm of PipeHawk PLC, who have had experience of dealing with the electromagnetic interference issues of wind turbines, for TV signals and data links.

G.1.2 This appendix is a summary of their findings and thoughts on the QinetiQ work. This was done after the first draft of the findings was complete and since then a number of the points raised by EMRAD have been addressed. These are noted in this appendix with footnotes.

G.2 EMRAD introduction

G.2.1 The Radar Cross-Section of a target is a measure of the target's ability to scatter electromagnetic energy in a specified direction and is a function of the electrical properties of the incident wave and the electrical and physical properties of the target.

G.2.2 The precise Radar Cross-Section of a complex target can only be calculated by solving Maxwell's equations with appropriate boundary conditions. Fortunately, Physical Optics can be used where the target is considerably larger than the wavelength of the incident wave; for example, modelling a wind turbine which has a rotor diameter of greater than 30m, illuminated by an incident wave which has a wavelength of just 10cm (3GHz). This approximation is adequate for smooth surfaces; furthermore, it reduces both the computational processing time and the complex mathematical algorithms required to solve Maxwell's equations. The Physical Theory of Diffraction (PTD) is particularly useful in the treatment of sharp edges and where the incident wave is circularly polarised.

G.2.3 The software model recently developed by QinetiQ for predicting the interaction of wind farms with radar uses two existing programs. The program developed specifically for this project is named WHIRL (Wind-farms Having Interactions at Radar Locations). WHIRL uses Ocellus to calculate the Radar Cross-Section of a single wind turbine and NEMESIS to calculate the propagation factors. WHIRL is a software simulation tool which models radar interaction with a wind farm. It displays the results on a virtual Plan Position Indicator (PPI) which resembles a map with the radar site at the centre of the display[1].

G.2.4 Ocellus uses the Physical Optics (PO) technique and the Physical Theory of Diffraction to determine the Radar Cross-Section of a single wind turbine.

G.2.5 The terrain plays a significant role in the propagation of radar and must be modelled appropriately. NEMESIS is used to determine the complex propagation coefficients for a predefined radar scenario. The program makes use of the Parabolic Equation Method (PEM) and the Fourier Split-Step Method to compute the effective refractivity over a specified range and terrain.

[1] For a full description of how the modules fit together see section 3.3 and figure 3.1 in the main report.

G.2.6 This report discusses all three programs and provides an unbiased opinion on the level of confidence to be placed in WHIRL.

G.3 Ocellus

G.3.1.1 The Radar Cross-Section (also known as the echo area) of a target is a function of its physical and electrical properties and the electrical properties of the incident wave.

G.3.1.2 Ocellus was originally written for MoD projects and was developed over several years under the ISO9000 quality system and has been verified against UK targets.

G.3.1.3 Ocellus is used to calculate the Radar Cross-Section of a single wind turbine by utilising well established analytical methods. The logical mathematical technique to be used for calculating the Radar Cross-Section of a complex target in the optical region, such as wind turbines being irradiated by a 3GHz radar pulse, is Physical Optics. This is because the physical structure of wind turbines[2] is invariably larger than the radar wavelength[3] and the surface of the turbine is predominantly smooth. Physical Optics is one of many techniques that may be used to approximate Maxwell's equations and is best suited to this application. The Finite Element Method could also be used for this application but it would require unreasonably large amounts of computer processing and memory. The use of other techniques, such as Method of Moments, is limited by computer memory and is best suited to electrically small objects, with well defined boundaries.

G.3.1.4 Ocellus detects sharp edges which may be present in the turbine structure and then uses the Physical Theory of Diffraction to determine the Radar Cross-Section of such elements. Furthermore, multiple bounce due to adjacent blades and the turbine tower and ground reflections have not been included at this stage because of the large computer overheads but could be included if required.

G.3.1.5 Ocellus requires an ASCII input file containing parameters relating to the radar antenna and scattering object.

G.3.2 Radar antenna

G.3.2.1 The main parameters relating to the radar antenna are the radar operating frequency and the positions of transmit and receive antennas. The program can compute the monostatic or bistatic Radar Cross-Section as selected by the user. Monostatic radar uses a common antenna to both transmit and receive the radar signal. In the bistatic arrangement a considerable distance separates the transmitter and receiver antennas. The ability of the program to model either types of radar is useful because both these methods are employed in UK radar.

G.3.3 Scattering material

G.3.3.1 The scattering material may be either a perfectly conducting material or a multilayer structure. Each layer in the multilayer structure can be allocated a thickness and complex permittivity. This facility is particularly useful when modelling turbine blades that have a metal lighting conductor extending from the hub to the tips of the blades and the blade

[2] The rotor diameter of wind turbines is generally greater than 20m
[3] The wavelength for UK radar is between 3cm and 50cm

itself is generally made from materials having significant electrical properties such as fibreglass reinforced composite material.

G.3.4 Output generated by Ocellus

G.3.4.1 Ocellus generates an output file containing vital information about those parts of the structure which are responsible for the stronger reflections. This file allows the user to examine which mathematical techniques predominately contribute in the calculation of the Radar Cross-Section: it is therefore essential that the user has some technical understanding of these procedures.

G.3.4.2 Ocellus also generates a file for WHIRL-COM; this file requires another program to translate it to binary format suitable for WHIRL-COM. For development it has been convenient to keep this as a separate program but in future it should be integrated into WHIRL-COM. The file contains a data library of the frequency sweep, Radar Cross-Section azimuth cut, either far-field or non-far-field Radar Cross-Section and the complex plane-wave reflection coefficient of the turbine as a function of frequency, angle of incidence and polarisation.

G.3.5 Ocellus validation

G.3.5.1 QinetiQ have verified Ocellus by comparing the predicted and measured Radar Cross-Section values for the wind turbine located at Swaffham.

G.3.5.2 The single wind turbine situated at Swaffham (N52:39:24 E00:41:00) is an Enercon E-66; its hub is located 67m above ground level. Each of its three fibreglass (reinforced epoxy) blades is 30.8m in length with a clockwise rotating rotor having a diameter of 66m. The range of speed is 10-22RPM, with a maximum tip speed of 76m/s.

G.3.5.3 The Radar Cross-Section of the wind turbine for various yaw and pitch angles were measured. A comparison of the predicted and measured results is shown in section 6.2 of this report. The general trend of the predicted Radar Cross-Section matches that of the measured data for all the measured yaw and pitch configurations. This is a good indication that the mathematical algorithms used in Ocellus are appropriate for modelling the Radar Cross-Section of wind turbines. However, there is a significant variation in the Radar Cross-Section level; the predicted Radar Cross-Section data is 4dB to10dB less than the measured Radar Cross-Section data depending on the wind turbine's yaw and pitch configuration[4].

G.3.5.4 The key reasons given for these significant discrepancies are stated by QinetiQ are as follows:-

- The wind turbine model has been developed from information gleaned from photographs, information directly from wind turbine manufactures and measurements which have been taken or provided.

[4] QinetiQ comment: In response to these comments QinetiQ has recalculated the predicted data at the exact same radar settings used in the trial (before there were small differences). This has improved the level of agreement between the measured and predicted data, however, in some cases the predictions are 4 to 6 dB lower than the measurements near some of the RCS peaks. The two reasons that have been identified to explain the 4 to 6dB variances are that the actual blade reflectivity is higher than assumed in the modelling and the modelling does not include "multiple-bounce" returns. For a more detailed explanation see section 6.2.8.

- PipeHawk's views on this statement:-
- QinetiQ have not indicated who the providers of these measurements are nor have they provided details of how these measurements were undertaken.
- It would seem that greater uncertainty has been introduced into the model by taking measurements from photographs. Unfortunately in many cases this was the only mechanism available to obtain the detail required.

- The wind turbine model simulates the turbine's blades as solid fibreglass.
  - PipeHawk's view on this statement:-
  - Modelling the wind turbine as a solid perfectly conducting material would be sufficient for the scenarios modelled. Generally, this is a conservative approach in ensuring the Radar Cross-Section is not underestimated.

- The wind turbine model simulates the turbine's blades without the centre conductor and the metal tips.
  - PipeHawk's view on this statement:-
  - This level of detail is unnecessary for scenarios where the scattering object is electrically large compared with the wavelength of the incident wave.

G.4 NEMESIS

G.4.1.1 The terrain plays a significant role in the propagation of radar; as the plane wave travels over a terrain the wave will decay with distance and it will diffract and reflect when faced with obstacles such as hilltops or lakes. Consequently, the terrain between the radar and wind farm must be modelled. NEMESIS was originally developed and verified for use by the MoD and is considered to be a comprehensive software suite. It is now being used to determine the propagation coefficients for a predefined radar scenario where the radar system and environmental features are taken into consideration.

G.4.1.2 The two mathematical methods used are the Parabolic Equation Method (PEM) and the Fourier Split-Step Method; both these methods are numerically efficient. The Fourier Split-Step Method is a numerical solution to the plane wave equation. PEM is used to set the boundary conditions and determine the diffraction over hilltops into shadowed areas. It is an approximation of the full wave equation which models propagation at small angular deviations with high accuracy.

G.4.1.3 NEMESIS generates a binary array file containing the propagation factor which is given as a function of range, above ground antenna height, azimuth angle and elevation angle. Unlike the output file generated by Ocellus, the file generated by NEMESIS does not require translating and can be readily accepted by WHIRL-COM; hence, not requiring a separate program to perform the translation.

G.4.2 Inputs required by NEMESIS

G.4.2.1 NEMESIS is capable of accepting an ASCII file containing the relevant data or the user may enter data through the Graphical User Interface (GUI).

G.4.2.2 Radar system information required by NEMESIS relates to the radar transmit power, transmit and receive gains, system noise and losses, polarisation, pulse duration and the most significant parameter of antenna elevation beam shape. Antenna positional data is

also required which includes its latitude and longitude, above ground height and elevation angle.

G.4.2.3 NEMESIS accepts terrain data in the form of Digital Terrain Elevation Data (DTED®).

G.4.2.4 The general parameters needed for the calculation are the maximum range over which the propagation coefficients are required, number of steps over the range, maximum above ground height and maximum elevation angle. The maximum elevation angle is limited to 15 degrees.

G.4.3 NEMESIS validation

G.4.3.1 QinetiQ have previously validated NEMESIS for other projects over several years. Therefore a good degree of confidence can be placed in both the accuracy and precision of the simulations produced by NEMESIS. However, further validation has been undertaken for the purposes of this project. This has been in the form of a comparison study, which compares propagation factors obtained using NEMESIS with those predicted by the Advanced Refractive Effects Prediction System (version 2.01.2014) for a given scenario. The study is documented in section 6.4; the comparison is detailed using two graphs showing general similarity between the one-way propagation losses predicted by the two programs. Using these graphs it is very difficult to compare propagation loss values at specific range and height locations. Given the extensive validation undertaken previously and the use of this program over several years this validation study is considered to be an acceptable compromise.

G.5 Wind Farms Having Interaction at Radar Locations (WHIRL)

G.5.1.1 QinetiQ have developed WHIRL specifically for analysing the interaction of wind turbines with radar installations. The program consists of two parts; the computation is performed by WHIRL-COM and the processed data is then displayed by WHIRL-DIS on a virtual Plan Position Indicator (PPI).

G.5.2 WHIRL-COM

G.5.2.1 WHIRL-COM reads the data files generated by Ocellus (Radar Cross-Section prediction program) and NEMESIS (propagation program). The GUI is used to input the filenames and set-up the turbine and aircraft positions. The program uses the data supplied by Ocellus and NEMESIS to compute the position of each turbine relative to the radar position. The total time for the simulation is determined by the aircraft's start and stop position together with its speed.

G.5.2.2 The simulated aircraft is assumed to be travelling in a straight line and at a constant speed. Although the program cannot represent every scenario this assumption is acceptable because it represents the general case. Each turbine is assumed to rotate at a constant rate, however, the individual turbines within the wind farm may be set to rotate at different rates. This is an excellent feature which can be used to determine the effects of multiple bounce for adjacent turbines, where each turbine's rotor speed is operated independently.

G.5.2.3 The rotor blades of each turbine can be set either to start at a user specified angle or at a random angle. This is another case where WHIRL-COM accurately simulates the real-

world scenario in which different turbines rotate asynchronously with respect to each other.

G.5.2.4 As in the real-world scenario the simulated radar antenna rotates at a constant speed that is independent of the turbine rotation period.

G.5.2.5 WHIRL-COM uses the standard monostatic radar equation to calculate the returned complex signal power from the aircraft target that has a constant Radar Cross-Section. The phase information contained in the complex echo signal is useful for Moving Target Indication (MTI) calculations.

G.5.2.6 WHIRL-COM simulates a simple MTI which suppresses stationary and slow moving targets while relatively fast moving targets are processed and displayed on the virtual PPI. Furthermore, the program has the ability to reject noise by using a user specified power threshold. If the power threshold is set too high then genuine targets are not processed, however, if it's set too low then invalid targets would be passed as genuine targets and displayed on the PPI. The user should therefore have some knowledge of the technical issues surrounding the power threshold and what constitutes a reasonable power threshold. Automatic gain control is achieved by using the user-specified dynamic range factor. The user should have some technical knowledge of the way in which the dynamic range factor influences the automatic gain control.

G.5.2.7 **Radar parameters:** A list of parameters pertaining to the radar is entered via the GUI. These parameters are:

- 3dB azimuthal beamwidth (Degrees)
- Radar pulse length (Seconds)
- Detection threshold relative to noise level (Decibels)
- Noise bandwidth (Hertz)
- Signal processing dynamic range (Decibels)
- Integration efficiency factor (0 to 1)
- Number of pulses integrated
- Initial azimuth angle of the radar antenna (Radians)
- Radar revolutions per minute
- Radar frequency (Hertz)
- Transmit power (Watts)
- Pulse repetition frequency (Hertz)
- 3D radar position (Meters)

G.5.2.8 The values for the majority of these parameters may be obtained from radar manufacturers.

G.5.2.9 **Turbine parameters:** Computer resources limit the number of turbines that can be entered into the model[5]. The turbines may have any number of blades, however three

[5] QinetiQ comment: This is a true statement, but does not cause any problems as large wind farms containing up to 100 turbines can be calculated on a standard PC with 512Mb of RAM. More RAM will allow larger farms to be considered.

blades are sufficient to model the majority of wind turbines found in the UK. For each turbine its spatial 3D co-ordinates, pitch, bearing, blade's start angle and the number of revolutions per minute are required. The blade can be initialized to start at a random angular position.

G.5.2.10 **Single target trajectory data:** In the real-world scenario an aircraft would be considered a single Radar Cross-Section target which would move independently of the terrain over which it flies. In the WHIRL-COM computer model however, the single target follows the contours of the terrain. Apparently the program does provide means by which the target's height may be made independent of the terrain, but this was not implemented during the development and validation of the program. Therefore WHIRL-COM is presently unable to simulate a real-world scenario where a wind farm is situated close to an aircraft landing strip with an aircraft coming in to land[6]. The consequences of not being able to simulate such scenarios are unknown, but are not relevant to the scenarios investigated during the current work, but may be important in future.

G.5.3 WHIRL-DIS

G.5.3.1 WHIRL-DIS accepts an output file from WHIRL-COM which contains the confirmed radar detections and then displays these radar detections in real-time on a virtual PPI. WHIRL-COM was initially used to perform this function; the program was later separated from WHIRL-COM so that it could be run on a portable computer and output in real-time.

G.5.3.2 A user-adjustable range-dependant threshold has been integrated into the software; this allows the operator to determine the level of clutter present in the PPI output.

G.5.4 Validation of WHIRL

G.5.4.1 The WHIRL model has been validated against radar data for a single wind turbine which is located at Swaffham and partially validated against a multiple wind turbine site located at Hare Hill.

G.5.4.2 **Single wind turbine:** The single wind turbine situated at Swaffham (N52:39:24 E00:41:00) is an Enercon E-66, its hub is located 67m above ground level. Each of its three fibreglass (reinforced epoxy) blades is 30.8m in length with a clockwise rotating rotor having a diameter of 66m. The range of speed is 10-22RPM, with a maximum tip speed of 76m/s.

G.5.4.3 Flight Refuelling Limited were contracted to collect the primary radar data over several days in the early part of July 2002. This data set was made available to QinetiQ. The Swaffham wind turbine is situated approximately 8.3km west of RAF Marham and is in line-of-sight of their radar (N52:38:40 E00:33:41).

G.5.4.4 **Multiple wind turbines:** The scenario used in the multiple wind turbine simulation is a general approximation of a video recording of the Prestwick PPI unit; the wind turbines' orientation and rotational speed were unknown. Consequently, these parameters were

[6] QinetiQ comment: This is a simple modification to the model if required. Changes in ground height are often small compared to the height of an aircraft so this following of the ground contours only amounts to minor fluctuations in the path of the aircraft.

selected by the operator's knowledge of the wind farm. This part of the validation is only intended to give a general feel for WHIRLs performance when it's used to model multiple wind turbines. Further work should be undertaken to validate WHIRL as a product for simulating the scattering from multiple turbines.

G.5.4.5 The multiple wind turbine site that was used in the partial validation process is situated at Hare Hill (N55:21:40 W04:07:24); this wind farm consists of twenty Vestas 650 wind turbines. The collated radar data are in the form of video recordings of the PPI unit at Prestwick aerodrome, showing the clutter caused by the Hare Hill wind farm. The comparison described in section 6.5.5, shows an expected agreement between the WHIRL simulation of the wind farm at Hare Hill and the video recording of the PPI unit at Prestwick. The area occupied by the simulated wind farm clutter is approximately 45% greater than the area actually occupied by the Hare Hill site. This is expected because of spreading effects caused by the radar antenna's antenna beamwidth.

G.6 Investigation of the Radar Cross-Section of a simple wind turbine blade section

G.6.1.1 The investigation of the propagation characteristics of radar signals via the WHIRL program showed that they reflect current practice in modelling features. Over a period of many decades a body of statistical information has been established and is well represented by the computer model.

G.6.1.2 The Ocellus program calculates one parameter for the turbine called the Radar Cross--Section. This parameter is easily measured and is used to assess the accuracy of the prediction. The comparison of the predicted and measured Radar Cross-Section shows that the computer model consistently underestimates the value of this parameter by 4dB to 10dB[7].

G.6.1.3 This error implies that the level of interference to the radar may be underestimated by this amount, and in a safety critical situation this could become dangerous if there were not adequate safety margins present. If the program were to be used in its present form the Radar Cross-Section would have to be adjusted by an appropriate amount to take into account the underestimation.

G.6.1.4 In order to provide guidance upon this issue PipeHawk has undertaken a short investigation into the key issues concerning the Radar Cross-Section of a wind turbine. To demonstrate the influence of the controlling parameters it is not necessary to use a full blade. The model adopted essentially treats part of the blade as a short length of cylinder, allowing the construction and behaviour of the Radar Cross-Section to be demonstrated.

G.6.1.5 A commercially available electromagnetic modelling package, which was developed by Computer Simulation Technology™ (CST) and called Microwave Studio (MWS®), was employed to facilitate the investigation. In an investigation such as this the validity of such a package must be demonstrated and in the next section it is employed to

[7] QinetiQ comment: In response to these comments QinetiQ has recalculated the predicted data at the exact same radar settings used in the trial (before there were small differences). This has improved the level of agreement between the measured and predicted data, however, in some cases the predictions are 4 to 6 dB lower than the measurements near some of the RCS peaks. The two reasons that have been identified to explain the 4 to 6dB variances are that the actual blade reflectivity is higher than assumed in the modelling and the modelling does not include "multiple-bounce" returns. For a more detailed explanation see section 6.2.8.

numerically determine the Radar Cross-Section of a perfectly conducting square plate. The analytical solution for this parameter is available to provide a comparison to and confidence in the numerical solution. It will be shown that the commercial software package is an effective way of computing the Radar Cross-Section of a scattering object.

G.6.1.6 Based upon this investigation CST-MWS® is employed to calculate the Radar Cross-Section of a short length of metal cylinder, representing a section of a metallic wind turbine's blade. The construction of the cylinder is then changed to be solid fibreglass in order to investigate the effects the material may have on the Radar Cross-Section. Finally, the construction of the cylinder is changed to an outer cylindrical shell of fibreglass, an air gap and an inner central metallic core. This may be closer to the real construction techniques employed in wind turbines.

G.6.1.7 The output from this investigation is then available to aid comment upon the applicability of the Ocellus program.

G.6.2 Radar Cross-Section of a perfectly conducting square plate

G.6.2.1 Initially the bistatic Radar Cross-Section of a square conducting plate was simulated; this was a quick and simple way of providing confidence in the commercial software employed. The bistatic and monostatic Radar Cross-Section of such an object can be calculated analytically by using the Physical Optics technique and makes comparison a simple matter. CST MWS® was used in two separate simulations to determine the Radar Cross-Section of a square conducting plate. Bistaic means the radar transmitter and receiver are at different locations and monostatic means the radar receiver and transmitter are in the same location. The frequency of the incident wave is 3GHz and the lengths of the sides of the plate for each simulation are 5λ and 10λ. The unit electric field vector propagates normal to the x-axis as shown in Figure G-1. The principal plane bistatic Radar Cross-Section for these simulations is shown in Figure G-2. The Physical Optics solution for these plates is shown in Figure G-3. The equations relating to the Physical Optics technique used to calculate these values are well know to the radar community and can be found in any radar literature and are given in section G.8.

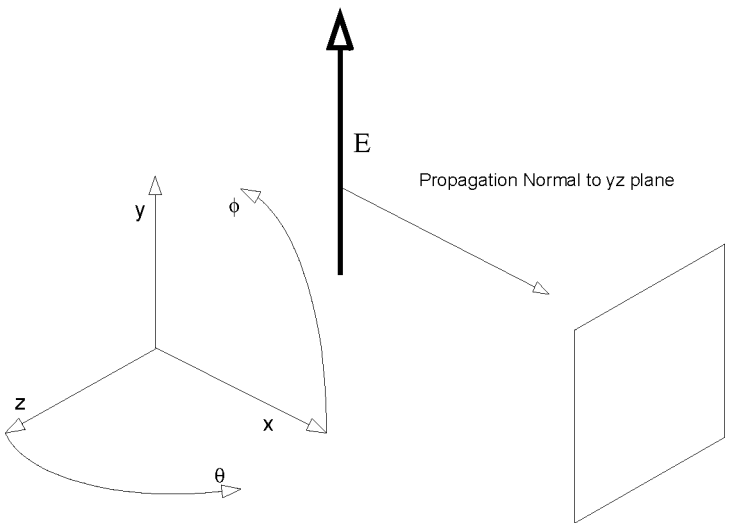

Figure G-1 Co-ordinate system used in the simulation of the RCS of a square plate.

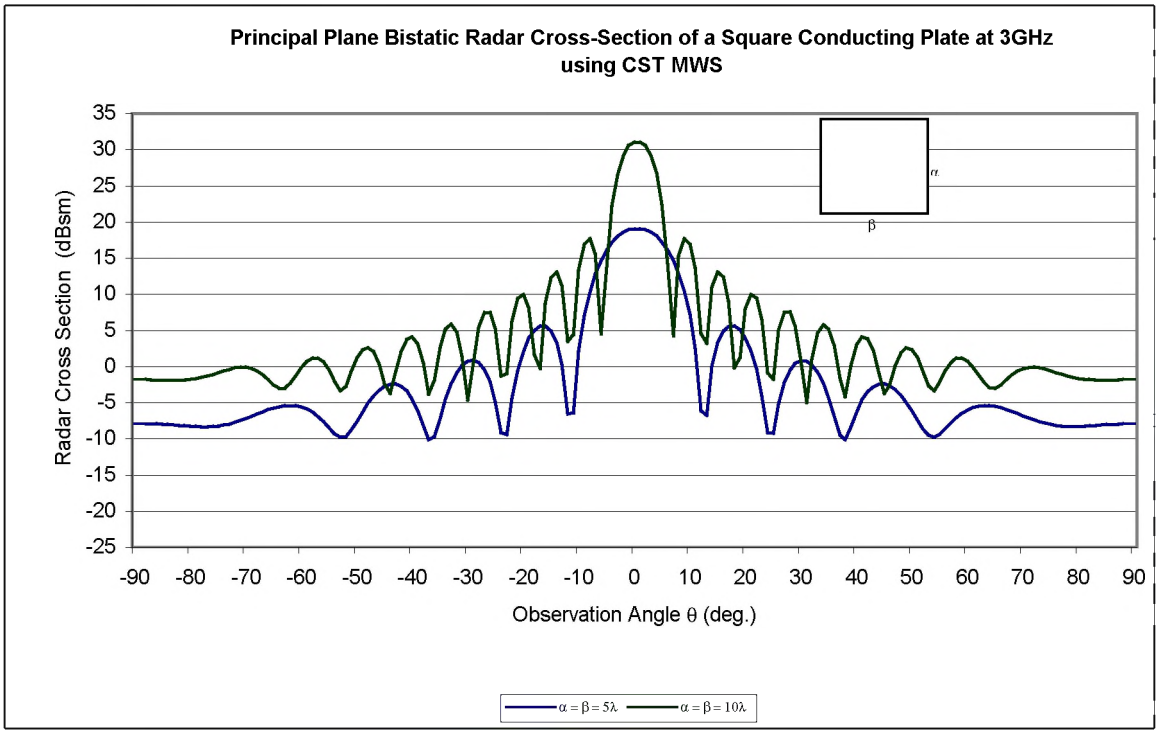

Figure G-2 Bistatic RCS of a conducting square plate using CST MWS®.

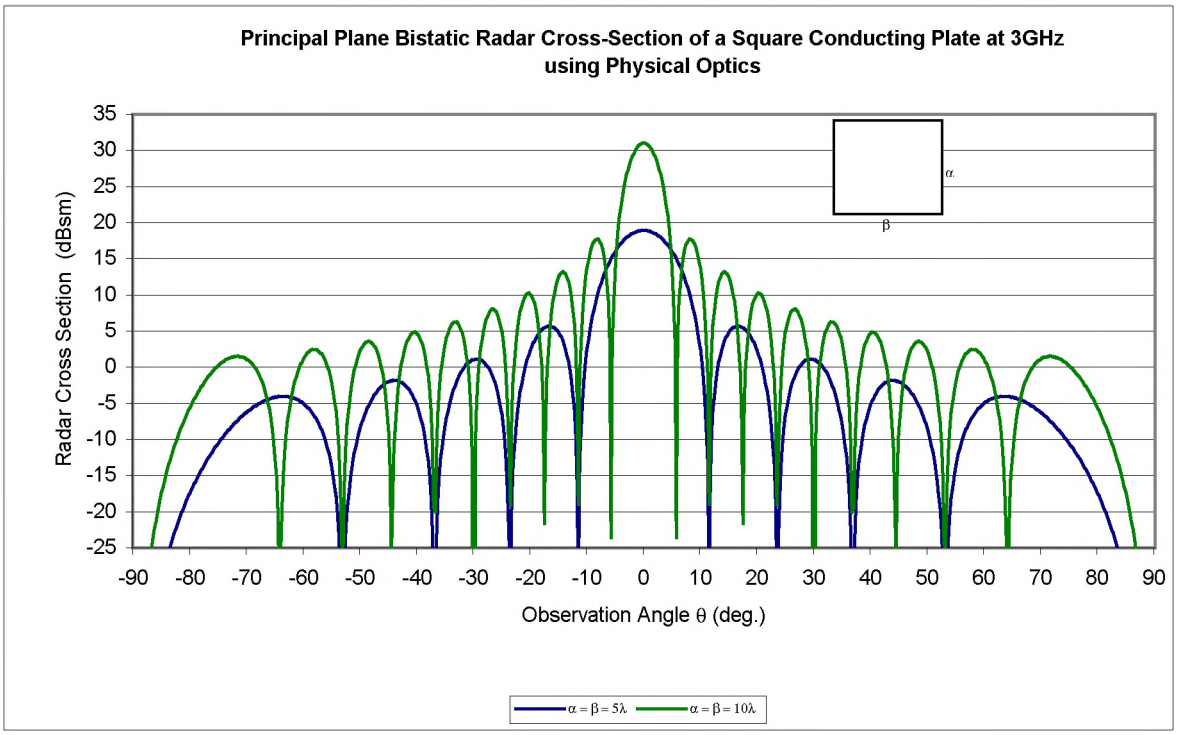

Figure G-3 Bistatic RCS of a conducting square plate using Physical Optics technique.

G.6.2.2 The monostatic and bistatic Radar Cross-Sections generated by CST MWS® show good agreement with the Physical Optics technique. This is to be expected, as the physical dimension of the square plate is much larger than the frequency of the incident wave. The small difference in the monostatic Radar Cross-Section generated by CST MWS® for a 5λ and 10λ plate is 0.04dB (0.9%) and 0.01dB (0.2%), respectively and is considered negligible.

G.6.3 Radar Cross-Section of an electrically large cylinder

G.6.3.1 CST MWS® is used to simulate the Radar Cross-Section of a solid conducting cylinder; it is then transformed into a fibreglass cylinder by simply changing it from a metallic material to a material with a dielectric constant of 4 and its Radar Cross-Section is then computed. The Radar Cross-Sections of the fibreglass and conducting cylinders may then be compared. The length and diameter of the cylinders are both 10λ. The frequency of the incident wave is 3GHz and the unit electric field vector propagates normal to the x-axis, as shown in Figure G-4. In this scenario it is perfectly reasonable to consider this cylinder as being a section of a turbine's blade.

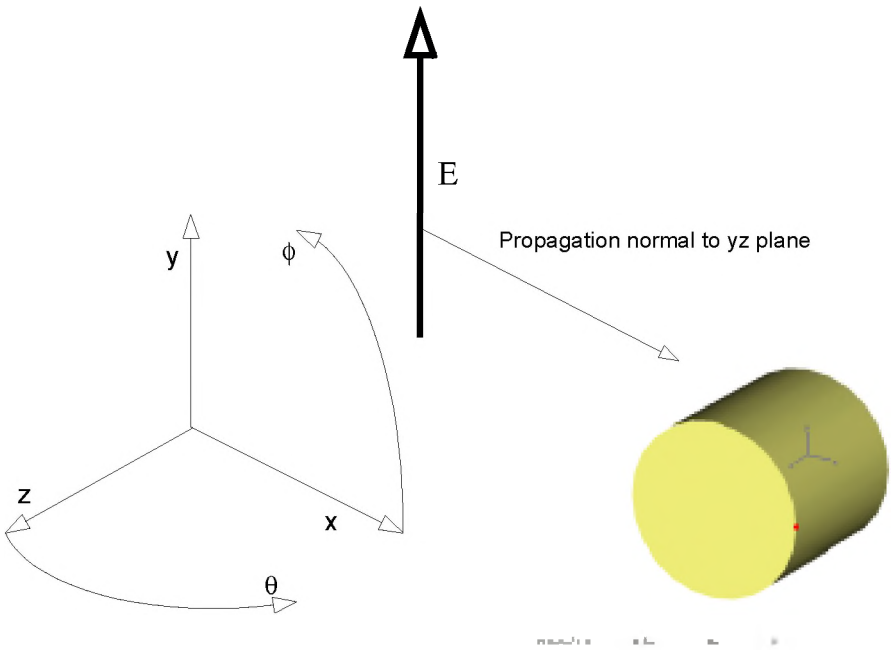

Figure G-4 Co-ordinate system used in the simulations of the RCS of a solid cylinder.

G.6.3.2 The monostatic Radar Cross-Section of an electrically large cylinder can be determined from a well known mathematical formula detailed in section G.8; for this cylinder the analytically calculated monostatic Radar Cross-Section when viewed normal to the YZ-plane (see Figure G-4) is 14.97dBsm. The simulated value for the Radar Cross-Section for this cylinder is 14.77dBsm suggesting that the model is calculating the Radar Cross-Section to an acceptable tolerance. This second comparison of the commercial software with an analytical model was considered desirable because the cylinder is a more extensive three-dimensional object, demanding significantly more computer resources. The principal plane bistatic Radar Cross-Section of the two types of cylinders is shown in Figure G-5. These simulations show that while the bistatic Radar Cross-Section is affected by the change in material, the monostatic Radar Cross-Section is almost identical. Therefore, it is reasonable to simplify the simulation by modelling the turbine's blades using perfectly conducting material rather than fibreglass. Consequently, the only technique required to calculate the Radar Cross-Section would be the Physical Optics method.

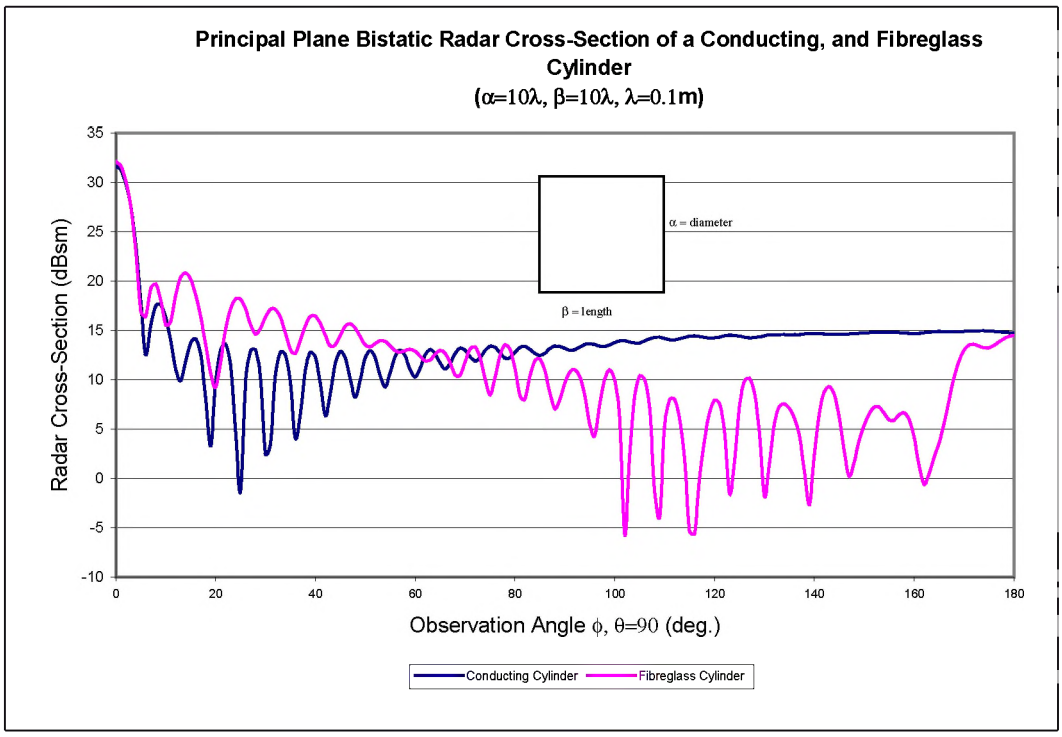

Figure G-5 Bistatic RCS of a conducting, and fiberglass cylinder.

G.6.4 Radar Cross-Section of a section of wind turbine

G.6.4.1 In this simulation an attempt is made to represent a detailed section of a wind turbine. The turbine section is formed from two concentric cylinders; a hollow fibreglass cylinder (wall thickness = $\lambda/2$) is used to form the exterior of the turbine and a solid conducting cylinder (radius = λ) forming some metallic parts of the wind turbine's blade, this represents the metallic root structure of the blade, the lighting conductor, or the air brake mechanism. The properties of the incident wave and the exterior dimensions of the turbine section are the same as in the previous simulation (length and external diameter are 10λ), as shown in Figure G-6.

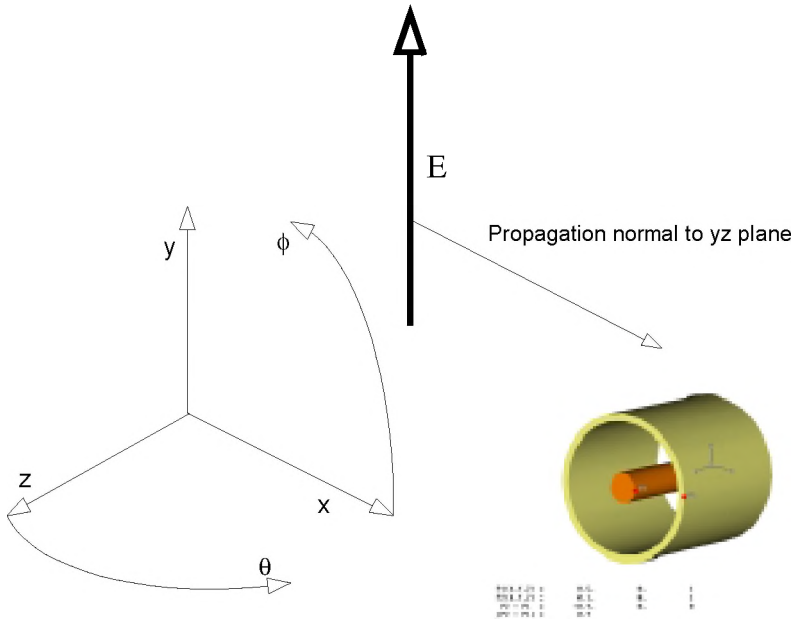

Figure G-6 Co-ordinate system used in the simulations of the RCS of a turbine section.

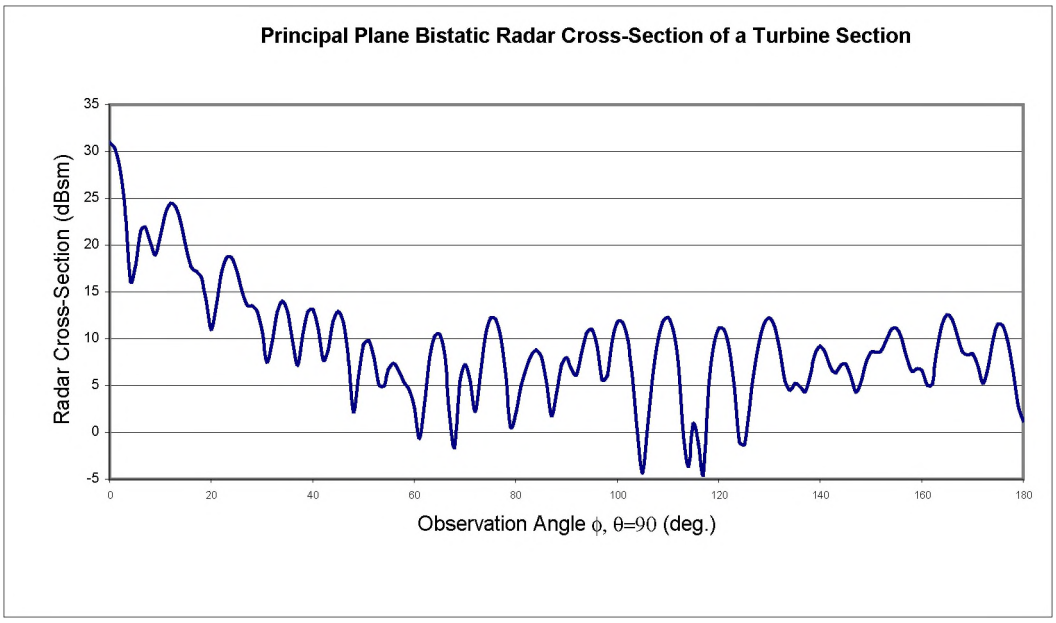

Figure G-7 Bistatic RCS of a wind turbine section.

G.6.5 Conclusions – Investigating the Radar Cross-Section of a turbine's blade

G.6.5.1 The investigation was carried out on a short length of blade represented by a cylinder cross-section. This may be considered a major simplification, but nevertheless some major conclusions may be drawn.

G.6.5.2 The details of the behaviour of the Radar Cross-Section have been presented. Table presents the key values for the three cylindrical geometries investigated. For the first two cases the peak in the backscattered Radar Cross-Section is in the monostatic direction.

G.6.5.3 For the third case it is a few degrees away from this direction. With a circularly symmetrical object like a cylinder this direction will never coincide directly with the true monostatic direction. With a more representative wind turbine's blade cross-section in which this symmetry is broken this peak could easily align with that direction.

G.6.5.4 In using the figures to investigate the consideration of wind turbines it is therefore relevant to compare all these figures in Table F-1.

G.6.5.5 The results in Table F-1 show that the details of the construction of the wind turbine's blade have little influence upon the peak Radar Cross-Section. In this example there is only 0.4dB reduction in the Radar Cross-Section in moving from an all metal conducting description to an all fibreglass construction. A further 2.1dB reduction occurs when the fibreglass is reduced to a shell construction with a metal insert.

G.6.5.6 In these examples the total variation caused by considering different construction materials and techniques is 2.8dB.

Case	Construction	RCS (dBsm)
1	A perfectly conducting (metal) cylinder 10 wavelengths in diameter and 10 wavelengths long.	14.9
2	A solid all fibreglass cylinder (dielectric constant 4; zero loss) 10 wavelengths in diameter and 10 wavelengths long	14.5
3	A fibreglass cylindrical shell 10 wavelengths in outer diameter and half a wavelength wall thickness filled with air but with a central metallic core 2 wavelengths in diameter.	12.1

Table G-1; The peak monostatic Radar Cross-Section of various cylindrical constructions (at 3GHz).

G.6.5.7 This investigation concludes that the variation in the construction of the blade is not an important issue in the overall prediction of the blade's Radar Cross-Section[8].

G.6.5.8 The prediction method forms part of a safety evaluation. A conservative approach, leaning towards safety, indicates that the turbine's blade should be featured as made up

[8] In our investigations of reflectivity, we found that blade reflectivity significantly effects the radar cross-section. The results shown here are correct, but with such simple shapes the results may not be applicable to complex wind turbine blades. We have carried out predications of the Enercon E-66 with metal blades and this gave peak values 10dB higher than the measured levels; i.e. the fibreglass predictions gave more accurate answers. Also if in the future new blade designs are developed with "stealthy" qualities then complex modelling including the blade reflectivity would be required to allow an assessment of these blades' ability to reduce radar clutter from turbines.

of a metallic skin. This may overestimate the Radar Cross-Section, but the margin is less than 3dB which may be less than the error in field measurements, and may be discounted.

G.6.5.9 The difference between the predicted and measured value for the Radar Cross-Section noted by QinetiQ are unlikely to arise from the simplification in the modelling of the turbine construction.

G.6.5.10 The investigation does however indicate the rapid spatial variation of Radar Cross-Section. Even with a ten wavelength long cylinder the lobes in the Radar Cross-Section, shown in Figure G-7, are six to seven degrees wide. The Swaffham blades are 30.8m long and at 3GHz this implies that they are at least three hundred wavelengths long. The equations in section G.8 indicate that the lobe structure for an actual turbine's blade will have lobes only 0.2 degrees wide.

G.6.5.11 This implies that a small variation in the angle of a wind turbine's blade in the direction of its length would cause a wide variation from minimum to maximum in the value of the Radar Cross-Section. This makes the detailed comparison of measured and predicted results demanding.

G.6.5.12 The computer model assumes a particular orientation for each blade and will calculate the scattered value for that angle. Most angles will be away from the peak of the maximum value, giving a prediction that is below the peak, at some intermediate level.

G.6.5.13 In practice the orientation of the length of the blade of the Swaffham machine may change by more than 0.2 degrees between the machine being on and off load, and even between the blades at the top and bottom of their rotation because of the vertical gradient of the wind. The blades flex by more than the width of the lobe of the Radar Cross-Section!

G.6.5.14 This implies that although the Ocellus program may predict the Radar Cross-Section corresponding to some value below the peak, the movement and flexing of the machine actually allows the radar to see the peak scattering condition.

G.6.5.15 This could possibly explain the discrepancy observed by QinetiQ between predicted and measured values.

G.6.5.16 The question then arises concerning how the Radar Cross-Section should be calculated in a manner that ensures the best responsible approach to safety.

G.6.5.17 The above discussion indicates that the lobe structure of the Radar Cross-Section of a wind turbine at 3GHz is so detailed and that it would be extremely difficult to accommodate. Not only would a most detailed model of the turbine need to be indicated, but also its dynamic characteristics in terms of its rotational movement under load. The pragmatic approach is simply to use the peak value.

G.6.5.18 Should the material details of the construction be included? The investigation showed that this has a small effect, less than 3dB. The pragmatic approach is simply to regard the wind turbine as a metallic or perfectly conducting construction. This requires the minimum of computation and with regard to safety is the conservative approach.

G.6.5.19 Should the shape of the blade be included? This is a question not directly addressed by the brief investigation carried out. At present the only recommendation that can be made

is that it may not be necessary in the initial assessment of a possible wind turbine site, but if that initial assessment indicates that the decision margins are small then it may be helpful if more detailed information is required[9].

G.7 Overall Conclusions

G.7.1 WHIRL has been developed by QinetiQ, with funding from the DTI managed by Future Energy Systems (FES) to advance the knowledge of the interaction between air radars and wind turbines. The UK is a small crowded landmass with many demands for development sites, and requires effective radar coverage. Introducing new energy systems into this crowded environment is demanding and there are many possible areas of conflict. Air safety is such an important issue that it should not be compromised.

G.7.2 Against this background there was little hard evidence to decide if sites could be developed for wind energy or development should be denied to protect radar. This was a highly contentious issue. There were some tools available such as that developed by PipeHawk for the CAA, but it had only been validated against scaled model measurements. Whilst this was a realistic approach with limited funds, it was not necessarily well understood by lay observers who preferred to see full-scale measurements.

G.7.3 The contribution of QinetiQ is valuable in that it has mobilised the resources of a major defence organisation to perform full-scale wind turbine measurements on site. It also allowed two of the four elements of predictive software to be used directly without further development based upon the extensive validation previously carried out for defence.

G.7.4 The contribution of Emrad, the technology division of PipeHawk plc, is to review the development of the other two packages called WHIRL-COM and WHIRL-DIS and position the work into an overall context particularly for the wind community.

G.7.5 NEMESIS describes the propagation of the radar signal between the radar transmitter and the wind turbine and the return path of the scattered signal back to the radar. Radio propagation studies are usually based upon statistical models with specific algorithms employed to describe the effects of hills and other similar obstructions. The validation of such a model does not involve the simple comparison of a few numbers but the detailed collection of statistics over a long period. This was well outside the scope of the work. The models and algorithms presented in the code appear to represent the modern view

[9] QinetiQ comment in response to the point raised in sections F.6.5.8 - F.6.5.19: The main objectives of the QinetiQ programme are summarised in section 1.3 of the main report. To achieve these aims QinetiQ proposed the development and validation of a computer model to simulate the effects of wind turbines on radar systems. In response to feedback from the radar sub-group and the Emrad review we have recalculated the predicted RCS data at the exact same radar settings used in the trial (before there were small differences). This has improved the level of agreement between the measured and predicted data, however, in some cases the predictions are 4 to 6 dB lower than the measurements near some of the RCS peaks. The two reasons that have been identified to explain the 4 to 6dB variances are that the actual blade reflectivity is higher than assumed in the modelling and the modelling does not include "multiple-bounce" returns. For a more detailed explanation see section 6.2.8.
The results generated by the project (parameter sensitivity modelling and field trials data) have enabled us to provide a much more detailed quantification of the complex interactions between wind turbines and radar systems than was previously available. Going forward, the model developed to support the project could be used in a number of ways, with one example being supporting the development of wind turbines designs with lower RCS signatures (where the ability to calculate intermediate as well as maximum RCS values will be an important requirement).

upon propagation effects built up over many decades of measurements to a large proportion of the radio community.

G.7.6 WHIRL calculates the Radar Cross-Section of a single wind turbine using the Ocellus block of code. This appears to present a valid calculation based upon the use of Physical Optics and the Physical Theory of Diffraction. Physical Optics is one of the most computationally efficient methods of calculating the scattering from smoothly curved extended surfaces, such as the major surfaces of a wind turbine's blade. Physical Optics is not valid at the edge and at other locations when diffraction occurs. At this location the basis of the model changes to the Physical Theory of Diffraction. Generally, only a small proportion of the energy scattered from a turbine's blade occurs as diffraction (except with an incident circularly polarised wave). Physical Optics precisely describes the scattering of the majority of the energy.

G.7.7 The limitation with this model despite its computational efficiency is the detail with which the blade must be described. Basic sampling theory dictates that spatial points to describe the blade are spaced at intervals less than half a wavelength apart over the whole area or volume of interest; ideally the points should be closer. For 3GHz radar the spatial points should be less than 5cm apart on a structure 30m long.

G.7.8 If the blade is metallic the points may be only on its surface but if the blade is made of a dielectric such as fibreglass the spatial points must be spread throughout the whole volume. The computational burden remains significant even with the Ocellus model making the assumption of a metallic blade.

G.7.9 The radar measurements carried out on site by QinetiQ although not directly available to PipeHawk appear to be of a high standard. In general the behaviour of the Radar Cross-Section of the wind turbine estimated from the movements accurately reflects the variations predicted. The angular structure of the measurements and the prediction is good. This provides much confidence in the quality of both.

G.7.10 The variation with angle of the blade's Radar Cross-Section indicates that the different contributions from Physical Optics and the Physical Theory of Diffraction are accurately mixed. The individual contributions will have different angular responses. The major discrepancy is in the level of the prediction versus the measurement.

G.7.11 The maximum values are greater than the predicted by 4dB to 10dB which indicates that it would be potentially dangerous to air safety to rely directly upon the prediction.

G.7.12 The simple investigation carried out by PipeHawk shows that the source of this discrepancy was unlikely to be the modelling of the material or construction of the blade. This produced a variation of less than 3dB.

G.7.13 It was shown that the most likely cause to the angular variation of the Radar Cross-Section, with a blade length of 30m at an operating frequency of 3GHz, and the lobes in the Radar Cross-Section are only 0.2 of a degree across. Flexing of the blade by this amount sweeps the value through both the maximum and minimum values. If the maximum value is consistently used, much of the discrepancy may disappear and the accuracy of the prediction may be greater.

G.7.14 Essentially, the full-scale measurements have validated the WHIRL model's underlying approach.

G.7.15 It is a valid approach, but before it can be relied upon for safety critical applications the source of the 4dB to 10dB underestimation of the Radar Cross-Section must be found and corrected[10].

G.7.16 It may be possible to further develop the code to use the peak of the blade's lobes only, rather than rely upon the detailed lobe structure which is too fine to be appropriate. This may provide the required correction.

G.7.17 Overall, the whole programme presented by both QinetiQ and PipeHawk is a valuable contribution to the overall understanding of the interaction of radio systems in general and radar systems in particular with wind turbines. It suggests a major increase in the overall volume of information available generally and to the wind energy community in particular for planning progress.

G.7.18 The problem of characterising the interaction of wind turbines is extremely demanding, and this work has demonstrated the degree of difficulty involved.

G.7.19 In the well-posed problem of a single blade, in section 5.2, QinetiQ demonstrate much precision in the agreement between theoretical predictions and measurements in a well-controlled compact range.

G.7.20 With a very large (in terms of wavelength) structure such as a complete wind turbine installed in the field, the challenge is much greater. To get similar agreement at 3GHz would require every detail of the metal and fibreglass structure, visible to the radar, including the internal structure of the blades to be fully modelled.

G.7.21 The spatial resolution required would be of the order of a fraction of a wavelength (~1cm) for the complete structure. It is unrealistic to include this level of detail in an electromagnetic model. It is unlikely that even QinetiQ could provide the computer resources to complete this task in a timely and cost effective manner. The resulting model would be entering new territory with regard to the stability of electromagnetic modelling and the return would be vanishing. It should not be considered.

G.7.22 What has been achieved in this work is the most detailed investigation of the Radar Cross-Section of a wind turbine that it is sensible to carryout given the current status of electromagnetic modelling and measurement techniques.

G.7.23 In considering the general spatial characteristics of the Radar Cross-Section of a wind turbine good general agreement was achieved between predictions and measurements. The agreement between the predicted and measured time-varying waveforms resulting from the cyclic variation in the Radar Cross-Section was not so good. The major discrepancy between measurements and prediction was in the absolute level of the Radar Cross-Section. Typically the difference was between 4dB and 10dB[11]. The measured signal was generally greater than the predicted signal level. This implies that particular

[10] QinetiQ comment: See section 6.2.8 for the QinetiQ explanation.

[11] QinetiQ comment: In response to these comments QinetiQ has recalculated the predicted data at the exact same radar settings used in the trial (before there were small differences). This has improved the level of agreement between the measured and predicted data, however, in some cases the predictions are 4 to 6 dB lower than the measurements near some of the RCS peaks. The two reasons that have been identified to explain the 4 to 6dB variances are that the actual blade reflectivity is higher than assumed in the modelling and the modelling does not include "multiple-bounce" returns. For a more detailed explanation see section 6.2.8.

care is required if the prediction is to be used for any purpose that is safety related. To be confident that the predicted scattering from the turbine is conservatively estimated, the worst-case figure of 10dB should be added to the predicted Radar Cross-Section.

G.7.24 One objective of the work is to aid the understanding of the interaction between wind turbines and radar to aid in co-siting planning issues. This work has focussed upon the interaction at the wind turbine, it does not address the influence of the signal scattered from the turbine upon the radar's performance. This includes issues such as whether the turbine appears upon the radar's Plan Position Indicator (PPI) as a target, or if the radar is desensitising in the shadow region behind the turbine.

G.7.25 The apparent jewel in this work is the radar field measurements although PipeHawk had no way of validating the precision achieved. Since the problem of electromagnetic interference arising from wind turbines was first identified with regard to interference to television broadcast, and subsequently with regard to microwave links there has been a major need for full-scale Radar Cross-Section measurements. The QinetiQ measurements are the most definitive in this regard because they employed a bespoke experimental radar, specifically designed for gathering this type of measurement rather than an operational radar operator in an unconventional manner to infer Radar Cross-Section information. The measured radar data now underpins the electromagnetic modelling techniques and provides the underlying justification for their use.

G.8 Mathmatics appendix

G.8.1 The bistatic and monostatic Radar Cross-Section of a square conducting plate may be found using the Physical Optics technique by the following equations:

$$\sigma_{(3D)Bistatic} = 4\pi\left(\frac{ab}{\lambda}\right)^2\left[\cos^2(\theta_i)\left(\cos^2(\theta_s)\cos^2(\phi_s)+\sin^2(\phi_s)\right)\right]\times\left[\frac{\sin(X)}{X}\right]^2\left[\frac{\sin(Y)}{Y}\right]^2$$

$$\sigma_{(3D)Monostatic} = 4\pi\left(\frac{ab}{\lambda}\right)^2\cos^2(\theta_i)\left[\frac{\sin\left[\frac{\pi b}{\lambda}(\sin(\theta_i))\right]}{\frac{\pi b}{\lambda}(\sin(\theta_i))}\right]^2$$

where,

$$X = \frac{\pi a}{\lambda}\sin(\theta_s)\cos(\phi_s)$$

$$Y = \frac{\pi b}{\lambda}(\sin(\theta_s)\sin(\phi_s)-\sin(\theta_i))$$

σ = Radar Cross-Section (dBsm)

a = length of side along the x-axis (m)

b = length of side along the y-axis (m)

λ = wavelength of the incident frequency (m)

θ_i = angle of incidence taken from the +z-axis toward the –y-axis (deg)

θ_s = scattering angle taken from the +z-axis toward the +y-axis (deg)

ϕ_i = angle of incidence taken from the +x-axis toward the +y-axis (deg)

ϕ_s = scattering angle taken from the +x-axis toward the +y-axis (deg)

G.8.2 The monostatic Radar Cross-Section of an electrically large conducting cylinder may be calculated using:

$$\sigma_{(Monostatic)} = \frac{2\pi ab^2}{\lambda}$$

where,

σ = Radar Cross-Section (dBsm)

a = radius (m)

b = length (m)

λ = wavelength of the incident frequency (m)

REFERENCES

1. BARRIOS, A. E., *A Terrain Parabolic Equation Model for Propagation in the Troposphere,* IEEE Transactions on Antennas and Propagation, vol. 42, no. 1, pp. 90–98, Jan 1994.

2. DONOHUE, D.J., and KUTTLER, J.R., *Propagation Modelling Over Terrain Using the Parabolic Wave Equation,* IEEE Transactions on Antennas and Propagation, vol. 48,no. 2, pp. 260–277, Feb 2000.

3. KUTTLER, J.R., and DOCKERY, G.D., *Theoretical Description of the Parabolic Approximation/Fourier splitstep Method of Representing Electromagnetic Propagation in the Troposphere,* Radio Science, vol. 26, no. 2, pp381–393, Mar–Apr 1991.

This page is intentionally blank